

INVESTIGATION OF FLUOROPHORE MOTIFS FOR PROTEASE DETECTION

THESIS

submitted for the degree of

DOCTOR OF PHILOSOPHY

in

Chemistry

at

Kingston University London

by

Luke James Bywaters

School of Life Sciences, Pharmacy and Chemistry,

Kingston University, Penrhyn Road,

Kingston-upon-Thames, Surrey, KT1 2EE.

December 2018



DECLARATION

This thesis entitled Investigation of Fluorophore Motifs for Protease Detection is based upon work conducted by the author in the School of Life Sciences, Pharmacy and Chemistry at Kingston University London between **October 2013 and May 2017**. All of the work described herein is original unless otherwise acknowledged in the text or by references. None of the work has been submitted for another degree in this or any other universities.

Luke James Bywaters

*“Where you arrive does not matter as much as what sort of person you are
when you arrive there.” - Seneca*

In Memory of My Mother Jan

Acknowledgments

First and foremost, I would like to thank my supervisor, mentor, and above all, friend Dr Adam Le Gresley, without whom there is not a chance that I would have survived long enough to reach this stage. Any words I could put to paper could not adequately describe the debt of gratitude I owe to him. He has provided me with constant support, guidance and an unwavering belief that I could get through this, especially when times were really tough. These characteristics in any person, in my opinion define a role model which we could, and should all aspire to. Secondly, I would like to thank Dr Alex Sinclair, who's hard work and lobbying provided me with the opportunity to undertake this PhD project, may he enjoy the very best of fortunes in his new career path.

I would also like to thank my friend Dr Jean-Marie Peron, the in house NMR 'don'. Who not only helped me out with the intricacies of both NMR and synthetic methodology on countless occasions, but also provided a sounding board for my perpetual complaining, swearing and general bad manner! Not only did he put up with me, but was always full of much needed advice and banter to bring a smile to my face when I needed it, often in the pub after a hard day in the lab.

I would also like to express my eternal gratitude to my friends Luke Stokes and Griff Williams, who were there in a flash when I really needed them, and continued to be there all through my troubled times. Without those guys and their support and faith in me, I don't know where I would be today. They showed me what a true friend really is.

It remains for me to thank my colleagues and friends from the LeGresley Research lab: the legendary Paddy Melia, one of my best friends and a more than worthy sparring opponent, who's banter I still bear the scars of! My friends Navid Shokri and Dr Rosa Busquets, who's consistent advice and unwavering confidence in me, even when I was seriously lacking them myself helped me indescribably. My Friend and contemporary Samerah Malik, who always maintained confidence in me with unconditional kindness and good advice even when my own faculties failed me, but without sparing the odd kick up the derriere when suitably required! My friend Alex Fudger who provided a shoulder to lean on with consistent good advice which kept me on track throughout the hard times.

Finally I would like to thank my lady Margarida, for her love, support, encouragement and for never giving up on me. She was always there to give me something to strive towards and look forward to, without which I couldn't have got through this. Furthermore I would also like to thank her for putting up with me and all the associated hassle and heartache that entailed. If trophies were awarded for such things, a large cabinet would be in order to house her collection.

All that remains is to thank Kingston University for providing the funding for this project, without which I am certain I could not have taken it on.

Abstract

There is an increasing and serious problem of antimicrobial resistance emerging where previously useful antibiotics are no longer effective. This causes a significant monetary and human cost in the healthcare system, and is a direct result of the misuse and over prescription of antibiotics. The development and implementation of rapid point of care diagnostics to conclusively identify problem pathogens such as *Staphylococcus aureus* could slow the emergence of antibiotic resistance by correctly targeted antibiotic therapy. The rapid and sensitive protease detecting LGX probe is an example of such a diagnostic test. The synthesis of this rhodamine based fluorogenic probe and the investigation of other fluorescence motifs for protease detection has been the focus of this project. Scale up and optimisation of the synthetic route to the previously produced LGX probe was achieved, allowing further testing in a healthcare environment. Previous work has failed to address the complexities associated with the use of conventional fluorescence motifs for probe generation, as well as the ways in which their fluorescence may be modulated. Herein we address these problems, and those encountered with the scale up of the 'LGX' probe. The lessons learned from the LGX synthesis provided the basis for development of a number of novel analogues of the orphan fluorophore class Singapore Green. A library of nine simplified and highly active fluorescent Singapore Greens were generated. These were exhaustively investigated and it was determined how structural variations effect both their spectral and fluorescence properties including quantum yield and extinction coefficient. The spectral characteristics of Singapore Green fluorescent motifs were found to be highly favourable allowing them to provide the central core of future probes. This work has also provided the synthetic methodology required to produce 'LGX' in the quantities required for eventual utilisation in healthcare environments. Furthermore it has provided the several novel platforms for the development of future probes. This is of potentially considerable value as it may not only contribute to the reduction of the problem

Abstract

pathogen *S. aureus* as well as slow the emergence of resistance, but also facilitate generation of other important protease detection systems.

Abbreviations

ACE	angiotensin-converting enzyme
Arg	arginine
BIOPEP	bioactive peptides
Boc	tertiary butoxycarbonyl
BODIPY	borondipyrrolmethine
br	broad
CA	coupling agent
Cbz	benzyloxycarbonyl
COMU	(1-cyano-2-ethoxy-2-oxoethylideneaminoxy)dimethylamino-morpholino-carbeniumhexafluorophosphate
d	doublet
DCM	dichloromethane
δ	chemical shift in parts per million
dd	doublet of doublets
DDAO	7-hydroxy-9H-(1,3-dichloro-9,9-dimethylacridin-2-one)
DDQ	2,3-dichloro-5,6-dicyano-1,4-benzoquinone
DIEA	diisopropyl ethylamine
DMF	dimethyl formamide
DMSO	dimethyl sulfoxide
DPP-4	dipeptidyl peptidase-4
EDCI	1-(3-dimethylaminopropyl)-3-ethylcarbodiimide hydrochloride
EEDQ	N-Ethoxycarbonyl-2-ethoxy-1,2-dihydroquinoline
eq	equivalent
ESBL	extended spectrum β - lactamases
EtOAc	ethyl acetate
FP-2	Falcpain-2
HABP	hospital acquired bacterial pneumonia
HATU	(1-[Bis(dimethylamino)methylene]-1H-1,2,3-triazolo[4,5-b]pyridinium-3-oxid hexafluorophosphate
HPLC	high performance liquid chromatography
HR MS	high resolution mass spectrometry
IR	infra-red
m	multiplet

Abbreviations

MAPKK	mitogen-activated protein kinase kinase
MDAP	mass directed auto purification
Me	methyl
MeOH	methanol
MRSA	methicillin resistant <i>Staphylococcus aureus</i>
MSSA	methicillin sensitive <i>Staphylococcus aureus</i>
m/z	mass to charge ratio
NMR	nuclear magnetic resonance
PCR	polymerase chain reaction
ppm	parts per million
Pro	proline
PRSP	penicillin resistant <i>Streptococcus pneumoniae</i>
PSMA	prostate specific membrane antigen
PyBOP	(benzotriazole-1-ylxoy)tris(pyrrolidino)phosphonium hexafluorophosphate
q	quartet
R _f	retention factor
Rho	Rhodamine 110
ROI	return on investment
rt	room temperature
SNAP	soluble <i>N</i> -ethylmaleimide-sensitive factor attachment protein
SNARE	soluble <i>N</i> -ethylmaleimide-sensitive factor attachment protein receptor
TFA	trifluoroacetic acid
THF	tetrahydrofuran
TLC	thin layer chromatography
VABP	ventilator acquired bacterial pneumonia
Val	valine
VRE	vancomycin resistant <i>enterococci</i>

Table of Contents

1. Chapter 1 - Introduction	19
1.1 Introduction to Proteases	20
1.1.1 Definition and Function	20
1.1.2 Organisation	22
1.1.3 Aspartic Proteases.....	22
1.1.4 Cysteine Proteases.....	23
1.1.5 Serine Proteases	23
1.1.6 Metalloproteases.....	23
1.2 Protease Activity	24
1.2.1 Accurate Antimicrobial Targeting <i>via</i> Protease Activity.....	24
1.3 Protease Detection	28
1.3.1 Detection Methods.....	28
1.3.2 Natural Substrate Turnover.....	29
1.3.3 Substrate Based Probes	31
1.3.4 Activity Based Probes	34
1.4 Fluorescence	37
1.4.1 The Fluorescence Process	37
1.5 Key Fluorophores	40
1.5.1 Coumarins	41
1.5.2 BODIPYs	43
1.5.3 Phenoxazines	46
1.5.4 Cyanines.....	48
1.5.5 Fluoresceins	51
1.5.6 Rhodamines.....	55
1.6 Aims	61
2. Chapter 2 – Results and Discussion	62
2.1 LGX Synthesis and Scale Up	63
2.1.1 Construction of the Boc-Val-Pro-OH Section of the Biomimetic Peptide.....	63

Table of Contents

2.1.2 Attachment of BocHN-Arg(Cbz) ₂ -OH to Rhodamine 110.....	64
2.1.3 Completing Attachment of the Biomimetic Peptide.....	72
2.1.4 The Hydrogenation Problem	76
2.1.5 Overcoming the Hydrogenation Problem	78
2.2 Routes to Novel Fluorophores.....	81
2.2.1 Reconsidering the Order of Probe Construction.....	81
2.2.2 Samarium Iodide.....	83
2.2.3 Directed Metalation	91
2.2.4 The Grignard Approach	97
2.2.5 Simplified Fluorophores	100
2.3 The Singapore Green Fluorophore.....	102
2.3.1 Properties and Synthesis	102
2.3.2 Synthesis of a Novel Singapore Green Library.....	107
2.3.3 Spectral Analysis of Singapore Greens.....	110
2.3.4 Fluorescence Quenching of Singapore Greens <i>via</i> Acylation.....	114
2.3.5 Spectral Analysis of Singapore Green Acyls	118
2.4 Conclusions	119
2.5 Future Work.....	120
3. Chapter 3 – Experimental	123
3.1 General Experimental Methods.....	124
3.1.1 Physical Methods.....	124
3.1.2 Reagents, Solvents and Reaction Conditions	125
3.2 Experimental Methods.....	127
4. Chapter 4 – References	168
5. Chapter 5 – Appendix	180
5.1 Excitation vs Emission Maxima for Singapore Greens	181
5.2 Plots for Fluorescence Quantum Yield Determinations of Singapore Greens.....	187

List of Tables

Table 1. Types of protease and their year of discovery.....	22
Table 2. The key fluorophore structures, classes and spectral properties.....	40
Table 3. Coupling agents and their best isolated yields of Rho-(Arg(Cbz) ₂ -NH ₂) ₂ 69 ...	70
Table 4. Hydrogenation conditions tested for selective deprotection of LGX precursor 92	77
Table 5. Oxidising conditions tested in order to re-form crucial functionality in LGX	80
Table 6. Reductive coupling reactions performed with the stoichiometries of xanthone 90 and acrylate 91 and corresponding conditions.....	90
Table 7. Reaction timings and equivalencies of Grignard 111 exposed to xanthone 108	98
Table 8. Spectral characteristics of the Singapore Green fluorophores SG1 – 9	111
Table 9. Comparative fluorescence, extinction coefficient and brightness values of SG1 116 and SG1Ac 136	118

List of Figures

Figure 1: The action of an endo and exopeptidase on a peptide	20
Figure 2. General representation of peptide cleavage through protease activity. Protease enzyme active site is regenerated following cleavage.....	21
Figure 3. Protease detection through natural substrate turn over	30
Figure 4. AMC/ACC substrate based probes produce a large fluorescence increase upon proteolysis	32
Figure 5. Substrate based protease detection <i>via</i> FRET	33
Figure 6. Fluorescently tagged activity-based probe, using an acyloxymethylketone electrophile for <i>in vivo</i> imaging and identification of target protease.....	36
Figure 7. A simplified Jablonski diagram showing the stages of the fluorescence process.....	37
Figure 8. 7-Aminomethylcoumarin (AMC, 1) and 4-Methylumbeliferone (4-MU, 2).....	41
Figure 9. The Pechmann condensation to produce the core fluorescent coumarins.....	42
Figure 10. Conversion of a triflate protected hydroxy coumarin 11 to the corresponding amino coumarin 14	43
Figure 11. Preparation of functionalised coumarin 17 <i>via</i> a Knoevenagel condensation	43
Figure 12. The simplest BODIPY core structure 18 and its stable tetramethyl analogue 3	44
Figure 13. The traditional Vilsmeier-Haack route to produce BODIPY dyes	45
Figure 14. Preparation of an aza-BODIPY dye 37 , followed by ligand substitution of the boron center to produce 23	46
Figure 15. Acid mediated condensation route to the phenoxazines: resorufin 4 and Nile red 27	48
Figure 16. Synthesis of phenoxazine analogue DDAO 30 <i>via</i> an alternative route	48
Figure 17. CyDyes, notable for their increase in $\lambda_{ex}/\lambda_{em}$ with central chain length	49
Figure 18. Synthetic route to cyanine 5 from an alkylindolinium salt 33 combined with triethyl orthoformate 34	50
Figure 19. Fusion of cyanines with other fluorophores results in enhanced tunability of spectral characteristics	51

List of Figures

Figure 20. Fluorescein 6 exists in equilibrium between non-fluorescent (left) and several fluorescent forms (right, far right).....	52
Figure 21. Addition of substituents and extension of conjugation produces bathochromic shifts, as well as variation in fluorescence quantum yield	53
Figure 22. Traditional condensation routes to fluorescein 6 require harsh conditions.....	53
Figure 23. Substituted phthalic anhydrides produce a difficult to separate mixture of substituted fluorescein isomers.....	54
Figure 24. Carbo- 44 and silafluoresceins 47 may be produced as single isomers from addition of organometallics, as long as suitable protection of other functionality is available.....	55
Figure 25. Synthesis of sulforhodamine B 50 and tetramethylrhodamine 53	56
Figure 26. Rhodamine 110 7 exists in equilibrium between a closed, non-fluorescent lactone form (left), and fluorescent quinoid forms (center, right).....	57
Figure 27. Buckwald-Hartwig cross coupling of a triflate functionalised carboxy fluorescein 55 produces a single isomer of carboxy rhodamine 53	59
Figure 28. Production of a silarhodamine from addition of an organolithium.....	59
Figure 29. The active compound in the fluorogenic <i>S. aureus</i> probe LGX 61	63
Figure 30. Generation of the dipeptide Boc-Val-Pro-OMe 64 using COMU 67	63
Figure 31. Coupling agent EDCI 65 , additive Oxyma 66 , and coupling agent COMU 82	64
Figure 32. Coupling of protected arginine 83 with rhodamine 110 22 to form the rhodamine bis-acylate, Rho-(Arg(Cbz) ₂ -NHBoc) ₂ 69	64
Figure 33. Solution equilibrium of rhodamine 110 7 and the effect on ring bound NH ₂ groups	66
Figure 34. Possible side products through coupling agent activation of the upper carboxyl group of rhodamine, accessible from its open fluorescent forms.....	67
Figure 35. De-guanidination occurs following an N ^ω -acylation side reaction of a non-exhaustively protected guanidine group. The following deprotection step results in both de-guanidination of arginine to form ornithine and simultaneous liberation of the corresponding substituted imidazolone	68
Figure 36. δ – lactam formation from an activated arginine residue. Cyclisation forms the δ – lactam as a result of the latent nucleophilicity of the un-protected guanidyl δ – NH group	68

List of Figures

Figure 37. Coupling agents EEDQ 71 , PPh ₃ Cl ₂ 72 , PyBOP 73 and HATU 74	69
Figure 38. Peptide coupling mechanism of HATU 74 and its improved efficiency facilitated by the neighboring group effect	71
Figure 39. Coupling of Rhodamine-(Arg(Cbz) ₂ -NH ₂) ₂ 75 to Boc-Val-Pro-OH 76 mediated by HATU 74 , to produce Rhodamine-(Arg(Cbz) ₂ -Pro-Val-NH-Boc) ₂ 77	73
Figure 40. Proton NMR spectrum of the Cbz- protected LGX precursor 77 compared to the reduced LGX 78 . Note the complete disappearance of the benzyl signals (A) signifying Cbz- deprotection along with the appearance of the benzyl proton signal (B) at around 6 ppm	76
Figure 41. Catalytic hydrogenation of the analogous phthalide ring system 79 results in cleavage to 80 , similar to that observed with our rhodamine 110 7 based probe	78
Figure 42. Modified scheme adopted in order to produce LGX in its active form 61	79
Figure 43. Non-fluorescent dihydro rhodamine 110 81 converts into fluorescent rhodamine 110 7 upon exposure to reactive oxygen species to form a fluorogenic intercellular probe	79
Figure 44. Modification to synthetic strategy to produce probes, amino acids (AA) will be added to a unfinished fluorophore core, after which the fluorophore will be completed	83
Figure 45. Symmetric 61 vs non-symmetric 84 fluorogenic probes. Symmetric varieties require two proteolysis events to achieve full brightness, non-symmetric probes require only one	84
Figure 46. Traditional condensation route used for production of un-symmetric rhodamines for coupling test	85
Figure 47. Condensation mechanism between phenols 86 , 87 and phthalic anhydride 56 to produce un-symmetrical rhodamine 85	85
Figure 48. General mechanism of reductive coupling of a ketone with an acrylate to form a γ – lactone	86
Figure 49. Reductive coupling reactions of xanthone 90 with acylates 91 or 93 in order to build the upper lactone ring to produce structures 92 or 94 respectively	87
Figure 50. Samarium diiodide mediates reduction of xanthone 90 to xanthene 95 in the presence of an alcohol proton donor such as s-BuOH	89
Figure 51. Imamoto's method to prepare SmI ₂ , using samarium metal and iodine	89

List of Figures

- Figure 52.** Samarium diiodide successfully forms the target lactone structure in the test reaction producing spiro lactone **97**.....91
- Figure 53.** Metalation occurs adjacent to the Directed metalating group (DMG) due to a complex induced proximity effect. This results in coordination of the lithium species to the Lewis basic DMG producing regioselectivity in lithiation. Treatment with an electrophile E⁺ then results in substitution at the lithiated position.....91
- Figure 54.** Benzoyl chloride **98** mediated acylation of dimethylhydrazine **99** produced both the target dimethylhydrazide product **100** and by-product **101**93
- Figure 55.** Treatment of the DMG *N,N'*-dimethylbenzohydrazide **100** with *s*-BuLi yielded lithium species **102**93
- Figure 56.** The target spiro-lactone **103** formed spontaneously following exposure of **96** to lithium species **102** and workup94
- Figure 57.** Formation of target product **104** following exposure of **90** to lithium species **102** and subsequent acidification with concentrated HCl95
- Figure 58.** ¹H-NMR spectrum and proton assignments of spiro[isobenzofuran-1(3H),9'-[9H]xanthen]-3-one **104**, previously unreported.....95
- Figure 59.** Synthesis of 3-amino-6-nitro-xanthen-9-one **108** *via* modification of A. Young-Hoon *et al*'s method96
- Figure 60.** Successful production of tertiary alcohol 9-phenyl-9H-xanthen-9-ol **110** through exposure of xanthone **90** to phenylmagnesium bromide **109**97
- Figure 61.** Proposed incorporation of upper ring by Grignard addition, followed by mild oxidation98
- Figure 62.** Tautomerism of 3-amino-6-nitro-xanthen-9-one **108** between the keto (left), and the imino (right) forms99
- Figure 63.** Infra-red spectrum of 3-amino-6-nitro-xanthen-9-one, compound **108**..... 100
- Figure 64.** Fluorescein **6**, front view (left) and top down view (right). The carboxyl group acts only to provide a rotational steric barrier to the top ring system, rendering it orthogonal to the lower xanthene system, the carboxyl is not essential for strong fluorescence and may be substituted with another sufficiently bulky group 101
- Figure 65.** The Singapore Green fluorophore **116** is a structural hybrid of Tokyo Green **115** and Rhodamine 110 **7**, possessing a portion of each structure as shown 103
- Figure 66.** Condensation of a substituted phthalic anhydride to produce an upper ring substituted rhodamine analogue yields a mixture of difficult to separate isomers. A Grignard reaction installing the substituted upper ring results in only a single isomer 104

List of Figures

Figure 67. Conversion of 3-amino-6-nitro-xanthen-9-one 108 to 3-methoxy-6-nitro-xanthen-9-one 118 <i>via</i> diazotization, hydrolysis and subsequent alkylation	104
Figure 68. Conversion of 3-methoxy-6-nitro-xanthen-9-one 118 to 3-amino-6-methoxy-xanthen-9-one 119 <i>via</i> reduction and subsequent trityl protection to yield 120	105
Figure 69. Conversion of xanthone 120 to SG1 116 <i>via</i> addition of Grignard reagent 121 , followed by acidic deprotection and dehydration of intermediate 122	105
Figure 70. Dehydration of 122 with concurrent imine formation results in decreased bond length and increased steric clash between the trityl group and the xanthone rings in 123	106
Figure 71. Test reaction to validate method of Grignard reagent generation	107
Figure 72. Expansion of aromatic region of ¹ H-NMR spectrum of fluorophore SG7 132 with associated aromatic proton assignments.....	109
Figure 73. Singapore Greens 1 – 9 (SG1, 2 – 9, 116 , 127 – 134). N.B. SG1 – 8.TFA, SG9.HCl	110
Figure 74. Disposition of methyl groups on SG3 128 oppose each other's electron donating effect, in SG6 131 they work in conjunction to enhance electron density in positions indicated. The result is a disproportionate increase in rate of PeT in SG6 131 over SG3 128 with corresponding drop in quantum yield, despite having the same relative electron density in the upper ring system.....	112
Figure 75. Comparison of SG4 129 , SG5 130 and SG7 132 fluorescence quantum yields. A large drop is observed between SG4 and SG5 despite only a modest increase in upper ring electron density, this is indicative of a threshold above which PeT becomes the dominant process.....	113
Figure 76. Fluorescence quantum yield decreases as upper ring electron density increases	113
Figure 77. Acylation of SG1 116 resulted in the spirocyclic bis-acyl analogue SG1BisAc 135 which rapidly decomposed in light to furnish the target product SG1Ac 136	115
Figure 78. Changes in aromatic region of ¹ H-NMR spectrum upon decomposition of SG1BisAc 135 to SG1Ac 136 in light over a 70 hour period. Specific timings marked under each spectrum	115
Figure 79. Changes in aliphatic region of ¹ H-NMR spectrum upon decomposition of SG1BisAc 135 to SG1Ac 136 with CH ₃ groups colour coded for clarity. Timings marked under each spectrum	116

List of Figures

- Figure 80.** Both bis-acylates SG5BisAc **137** and SG8BisAc **139** are highly resistant to photolysis under normal lighting and UV irradiation of 365 or 254 nm..... 117
- Figure 81.** Extension of lower xanthene ring systems on Singapore Green precursors. $R^1 = \text{CH}_3, \text{C}_2\text{H}_5, \text{C}_3\text{H}_7$ etc 120
- Figure 82.** Synthesis of Singapore Greens with extended lower xanthene ring systems as well as variation of ring substituents R^1, R^2 and R^3 to determine their effects on spectral characteristics. $R^1 = \text{CH}_3, \text{C}_2\text{H}_5, \text{C}_3\text{H}_7$; $R^2 = \text{CH}_3, \text{OCH}_3, \text{CF}_3$; $R^3 = \text{H}, \text{CH}_3, \text{OCH}_3, \text{CF}_3$ etc 121
- Figure 83.** The most favorable Singapore Green analogue would be used as the core for a next generation *S. aureus* probe using the proven synthetic route to LGX..... 122

Chapter 1 – Introduction

1.1 Introduction to Proteases

1.1.1 Definition and Function

The term protease and proteinase are often used interchangeably in literature, by definition however, a protease refers to either an endo or exopeptidase, while proteinases refer specifically to endopeptidases.¹ They are simply enzymes that function to induce proteolysis. Proteolysis is achieved through catalysing the cleavage of an amide bond between two amino acids of the peptide chain. This can occur in either the main body of a peptide, in which case they are denoted endopeptidases, or at the final amino acid at the carboxyl (C-) or amino (N-) terminus, denoting them as exopeptidases.² The proteolysis produces two shorter peptide chains from the original larger single chain. Countless biological functions are reliant upon this process, including protein digestion, wound healing, cell division and immune system activation to name but a few.³

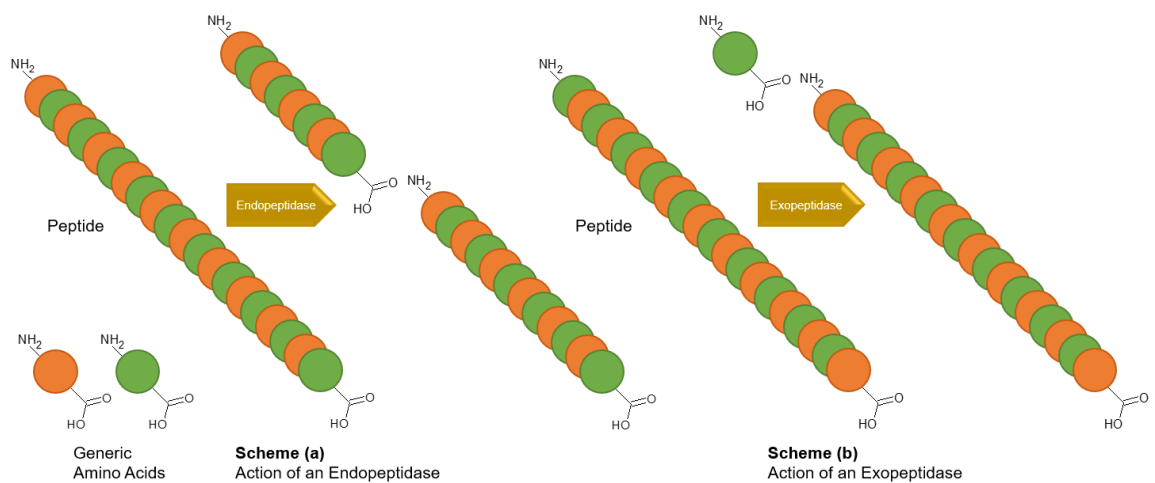


Figure 1. The action of an endo and exopeptidase on a peptide.

Substrate selectivity is extremely important to the function of a protease, as lack of discrimination between substrates may lead to unwanted cleavage and detrimental downstream effects. In light of this, many proteases exhibit high specificity and recognise only a very limited number of peptide sequences. Conversely, some exhibit a surprisingly broad selectivity, enabling them to cleave a wide variety of substrates. These variations in

Chapter 1 - Introduction

selectivity are attributed to the precise shape, size and orientation of the catalytic site in question. The catalytic properties and specificity of a protease are determined by the order of its primary amino acid sequence. The variable mechanisms associated with these, as well as regulation of substrate and proteolytic access have been, and continue to be, the subject of much research.^{4,5,6,7}

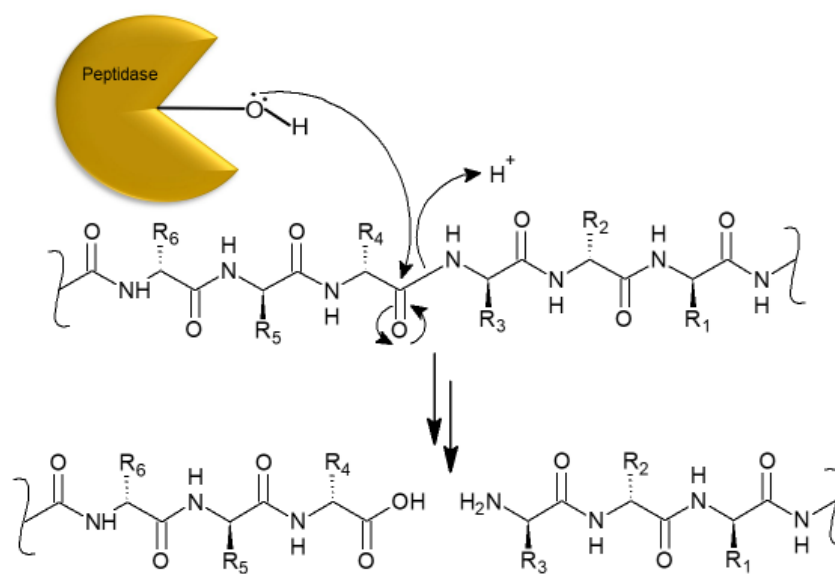


Figure 2. General representation of peptide cleavage through protease activity. Protease enzyme active site is regenerated following cleavage.

Interest in proteases arises from but is not limited to the fact that abnormal protease activities are linked to an array of diseases. In humans, around 1.7 % of genes code for proteases, which corresponds to approximately 400 individuals, of which at least 14 % are under investigation as therapeutic targets for diseases, including cancers, Alzheimer's disease, thrombosis, diabetes, and HIV.^{8,9,10,11,12} In view of the compelling reasons for the study of proteases their mechanisms and inhibitors, it is clear why this field of research is important and justifies the extensive investigation which continues to be devoted to the development of sensitive, selective and robust assays for their detection and quantification.

1.1.2 Organisation

There are seven well defined families of proteases, named after residues important to their catalysis, these are: Aspartic, Cysteine, Glutamic, Metallo, Asparagine, Serine and Threonine. In addition to this, there are two further members consisting of mixed catalytic family or unknown catalytic mechanism. Of the seven main families, four are large and of major therapeutic interest (Aspartic, Cysteine, Serine and Metallo), with the remaining three which are either less-well understood, have few members, or possess little apparent therapeutic application. The well-defined families and the year they were first characterised are as follows in Table 1.¹³

Protease	Year of discovery	Catalytic residue nature
Aspartic-	1993	Aspartamate carboxylic acid
Cysteine-	1993	Cysteine thiol
Serine-	1993	Serine alcohol
Metallo-	1993	Metal based, often Zinc
Threonine-	1997	Threonine alcohol
Glutamic-	2004	Glutamate Carboxylic acid
Asparagine-	2010	Asparagine

Table 1. Types of protease and their year of discovery.

1.1.3 Aspartic proteases

Aspartic Proteases are classed as such due to the two aspartic acid residues housed within their active site which are largely responsible for their activity. It has been deduced and generally accepted that an acid-base mechanism is responsible for their catalytic activity. This arises through the two active site aspartate residues playing the part of acid-base proton shuttles. They work together to activate a water molecule which is in turn responsible for the proteolysis, this is believed to be initially localised between the two aforementioned aspartates and commences the proteolytic activity.¹⁴

1.1.4 Cysteine proteases

Like the others, the cysteine family of proteases are named after the important residue in their active site. Their catalytic activity is made possible by the presence of this nucleophilic residue, along with a basic histidine in close proximity. In addition, an aspartate residue usually accompanies the two others in order to form a catalytic triad. The aspartate residue is important for orientation and polarisation of the histidine residue in order to facilitate proteolysis *via* enabling efficient proton transfer between them, forming the initial Cys-S⁻/His-NH⁺ ion pair which commences the proteolysis leading to an oxyanionic transition state. Collapse of the transition state results in elimination of the carboxyl end of the substrate. Repetition of the catalytic steps then lead to elimination of the NH₂ side of the substrate along with regeneration of the catalytic site.^{15,16,17,18}

1.1.5 Serine proteases

The active site of the serine protease again contains the catalytic triad charge relay system, consisting of the nucleophilic serine (after which these proteases are named), a basic histidine, and aspartate residues which in combination are responsible for their activity.¹⁹ The generally accepted catalytic mechanism for serine proteases is similar to cysteine proteases and proceeds *via* two steps. The initial step involves acylation of the serine residue. This leads to a tetrahedral oxyanion intermediate following deprotonation of serine by histidine. The intermediate then collapses expelling the NH₂ side of the substrate, assisted by proton transfer. The second catalytic step involves elimination of the carboxyl side of the substrate *via* de-acylation to regenerate the catalytic site for further catalysis.¹⁹

1.1.6 Metalloproteases

Metalloproteases are a wide-ranging family of protease enzymes in which a metal ion is central to their catalytic activity. Within the active site, the metal ion is coordinated to the surrounding protein *via* three amino acid residues which consist of aspartate, glutamate, and either histidine or lysine. A vast majority of the metalloproteases contain zinc as the

active metal. However, others containing cobalt or calcium are known but the metal ion always appears as a divalent cation.^{20,21}

Their catalysis in general relies on the coordination of a water molecule to the cationic metal centre (in this case zinc) imparting polarisational activation. A tetrahedral oxyanionic transition state is formed, stabilised by the Lewis acidity of the zinc centre. Other steps precede proton transfer between the enzyme's active carboxylic acid group and the terminal carboxylate group of the substrate which completes proteolysis regenerating the enzymes active site.^{20,21,22}

1.2 Protease Activity

1.2.1 Accurate Antimicrobial Targeting via Protease Activity

There is an ongoing problem of antimicrobial resistance emerging for previously treatable illnesses. This is a result of the lack of new antibiotics coming to market as well as poor management and use of those currently available. This is a well-established problem that has appeared at a time when both antibacterial research and productivity has dropped to an all-time low, with few new agents on the horizon.²³

Balancing the system to facilitate the supply of new antibiotics while improving the effectiveness of those currently available in order to suppress the rise of resistance has become difficult. The lack of new antibiotics being released leads to a steady increase in resistance to those currently available, at great cost.²⁴

Two main factors have contributed to the crisis of emerging antibiotic resistance. Firstly, the reduction in the number of pharmaceutical companies over the years since modern antibiotics were initially developed. Where there once were many individual competing companies, mergers and acquisitions have reduced the number of companies with the capacity to develop such agents. This has led not only to a decrease in competition

(contentious in itself), but also to a decrease in the number of individual antibiotic compounds in development.²⁵ This, coupled with those same companies developing other pharmaceutical agents with higher chances of success and return on investment (ROI), gives an indication as to why so many have abandoned antibiotic research altogether.²⁶

Secondly, but equally important, is the long term misuse of the currently available antibiotics. This facet of the developing antibiotic resistance problem could be attributed to both convenience and ignorance in relation to antibiotic use. Currently, antibiotic therapy is based upon the empiric model. This could be likened to an “educated guess”, whereby a healthcare professional will prescribe a particular course of antibiotics based upon various signs and symptoms. The caveat is that there is rarely a definitive diagnosis as to the identity of the problem pathogen (if one is even present), and this often leads to less than ideal antibiotic use.²⁷ That is not to say that this model of antibiotic therapy has not been effective in the past, with many lives saved and significant societal advances as a consequence. However, the downside of antibiotic use directed by the empiric model is the high costs paid by the misprescribed patients, whether they be human or otherwise. Unnecessary courses of antibiotics prescribed for uninfected patients leads to needless side effects, damage to the human microbiome, and most importantly, antibiotic resistance.²⁷ This erroneous use could be reduced, or even eradicated if testing for pathogen identity were undertaken before antibiotic therapy commenced. Unfortunately this is often unfeasible, as testing is generally slow, too expensive, or impractical in many cases.²⁷

There are a number of particular bacterial strains which have been shown to pose the greatest threat in terms of antibiotic resistance. Studies on the impact of said resistance in terms of mortality and length of hospitalisation have highlighted these bacteria as: methicillin-resistant *Staphylococcus aureus* (MRSA), penicillin-resistant *Streptococcus pneumoniae* (PRSP), extended spectrum β – lactamases (ESBLs) in *Escherichia coli* and *Klebsiella pneumoniae*, vancomycin-resistant *Enterococci* (VRE) and carbapenem-

resistant *Pseudomonas aeruginosa*.²⁸ These studies concentrated on a range of common problem infection sites including urinary tract, soft tissue, blood, respiratory and skin. The results quantified the additional burden caused by these to be approximately 25,000 deaths, 400,000 infections and 2 - 5 million extra hospital days per year in the EU alone. The monetary cost was estimated to total approximately € 900 million per year, with a concurrent loss of 600 million days of productivity.²⁹ The WHO has placed infections resulting from antibiotic resistant bacteria at the top of their preliminary ranking of pharmaceutical gaps, above cardiovascular disease, diabetes types I and II, and even cancer.³⁰ Furthermore, lower respiratory infections caused by bacterial pathogenesis are ranked first on the list of global burden of disease.³¹ The two most common healthcare associated infections in the United States are hospital acquired bacterial pneumonia (HABP) and ventilator acquired bacterial pneumonia (VABP), with the leading cause of these complications being *Staphylococcus aureus*.^{32,33} Adverse outcomes related to these infections can be lessened or avoided altogether *via* the swift administration of correctly targeted and dosed antibiotic therapy.^{34,35,36}

With this in mind it is not surprising that a general agreement has arisen that a transformational effect in the use and effectiveness of antibiotics would be seen if superior methods of detection of problem pathogens were employed. These would have to be equally accurate, but much faster and cost effective than those currently utilised. Therefore, the answer is adoption of rapid point of care tests to improve decision making in the treatment of bacterial infections. This is particularly important in the early stages of treatment where conclusive identification of the pathogen is crucial to avoid the use of the empiric method of antibiotic prescription. Therefore, the change in practice from empiric to accurate and appropriately targeted antibiotic use following a conclusive identification could achieve the aforementioned transformational effect, suppressing the rise of resistance.³⁷ This point is reflected in the WHO's report stating that "Governments and partners need to work closely with industry to encourage greater investment in research and development of new diagnostics that can improve decision making".³⁸

Chapter 1 - Introduction

The message is therefore clear, the continued development of simple, cheap, efficient and accurate point of care tests is the key solution for addressing the emergence of antibiotic resistance. These tests provide the opportunity to break the current cycle of inaccurate antibiotic therapy by allowing rapid and accurate identification of problem pathogens. This would then allow antibiotic therapy to commence only after positive identification and determination of antibiotic susceptibility. These tests can operate *via* targeting a specific protease enzyme expressed by the problem pathogen, providing conclusive results many times faster than traditional culture or polymerase chain reaction (PCR) methods. Furthermore, these rapid diagnostics could also expedite the development of new antibiotic classes, addressing the other major problem faced by the healthcare industry. This could be achieved by improving the cost effectiveness of clinical trials by identifying only the correct patient populations to be tested, ruling out those carrying several bacterial infections treatable by currently available antibiotics.^{39,27}

It is therefore clear that development of rapid diagnostics for identification of common healthcare infections for which resistance is emerging is of paramount importance. These bacterial protease targeting probes could form the basis of a modern antibiotic stewardship strategy, optimising clinical outcomes while minimising harmful consequences of antibiotic use. If this strategy is not implemented, along with the lack of new antibiotics in development, multidrug resistant bacterial infections will become more and more commonplace. The final result of this being, in the not too distant future, traditional antibiotic therapy will have been confined to the pages of history, and the 'post antibiotic era' will have begun. If the human race is to remain resident on planet earth for generations to come, this must be avoided at any cost.

1.3 Protease Detection

1.3.1 *Detection Methods*

The detection of protease activity has been crucial to the understanding of their function and importance in physiology. Quantification of their activity has profoundly deepened the understanding of these proteins as the driving force behind not only important biological functions, but also numerous diseases. Therefore, protease detection methods must be constantly developed and improved so as to be able to fully understand them in a clinical and biological context; more specifically, to allow their exploitation as therapeutic targets for the treatment of diseases. To address this, significant research is ongoing in this area.

The ability of a protease to distinguish its proper substrate from among many candidates is very important in maintaining the biological function for which it is designed. The selection of the enzyme's substrate is regulated by various factors, including the location and timing of expression, enzyme and substrate concentrations, and the requirement of cofactors. However, the dominant principle in determining protease specificity is the structure of its active site which is dictated by its specific amino acid sequence. This in turn determines its shape, size, polarity and consequently which substrates it has affinity for, as a result of their complimentary properties. The area of the active site which dictates the affinity may be referred to as the specificity pocket. The properties of which are heavily based upon the side chains of the substrate and enzyme residues, as well as the steric and electronic interactions between them.

Determination of the substrate specificity of a protease and characterisation of its active site is of paramount importance in understanding the role that protease plays in a complex biological pathway. In defining the specificity of a protease for a particular substrate, the initial basis for design of selective inhibitors for that enzyme is provided. This enables study of the action of the protease in its biological context, which may then allow its manipulation for medicinal or other purposes through activity modulation.⁴⁰

Protease activity may be detected through a myriad of different techniques; though they may be broadly grouped into one of three categories based upon the method of monitoring said activity. The three categories consist of: Natural substrate turnover, Substrate based probes and Activity based probes, each of which has its own advantages and disadvantages.⁴⁰

The most direct method of detection is *via* natural substrate turnover, in which an active protease may be detected *via* cleavage of its natural substrate. It is then possible to directly measure protease cleavage events *via* quantification of the peptide fragments produced by proteolysis of the substrate. However, in this case the substrate fragments must be isolated, purified and quantified from the complex mixture of products produced.⁴¹ On the other hand, substrate based probes are able to generate a signal directly following a proteolytic event, simplifying the detection of activity.⁴² Activity based probes, the third category, are able to monitor protease activity indirectly by using a substrate like region which binds covalently instead of being cleaved by the protease. Therefore, quantification of binding reveals protease activity.^{43,44}

1.3.2 Natural Substrate Turnover

Protein substrates are cleaved by active protease enzymes, a simple example of this would be autoprolysis, in which a protease cleaves an inactive form of itself to produce its active form.^{45,46} A common way of measuring the proteolysis of individual substrates is *via* resolution of the substrate fragments through electrophoresis, using sodium dodecylsulphate polyacrylamide gel (SDS-PAGE). This is then followed by immunoblotting or Coomassie staining to visualise the individual substrate fragments. A prominent limitation of this procedure is that substantial prior knowledge of the substrates to be measured is required. Changes in migration of the substrate fragments through the gel indicate proteolysis of the substrate. As an alternative to visualisation techniques, mass spectrometry may be used in tandem with SDS-PAGE, to simultaneously measure substrate turnover of all fragments; monitoring of several proteases at the same time is

therefore made possible.⁴⁷ Furthermore, gel-free techniques have been developed in order to separate proteolysis fragments from several different proteases at the same time. This then facilitates identification and quantification of most fragments from the sample through exploitation of the unique α -amino group liberated from the substrate.⁴⁸ Commonly cleaved substrate sequences suggest catalytic recognition motifs, while the pathways into which the substrates fall may indicate the function of the protease in question. A schematic of the steps involved in these techniques is shown in Figure 3.⁴⁹ Both gel-based and gel-free methods have proved effective in separating closely related physiological functions of proteases, assisting in the design of selective activity and substrate based probes.

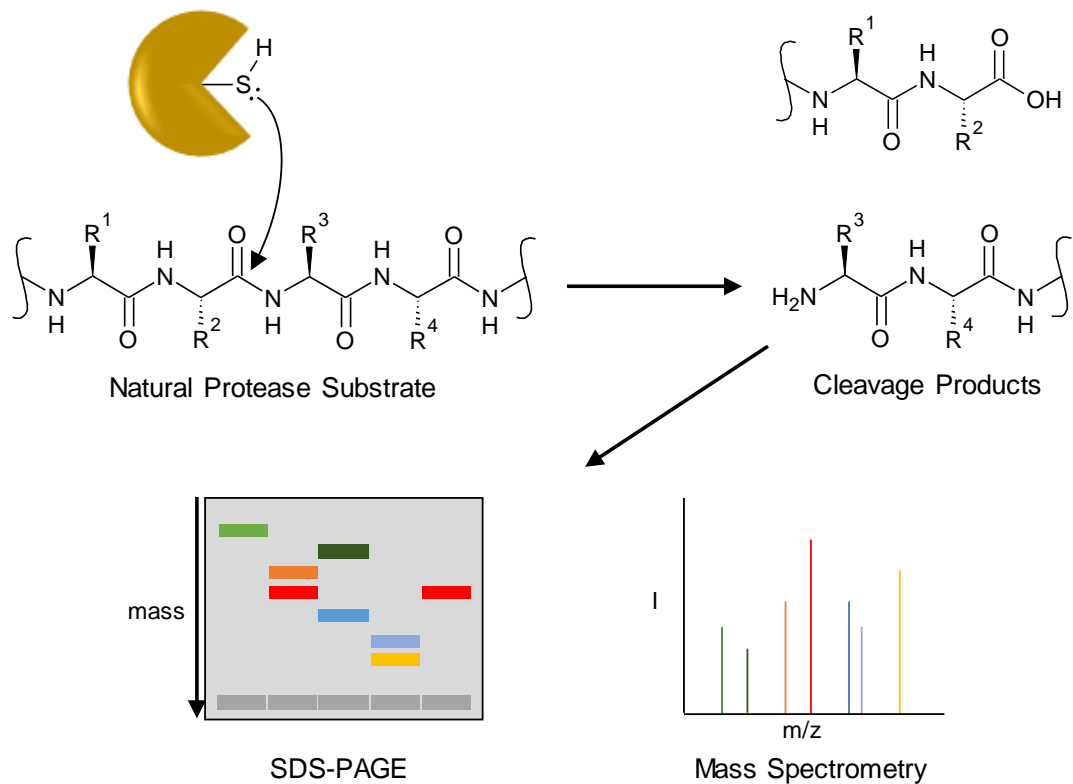


Figure 3. Protease detection through natural substrate turn over.

1.3.3 Substrate Based Probes

As mentioned before, quantification of proteolytic cleavage of natural substrates requires isolation and identification of the resulting peptide fragments. This is a significant limitation if the function of the protease is thus far unknown. However, substrate-based probes are able to measure protease hydrolysis activity without the need for complex isolation and characterisation procedures. These probes generally consist of two parts, the recognition sequence which binds to the active site of the protease in question, and a reporter which provides a detectable signal upon cleavage of the probe. The selectivity and sensitivity of the probe is critically dependent upon the design and identity of the recognition sequence, as this is the part of the probe which confers specificity and is cleaved by the target protease.⁵⁰ The recognition sequence is usually identified and synthesised based on one of two ways. Either through prior knowledge of the natural protease substrate and its reproduction, or identification of a specific sequence through cleavage patterns obtained from synthetic peptide libraries screened against the protease in question.⁴² Following identification of the correct recognition sequence, it is coupled to the reporter to form the active protease probe. Countless examples of substrate-based probes exist, particularly the fluorogenic variety which are simple, robust and used frequently to reflect this. An example of which combines a fluorophore such as 7-hydroxy-4-methylcoumarin (AMC, **1**) or 7-amino-4-carbamoylmethylcoumarin/4-methylumbiliferone (ACC/4-MU, **2**), with an amino acid recognition sequence targeted by the protease of interest. The fluorescence of the probe is minimal when the recognition sequence is attached, and upon cleavage a large increase in fluorescence is observed as the free fluorophore is released, Figure 4.⁴⁰

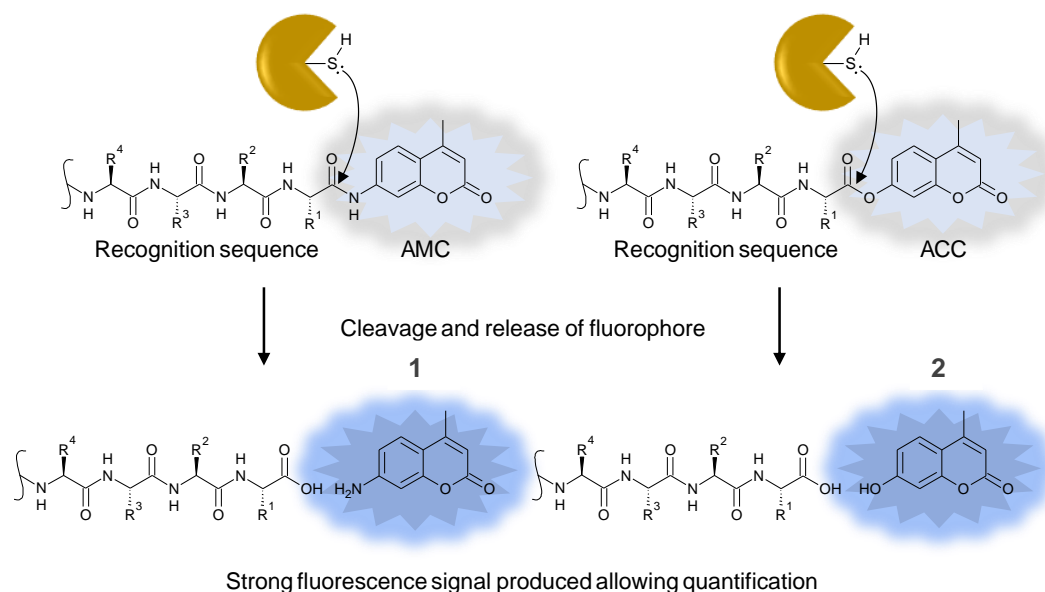


Figure 4. AMC/ACC substrate based probes produce a large fluorescence increase upon proteolysis.

The design of fluorogenic probes is relatively simple in principle but their selectivity can be limited as the recognition sequence binds to the active site at the non-prime side. However, this limitation is not common to all fluorogenic substrate based probes as some have recognition sequences which bind across both prime and non-prime sides of the active site. Fluorescence resonance energy transfer (FRET) probes are an example of this, these contain a fluorophore and quencher attached to either end of a recognition sequence.⁴² Cleavage of the recognition sequence releases the quencher, which diffuses away from the fluorophore leading to a measurable change in fluorescence. Changes in fluorescence observed when using these probes are detected and quantified by plate reader, fluorescence microscopy or *in vivo* imaging, (Figure 5).⁴⁰

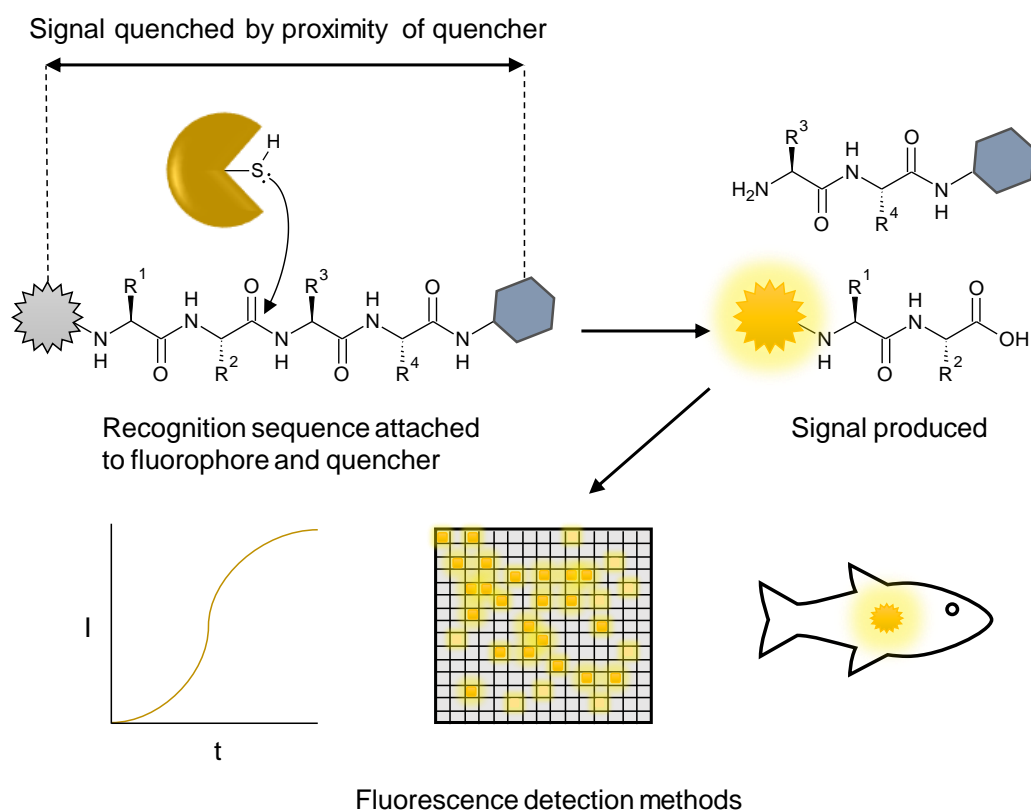


Figure 5. Substrate based protease detection *via* FRET.

Examples of Bioluminescence resonance energy transfer (BRET) probes using similar recognition sequence arrangements have also been demonstrated, as well as colour changing gold nanoparticle-based probes.^{51,52} Substrate based probes are not only limited to detection by fluorescence, other detection methods have also been demonstrated. For example, clinical varieties have been developed, an example of which is a probe containing a ^{19}F trifluoromethoxybenzylamide with an accompanying Gd^{3+} chelator has been used for magnetic resonance imaging (MRI). The probe acts as an MRI contrast agent, in which the signal is minimal when intact due to quenching by the paramagnetic Gd^{3+} cation, but when cleaved this effect is lost and a strong MRI signal is observed.⁵³ Many other types of substrate-based probes also exist, but their general design characteristics are analogous to that of the discussed examples.

The study of proteases using substrate-based probes benefits from several advantages over the use of other probe types. Their properties allow a diverse library of designs to be

created with few limitations. Any chemical group that can be bonded to an amide or carboxylic acid can be included in the structure allowing a near limitless range of possibilities. There have even been examples of genetically engineered substrate-based probes in which a FRET donor-acceptor fluorescent protein pair are attached to each end of the recognition sequence.⁵⁴ Further advantages include the high signal to noise ratio achieved by substrate-based probes, in part due to the rapid signal increase produced as each enzyme is able to rapidly cleave multiple probes. This is in addition to their applicability to high throughput screening. With these advantages in mind, it is not surprising that fluorogenic probes of this type are frequently used for substrate specificity and inhibitor screening. This enables the design of selective inhibitors, activity-based probes, and the discovery of novel recognition sequences.⁵⁵ Of course substrate-based probes are not without their limitations, the most prominent of which is the difficulty in distinguishing which specific protease is responsible for substrate cleavage. This information can only be deduced using some prior knowledge of substrate specificity of the protease in question. Another minor disadvantage is that after cleavage, diffusion of the reporter leads to a blurred signal, which complicates location or isolation of the protease of interest, if indeed this is required.⁴⁹ The simplicity and flexibility of substrate-based probes lends itself to ever more ingenious designs limited only by the ever-expanding synthetic toolkit available, and the imagination of the designer.

1.3.4 Activity Based Probes

The third form of protease detectors are the so-called activity-based probes. These differ from the other two in that when activated, they bond covalently and irreversibly to the target protease. This covalent bond is the result of either electrophilic attack from a nucleophilic residue housed within the enzyme's active site, or in some cases the action of a photoactivatable crosslinker which can bond to a non-catalytic residue in the active site. Activity based probes are composed of three parts, the reactive functional group from which the covalent bond to the enzyme is formed, the recognition sequence, and a

reporter which produces a signal to indicate activity. As with the other probe types, a recognition sequence is used to confer protease specificity so only catalytically active proteases are detected. Like substrate based probes, commonly a fluorophore is attached to the recognition sequence as the reporter, so as to produce a signal from which to gather activity information.^{43,44} Various detection methods have been utilised for activity-based probes. These include the time consuming SDS-PAGE methodology, which may or may not be complimented with mass spectrometry, fluorescence microscopy and *in vivo* imaging techniques, as detailed in Figure 6. The covalent linkage between the probe and the target protease is considered an advantage of activity-based probes as it indicates the protease location and can aid isolation if this is required. Additionally, it may be able to indicate potential incorrect drug targeting as well as highlighting ancillary proteases in physiological processes.^{40,49}

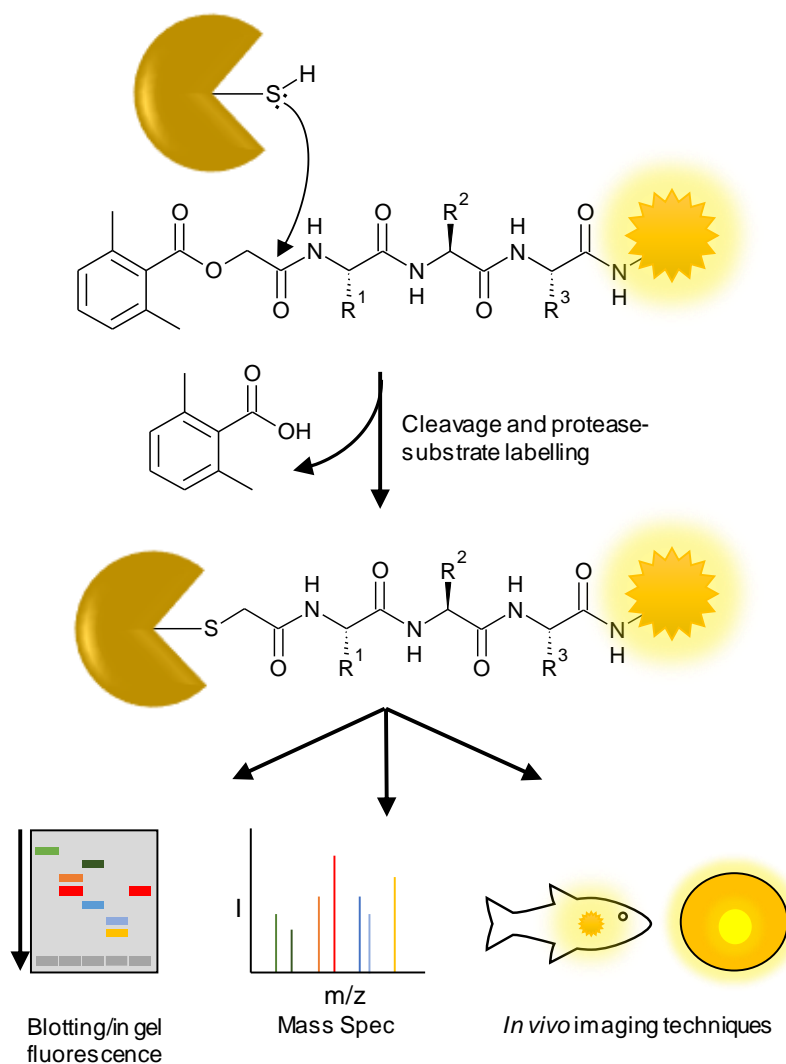


Figure 6. Fluorescently tagged activity-based probe, using an acyloxymethyl ketone electrophile for *in vivo* imaging and identification of target protease.

It should be well noted that the design of such probes would be near impossible without the prior knowledge gained through the use substrate-based probes (initial identification of individual proteases themselves, identification of their catalytic recognition sequences etc). Another disadvantage of activity-based probes is their requirement for the incorporation of a reactive electrophile or photo-crosslinker which, even with careful design produces significant/notable cross reactivity.^{56,57} This along with the total inactivation of the target protease upon binding could affect the physiological process in question and lead to non-representative results. In order to minimise the alteration of the studied biological process and their downstream compensatory mechanisms, only a small

percentage of the active enzyme is usually modified, which of course leads to weak signal.^{49,58}

1.4 Fluorescence

1.4.1 The Fluorescence Process

The process of fluorescence results from three stages which can occur in certain types of molecules that possess certain characteristics. These include but are not limited to poly-aromatic hydrocarbons, heterocycles and mixed molecules which show extended conjugation. Some form of extended conjugation is generally a requirement for a molecule to exhibit fluorescence. This is due to the electrons occupying the extended molecular orbitals being of similar energy to the photon energy associated with that particular fluorescence process. Molecules which exhibit fluorescence are known as fluorophores, and often share similar characteristics to coloured molecules known as chromophores. Fluorescent probes often consist of a fluorophore linked to another moiety, designed to show varying fluorescence characteristics which respond to specific stimulus, or localise to a particular area of interest in an analytical sample.⁵⁹

The three key stages of fluorescence and the associated electronic transitions of the fluorophore may be explained with the aid of a Jablonski diagram, Figure 7.⁵⁹

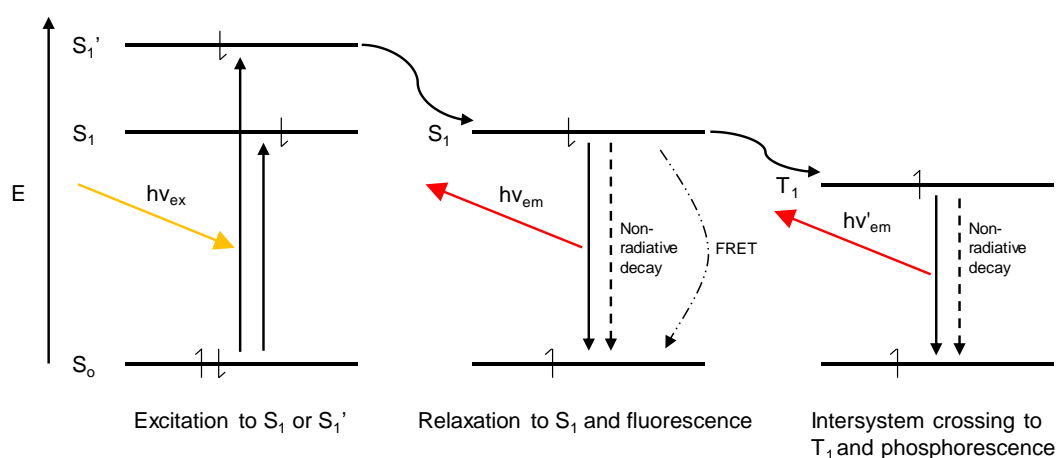


Figure 7. A simplified Jablonski diagram showing the stages of the fluorescence process.

Chapter 1 - Introduction

A fluorophore absorbs a photon of energy $h\nu_{\text{ex}}$, the energy of this incident photon matches the gap between the ground singlet electronic state (S_0) and the excited singlet electronic state (S_1') to which the electron is promoted. This photon is usually provided by either an incandescent lamp or laser of the correct wavelength. Following excitation, the electron remains in the (S_1') state for a finite period or lifetime (τ), usually in the region of 1-10 ns. In this time energy is lost through conformational changes taking in place in the fluorophore as well as rapid reorganisation of solvent molecules and other interactions around the modified dipole of the conformationally changed fluorophore. This result of this energy loss is the reversion of the fluorophore to a relaxed singlet excited state (S_1), it is this state from which emission of a photon of $h\nu_{\text{em}}$ and fluorescence occurs. An important point to note is that not all the excited molecules relax back to their ground state by emission of a photon, several other competing processes also act to depopulate the S_1 state. These other processes allow the fluorophore to return to its ground state through non-radiative means such as collisional quenching, bond rotation, photoinduced electron transfer (PeT) or Fluorescence resonance energy transfer (FRET) to an acceptor molecule. An additional possibility is intersystem crossing achieved *via* a spin inversion of the excited electron to yield an excited triplet state (T_1). Photon emission is also possible from the T_1 state, however the lifetime of this excited state tends to be significantly longer and the emission wavelength also longer, as a result of this emission from T_1 is termed phosphorescence.

Upon emission of a photon $h\nu_{\text{em}}$ through fluorescence or phosphorescence, the fluorophore returns to its ground electronic state (S_0) and the sequence may begin again. As a result of the energy dissipated during the lifetime of the excited state, the energy of the photon $h\nu_{\text{em}}$ is lower than that of the incident photon $h\nu_{\text{ex}}$ and consequently of longer wavelength. The difference between the energy of the incident and emitted photon ($h\nu_{\text{ex}} - h\nu_{\text{em}}$) is known as the Stokes shift. This shift is significant for the sensitivity and subsequent usefulness of the fluorophore as it defines the gap between excitation and

emission photons. This is important for the ease of detection of the emitted photon against a low background and in isolation from the excitation photon.

A number of key properties of a fluorophore arise from the aforementioned sequence. The Stokes shift mentioned previously denotes the difference between energy of excitation ($h\nu_{\text{ex}}$) and emission ($h\nu_{\text{em}}$), a general rule states $h\nu_{\text{ex}} > h\nu_{\text{em}}$ under normal circumstances. Multiphoton absorption is however possible, whereby two or more photons are absorbed simultaneously leading to $h\nu_{\text{ex}} < h\nu_{\text{em}}$. The fluorescence quantum yield (Φ), is a measure of the quotient of photons absorbed to those re-emitted as fluorescence and is a direct indication of the efficiency of the fluorescence process. In addition to these the extinction coefficient (ϵ) is a measure of how strongly the molecule absorbs light of a particular wavelength, per unit concentration. Excited state lifetime (τ), is the average time between absorption and emission and is an important property, it is dependent on the relative rates of fluorescence and other competing non-radiative processes. Finally, a useful measure of fluorophore brightness is derived from the product of ϵ and Φ , this provides a relative comparison of photon yield between differing fluorophores under the same incident light intensity.^{59,60}

1.5 Key Fluorophores

The study of fluorescence has been ongoing for more than 100 years, and to date a huge number of fluorophores have been classified. However, a large proportion of these are derivatives of but a few main classes which have enjoyed the most widespread use. These broadly fall into six important classes, which are most commonly used as probes for chemical or biological detection. The six main classes, along with their prototypical structures and corresponding optical properties are shown in Table 2, and will be discussed briefly below.

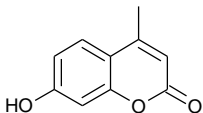
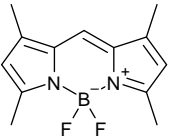
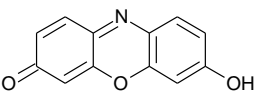
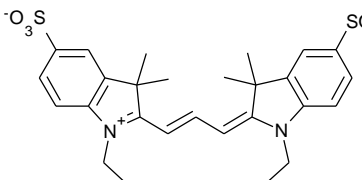
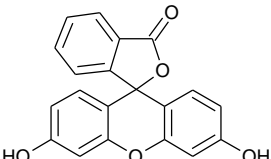
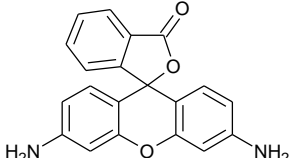
Structure	Name	λ_{abs} (nm)	λ_{em} (nm)	ϵ ($\text{M}^{-1}/\text{cm}^{-1}$)	Φ
 2	Coumarins	360	450	1.7×10^4	0.63
 3	BODIPYs	505	516	9.1×10^4	0.80
 4	Phenoxazines	572	585	5.6×10^4	0.74
 5	Cyanines	554	568	1.3×10^5	0.14
 6	Fluoresceins	491	510	9.0×10^4	0.86
 7	Rhodamines	498	521	6.8×10^4	0.98

Table 2. The key fluorophore structures, classes and spectral properties.^{60,61,62,63,64,65,66,67,68,69,70}

1.5.1 Coumarins

Coumarin is one of the most common and widely used fluorescent molecules seen in organic chemistry. The unsubstituted parent coumarin structure is traditionally modified at the 7-position (Figure 8 arrowed) with electron donating heteroatoms in order to produce molecules showing strong fluorescence. The most common modifications include addition of a hydroxyl or amine group to yield 7-hydroxy-4-methyl-coumarin (4-methylumbelliferone, 4-MU, **2**) or 7-amino-4-methyl-coumarin (7-aminomethylcoumarin, AMC, **1**), as per Figure 8.

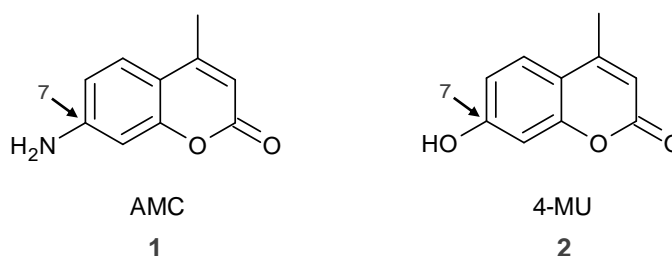


Figure 8. 7-Aminomethylcoumarin (AMC, **1**) and 4-Methylumbelliferone (4-MU, **2**).

Due to the ease with which coumarins may be chemically bonded to other molecules *via* either their hydroxyl or amine groups, many fluorogenic probes, labels and enzyme substrates exist, some dating back many decades.⁷¹ The fluorescence properties of hydroxy coumarins are moderately sensitive to pH due to the relatively low pKa of 7.8 of their hydroxyl group. This property may be modified *via* attachment of electron withdrawing groups such as halogens, these act to decrease delocalised electron density and lower the pKa of the hydroxyl group, thus reducing pH sensitivity.⁷² Amino coumarin conjugates see frequent use as enzyme substrates, especially proteases enzymes as a result of their ability to form amide bonds to peptides. They do not suffer from the same pH sensitivity as their hydroxy analogues which broadens their usability. Amino coumarin derivatives such as compound **14** (Figure 10) ($\lambda_{\text{ex}}/\lambda_{\text{em}} = 380/444 \text{ nm}$, $\epsilon = 1.8 \times 10^4 \text{ M}^{-1}\text{cm}^{-1}$) which contains a carboxyl linker, grants it the ability to act as a substrate for lipoic acid ligase. This then further enables the molecule to fluorescently label specific proteins which contain the corresponding short peptide recognition sequence.⁷³

Acylation of the amino group of the amino coumarins results in a hypsochromic shift and drop in quantum yield. This comes about due to lowering of conjugated electron density and the increased possibility of shedding excess energy through non-radiative means. This property grants the fluorophore the useful ability to act as a fluorogenic enzyme substrate.⁷⁴ Conversely, alkylation of the amine group results in a bathochromic shift due to the increase in electron density from the positive inductive effect of the alkyl group. Molecule **17** (Figure 11) shows comparatively long absorption and emission maxima for a probe of this type ($\lambda_{\text{ex}}/\lambda_{\text{em}} = 444/514 \text{ nm}$).⁷⁵

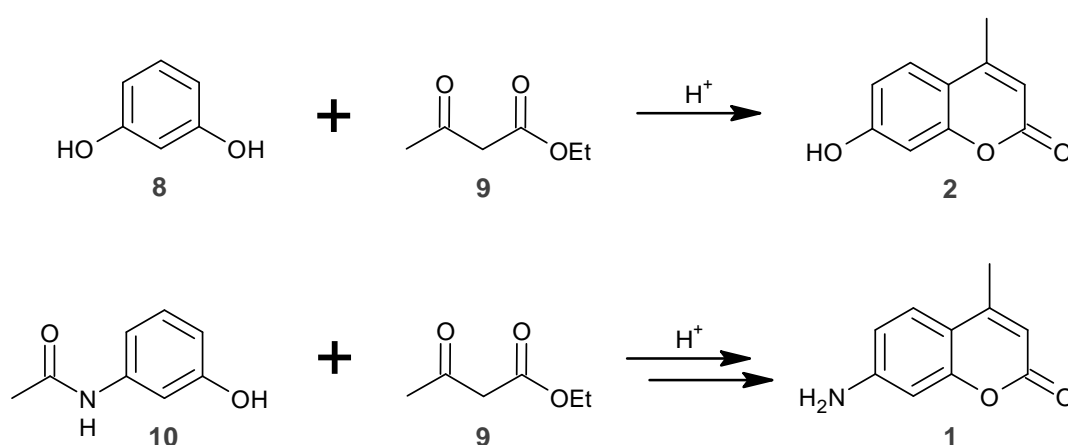


Figure 9. The Pechmann condensation to produce the core fluorescent coumarins.

The synthesis of coumarins commonly proceeds *via* a Pechmann condensation of a phenol with a β -carbonyl ester under acid catalysis.⁷⁶ Synthesis of the typical coumarin, 4-MU **2**, involves the addition of resorcinol **8** to ethyl acetoacetate **9**, (Figure 9). The reaction gives high yields when producing 7-hydroxy coumarins or N-acylated 7-amino coumarins. However, synthesis of unprotected amino coumarins is difficult and usually requires protection of the aniline group for good yields, acylation is often used for this purpose.⁷⁷ A more up to date route to 7-aminocoumarins utilises palladium catalysed Buchwald-Hartwig cross coupling to convert 7-hydroxy coumarins into the analogous amino coumarin. In this reaction the coumarin is converted into the triflate, coupled with an imine, and then subjected to acid catalysed hydrolysis to yield the required 7-aminocoumarin in reputedly good yield.⁷⁸

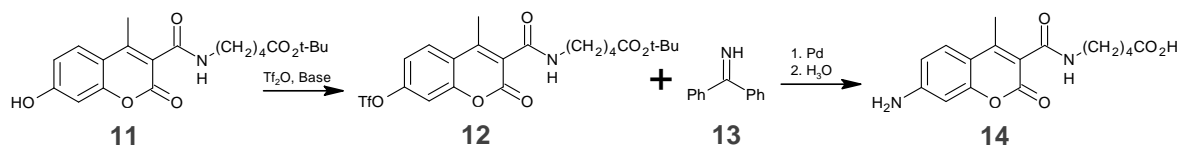


Figure 10. Conversion of a triflate functionalised hydroxy coumarin **12** to the corresponding amino coumarin **14**.

In addition to this, the coumarin core may be produced through a Knoevenagel condensation of a 2-formylphenol and a β -substituted carboxylic acid or ester of choice. This route has the advantage that it may be used on multi functionalised molecules without experiencing significant side reactivity.⁷⁹

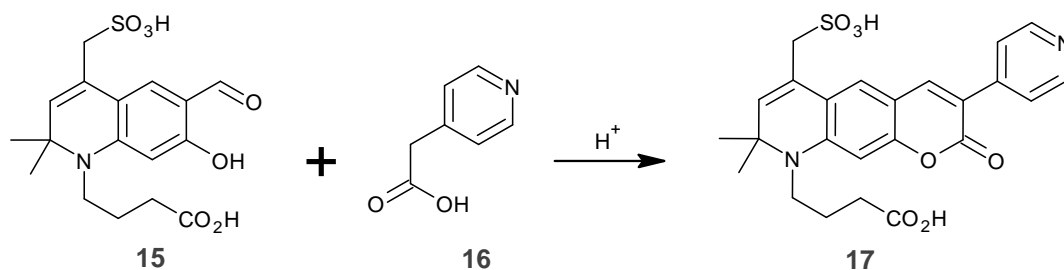


Figure 11. Preparation of functionalised coumarin **17** via a Knoevenagel condensation.

It is clear that the utility of coumarins as fluorescent labels, probes and fluorogenic substrates cannot be overstated. In light of the ability to modify their spectral properties *via* structural changes they have enjoyed wide use in synthetic chemistry and chemical biology; they are not however, without their drawbacks. The relatively low quantum yields, and predominantly short wavelengths of excitation and emission reduce their usefulness in live imaging and when probing deeper into samples. This is, in part, due to the damaging effects of shorter wavelength irradiation as well as autofluorescence, coupled with the relatively high intensity of light required to produce good signal to background ratios.

1.5.2 BODIPYs

This fluorophore class consists of a **boron dipyrromethene** core skeleton from which the abbreviated name is derived, although the full IUPAC name of the core is 4,4-difluoro-4-

bora-3a,4a-diaza-s-indacene **18**. Again, these enjoy widespread use in synthetic chemistry and are noted for their versatility, as a result of their favourable spectral properties: They have an exceptionally short Stokes shift, a net neutral charge, very high quantum yield in a wide range of solvents including water, sharp excitation and emission maxima and show little sensitivity to environmental changes. The insensitivity of their spectral characteristics to polarity changes is mainly attributed to their mutually orthogonal dipole moment and transition dipole.^{80,81} The simplest unfunctionalized BODIPY **18** decomposes above -30 to -40 °C and consequently wasn't synthesised until 2009. On the other hand, the tetramethyl BODIPY **3** and more complex versions are stable at room temperature and therefore readily available.^{82,83}

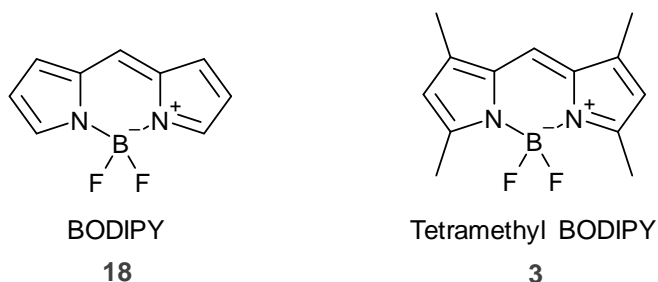


Figure 12. The simplest BODIPY core structure **18** and its stable tetramethyl analogue **3**.

The tetramethyl compound **3** and its derivatives exhibit a notably higher photostability than fluorescein.⁸⁴ The BODIPY class has no exocyclic donor or acceptor groups, which is quite unusual for a useful fluorophore. This however endows it with the possibility of modification at almost any position in order to tailor its spectral characteristics. An example in which conjugation has been extended *via* addition of four aromatic groups, as well as replacement of the bridging carbon with a nitrogen is **22**, (Figure 14). This compound is known as an aza-BODIPY due to replacement of the bridging carbon with nitrogen, it shows a large bathochromic shift in comparison with the parent compound, as well as a dramatic drop in quantum yield ($\lambda_{ex}/\lambda_{em} = 642/688$ nm, $\Phi = 0.07$).⁸⁵ The extension of conjugation acts to lower the energy of the HOMO, and the extra substituents allow the depopulation of the excited electronic state *via* non radiative means. Furthermore, even the boron ligands may be substituted, another example of which

bridges and incorporates the previously added phenol substituents of **23**. This further extends conjugation leading to an additional bathochromic shift, while the added rigidification significantly increases the quantum yield ($\lambda_{\text{ex}}/\lambda_{\text{em}} = 728/746 \text{ nm}$, $\Phi = 0.51$).⁸⁵

The historic synthesis of the tetramethyl BODIPY core **3** relied on an analogue of the Vilsmeier-Haack reaction. It is initiated by condensation of dimethyl-pyrrole **20** with 2-formyl-3,5-dimethylpyrrole **19** followed by BF_3 treatment to complete the synthesis, (Figure 13).⁶² The flexibility of this synthetic route invited the production of numerous unsymmetrical BODIPY derivatives.

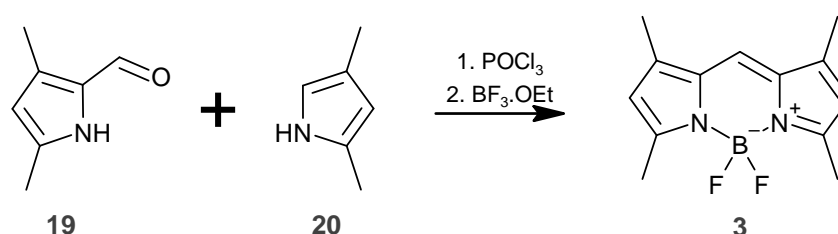


Figure 13. The traditional Vilsmeier-Haack route to produce BODIPY dyes.

Symmetrical versions of the dye are also obtainable through condensation of an aldehyde with two pyrrole equivalents. Through substitution of the aldehyde, the functionality of the bridging carbon may be modified for additional variation in spectral characteristics.⁸⁶ Furthermore, the so called nitrogen bridging aza-BODIPY dyes may also be created *via in situ* generation of the pyrrole rings.⁸⁷ The aforementioned BODIPYs **22** and **23** may be synthesised from diarylpropanone starting material **21** through treatment with ammonium acetate, followed by BF_3 . Demethylation and incorporation of the phenol substituent into the boron system is achieved through treatment with BBr_3 to produce **38**.⁸⁵

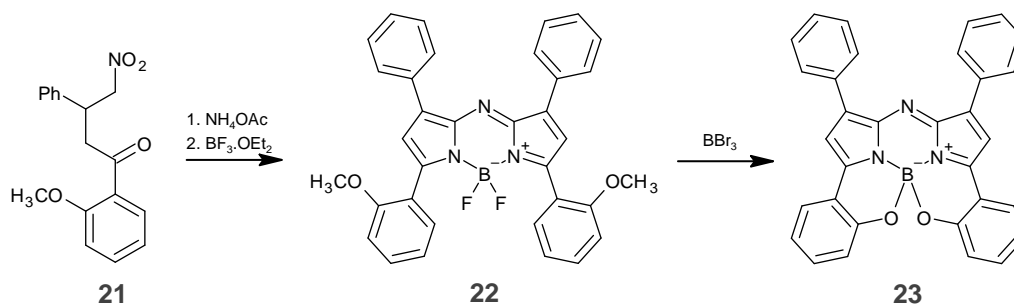


Figure 14. Preparation of an aza-BODIPY dye **22**, followed by ligand substitution of the boron centre to produce **23**.

The exceptional flexibility of the BODIPY core for modification and spectral tailoring has earned it significant interest from the synthetic community. Unsurprisingly, this has led to the production of numerous BODIPY based fluorophores with many and varied uses. BODIPYs have been used effective bioluminescence/fluorescence energy transfer (BRET/FRET) donors, reactive labels for certain species, as well as fluorogenic probes.^{88,89,90} However, some problems may occur due to the very small Stokes shift, which can lead to spectral overlap and self-absorbance.

1.5.3 Phenoxazines

Phenoxazines are an old class of fluorescent dye and possess a long and varied history in stains, laser dyes, and fluorescent probes.^{91,92} They exhibit high sensitivity to polarity and their surrounding environment, in light of this a derivative thereof comprises the core component of the pH indicator litmus.⁹² The phenoxazines possess a similar core to that of the xanthene based fluoresceins and rhodamines, albeit with a relative bathochromic spectral shift as a result of the oxazine nitrogen.

The archetypal phenoxazine dye is known as resorufin **4** (Figure 15) and this compound shows favourable spectral characteristics when existing in its anionic form ($\lambda_{\text{ex}}/\lambda_{\text{em}} = 572/585$ nm, $\epsilon = 5.6 \times 10^4$ M⁻¹cm⁻¹ $\Phi = 0.74$). The sensitivity to pH exhibited by this molecule is a factor to be taken into account however, as the pKa of the hydroxyl group is 5.8.⁶⁴ Resorufin **4** and other variants of this core structure show strong fluorescence

quenching effects when the hydroxyl group is either alkylated or acylated, this effect is also accompanied by a moderate hypsochromic shift. This property makes resorufin **4** and its analogues a useful core for fluorogenic enzyme substrates and labels.^{93,94} Resorufin **4** also shows redox active spectral properties, which allow it to act as a redox probe for peroxidases as a result of the lack of fluorescence of its oxidised and reduced forms.⁹⁵

Spectral characteristics of this class may be further modified through incorporation of other groups into the core, such as fused benzo rings or exocyclic alkyl amino groups which extend conjugation. Also, replacement of the oxazine oxygen with other atoms elicits further spectral changes. An exemplar of the changes such modifications produces results in the Nile red fluorophore **27** (Figure 15). The extended conjugation of this molecule causes a bathochromic shift compared to the parent compound when in aqueous solution ($\lambda_{\text{ex}}/\lambda_{\text{em}} = 523/565 \text{ nm}$). It is however sensitive to polarity, and a hypsochromic shift is observed when in non-polar solvents such as xylene, and this is accompanied by a 100 fold increase in fluorescence quantum yield. This polarity dependent spectral shift allows the molecule to be utilised as a lipid stain for live cell imaging, or visualisation of cell membranes in microscopy.^{96,97} Replacement of the phenoxazine oxygen with a geminal-dimethyl group and addition of two chlorine atoms to the quinone ring system produces the compound 7-hydroxy-9H-(1,3-dichloro-9,9-dimethylacridin-2-one) known as DDAO **30** ($\lambda_{\text{ex}}/\lambda_{\text{em}} = 646/659 \text{ nm}$, $\epsilon = 5.6 \times 10^4 \text{ M}^{-1}\text{cm}^{-1}$, $\text{pK}_a = 5.0$) (Figure 16). Derivatives of this compound have been demonstrated as substrates for aryl sulfatases, β -galactosidases, and as a caged fluorophore system.^{98,99} As before, alkylation of the phenolic hydroxyl produces a dramatic change in fluorescence which lends itself to these applications.

Traditionally, the synthesis of phenoxazines proceeds through the acidic condensation of phenols with nitrosylated aromatics. The prototypical phenoxazine resorufin **4** is produced in this way, *via* condensation of resorcinol **8** with 4-nitrosoresorcinol **24** in H_2SO_4 .¹⁰⁰ Nile

red **27** is produced in the same way, *via* reaction of 1-naphthol **26** and substituted 3-aminophenol **25**.⁹¹

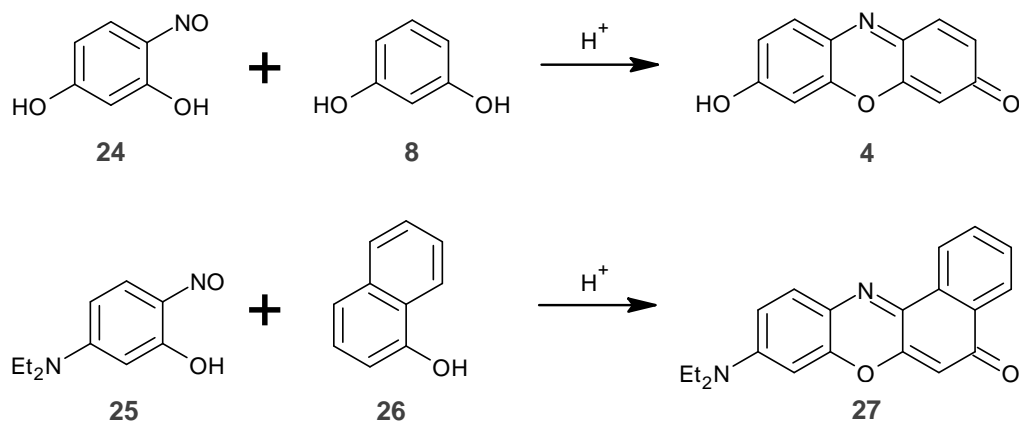


Figure 15. Acid mediated condensation route to the phenoxazines: resorufin **4** and Nile red **27**.

Other routes are however possible, DDAO **30** is synthesised by treatment of phenol **28** and chloramine **29** with base, reduced, condensed with acid and finally oxidised to yield the product **30**, (Figure 16).⁹⁸

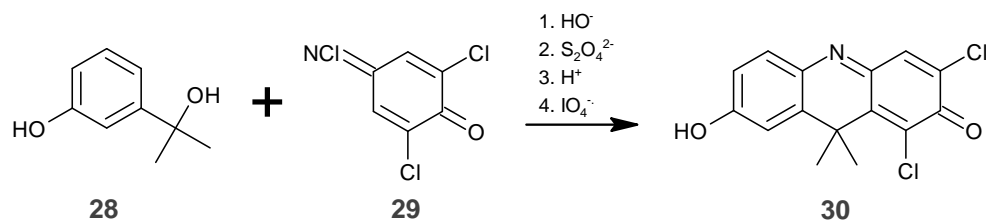


Figure 16. Synthesis of phenoxazine analogue DDAO **30** *via* an alternative route.

The number of steps required in this synthesis somewhat limits its applicability and therefore lends itself to further innovation to simplify its production.

1.5.4 Cyanines

The cyanines are a class of fluorescent dye that conform to the general structure $R_2N-(CH=CH)_n-CH=NR_2^+$ and as such are a diverse group. They generally exhibit a large extinction coefficient, are resistant to photobleaching and enjoy good absorption and emission tunability through structural modification. They have only relatively recently

(1993) had their usability expanded significantly, through development of structural hybrids. This development has led to advances in their utility as a result of the invention of the so called CyDyes. These are indocarbocyanine sulfonates, an example of which is Cy3 **5** ($\lambda_{\text{ex}}/\lambda_{\text{em}} = 554/568 \text{ nm}$, $\epsilon = 1.3 \times 10^5 \text{ M}^{-1}\text{cm}^{-1}$ $\Phi = 0.14$). The sulfonate group imparts greater solubility to the dye, this along with further functionalisation has provided handles for bioconjugation and labelling of proteins and nucleic acids.^{66,101} As well as their somewhat limited applications as stains for cell membranes and DNA.^{102,103} The practicality of the CyDyes stems from the fact the excitation and emission maxima may be tailored simply by extension of the central polymethine chain. Extension of this chain produces a bathochromic in both excitation and emission wavelengths. The numerical suffix of the CyDye nomenclature corresponds to the number of carbon atoms in the central chain (Figure 17).⁶⁷

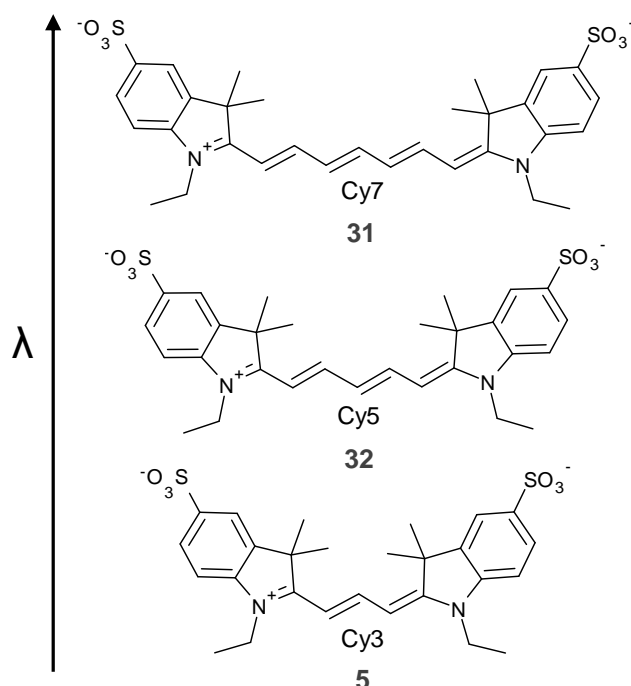


Figure 17. CyDyes, notable for their increase in $\lambda_{\text{ex}}/\lambda_{\text{em}}$ with central chain length.

Not unlike the BODIPY class's core structure, the cyanines contain no exocyclic donor or acceptor groups, this somewhat limits their usefulness as strategies for modifying the spectral characteristics seen in other fluorophores are not applicable. Methods have

however been developed to partially overcome this limitation and these involve the fusion of the cyanine with another class of fluorophore such as rhodamine. An example of this fusion is **37** (Figure 19) and the joining of the two leads to an excitation maximum at longer wavelength with decent fluorescence properties ($\lambda_{\text{ex}}/\lambda_{\text{em}} = 720/750 \text{ nm}$, $\epsilon = 1.25 \times 10^5 \text{ M}^{-1}\text{cm}^{-1}$ $\Phi = 0.30$). Other combinations of fluorophore also exist such as cyanine-fluorescein and cyanine-coumarin both of which allow modification of their spectral properties through functionalisation of the non-cyanine structure.^{104,105,106}

Generally the synthetic route used to produce the cyanines involves addition of an aldehyde equivalent to an activated carbon species like a 2-alkylindolinium salt.¹⁰⁷ For example the Cy3 dye **5** is produced in this manner through condensation of the indolinium salt **33** with triethyl orthoformate **34**, to yield the product (Figure 18).¹⁰¹

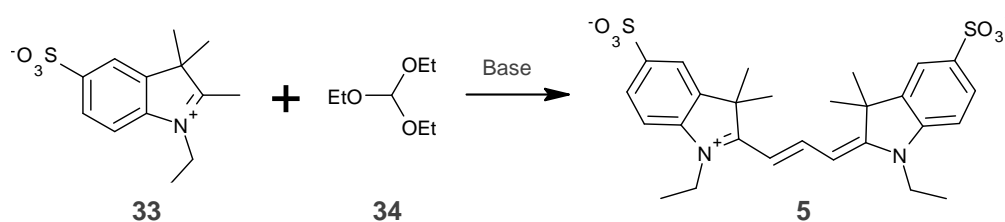


Figure 18. Synthetic route to cyanine **5** from an alkylindolinium salt **33** combined with triethyl orthoformate **34**.

Chromenylium compound **35** may also be fused with aldehydic cyanine precursor **36** in an analogous manner to form a hybrid fluorophore **37** with enhanced tunability (Figure 19). Substitution of the chromenylium portion enables generation of various hybrid structures with properties tailorable for desirability.¹⁰⁸

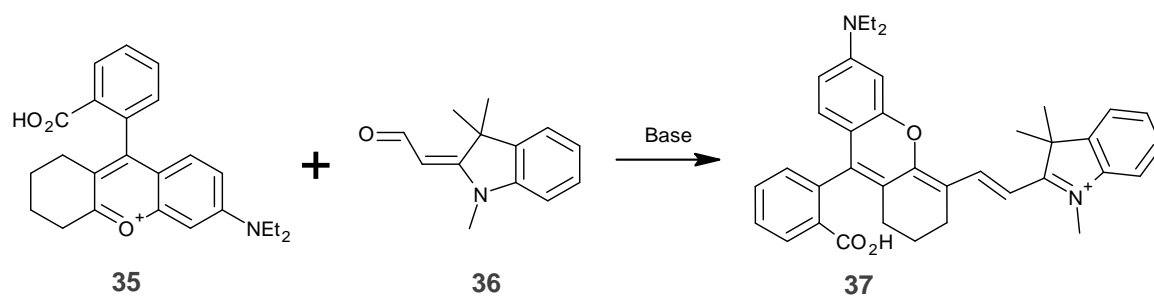


Figure 19. Fusion of cyanines with other fluorophores results in enhanced tunability of spectral characteristics.

Most commonly the cyanine fluorophores are used as fluorogenic labels or stains for targeting nucleic acids or proteins, showing a large fluorescence increase upon binding.⁶³ They have also been found to be useful in several other applications including pH sensing fluorescent indicators, and as FRET donor-acceptor pairs wherein two different cyanine dyes are bound together by a targeted cleavable linker.^{109,110}

1.5.5 Fluoresceins

Fluorescein **6** is one of the oldest synthetic fluorophores, having been first synthesised in 1871 by Adolf von Bayer.¹¹¹ It does however remain one of the most commonly used fluorophores with countless applications in medicine, industry and science. The phenolic hydroxyl of fluorescein is moderately acidic with a pKa of 6.4. The compound is most fluorescent in its dianionic form and is commonly used for fluorescence detection ($\lambda_{\text{ex}}/\lambda_{\text{em}} = 491/510 \text{ nm}$, $\epsilon = 9.0 \times 10^4 \text{ M}^{-1}\text{cm}^{-1}$ $\Phi = 0.86$).¹¹² The fluorescence profile of fluorescein is pH sensitive because of its relatively low pKa, however, addition of electron withdrawing substituents such as halogens to the phenolic rings lowers its pKa decreasing its pH sensitivity and enhancing photostability.¹¹³ Fluorescein **6** exists in an equilibrium between a non-fluorescent closed lactone form and an open highly fluorescent form, Figure 20.

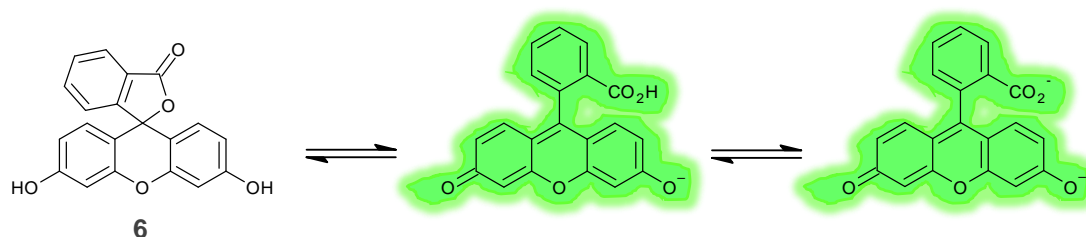


Figure 20. Fluorescein **6** exists in equilibrium between a non-fluorescent (left) and several fluorescent forms (right, far right).

This equilibrium may be modified through functionalisation of the phenolic hydroxyl groups. This acts to lock the molecule into the non-fluorescent closed lactone form. The ability to lock the molecule into the non-fluorescent through functionalisation allows useful fluorogenic enzyme probes to be produced.¹¹⁴ These develop a large increase in fluorescence upon enzymic cleavage and release of the fluorophore which contributes to an excellent signal to background ratio.

The brightness of fluorescein is relatively easy to modify through simple changes to its structure, however the excitation and emission maxima are more difficult to adjust without subsequent loss in fluorescence intensity. Rose Bengal **38** is an example of this drop in intensity after modification. The molecule also shows a bathochromic shift compared to the parent compound, most tellingly this shift is accompanied by a large decrease in quantum yield ($\lambda_{\text{ex}}/\lambda_{\text{em}} = 548/566 \text{ nm}$, $\Phi = 0.018$).¹¹⁵ Bathochromically shifted fluoresceins have, however, been produced for use as labels, achieved through the fusion of additional rings and extension of the lower phenolic ring systems (Figure 21).¹¹⁶ These extended molecules were coined seminaphtho- **39** and naphthofluoresceins **40**, and have found application as fluorescent indicators and cellular stains.^{117,118,119,120}

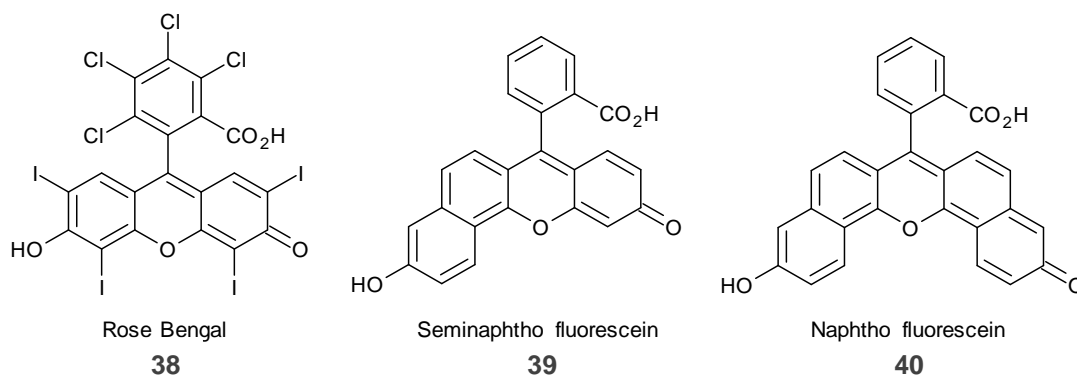


Figure 21. Addition of substituents and extension of conjugation produces bathochromic shifts, as well as variation in fluorescence quantum yield.

In addition to this, modification to the core xanthene moiety of fluorescein **6** has been shown to effectively change the spectral characteristics, Figure 24. For example, replacement of the xanthene oxygen with a geminal dimethyl group produces a carbofluorescein **45** which shows a bathochromic shift compared to the parent compound ($\lambda_{\text{ex}}/\lambda_{\text{em}} = 544/567 \text{ nm}$, $\epsilon = 1.08 \times 10^5 \text{ M}^{-1}\text{cm}^{-1}$ $\Phi = 0.62$), along with a pKa of 7.4.⁶⁸ Furthermore, replacement of the aforementioned oxygen with a dimethylsilyl group produces silafluorescein **47**, which exhibit an even larger bathochromic shift ($\lambda_{\text{ex}}/\lambda_{\text{em}} = 582/598 \text{ nm}$, $\epsilon = 1.1 \times 10^5 \text{ M}^{-1}\text{cm}^{-1}$ $\Phi = 0.42$).¹²¹

Historically, the synthesis of fluorescein has involved the condensation of resorcinol **8** with phthalic anhydride **41** in a melt of ZnCl_2 at $180 \text{ }^\circ\text{C}$, or in a neat acid such as $\text{CH}_3\text{SO}_3\text{H}$ at lower temperatures around $85 \text{ }^\circ\text{C}$, Figure 22.^{111,112,113}

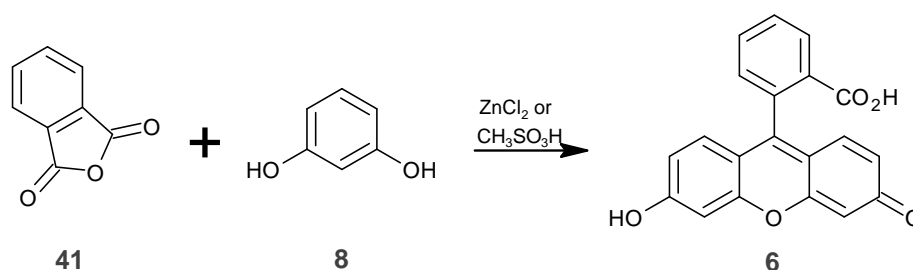


Figure 22. Traditional condensation routes to fluorescein **6** require harsh conditions.

The use of nitro or carboxy substituted phthalic anhydrides results in the production of fluoresceins substituted on the upper ring. These substitutions are useful as

bioconjugation handles, however a mixture of isomers is formed (Figure 23) and these require separation. This is usually attempted *via* derivatisation and subsequent crystallisation.^{112,113}

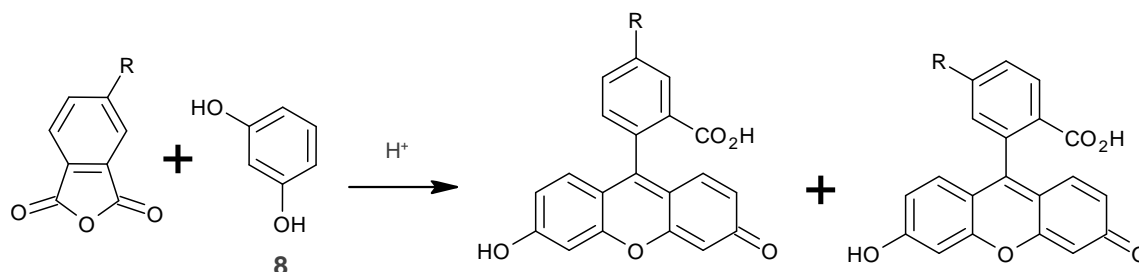


Figure 23. Substituted phthalic anhydrides produce a difficult to separate mixture of substituted fluorescein isomers.

The carbo- **44** and silafluorescein **47** (Figure 24) cannot be produced through the same acid mediated method as the parent compound. They are instead synthesised through the addition of an organometallic aryl group to a benzophenone derivative. For example carbofluorescein **44** is produced through the addition of a Grignard reagent **43** to a protected anthracene derivative **42**, which upon deprotection yields the required compound.⁶⁸ Similarly, silafluorescein **47** is produced through the addition of an aryl lithium **46** to protected silanone **45**.¹²¹ These reactions produce only single isomers (Figure 24), however the protection of ancillary groups must be robust and this can be a limiting factor.

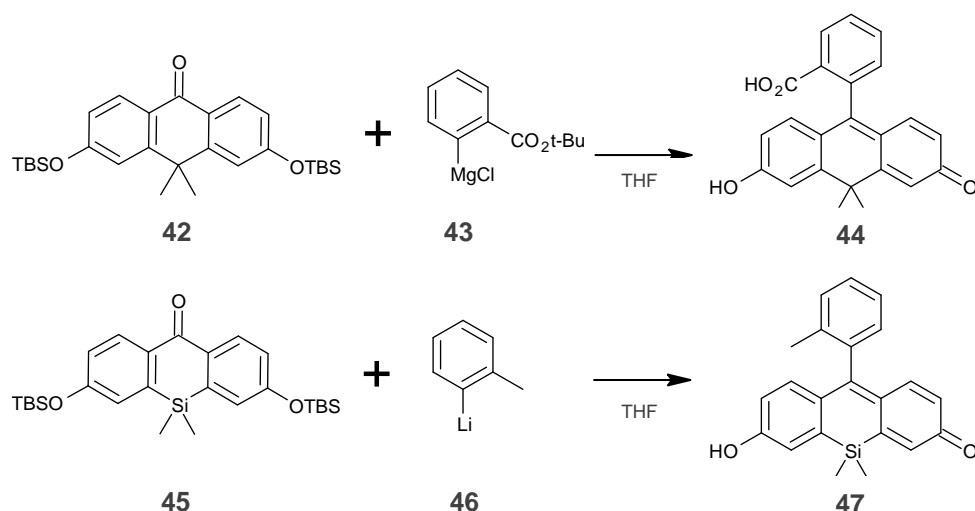


Figure 24. Carbo- **44** and silafluoresceins **47** may be produced as single isomers from addition of organometallics, as long as suitable protection of other functionality is available.

The usefulness of the fluoresceins stems from the augmentation of the open-closed equilibrium through simple functionalisation of the phenolic oxygens *via* alkyl- or acylation. As the removal of these groups *via* enzymic or other cleavage results in a large increase in fluorescence, a broad variety of possibilities for fluorogenic enzyme probes, sensors, and photoactivatable dyes exists.^{122,123,124}

It is unsurprising that fluorescein continues to be the subject of extensive research with further structural modifications yielding new and useful compounds for a myriad of applications. The production of bathochromically shifted fluoresceins with good brightness has provided the basis for a number of new and useful ion indicators and enzyme substrates.^{121,125} There is, as always, scope for further development and no doubt many more improvements and advances will be seen as research continues.⁶⁰

1.5.6 Rhodamines

Rhodamines are another older class of fluorophore similar to fluorescein **6**, the first synthesis of which was recorded as far back as the 1880s. These fluorophores are essentially the amino analogue of fluorescein **6**, they do however have a number of advantages over fluorescein **6**, including lower pH sensitivity, better photostability and

improved tunability. The prototypical rhodamine, sulforhodamine B **50** (Figure 25), was first described in a patent dating back to 1887.¹²⁶ This fluorophore strongly absorbs in the green region with a strong emission in the yellow region ($\lambda_{\text{ex}}/\lambda_{\text{em}} = 565/586 \text{ nm}$, $\epsilon = 8.4 \times 10^4 \text{ M}^{-1}\text{cm}^{-1}$ $\Phi = 0.45$).⁶³ Rhodamine **50** has frequently been used as a laser dye, and its sulfonyl chloride counterparts are commonly used to label amino containing molecules. Tetramethyl rhodamines **53** (Figure 25) are another example of conjugatable rhodamines, which are attached by the second carboxyl group of the upper ring system to biomolecules or ion sensing groups.¹²⁷ The structural change from sulfonate to carboxylate produces a weak hypsochromic shift in both the excitation and emission maxima ($\lambda_{\text{ex}}/\lambda_{\text{em}} = 548/572 \text{ nm}$, $\epsilon = 7.8 \times 10^4 \text{ M}^{-1}\text{cm}^{-1}$).⁶⁸

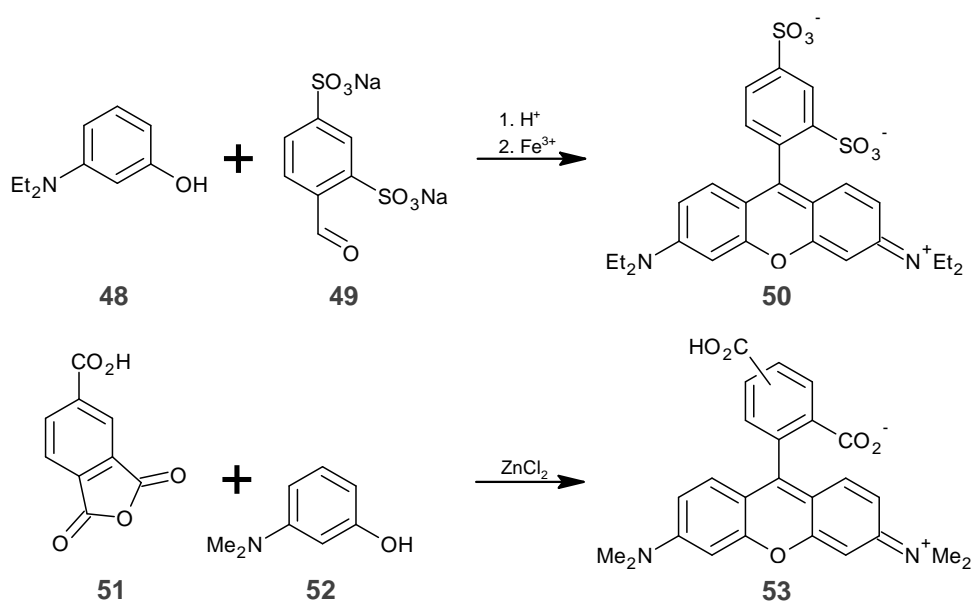


Figure 25 Synthesis of sulforhodamine B **50** and tetramethylrhodamine **53**.

Variation of the amine substituents in rhodamines also produces variations in the spectral properties of the dye. A hypsochromic shift is observed from the non-alkylated rhodamine 110 **7** when compared to its tetramethyl counterpart **53**, rendering it spectrally similar to fluorescein ($\lambda_{\text{ex}}/\lambda_{\text{em}} = 496/517 \text{ nm}$, $\epsilon = 7.4 \times 10^4 \text{ M}^{-1}\text{cm}^{-1}$ $\Phi = 0.88$).^{68,69,70,128} The ability to conjugate peptides and other biomolecules to the available amine groups of rhodamine 110 **7** has led to its common use as a fluorescent label.¹²⁹ Rhodamine 110 **7** is also widely used as a core for fluorogenic probes and detectors. Similarly to fluorescein **6**, the

molecule exists in equilibrium between a non-fluorescent closed lactone form and several highly fluorescent quinoid forms. This equilibrium may be forced towards the closed and non-fluorescent form *via* acylation of the amine groups. Subsequent removal of the acyl groups *via* enzymic cleavage or other means produces a large increase in fluorescence. This highly exploitable property has led to many fluorogenic derivatives which have proven useful for the detection of enzymic activity, as well as activity measurement labels in fluorescence microscopy.^{122,130,131}

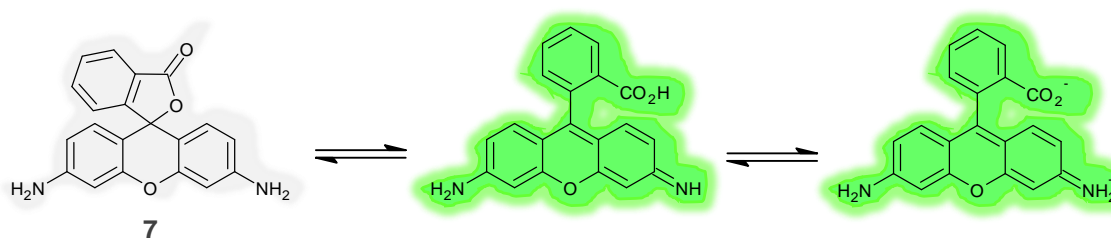


Figure 26. Rhodamine 110 **7** exists in equilibrium between a closed, non-fluorescent lactone form (left), and fluorescent quinoid forms (centre, right).

Further modification of the rhodamine core through substitution of the xantheno oxygen with atoms such as carbon, silicon, germanium and tellurium has also been shown to vary its spectral properties.^{68,132,133} Substitution for carbon yields carborhodamines, the simplest of which exhibits a bathochromic shift compared to the parent compound ($\lambda_{\text{ex}}/\lambda_{\text{em}} = 552/577$ nm, $\epsilon = 6.5 \times 10^4$ M⁻¹cm⁻¹ $\Phi = 0.64$).⁶⁸ Larger bathochromic shifts may be produced through substitution of the xantheno oxygen with silicon, to produce silarhodamine **60** ($\lambda_{\text{ex}}/\lambda_{\text{em}} = 691/712$ nm, $\epsilon = 1.0 \times 10^5$ M⁻¹cm⁻¹ $\Phi = 0.12$) (Figure 28). This shift brings the excitation and emission maxima close to the infrared region and creates a useful core for the production of compounds for *in vivo* imaging.¹³⁴

The initial synthesis of sulforhodamine **50** involved an acid catalysed condensation of benzaldehyde **49** with aminophenol **48**, followed by FeCl₃ mediated oxidation (Figure 25).¹²⁶ The standard carboxy rhodamines, bearing an additional o-carboxyl group on their upper ring may be produced through condensation of a phthalic anhydride with two equivalents of a substituted 3-aminophenol. An example is the production of **53** which is

generated as an isomeric mix of the 5/6-carboxy- analogue by condensation of two equivalents 3-(dimethylamino)phenol **52** with trimellitic anhydride **51** in ZnCl_2 (Figure 25).¹²⁷ An alternative set of conditions which have proved successful involves dissolution of the two starting materials in propionic acid with a catalytic quantity of TsOH .¹²²

Production of rhodamines through the aforementioned condensation route has a number of notable disadvantages. The use of substituted phthalic anhydrides leads to the production of a mixture of difficult to separate isomers, which require complex and time-consuming separation to yield any single isomer. Although single isomers are commercially available, they are prohibitively expensive for most applications. In addition, the limited availability of 3-aminophenol derivatives can also prove problematic. Furthermore, the strongly acidic conditions used for the condensation are not well tolerated by many functional groups, and this further limits the applicability of this route. An example of some of the problems encountered is shown when using the condensation route for the synthesis of 5-carboxyrhodamine 110 **53**. Although its production is possible *via* this route, not only a mixture of isomers is formed but hydrolysis of the product to rhodols and fluoresceins is also observed, significantly complicating the purification.¹³⁵

After much research into the synthesis of rhodamines a number of alternatives to the condensation have proven viable. One such strategy converts fluoresceins into rhodamines *via* conversion to triflates, followed by a Buchwald-Hartwig cross coupling to yield the corresponding rhodamine. For example, the single isomer 5-carboxyrhodamine 110 **53** may be generated from the t-butyl protected 5-carboxyfluorescein triflate **55** followed by deprotection (Figure 27). This approach simplifies the production of such single isomers and even allows the synthesis of N-aryl and N-acyl rhodamines. This useful transformation also circumvents the difficulty of acylating rhodamines in light of the low reactivity of the aniline nitrogen of rhodamine.¹³⁶ Carbofluoresceins have been successfully converted into carborhodamines using this same method, giving rise a diverse collection of bathochromically shifted rhodamines.⁶⁸

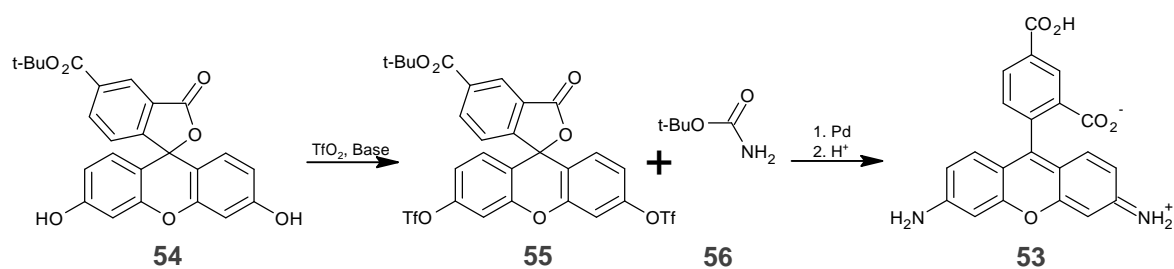


Figure 27. Buckwald-Hartwig cross coupling of a triflate functionalised carboxy fluorescein **55** produces a single isomer of carboxy rhodamine **53**.

One other successful method has applied organometallic compounds to add to N-tetra alkylated xanthenes, to generate a variety of other rhodamines.^{137,138} Silarhodamine **60** was successfully synthesised from addition of organolithium **59** to the xanthone analogue diaminosilanone **58**, yielding the product **60** after amine deprotection (Figure 28).⁶⁰

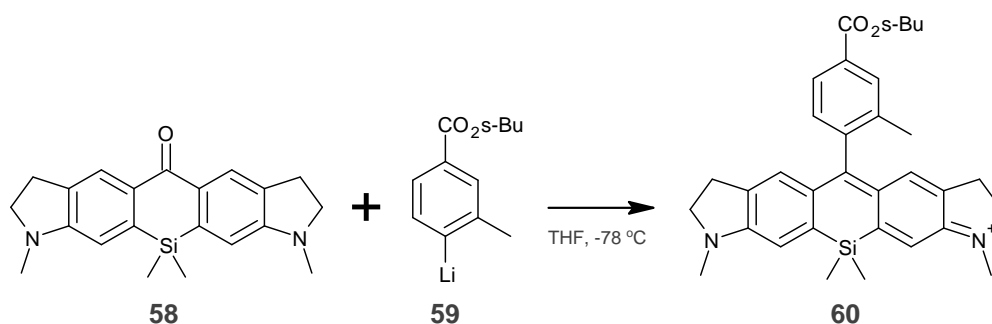


Figure 28. Production of silarhodamine **60** from addition of an organolithium.

As a result of the improved customisability of the rhodamine core over its counterparts, it is not surprising that rhodamines remain the most useful of all the fluorophores. Their application for the production of fluorescent probes and labels is unrivalled, with the implementation of carbo and silarhodamines significantly advancing probe and label based imaging capabilities *in vivo*.^{68,133,134,138} Combinatorial libraries are now accessible and enable tuning of probes to specific biological targets.¹³⁹ Along with this, photoactivatable rhodamines have also been developed, and the carborhodamines have proven useful in super-resolution microscopy.¹²²

As the understanding of the factors controlling the open/closed equilibrium of rhodamine has deepened, as has their usefulness and applicability to new and improved applications. The carbo- and silarhodamines shift this equilibrium towards the closed form which

reduces their overall brightness. There is however a concurrent increase in cell permeability as a result of the higher contribution from the reduced polarity closed form.^{68,138} Alongside this it has been found that modification of the upper ortho substituent also effects the equilibrium. Substitutions of this group have allowed production of lactam based photoactivatable fluorophores as well as various sensors.^{140,141,142} There is still room for advancement of the properties of this class of fluorophore, and as research continues it is inevitable that these will be made.

1.6 Aims

This research project set out to re-synthesis the *S. aureus* probe LGX for further testing both in-house at Kingston University and externally as part of its development as a next generation point of care test for the microorganism. Following this the synthesis was to be re-examined and improved upon in order to facilitate the synthetic scale up required in order to be produced on a larger scale industrially. Having achieved this, further down the line it was the responsibility of the writer to investigate routes to new fluorophores. This investigation would allow not only allow the production of novel fluorophores of value to the synthetic community, but facilitate the development of new protease probes. Having synthesised a small library of novel fluorophores, the most promising candidate would be put forward for production of a next generation *S. aureus* probe with desirable features such as a simplified synthesis and improved sensitivity.

Chapter 2 – Results and Discussion

2.1 LGX Synthesis and Scale Up

2.1.1 Construction of the Boc-Val-Pro-OH Section of the Biomimetic Peptide

LGX was a *Staphylococcus aureus* probe previously developed by the Le Gresley lab with high sensitivity and proven efficacy in detection of the bacteria. Its effectiveness was based upon targeting a bacterial protease expressed by 95 % of the bacteria in question.⁷⁰ Previous syntheses of the compound were met with difficulty and its production was notably of low yield (~1.8 %).

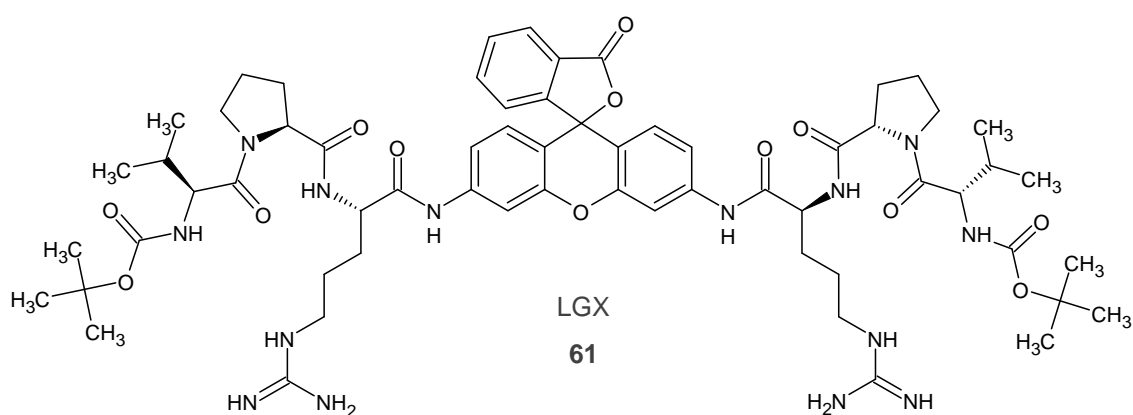


Figure 29. The active compound in the fluorogenic *S. aureus* probe LGX **61**.

The exploratory synthesis and scale up of LGX **61** commenced with the coupling of protected amino acid Boc-NH-Val-OH **62** with HN-Pro-OMe **63** for production of part of the biomimetic tripeptide Boc-NH-Val-Pro-OMe **64**. Commercially available protected amino acids **62** and **63** were obtained, and solution phase peptide coupling undertaken. A range of conditions were tested in order to ascertain the most effective route to the dipeptide. The dipeptide Boc-NH-Val-Pro-OMe **64** would later be required in significant quantities to allow optimisation of the synthetic route.

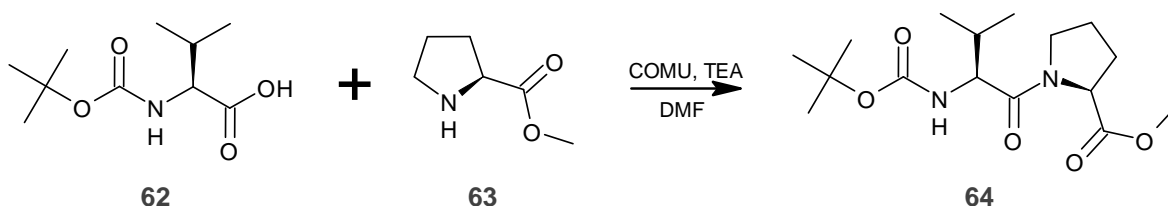


Figure 30. Generation of the dipeptide Boc-Val-Pro-OMe **64** using COMU **67**.

Previous work had produced the dipeptide in moderate yields using solution phase peptide coupling techniques with the coupling agent 1-ethyl-3-(3-dimethylaminopropyl)carbodiimide (EDCI) **65**, and the additive ethyl cyanohydroxyiminoacetate (Oxyma) **66** to suppress racemisation in the presence of triethylamine (TEA) base.⁷⁰

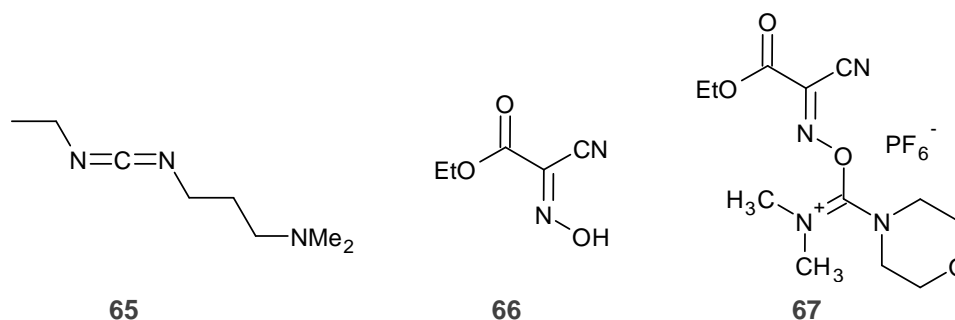


Figure 31. Coupling agent EDCI **65**, additive Oxyma **66**, and coupling agent COMU **67**.

This route was found to produce yields of around 50 %; improvements were achieved by substitution of EDCI **65** with (1-cyano-2-ethoxy-2-oxoethylideneaminoxy)dimethylamino-morpholino-carbeniumhexafluorophosphate (COMU **67**) which improved yields to a consistent 60 - 70 %.

2.1.2 Attachment of Boc-Arg(Cbz)₂-OH to Rhodamine 110

Having improved the synthetic route and produced sufficient quantities of the protected dipeptide, attention was directed toward the coupling of rhodamine 110 **7** with the protected arginine, HO-(Arg(Cbz)₂-NHBoc)₂ **68**.

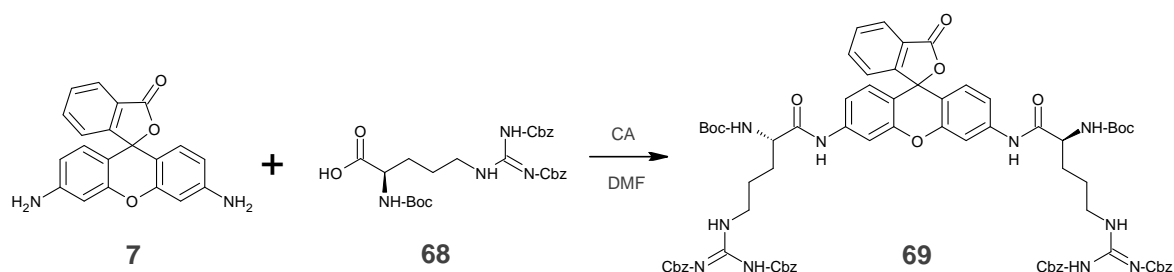


Figure 32. Coupling of protected arginine **68** with rhodamine 110 **7** using coupling agent (CA) to form the rhodamine bis-acylate, Rho-(Arg(Cbz)₂-NHBoc)₂ **69**.

Both rhodamine 110 **7** and the protected arginine **68** were obtained commercially; rhodamine as the HCl salt and arginine with NH t-butoxycarbamate (Boc-) protection and double side chain carboxybenzyl (Cbz-) protection, (Figure 32). Initial coupling attempts followed that of previous work: solution phase peptide synthesis with EDCI **65** in combination with Oxyma **66** in the presence of TEA base. These coupling conditions proved ineffective, producing complex intractable mixtures in all instances. Numerous variations in the number of coupling agent and base equivalents were tested, along with both DMF and DCM as solvent choices. Other solvents were unable to dissolve the reagents and only the activated amino acid was found to dissolve in DCM. Numerous workup conditions were also tested in tandem on each reaction in order to ascertain the most effective. These test workups included copper sulphate washes for removal of uncoupled amine, as well as standard acid and base workup steps. Traditional flash column chromatography was employed for purification, using both gradient and isocratic mobile phases. After many trials of the aforementioned coupling conditions, they were ruled out as too inefficient with remarkably poor yields of only moderate purity. The quantities produced using these methods precluded continuation of the synthesis and so a more effective route was sought.

Following the lack of success of the previous EDCI **65** based coupling route, attention was turned toward the previously successful coupling agent COMU **67**. This reagent had recently garnered significant attention from the synthetic community due to its high efficiency in coupling hindered and bulky amino acids.¹⁴³ In addition to the success reported by other researchers, it was rationalised that the improved water solubility of the COMU **67** by products may simplify workup. This would be advantageous as purification had been problematic when using EDCI **65** coupling route.

The general coupling procedure optimised by the inventors of COMU **67** for solution phase was initially employed for synthesis.¹⁴³ A similarly complex reaction mixture was observed upon TLC analysis, this was inferred to be a selection of mono, bis and other

variations of coupled products. It is worthy of note that as rhodamine 110 **7** exists in equilibrium between at least three forms in solution, coupling is capricious. As a further complication each of these forms suffer from an intrinsic lack of NH_2 nucleophilicity.¹⁴⁴ The equilibrium consists of a colourless closed lactone form containing two anilino type NH_2 groups (Figure 33, left), a coloured open quinone form in which one of the amine groups exists as a zwitterionic iminium species (Figure 33, centre), and an open and coloured form in which one amine exists as an imine, (Figure 33, right).

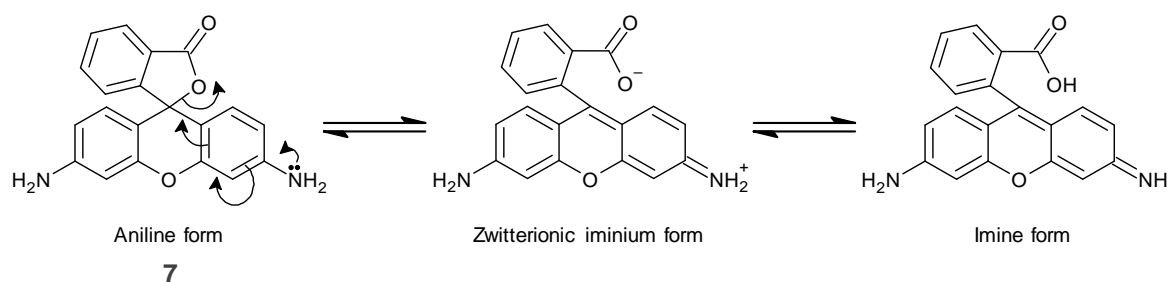


Figure 33. Solution equilibrium of rhodamine 110 **7** and the effect on ring bound NH_2 groups.

Both open forms are significantly less reactive towards acylation as the nucleophilic electron pair is far less available. This effect is introduced not only due to a contraction of the outer orbital through rehybridization from sp^3 to sp^2 , significantly increasing in s character, but also the reduction of availability through initial cationic iminium formation when converting from the anilino form. It is therefore likely that only the anilino form would possess the nucleophilicity required to undergo acylation to any appreciable extent. Furthermore, as the open forms are favoured in polar solvents, these effects, when combined with the low nucleophilicity of aniline groups especially when heavily conjugated, goes some way to explain the difficulty in bis acylation of rhodamine 110 **7**. A further noteworthy observation is that, in polar solvents such as those employed herein the solution is strongly fluorescent.

Yet another complication associated with acylation of rhodamine 110 **7**, is that when the upper carboxylic acid group is exposed in the open forms, it is possible for it also to be activated by the coupling agent. This therefore enables rhodamine-rhodamine homo-

coupling and polymerisation to compete with the intended coupling, as shown in Figure 34.

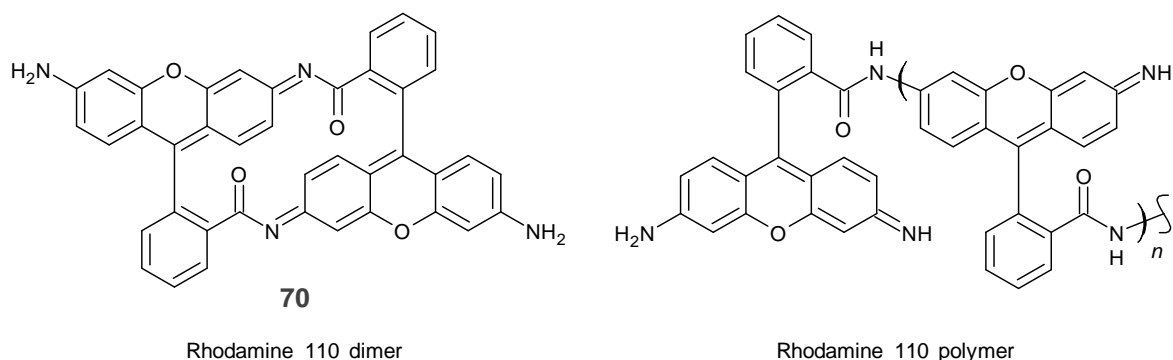


Figure 34. Possible side products through coupling agent activation of the upper carboxyl group of rhodamine, accessible from its open fluorescent forms.

After consideration of the potential issues the nature of rhodamine 110 **7** contributed to the synthesis of the bis-arginine intermediate, the complexities associated with arginine itself were also considered. It is common knowledge that arginine is one of the most problematic amino acids, not only due to its steric bulk, but also because of the guanidine group at the distal end of the side chain. As the guanidine moiety is reactive to both nucleophiles and electrophiles it is usually protected in peptide synthesis to avoid such side reactions. However, exhaustive Cbz- protection of the guanidine group of arginine is very difficult, and so double protection is usually the most robust available. Two main side reactions are associated with arginine, de-guanidination and δ -lactam formation.^{145,146}

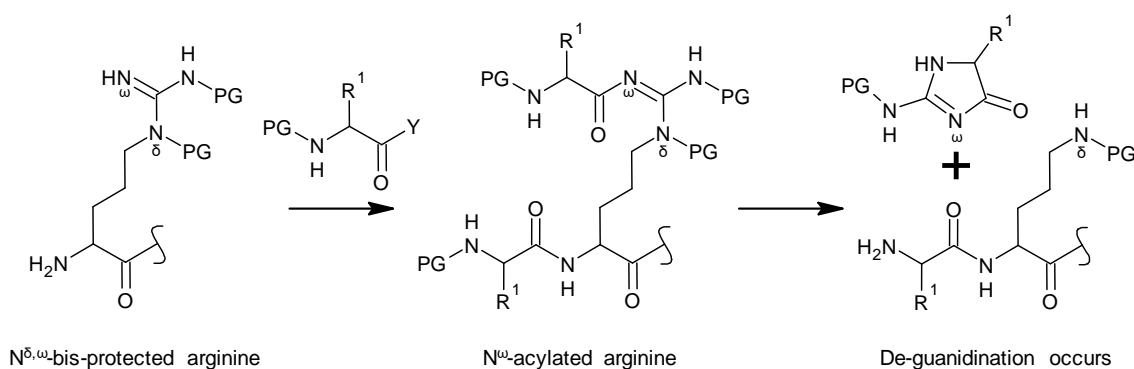


Figure 35. De-guanidination occurs following an N^{ω} -acylation side reaction of a non-exhaustively protected guanidine group. The following deprotection step results in both de-guanidination of arginine to form ornithine and simultaneous liberation of the corresponding substituted imidazolone.

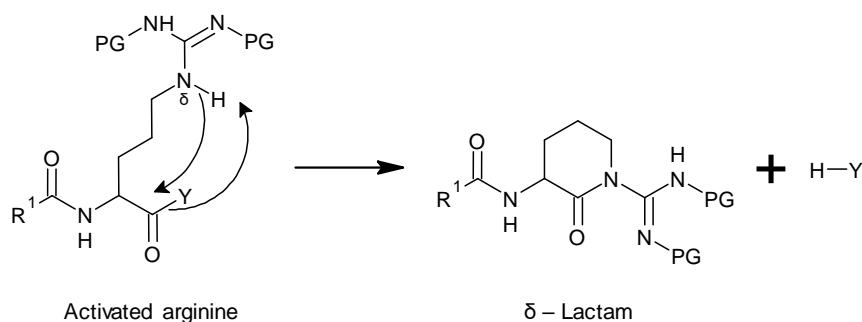


Figure 36. δ – lactam formation from an activated arginine residue. Cyclisation forms the δ – lactam as a result of the latent nucleophilicity of the un-protected guanidyl δ – NH group.

These side reactions (Figure 35 and 36) may be suppressed, but are rarely eliminated through side chain protection. One of the most effective protecting groups for minimisation of these side reactions has been found to be the carboxybenzyl group (Cbz).¹⁴⁵ This protection was selected in light of this and a number of other factors. These included its high stability to both acid and basic conditions, permitting the orthogonal and acid labile Boc- protecting group to be removed without affecting it. Moreover, the simplicity of its removal *via* hydrogenation was the deciding factor, leading to its selection over others. This was because later in the synthesis when the molecule is large and complex, deprotection could be achieved very simply without further purification, vastly simplifying the final synthetic step.

Again, significant time was devoted to investigating COMU **67** as a coupling agent to produce Rho-(Arg(Cbz)₂-NH₂)₂, **69**. Initially the standard optimised procedure was adopted as with generation of the aforementioned dipeptide.¹⁴³ Several small scale test reactions were initiated, with increasing numbers of arginine equivalents to investigate saturation effects on coupling efficiency. Careful TLC analysis revealed that as the number of arginine equivalents increased, as did reaction mixture complexity. This indicated a concurrent increase in side reactivity with arginine saturation. It was found that using only a slight excess in the region of 1.1 arginine equivalents per reaction site was the most effective reaction stoichiometry. This appeared to minimise the number of side reactions and facilitated the effective removal of unreacted arginine in reaction workup. Extension of reaction time up to 168 hours was also tested, however above 48 hours provided no advantage and in fact led to a more complex crude mixture. Modest recovered yields of around 8 % were achieved with COMU **67**, consequently it was deemed necessary to continue investigation of the coupling procedure.

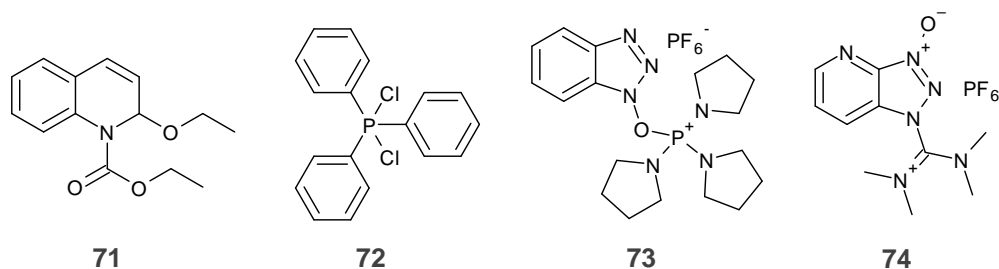


Figure 37. Coupling agents EEDQ **71**, PPh₃Cl₂ **72**, PyBOP **73** and HATU **74**.

Several other coupling agents were employed in order to enhance the efficiency of the coupling procedure. These were investigated through a selection of tandem reactions to screen the for applicability to this difficult coupling. The selection of coupling agents was influenced by their reported effectiveness in the promotion of difficult couplings.¹⁴⁷ They included N-Ethoxycarbonyl-2-ethoxy-1,2-dihydroquinoline (EEDQ) **71**, Dichlorotriphenylphosphorane (PPh₂Cl₂) **72** (benzotriazole-1-ylxoy)tris(pyrrolidino)phosphonium hexafluorophosphate (PyBOP) **73**, and (1-[Bis(dimethylamino)methylene]-1H-1,2,3-triazolo[4,5-b]pyridinium-3-oxid

hexafluorophosphate (HATU) **74**. Their effectiveness in promoting the coupling is shown in Table 3.

Coupling Reagent	Isolated yield
EEDQ 71	-
PPh ₃ Cl ₂ 72	-
EDCI 65	5 %
PyBOP 73	8 %
COMU 67	8 %
HATU 74	25 %

Table 3. Coupling agents and their best isolated yields of Rho-(Arg(Cbz)₂-NH₂)₂, **69**.

Notably, most coupling agents performed worse than COMU **67** in coupling arginine to rhodamine 110, with only PyBOP **73** approximately equalling the efficiency of COMU **67**. However, HATU **74** was found to vastly increase the efficiency of coupling with a concurrent improvement in isolated yield. Moreover, the crude reaction mixture was found to contain fewer by products than that obtained with COMU **67** coupling, likely as a consequence of the higher reactivity of HATU **74** over COMU **67**. Like most peptide coupling agents, the reaction pathway of both COMU **67** and HATU **74** is thought to essentially pass through the same stages. However, the final stage in the case of HATU **74**, in which the activated ester is attacked by the nucleophile, benefits from a neighbouring group effect not seen in COMU **67**. This neighbouring group effect is brought about by the nitrogen lone pair of the azotriazole ester formed in the HATU **74** coupling pathway as shown in Figure 38. The result is improvement of orientation of the incoming amine providing an improved and faster reaction pathway, leaving less time for side reactions to take place. It is believed that the improvement in yields and reduction of side reactions observed was a result of this effect.

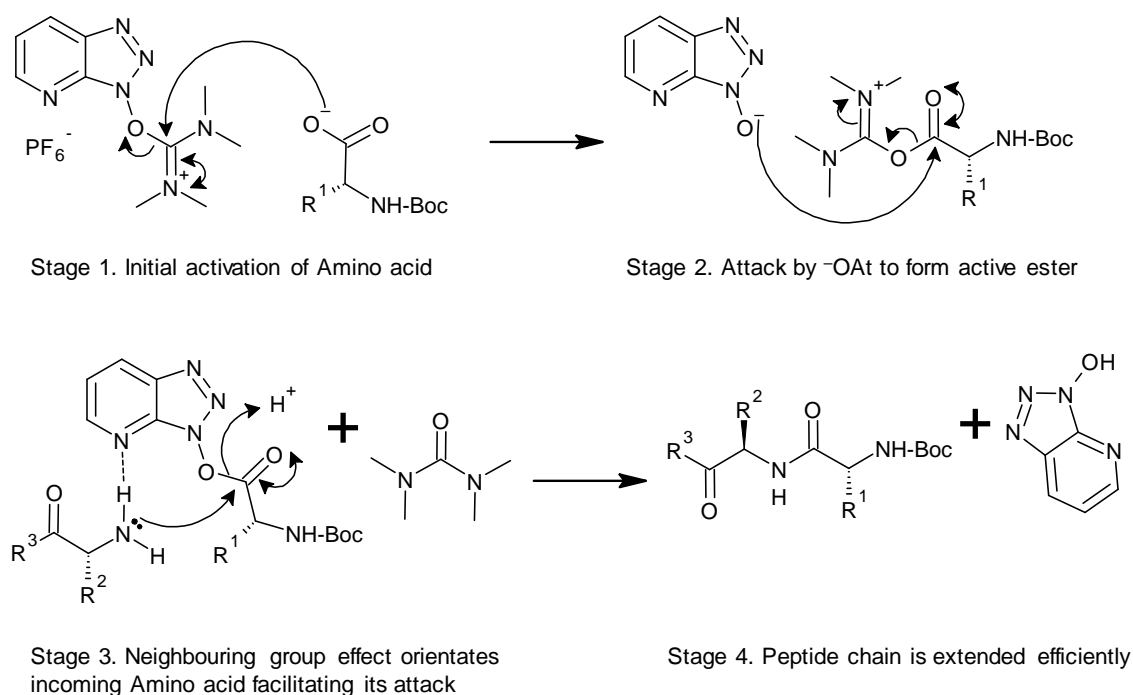


Figure 38. Peptide coupling mechanism of HATU **74** and its improved efficiency facilitated by the neighbouring group effect.

With a more effective coupling agent in hand, optimisation of the coupling procedure was undertaken. Varying quantities of coupling agent and amino acid were tested, again under the pretence that saturation of rhodamine with increasing numbers of arginine equivalents would increase efficiency. The rationale behind this was that increasing saturation with arginine would concurrently increase the probability of collision of mono-acylated rhodamine with the amino acid while in the minor anilino form, forming the bis-acyl. Once again this was found to be largely ineffective with increasingly complex mixtures observed *via* TLC as ratios of amino acid to rhodamine increased. Eventually it was determined that only a slight excess of amino acid, in the region of 1.1 - 1.2 equivalents per reaction site was most effective, similar to COMU **67**.

Attention was now directed at its purification, predictably this provided its own challenges. Flash column chromatography was employed, with a broad selection of mobile phases tested. These ranged from ethyl acetate/petroleum ether to acetonitrile/DCM in an attempt to take full advantage of the elutropic series. Perturbations in the order of elution

of fractions of interest were observed upon substitution of mobile phase. Nevertheless, the complexity of the crude reaction mixture even after optimisation of workup precluded any noteworthy improvement to isolable yield.

An explanation as to the problems encountered in purification is that compound of interest appeared to be unstable on silica. Decomposition from colourless, with only a 254 nm absorbance, to fluorescent yellow under both 254 and 365 nm irradiation was observed in only minutes *via* TLC. This was initially attributed to the moderate acidity of silica, which, in the presence of a nucleophilic solvent such as methanol may promote hydrolysis. As this effect appeared most swiftly in the presence of methanol, this solvent was substituted for one less nucleophilic. The decomposition was however also noted when using other non-nucleophilic solvent combinations such as ethyl acetate/hexane, albeit more slowly. To address the apparent silica facilitated de-acylation of rhodamine, TEA treated silica and both neutral and basic alumina were employed. Confoundingly, all of these appeared to produce the same effect to a more or less of an extent. Reverse phase techniques were then tested, but even these proved no more effective at quelling the apparent decomposition. After much investigation it was found that only mild degradation was seen when using a 3:7 ethyl acetate:chloroform mobile phase on untreated silica. These conditions allowed sufficient time for isolation, while providing a favourable loading capacity.

Having optimised the coupling procedure and purification, isolated yields rose to 25 %, a more than three-fold improvement over those previously reported. As a result of this improvement, sufficient quantities for continuation of synthesis could now be produced, therefore the next synthetic step was addressed.

2.1.3 Completing Attachment of the Biomimetic Tripeptide

With sufficient quantities of Rho-(Arg(Cbz)₂-NH₂)₂ **69** in hand, Boc- deprotection of the parent compound was undertaken. This provided the di-amine Rho-(Arg(Cbz)₂-NH₂)₂ **75** for the next stage of synthesis, coupling of **75** to Boc-NH-Val-Pro-OH **76**. HATU **74** was

utilised with the optimised solution phase coupling procedure to generate Rho-(Arg(Cbz)₂-Pro-Val-NH-Boc)₂ **77**.

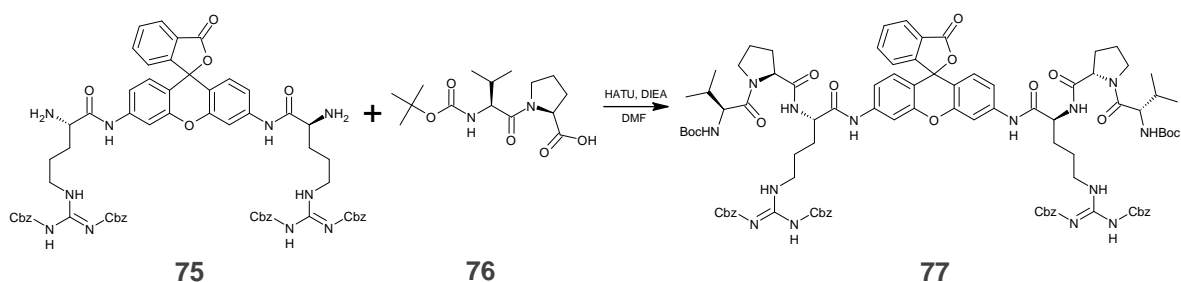


Figure 39. Coupling of Rhodamine-(Arg(Cbz)₂-NH₂)₂ **75** to Boc-Val-Pro-OH **76** mediated by HATU **74**, to produce Rhodamine-(Arg(Cbz)₂-Pro-Val-NHBoc)₂ **77**.

This was achieved in consistently good yields of around 67 %. It was once again noted that the compound decomposed on silica similar to that seen with the parent compound Rho-(Arg(Cbz)₂-NHBoc)₂ **69**. As the current intermediate was of large molecular weight, a high polarity mobile phase was required for purification. To address this, as well as provide sufficient resolution, methanol/DCM mixtures were initially employed. These were found to be of limited use due to significant and rapid decomposition. After a number of TLC trials, it was determined that a pure ethyl acetate mobile phase provided sufficient polarity for separation, while minimising said decomposition. Employment of this mobile phase allowed sufficient quantities of the product Rho-(Arg(Cbz)₂-Pro-Val-NHBoc)₂ **77** to be isolated effectively. An optimised synthetic route to the precursor **77** of the active LGX compound **61** had now been established, with improvements to both simplicity of synthesis and isolated yields. These improvements would facilitate further up scaling of production of the protected LGX precursor **77** in a proposed future industrial setting. Quantities of said precursor **77** could therefore be produced and stored in the desirable inactive form. Then, in theory when required, the less stable active compound **61** may simply be generated through Cbz- deprotection, needing no further purification!

Following the successful synthesis of the active compound precursor, efforts were turned toward an efficient deprotection strategy. Conditions for guanidine Cbz deprotection of the Rho-(Arg(Cbz)₂-Pro-Val-NHBoc)₂ **77** were employed in light of the near quantitative

yields previously reported.⁷⁰ Initial tests used the same 5 % Pd/C under one atmosphere hydrogen pressure. Deprotection was indicated to have occurred over a 24 hour period through TLC analysis, the result of which was a baseline spot. Removal of the catalyst was achieved *via* filtration through a celite bed, leaving what appeared to be the pure compound in near quantitative yields. Analysis *via* ¹H- NMR spectroscopy showed the disappearance of the Cbz- aromatic proton signals around 7.1 ppm as well as complete disappearance of the associated benzyl protons at 5.1 ppm. This provided good confirmation as to the successful Cbz- deprotection of guanidine's side chains.

The *S. aureus* probe LGX was then constituted in the manner previously reported, using the freshly synthesised Rho-(Arg-Pro-Val-NHBoc)₂ **61**.⁷⁰ It was then tested on coagulase positive *S. aureus* in order to ensure its activity and reproducibility when compared to previous studies.⁷⁰ Bewilderingly, no fluorescence response was observed when these tests were carried out, even when the bacterial concentration was vastly increased in the test cultures. Further batches of the bacterial culture were tested as well as newly synthesised active compound, all of which yielded the same result. After eradication of the possibility of a problem with the bacteria, it became clear that there was a problem with the LGX.

Exhaustive examination of ¹H-NMR spectra of the newly synthesised batch of Rho-(Arg-Pro-Val-NHBoc)₂ **61**, and comparison to the active LGX reported by the Le Gresley lab showed one slight difference which had so far gone un-noticed. A singlet proton signal had appeared at around 6 ppm, this transformation had not been previously been observed and hence overlooked as a slight impurity picked up from celite or another source. Mass spectrometry was employed in order to further investigate what this new signal could correspond to. The result was a molecular ion peak two Daltons heavier than that expected from the active compound, once again easily overlooked and attributable to proton capture during ionisation in MS. This information when combined with the

additional proton peak observed at around 6 ppm, and the general downfield shift in the aromatic region signified a structural change previously unobserved.

Considering the resonance region in the spectrum in which this new signal resided, it was rationalised to be unlikely to correspond to a shifted aromatic signal. The region in which it was found did however permit a strongly deshielded benzylic proton. Examination of the COSY spectrum also confirmed no short-range coupling, as would be expected of such a proton. It was subsequently inferred that hydrogenation had occurred simultaneously on the upper benzylic position while undergoing Cbz- deprotection. The two Dalton increase in mass was also explained by addition of two hydrogens, one at the benzyl position and one on the upper carboxylic acid. This was also the reason as to why when testing the newly made compound no fluorescence response was observed. It is well known that rhodamines, when reduced at the benzylic position are non-fluorescent due to breakdown of molecular conjugation. This further confirmed the credibility of the described structural change in the compound. Nevertheless, it did not explain why the exact same hydrogenation conditions previously used for Cbz- deprotection were now causing over hydrogenation and consequent inactivation of the compound. One further mystifying point was the exact same batch of Pd/C was used for deprotection, even coming from the same jar.

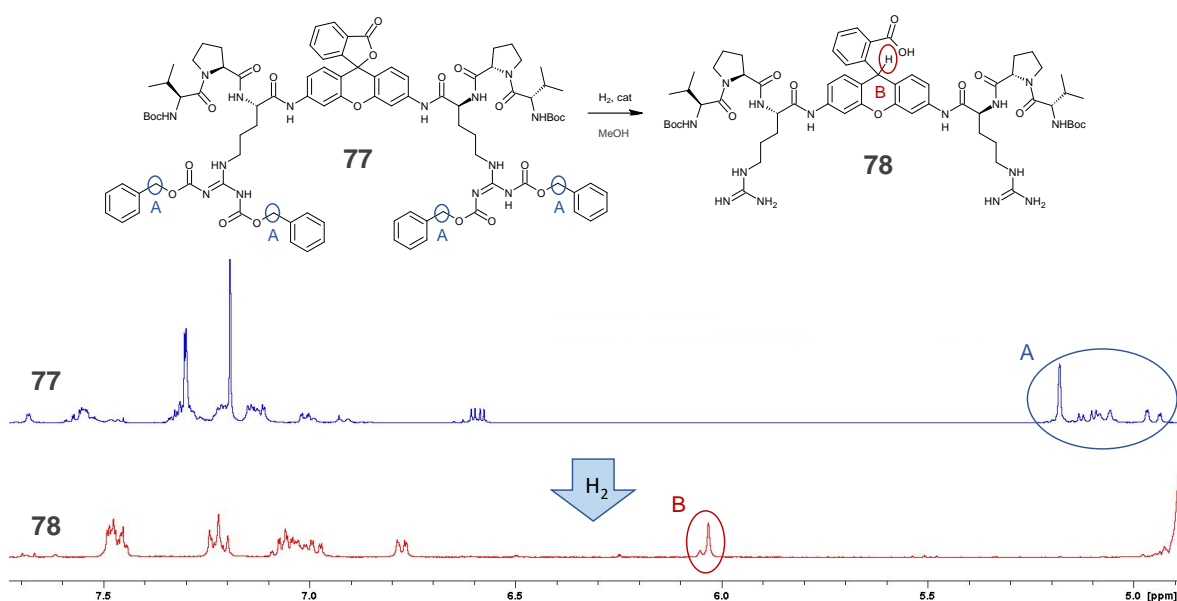


Figure 40. Proton NMR spectrum of the Cbz- protected LGX precursor **77** compared to the reduced LGX **78**. Note the complete disappearance of the benzyl signals (A) signifying Cbz-deprotection along with the appearance of the benzyl proton signal (B) at around 6 ppm.

2.1.4 The Hydrogenation Problem

Following conclusive identification of the cause of inactivity of the newly synthesised compound **78**, focus was directed toward overcoming it. Exhaustive testing of hydrogenation conditions were undertaken in an attempt to increase the selectivity of the hydrogenation. Attempts were made to remove only the Cbz- protection while leaving the upper benzylic lactone intact, as it is crucial for activity.

Initial testing varied the stoichiometry of the catalyst as well as solvent choice. Monitoring *via* TLC and NMR proved this to be ineffective, with over hydrogenation of the crucial upper lactone ring prevailing in all instances. Subsequent variations in catalyst loadings were also tested, as well as reduction in hydrogen pressure from one atmosphere to simply charging the catalyst with hydrogen and running the reaction under nitrogen in an attempt to limit the available hydrogen. This was again met with similar results. The central lactone being reduced faster than global Cbz- deprotection was now becoming increasingly probable. With this in mind, coupled with the expense and tedious nature of preparing the LGX precursor **77** and then wasting it, the decision was made that material

must be conserved and a more thorough approach adopted. Employment of sensitive autoclave equipment was deemed the only realistic option as this could provide a stoichiometric quantity of hydrogen, just enough to deprotect the guanidine groups in theory leaving the crucial functionality untouched. In the absence of such equipment, Peakdale Molecular were instructed to exhaustively test hydrogenation conditions, which they did.

Conditions	Result
Pd/C (Kingston) and PtO ₂ , 1 atm H ₂ , EtOH, 16 h	Complete conversion to 77
PtO ₂ , 1 atm H ₂ , EtOH, 16 h	78 + intermediates with some Cbz intact
Pd/C (Kingston), 1 atm H ₂ , EtOH, 16 h	78 + intermediates with some Cbz intact
Pd/C (Kingston), 1 atm H ₂ , IPA, 16 h	Mainly single Cbz removed + 77
Pd/C (Kingston), 1 atm H ₂ , MeOH, DIPEA, 16 h	78 + intermediates with some Cbz intact
Pd/C (Peakdale), 1 atm H ₂ , THF, 16 h	Mainly single Cbz removed + 77
Pd/C, 1 atm H ₂ , MeOH, RT, 24 h	Mainly 78 observed
Pd/C 1 atm H ₂ , IMS, RT, >5 days	Mainly 78 observed
Pd/C, 30 bar H ₂ , MeOH, RT, 24 h	Mainly 78 observed
Pd/C, 30 bar H ₂ , IMS, RT, >5 days	Mainly 78 observed
1 % Pd/C, 1 atm H ₂ , MeOH, RT, 3 days	Mainly 78 observed
1 % Pd/C, 1 atm H ₂ , 1:1 IMS-AcOH	Incomplete after 2 days. Intermediates observed indicated ring opened material

Table 4. Hydrogenation conditions tested for selective deprotection of LGX precursor **77**.

A multitude of deprotection conditions were screened as shown in Table 4. It was determined that LGX precursor Rho-(Arg(Cbz)₂-Pro-Val-NHBoc)₂ **77** could not be selectively deprotected under standard or non-standard hydrogenation conditions as evidenced in their report, the results of which are included in Table 4. Indeed, the rate of hydrogenation of the central benzyl ester was proven to be greater for Rho-(Arg(Cbz)₂-Pro-Val-NHBoc)₂ **77** than the rate of loss of Cbz- protection.⁶⁹ Moreover, analogous cyclic benzyl esters in the form of phthalides have been shown to be highly prone to reduction

under countless hydrogenation conditions, resulting in cleavage and saturation comparable to that observed.¹⁴⁸

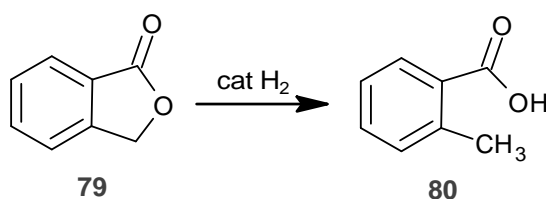


Figure 41. Catalytic hydrogenation of the analogous phthalide ring system **79** results in cleavage to **80**, similar to that observed with our rhodamine 110 **7** based probe.

Production of the LGX **61** probe for use in both clinical and non-clinical environments relies on the specificity of the final Cbz- deprotection step. The same specificity is also required for generation of other rhodamine-based protease probes containing Cbz-protected functionality. This is because non-specific deprotection renders the probe inactive as the reduced rhodamine core is non-fluorescent, as was observed. Exposure to the target protease and subsequent cleavage therefore liberates a non-fluorescent molecule, rendering the probe ineffective.

2.1.5 Overcoming the Hydrogenation Problem

Despite exhaustive testing of hydrogenation conditions, it was not to be possible to preserve the upper lactone while removing the Cbz- protection during scale up. In view of this, an alternative approach was adopted. If loss of the lactone is unavoidable, would it be possible to selectively reform the required functionality through subsequent oxidation (Figure 42)?

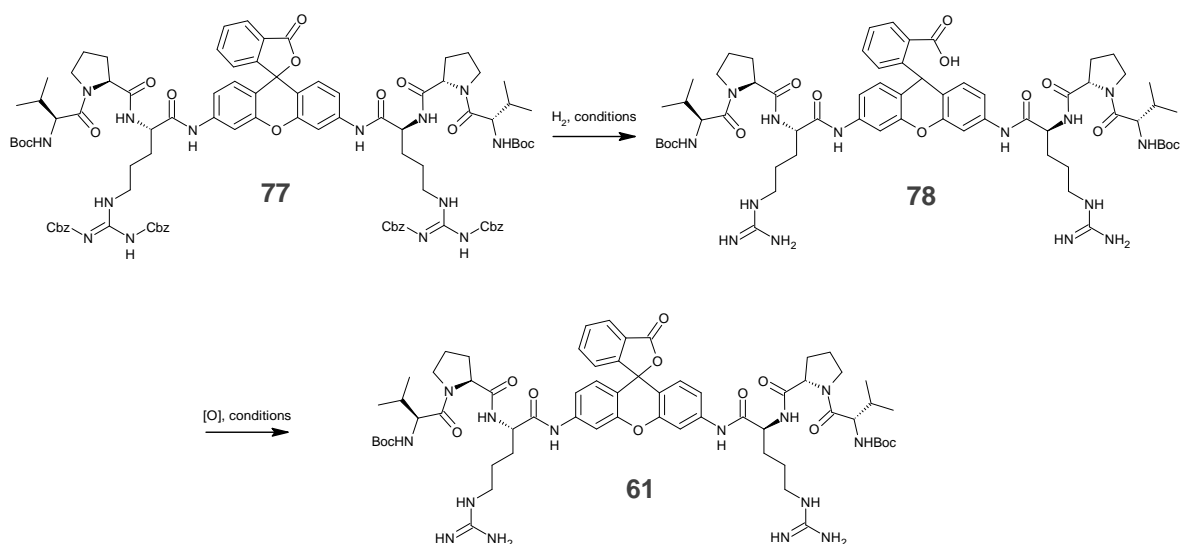


Figure 42. Modified scheme adopted in order to produce LGX in its active form **61**.

Examination of the literature provided information on the ability of dihydro rhodamine 110 **81** (and others) to act as an intracellular oxidant sensors in tissues such as tumour cells. These dihydorhodamines are, in their reduced form, both colourless and non-fluorescent. However, when exposed to intracellular reactive oxidant species, they are oxidised to their coloured fluorescent forms. This produces a fluorescence contrast change signalling a positive test result.¹⁴⁹

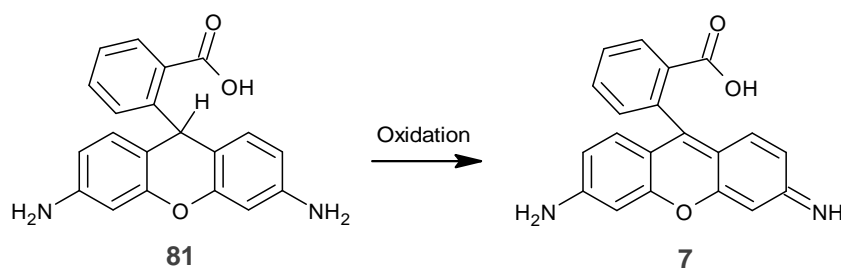


Figure 43. Non-fluorescent dihydro rhodamine 110 **81** converts into fluorescent rhodamine 110 **7** upon exposure to reactive oxygen species to form a fluorogenic intercellular probe.

With this transformation in mind, it was attempted to apply it to the reduced LGX probe **78** in order to test if selective oxidation was achievable. Oxidation of our probe by peroxide or similar species commonly targeted by dihydro rhodamines was found to be ineffective. Additionally, such conditions had not been shown to reform the upper lactone ring, instead yielding the fluorescent open form.¹⁴⁹ Hence, a more selective reagent was sought out.

Chapter 2 – Results and Discussion

Exhaustive testing of oxidants was now undertaken in an effort to restore the crucial functionality, these are listed in Table 5 below.⁶⁹

Conditions	Result
DBU, DMF, bubbling air, 3 h	No reaction
H ₂ O ₂ , 3 h	No reaction
PhI(OAc) ₂ , KBr, DMF, 16 h	No 78 or desired product observed. LCMS showed no significant mass.
PhI(OAc) ₂ , KBr, DCM, 16 h	No 78 or desired product observed. LCMS showed no significant mass. ¹ H NMR showed slight shift in “benzylic proton”
1 M NaOH, MeOH, 16 h	78 + more polar product with no significant mass associated with it
PtO ₂ , EtOH, 6 h	No reaction
Pd/C, IMS, 16 h	No reaction
DDQ, MeOH, 16 h	No reaction, Tentative 61 at high excess
DDQ, DMSO, 16 h	Mainly 78 and DDQ by products. Possible product mass in LCMS, but peak associated comes off in wash
DDQ, DMF, 16 h	Mainly 78 and DDQ by products. Possible product mass in LCMS, but peak associated comes off in wash
DDQ, DCM/H ₂ O 9:1, 16 h	No reaction – insoluble
DDQ, MeCN/MeOH 9:1, 16 h	No reaction
MnO ₂ , MeOH, 16 h	No reaction

Table 5. Oxidising conditions tested in order to re-form crucial functionality in LGX probe.

After testing numerous oxidants and conditions, 2,3-dichloro-5,6-dicyano-1,4-benzoquinone (DDQ) appeared to show promise. It is noted for its oxidative coupling ability, and so a further test reaction was set up. Dissolution of the inactive product in MeOD with excess DDQ allowed reaction progress to be monitored by proton NMR at 60 second intervals. Delightfully, regeneration of the lactone functionality was implied through disappearance of the offending benzylic proton signal at around 6 ppm. Optimisation of this oxidation method followed, it was then applied to the bulk of the reduced probe.

Restoration of the crucial functionality was found to be successful by application of this method. The result was completion of a successfully scaled up synthesis of LGX **61**, using the optimised 8 equivalents of DDQ in methanol. Under these conditions it was possible to re-form the central lactone of the rhodamine core to yield the active compound while leaving the peptide side chains intact. The yield of this reaction was high (83 %) and the correct structure was verified by both NMR and HR MS, with successful cross referencing to previous data on the active compound.⁷⁰

Having successfully solved the LGX over hydrogenation problem *via* DDQ re-oxidation to restore the critical functionality, the synthesis of the LGX *S. aureus* probe could undergo scale up and further testing for use in healthcare and other environments. This may in future form part of an updated and ultra-fast first line of defence for the detection and control of troublesome bacterial strains, with an aim to reduce the morbidity rate of bacterial infection *via* accurately targeted antibiotic therapy.

2.2 Routes to Novel Fluorophores

2.2.1 Reconsidering the Order of Probe Construction

Having considered the problems associated with the scale up of the LGX probe **61**, it became apparent that the fundamental issues limiting the utility of rhodamines in this context has not been fully addressed thus far. These issues relate to the difficulty in using rhodamine-based fluorophores to generate probes. As was shown, they are not only unreactive towards derivatisation, but also prone to a multitude of side reactions resulting from their structural equilibria. This may go some way toward explaining why despite finding widespread use as fluorogenic probes, the chemistry of these is somewhat limited and has advanced little since the 1980's.¹⁵⁰ In order to improve upon and increase the usefulness of these xanthene based fluorophores, a modified approach is required. This

revised approach would attempt to reverse the order of probe construction in an effort to simplify synthesis.

As mentioned before, rhodamine 110 **7** exists in equilibrium between several forms in solution, with the conjugated lone pairs of the NH₂ groups undergoing resonance, thus reducing their availability and subsequent nucleophilicity. It was rationalised that this limitation could be overcome through reduction of some of the conjugation through removal of the top lactone aromatic (phthalide). Removal of this system should reduce the number of possible canonical forms with a consequent increase in NH₂ nucleophilicity. This would theoretically improve the efficiency of the amino acid coupling procedure, simplifying purification and improving yields. The upper lactone ring would be introduced at a later stage to complete the fluorophore core, after amino acid coupling was complete, Figure 44.

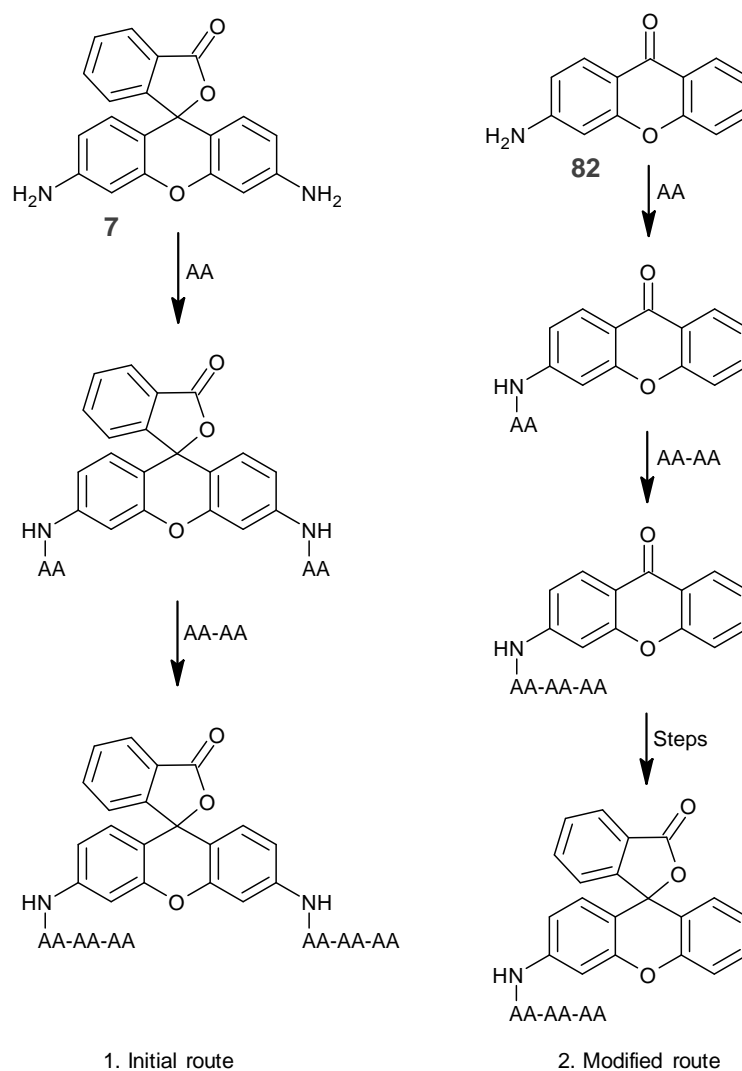


Figure 44. Modification to synthetic strategy to produce probes, amino acids (AA) will be added to a unfinished fluorophore core, after which the fluorophore will be completed.

2.2.2 Samarium Iodide

The method would commence with the synthesis of a parent xanthenone such as **82** (Figure 44), which, following addition of the amino acid chain would be modified to produce the desired rhodamine analogue. An advantage that building up the xanthenone core first provides, is that access to unsymmetrical structures is possible. This would enable not only a selection of novel unsymmetrical rhodamine analogues to be constructed, but also the probes built upon them would possess simplified kinetic profiles. This is because the previously produced LGX probe **61** contained two biomimetic arms, cleavage of the first

arm yields only the moderately fluorescent compound **83**. However, in order to display maximum fluorescence the second arm must also be cleaved to liberate rhodamine 110 **7**, (Figure 45). This leads to a more complex second order fluorescence profile with respect to the fluorophore, limiting the linear dynamic range of detection. This would complicate simple kinetic rate analysis being performed upon the microorganism of interest. However, if maximum fluorescence were achieved in but a single cleavage event, analysis could easily be performed upon the target of interest, directly correlating the rate of change of fluorescence with the rate of cleavage. This could potentially allow quantification of the microorganism, as opposed to mere detection.

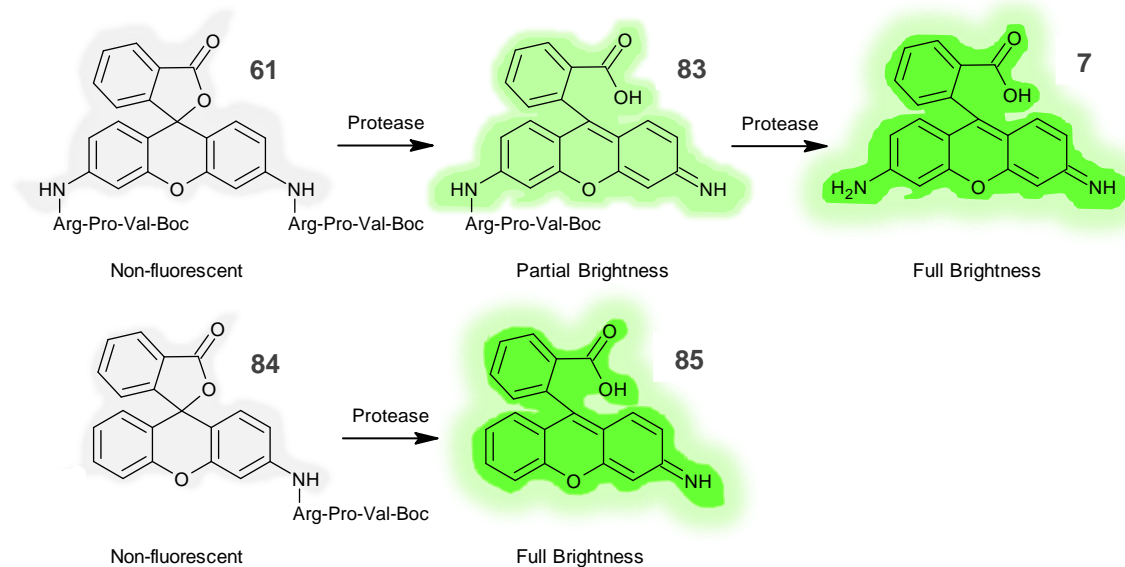


Figure 45. Symmetric **61** vs non-symmetric **84** fluorogenic probes. Symmetric varieties require two proteolysis events to achieve full brightness, non-symmetric probes require only one.

Before undertaking the new route toward un-symmetric probes, a small set of un-symmetric rhodamine analogues were prepared and tested for coupling efficiency. This was to confirm that the only logical option for improvement of coupling were to remove the aforementioned upper ring system. These were synthesised *via* the traditional route in which phthalic anhydride is condensed with various phenols in acid at high temperatures (140 °C) for extended periods (~2 days).¹⁵¹ This route, although aggressive and tedious,

did indeed allow production of various rhodamine analogues, albeit in low yields after long and difficult purifications.

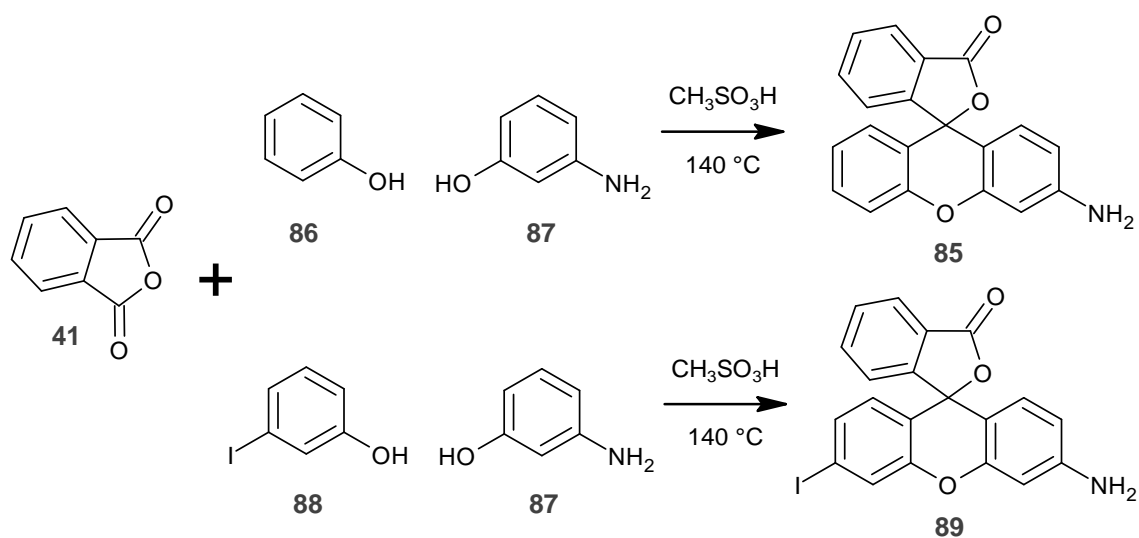


Figure 46. Traditional condensation route used for production of un-symmetric rhodamines for coupling test.

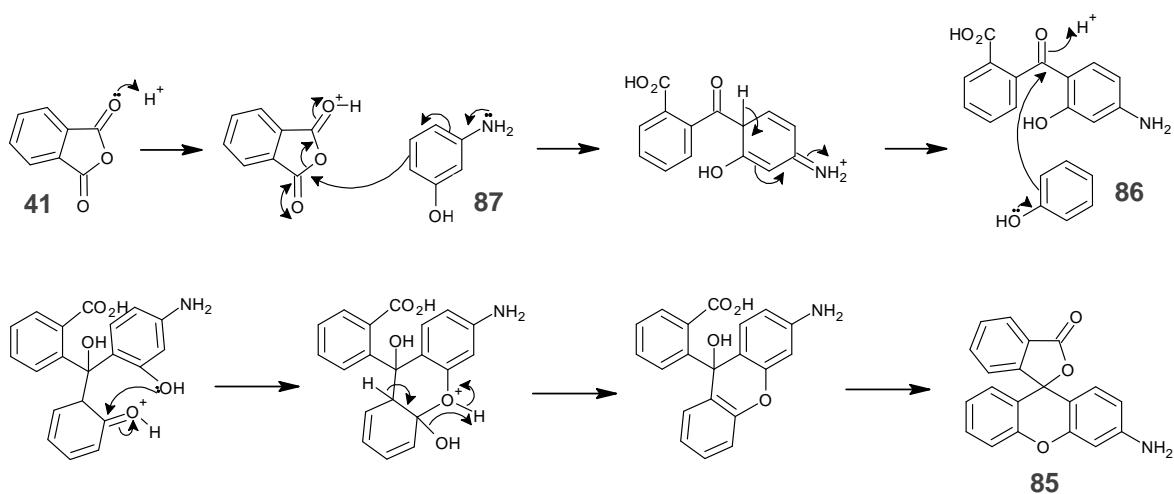


Figure 47. Condensation mechanism between phenols **86**, **87** and phthalic anhydride **41** to produce un-symmetrical rhodamine **85**.

The optimised coupling method used previously on rhodamine 110 **7** was applied to the two newly synthesised rhodamine analogues. Several HATU **74** mediated test couplings were attempted, using both mono-amino rhodamine **85** and iodorhodamine **89**. The crude reaction mixtures were examined *via* TLC and GC-MS for coupling effectiveness. The results were found to be similar to that of rhodamine 110 **7** coupling, yielding complex

near intractable mixtures. With these results in mind, our newly proposed route in which the un-symmetrical fluorophore is built up last was confirmed as the next logical next step, with other possibilities effectively ruled out.

Following the aforementioned confirmation, and with a general plan in mind, the literature was scoured for transformations that when applied to xanthone, would result in the required functionality. Before applying the new transformations to more complex xanthenes, they were trialled on the simplest unfunctionalized and commercially available xanthone core **90**. Testing of experimental conditions on this cheap and easily obtainable precursor allowed determination of transformations viable to the more complex xanthenes later on.

During our investigation, samarium diiodide (SmI_2) appeared as an interesting possibility. It was reputed to induce reductive coupling between α, β – unsaturated esters and carbonyl compounds. This resulted in production of γ – lactones in a one pot reaction, with broad scope in applicable substrates. There are numerous examples of this reagent rapidly and efficiently forming 5 – member spirocyclic ring systems like that found in rhodamine.^{152,153,154}

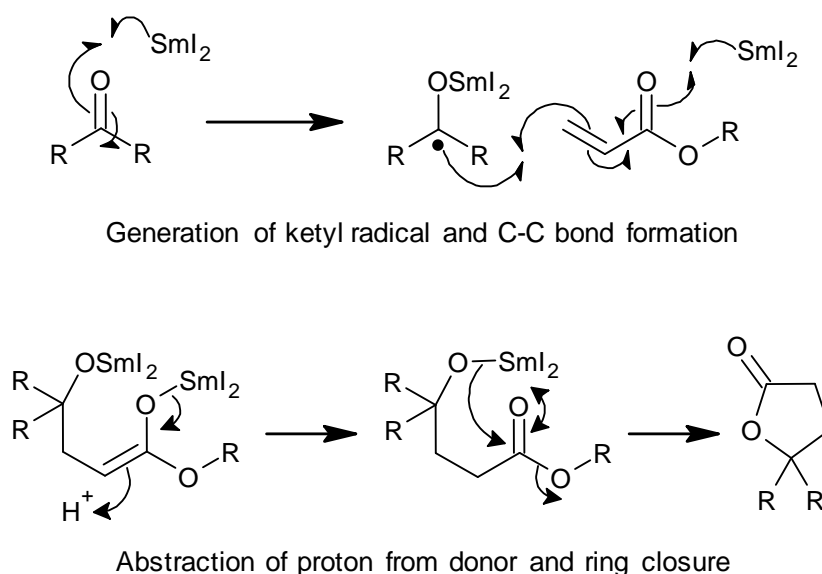


Figure 48. General mechanism of reductive coupling of a ketone with an acrylate to form a γ – lactone.

Moreover, the rapidity of many of its reactions under surprisingly mild conditions allow it to be used with high selectivity in polyfunctional systems similar those in question.

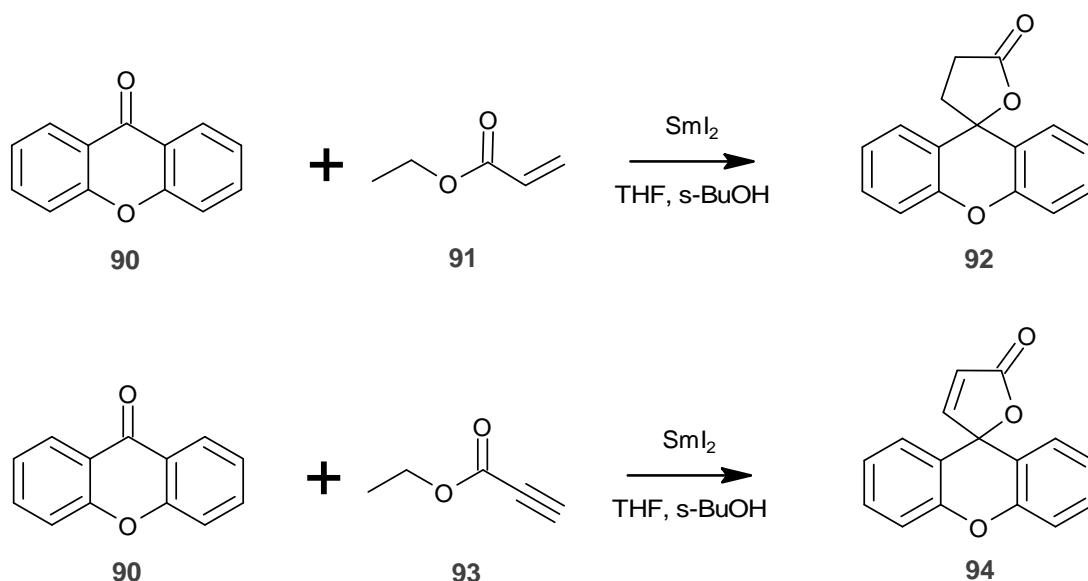


Figure 49. Reductive coupling reactions of xanthone **90** with acrylates **91** or **93** in order to build the upper lactone ring to produce structures **92** or **94** respectively.

The primary viability testing of SmI_2 was undertaken on unfunctionalized xanthone using commercially available 0.1 M SmI_2 solution obtained from Sigma-Aldrich. Initially the reaction was carried out at room temperature with a equimolar ratio of xanthone, ethyl acrylate, and the proton donor *s*-butanol, treated with 2.5 equivalents of SmI_2 . This followed the standard reductive coupling procedure.¹⁵² Reaction progress was monitored by TLC and it was noted that after four hours the reaction mixture appeared to have reached a steady state. In addition to this, a solution colour change had occurred from the deep blue indicative of SmI_2 , to the yellow of SmI_3 signifying consumption of the reagent. TLC examination of the crude indicated that xanthone **90** and acrylate **91** starting materials had not been fully consumed. Gas Chromatography-Mass Spectrometry (GC-MS) analysis of the crude reaction mixture revealed no trace of the target lactone **92**. $^1\text{H-NMR}$ analysis also showed only starting materials, again with no trace of lactone **92** formation for which two triplets were expected at around 2 and 2.7 ppm based on spectroscopic data obtained for similar spiro-lactones. With no evidence of the target molecule in four hours, reaction time was increase to 20 hours, hopefully sufficient to

produce the target. Conditions were held constant and progress was again monitored by TLC. Examination of the crude mixture after 20 hours yielded essentially the same results, tentative evidence however of a new but weak TLC spot at lower R_f was revealed after KMnO_4 visualisation. Normal workup procedure was employed after which the new TLC spot was no longer visible. Examination of the crude *via* GC-MS, ^1H , and COSY NMR provided no evidence of target molecule **92**, with only starting materials **90** and **91** were observed. The tentative evidence given by the higher polarity TLC spot which curiously disappeared after workup may imply the reaction mixture contained an unstable organo-samarium(III) compound, readily hydrolysed back to starting materials in the workup.

Given that no solid evidence of the formation of desired lactone **92** was observed for the reactions at room temperature, it was decided that it be tested at reflux. This would hopefully provide sufficient energy to overcome whatever barrier was inhibiting formation of desired lactone **92**. Even at reflux, TLC analysis after 20 hours showed incomplete consumption of the starting materials. However, in addition to the transient low R_f spot previously observed, a new higher R_f spot with strong absorption at 254 nm was seen. As target lactone **92** should be more polar than the starting materials, this new spot appeared inconsistent with the expected results, however, attention was nonetheless directed towards it. Examination of the ^1H -NMR spectrum of the crude gave no indication of the desired product **92** once again, showing only starting materials **90** and **91** and a small amount of the reduction product, xanthene **95**. It appeared that some xanthone had had the ketone group reduced to CH_2 . The condensing of the four characteristic aromatic peaks of xanthone **90** into two multiplets implied this, along with the appearance of a singlet resonance at 4 ppm courtesy of the aforementioned xanthene CH_2 . Cross reference with known data for the compound confirmed this.¹⁵⁵

As conducting the reductive coupling at reflux had still not promoted formation of the desired lactone, the number of SmI_2 equivalents was doubled to five. This attempted to address the commercially obtained SmI_2 solution being of lower concentration than that

stated, as this has been extensively stated and studied in the literature.¹⁵⁶ After 20 hours and five SmI_2 equivalents, analysis of the crude showed similar results to before, no evidence of target lactone **92**. One notable difference however was that xanthone **90** had been consumed much more significantly, with a corresponding increase in production of the reduction product, xanthene **95**.

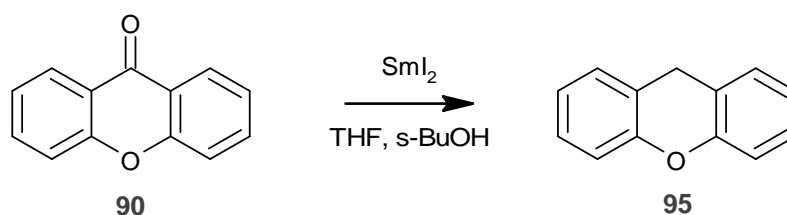


Figure 50. Samarium diiodide mediates reduction of xanthone **90** to xanthene **95** in the presence of an alcohol proton donor such as s-BuOH.

A further attempt was made to produce the lactone of interest **92**, on this occasion SmI_2 was freshly produced in house using Imamoto's method, with standardisation against a volumetric solution of ultra-pure iodine in THF.¹⁵⁷



Figure 51. Imamoto's method to prepare SmI_2 , using samarium metal and iodine.¹⁵⁷

Following standardisation to a high degree of accuracy, the fresh SmI_2 solution was used immediately for two further reactions, both at room temperature and for 20 hours, using exactly 2.5 equivalents of SmI_2 . One was performed with the s-BuOH additive, and one without, so as to be directly comparable to previous results. This ruled out the possibility of reaction failure either due to inconsistent SmI_2 stoichiometry, or inclusion of the alcohol proton donor usually required for coupling. Both reactions showed little change to that previously seen, with the crude $^1\text{H-NMRs}$ of both showing predominantly starting materials. One final reaction with only xanthone **90** and SmI_2 was undertaken to ascertain whether xanthone **90** showed any notable reactivity towards SmI_2 , this yielded only starting material **90**.

Xanthone (eq)	Acrylate (eq)	Sml ₂ (eq)	s-BuOH (eq)	t (h)	T (°C)
1	1	2.5	1	4	20
1	1	2.5	1	20	20
1	1	2.5	1	20	reflux
1	1	5.0	1	20	20
1	1	2.5	0	20	20
1	1	2.5	1	20	20
1	0	2.5	0	20	20
1	0	2.5	1	20	20
1	1	2.5	1	20	20

Table 6. Reductive coupling reactions performed with the stoichiometries of xanthone **90** and acrylate **91** and corresponding conditions.

To ensure the reductive coupling procedure actually worked and did indeed furnish the intended product, a reaction between cyclohexanone **96** and ethyl acrylate **91** with the same stoichiometries was set up. This proceeded smoothly to yield the expected spirocyclic lactone **92** in good yield, the structure of which was confirmed *via* NMR and HR MS. The success of this reaction confirmed that the Sml₂ mediated reductive coupling was incompatible with xanthone **90** and by extension the xanthone species in general. This was conceivably due to stabilisation and quenching of the ketyl radical species formed in the first step. This conjecture agreed with studies undertaken by Martinez *et al.* who's findings demonstrated that numerous xanthenes were able to efficiently deactivate free radicals. This occurred due to their high electron affinity and was shown to be especially efficient if the xanthone were in its neutral state.¹⁵⁸

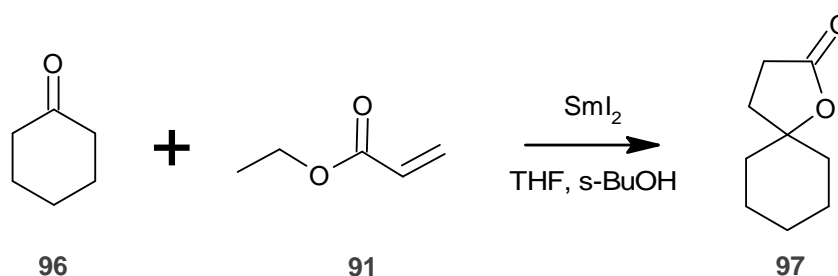


Figure 52. Samarium diiodide successfully forms the target lactone structure in the test reaction producing spiro lactone **97**.

After successfully demonstrating the incompatibility of samarium induced reductive coupling with xanthone **90**, this approach could be ruled out with confidence. The requirement for a new route was now apparent. Consequently, the literature was once again examined for transformations which would result in the required functionality.

2.2.3 Directed Metalation

The process of directed ortho metalation (Figure 53) was highlighted as one of the better-known routes towards aryl containing scaffolds, and its investigation appeared to show promise.

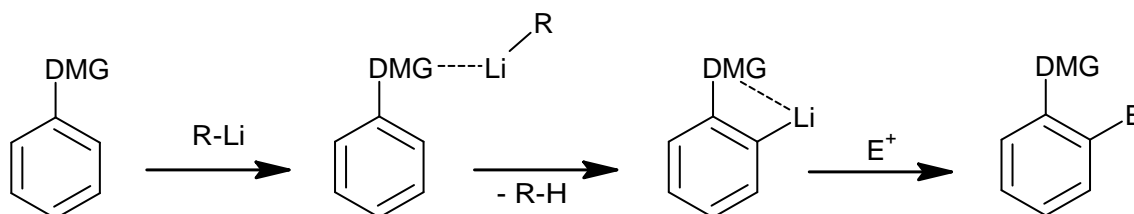


Figure 53. Metalation occurs adjacent to the Directed metalating group (DMG) due to a complex induced proximity effect. This results in coordination of the lithium species to the Lewis basic DMG producing regioselectivity in lithiation. Treatment with an electrophile E^+ then results in substitution at the lithiated position.

The Wuts group was found to have explored and successfully applied dialkyl hydrazides to directed lithiation.¹⁵⁹ The rationale behind their investigations were that amides had seen traditional use as efficient ortho metalating agents. Their limitation was that strongly acidic conditions were often required to hydrolyse the amide, subsequently cleaving other

labile groups. This had limited the applicability of such agents, especially to more delicate substrates. Therefore, as dialkylhydrazides 'look' similar to primary amides, they ought to exhibit similar ortho metalating properties, but with the added benefit of being far more labile than their amide counterparts. This meant that hydrolysis could be achieved selectively in the presence of sensitive ancillary groups, under milder conditions.¹⁵⁹

It was shown that ortho lithiation of dimethyl hydrazide could be achieved with *s*-butyl lithium (*s*-BuLi), *n*-butyl lithium on the other hand had been insufficiently basic at below -10 °C. The lithiated product was then exposed to a number of standard electrophiles, generating the free acid ortho addition product after oxidation. This was consistent with previously demonstrated directed metalation chemistry differing only by the mild nature of the oxidants required, such as CuCl₂ or H₅IO₆. Strikingly though, if the electrophile had aldehyde or ketone functionality, lactonization was often spontaneous during the workup procedure.¹⁵⁹ This would lead to a spirocyclic phthalide or aromatic lactone in the case of addition to cyclohexanone, similar to the core structure of rhodamine. By extension, if this chemistry could be applied to xanthenes, it may lead to a novel and cost-effective route to rhodamine conjugates. This could potentially facilitate the generation of novel rhodamine analogues and rhodamine-based probes.

With the hypothesis in place, attention was directed to synthesis of the directed 'lithiating' agent *N,N'*-dimethylbenzohydrazide **100**. This was initially attempted through condensation of benzoyl chloride **98** and dimethyl hydrazine **99** in the presence of triethylamine. Recrystallisation then yielded both needle like, and hexagonal prismatic crystals, the majority of which were the prismatic variety. Examination by ¹H-NMR confirmed formation of the target compound **100** as the needle like crystals, however the major product was determined to be the bis acylated compound *N*-benzoyl-*N,N'*-dimethylbenzohydrazide **101**, which was confirmed by ¹H-NMR and HR MS.

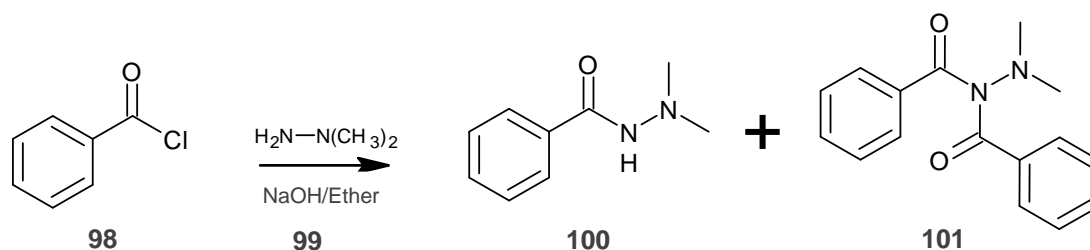


Figure 54. Benzoyl chloride **98** mediated acylation of dimethylhydrazine **99** produced both the target dimethylhydrazide product **100** and by-product **101**.

The synthesis was improved through utilisation of Schotten-Baumann conditions, employing a biphasic aqueous NaOH/diethyl ether mix at 0 °C with maintenance of a pH above 11. This method minimised the side reaction and furnished target compound **100** in vastly improved yield after a simple recrystallisation.

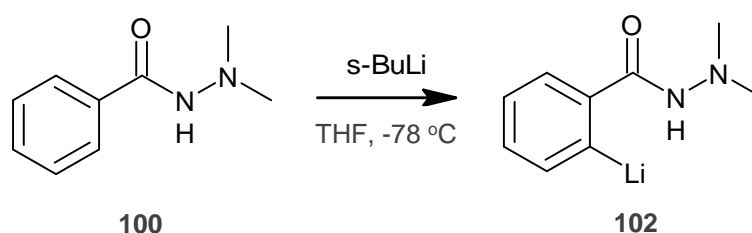


Figure 55. Treatment of the DMG *N,N'*-dimethylbenzohydrazide **100** with s-BuLi yielded lithium species **102**.

Next, lithiation of hydrazide **100** to produce lithium species **102** was achieved with s-BuLi in the presence of tetramethylethylenediamine (TMEDA), at -78 °C in 30 minutes. The resulting solution was stirred for a further 210 minutes, after which the cyclohexanone **96** substrate was added, and stirred overnight. The standard quenching and workup procedure followed, after which the crude was examined by ¹H-NMR for evidence of the target compound. NMR examination showed good evidence of the compound by examination of the aromatic region, the reaction having proceeded with satisfying efficiency. The pure compound **103** was then isolated *via* column chromatography in good yield. Further inspection showed that the spontaneous cyclisation had occurred, exclusively forming product **103**. As expected, hydrolysis of the hydrazide intermediate had taken place in the workup procedure without the need for aggressive conditions.

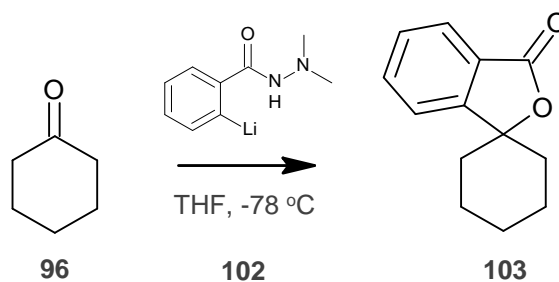


Figure 56. The target spiro-lactone **103** formed spontaneously following exposure of **96** to lithium species **102** and workup.

Having successfully confirmed that directed metalation can produce the core lactone in a single step, attention was directed towards its application to xanthone **90**.

Again, the hydrazide was generated in the same manner as before, after which xanthone **105** was added, stirred for 210 minutes and allowed to rise to room temperature. The reaction was monitored by TLC which showed a complex mixture up to and after 16 hours. The consumption of xanthone **90** was also found to be incomplete after this time. Purification of the intractable mixture was not possible using the standard workup which was previously successful. Several further attempts were made with little success, however, evidence of the product of interest was observed by LRMS. Reducing the number of xanthone **90** equivalents was found simplify the crude reaction mixture, however, the pure product remained elusive. Following confirmation of the presence of the target *via* MS, attention was turned toward the workup procedure. Eventually it was found that the target compound could be crystallised by acidification with concentrated HCl following the standard workup. Acidification appeared to have induced cyclisation of the product to produce needle like crystals of pure product. Cyclisation to form the target lactone was inferred to have probably occurred *via* a intramolecular Fischer type esterification.

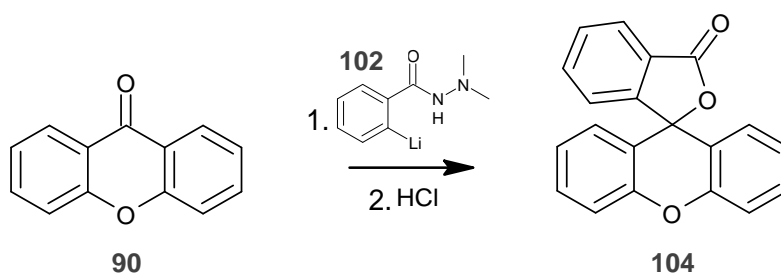


Figure 57. Formation of target product **104** following exposure to lithium species **102** and subsequent acidification with concentrated HCl.

Full spectral analysis of target compound **104** confirmed its identity, the unfunctionalized version of the rhodamine core. Examination of the literature revealed that this was a novel route to spiro[isobenzofuran-1(3H),9'-[9H]xanthen]-3-one **104**, a previously uncategorised structure. This was the first verified synthesis of compound **104** backed by a full spectroscopic dataset, (Figure 58).

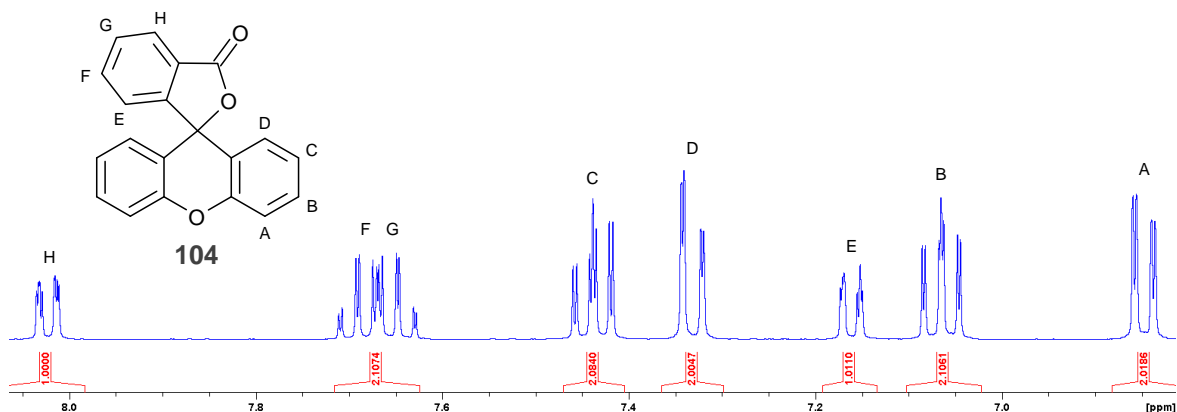


Figure 58. $^1\text{H-NMR}$ spectrum and proton assignments of spiro[isobenzofuran-1(3H),9'-[9H]xanthen]-3-one **104**, previously unreported.

After the success of the directed metalation approach in generating the core rhodamine structure **104**, the conditions would now be applied to functionalised xanthenes to ascertain if the route was compatible. Synthesis of the functionalised xanthenes was then commenced.

The synthetic methodology adopted for production of the parent xanthone was adapted from that of Young-Hoon *et al.*, the procedure was originally developed to produce a rosamine library through combinatorial synthesis.¹⁶⁰ These conditions were employed to

produce the initial 3-amino-6-nitro-xanthen-9-one **108**, which would later be modified aiming to form novel unsymmetrical rhodamine analogues.

Production of **108** commenced with an Ullmann condensation of 2-chloro-4-nitrobenzoic acid **105** with N-(3-hydroxyphenyl)acetamide **106**, requiring high temperatures and extended reaction times. The reaction pathway passes through biaryl ether **107** which was not isolated. Instead, workup in hot concentrated sulphuric acid induced secondary ring closure to yield **108** in consistent yields of 30 %.

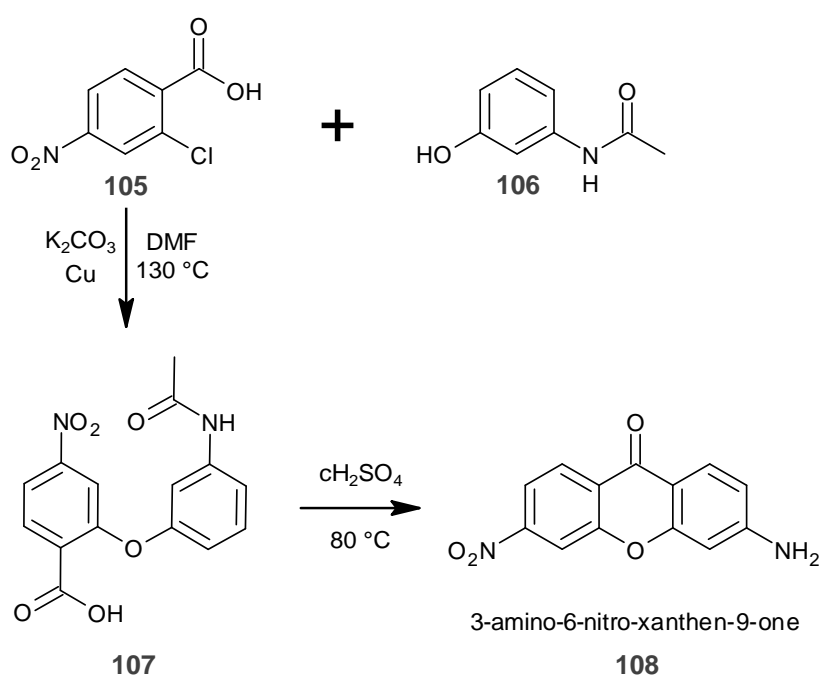


Figure 59. Synthesis of 3-amino-6-nitro-xanthen-9-one **108** via modification of A. Young-Hoon *et al*'s method.

Multiple attempts at functionalisation of the ketone group of unsymmetrical xanthenone **108** were undertaken, using lithium species **102**. These all resulted in intractable mixtures. Conceivably this was due to incompatibility with the nitro amino arrangement alongside the highly basic nature of the organo-lithium nucleophile. Further examination yielded no evidence to the formation of the target compound *via* LRMS.

2.2.4 The Grignard Approach

Following determination that functionalised xanthone **108** was incompatible with the organo-lithium reagent **102**, its less aggressive organo-magnesium Grignard counterparts were tested. If this approach were successful, acylation of the NH_2 of **108** with an appropriately protected amino acid such as $\text{BocNH-Arg}(\text{Cbz})_2\text{-OH}$ **68** to give an acylated rhodamine precursor would be the next step. An attempt at introduction of the lactone to the acylated xanthone would follow this, which, if successful would signal an initial success of this route.

In order to determine compatibility of Grignard reagents with the xanthenes, a test reaction of phenylmagnesium bromide **109** on xanthone **90** was carried out with success, to yield tertiary alcohol **110**, confirmed by MS.

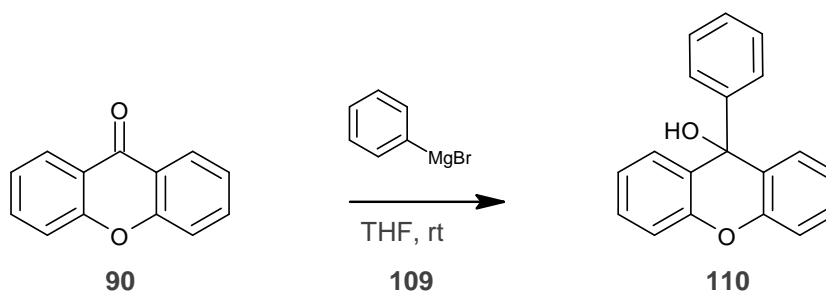


Figure 60. Successful formation of tertiary alcohol 9-phenyl-9H-xanthen-9-ol **110** through exposure of xanthone **90** to phenylmagnesium bromide **109**.

Following the success, the conjecture that acetal protected Grignard reagent **111** could be exposed to xanthone **108** to produce alcohol **112** was tested. Acid hydrolysis would then follow to produce **113**, followed by oxidation to complete the upper lactone, yielding product **114**, Figure 61.

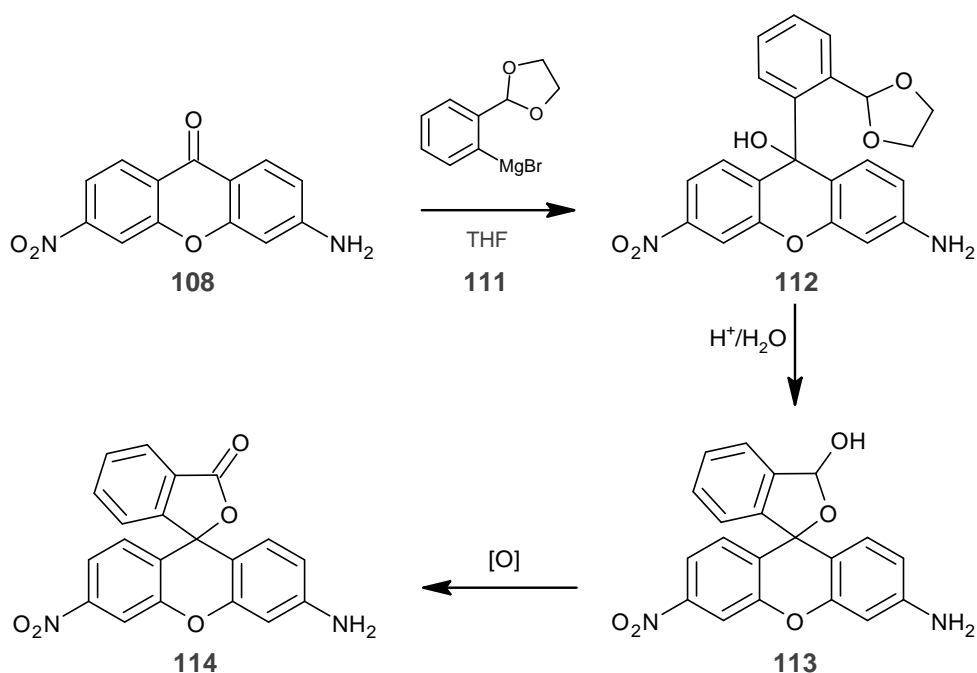


Figure 61. Proposed incorporation of upper ring by Grignard addition, followed by mild oxidation.

Several attempts at the first step of incorporation of the upper lactone to form intermediate **112** by Grignard addition of **111** to **108** were met with little success. Examination of the crude mixtures showed no evidence of the product *via* NMR or MS. A complex intractable mixture which rapidly became purple was instead produced in all cases. The synthetic attempts and their associated stoichiometries are included below (Table 7).

Grignard (eq)	Xanthone (eq)	Reaction time (h)
1.1	1	4
2	1	4
3	1	4
4	1	4
5	1	4
1.1	1	20
2	1	20
3	1	20
4	1	20
5	1	20

Table 7. Reaction timings and equivalencies of Grignard **111** exposed to xanthone **108**.

The surprising lack of success of the Grignard reaction, alongside the striking colour change warranted further investigation. Upon which the Bartoli indole synthesis reaction was uncovered.¹⁶¹ This synthesis described the reaction of Grignard reagents with aryl nitro compounds to yield indoles, thus demonstrating the reactivity of these toward such reagents. It was inferred that Indole formation *via* the Bartoli route was causing the issues we encountered, however their formation was not explicitly confirmed *via* spectroscopic means. This, coupled with the characteristically purple colour of many indole analogues was deemed an adequate explanation in this instance. It is likely that attack on the deactivated ketone group of xanthone **108** is slower than on the nitro group, further highlighting their incompatibility. The ketone group in our xanthone **108** also suffers from deactivation through conjugation into the flanking aromatics. This is in part due to the contribution of the tautomeric imine form it is able to adopt, which further reduces the electrophilicity of the ketone group. Extra stabilisation of this form is conferred by the extended conjugation gained over the entirety of the planar molecule, increasing its favourability. As further confirmation of the imino contribution, examination of the Infra-red spectrum of **108** showed a markedly decreased carbonyl band intensity to that which would be expected.

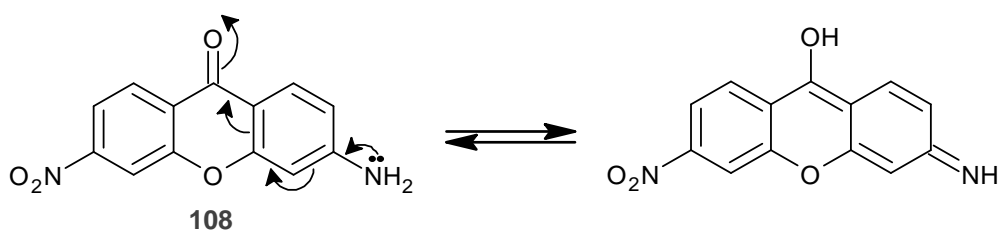


Figure 62. Tautomerism of 3-amino-6-nitro-xanthen-9-one **108** between the keto (left), and the imino (right) forms.

Having experienced a few setbacks in the pursuit of constructing rhodamine cores as a result of chemical incompatibility, the literature was again scoured. Interestingly it was found that analogous fluorophores could be constructed without the need for the upper lactone. This could reduce the number of possible side reactions through removal of the

upper carboxylic acid group as well as eliminating the open close equilibrium, which contributed to the lack of aniline group nucleophilicity.

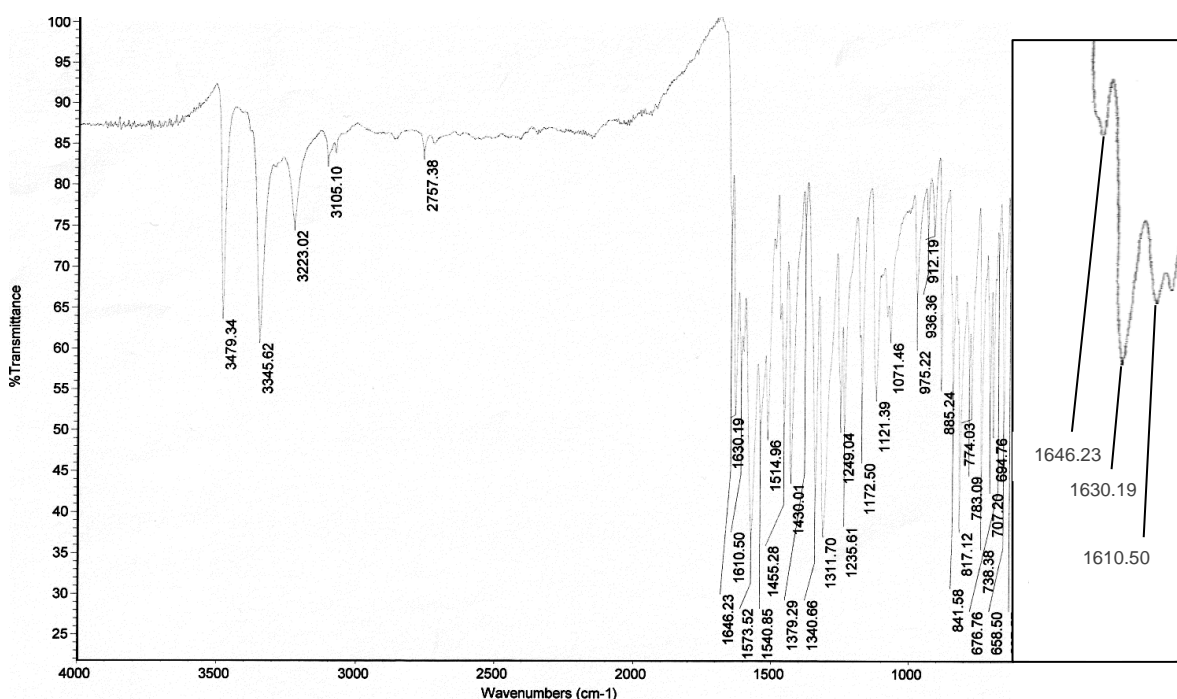


Figure 63. Infra-red spectrum of 3-amino-6-nitro-xanthen-9-one, compound **108**, weak carbonyl band expanded for clarity.

2.2.5 Simplified Fluorophores

The specific mechanism controlling the fluorescence in rhodamines and fluoresceins had been unclear for a long period, largely ignored with only empirical observations contributing to its understanding.¹⁶² Published research had shown that the upper carboxyl group involved in lactonization was indispensable for fluorescence, as its removal resulted in a sharp reduction in fluorescence quantum yield.¹⁶³ Later on however, it was proven that the carboxyl group played no part in the fluorescence properties, it merely acted as a steric barrier to force the upper ring to orientate itself orthogonally to the lower xanthen system and restrict rotation. In the case of fluorescein **6**, this supposed indispensability was countered through demonstration *via* replacement of the upper carboxyl group with a methyl group. This produced a new fluorescein analogue coined 2-Me Tokyo Green **115** (Figure 65), which had a near identical fluorescence quantum yield, absorbance and

emission maxima to fluorescein **6**. Furthermore, it demonstrated that even the small methyl group provided a sufficient rotational steric barrier to induce orthogonality, paving the way for the creation of additional analogues.¹⁶⁴

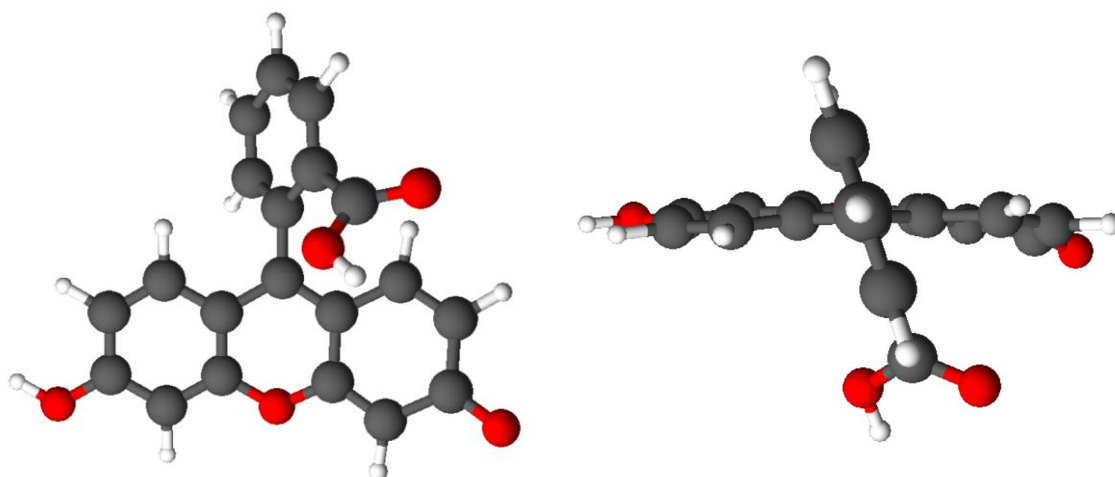


Figure 64. Fluorescein **6**, front view (left) and top down view (right). The carboxyl group acts only to provide a rotational steric barrier to the top ring system rendering it orthogonal to the lower xanthene rings. The carboxyl is therefore not essential for strong fluorescence and may be substituted with another sufficiently bulky group.

The research into Tokyo Greens also revealed that the fluorescence quantum yield of that class of fluorophores was directly dependent on the electron density of the upper ring system.¹⁶⁴ It was shown that as electron density in the upper ring increased, the quantum yield decreased down to a point at which essentially no fluorescence was visually observable. Fluoresceins and Tokyo Greens were described as directly linked donor-acceptor systems, in which Photoinduced electron Transfer (PeT) determined their quantum efficiency of fluorescence. As electron density in the upper ring increased, so did the rate of PeT, progressively quenching fluorescence and reducing quantum yield.¹⁶⁴ This quenching mechanism was in addition to that observed upon acylation of the hydroxyl groups, the basis for the on/off fluorescence exploited in fluorescent probes. This second quenching mechanism (also observed for NH_2 acylation in rhodamines) not only reduces the hydroxyl lone pair donation into the main body of the fluorophore, but also

locks the molecule into the lactone form, disrupting molecular conjugation. Breaking of molecular conjugation in the Tokyo Greens cannot happen in this manner due to lack of the upper carboxylic acid group. Therefore the quenching mechanism when acylated is due in part to reduction in back donation of hydroxyl lone pairs (NH_2 lone pairs in rhodamines), sometimes referred to as the push/pull effect. Further quenching is endowed though the ability to shed additional energy through the increase in vibrational deactivation. This results from the improved vibrational freedom imbued by additional lower ring-bound functionality.

2.3 The Singapore Green Fluorophore

2.3.1 *Properties and Synthesis*

Inspection of the literature revealed a further related, but orphan family of fluorophore which possessed desirable characteristics. These were both an un-symmetric structure, and the lack of troublesome upper carboxylic acid group. This orphan fluorophore was coined Singapore Green (SG), and had built on the lessons learned from stripping down fluoresceins while maintaining the upper rotational steric barrier. It was a hybrid of rhodamine and Tokyo Green, possessing both an NH_2 and OMe group, the upper ring bore only a methyl group, (Figure 65). The NH_2 could act as a handle for recognition sequence attachment, while the methyl group masked OH reactivity or could be substituted for solid support attachment.¹⁶⁵ As these features were both desirable for the research, and very little investigation of this class had been undertaken, an excellent opportunity had presented itself. A library of novel analogues could be synthesised and investigated for the effect that variation of the upper ring had on spectral properties. This would indicate whether the same mechanism modulating fluorescence intensity in the Tokyo Greens also applied to the Singapore Greens. Accordingly, the most promising candidates could then be put forward for next generation probe development.

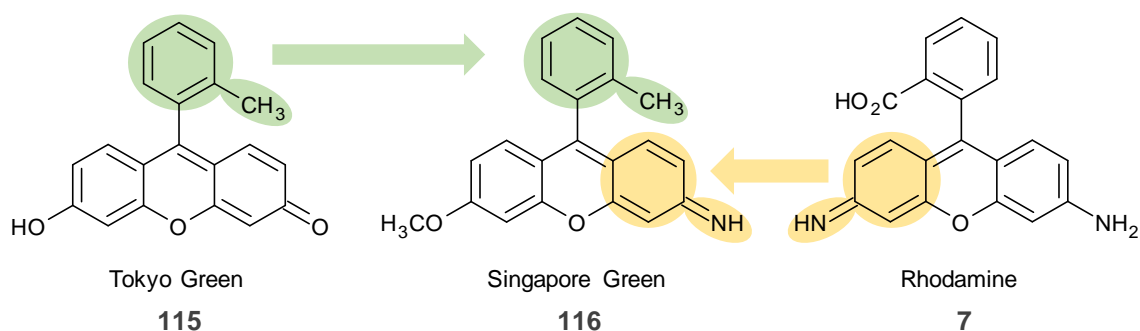


Figure 65. The Singapore Green fluorophore **116** is a structural hybrid of Tokyo Green **115** and Rhodamine **110 7**, possessing a portion of each structure as shown.

Pursuit of this route provided a synthetic advantage over the previous, particularly as the problematic upper lactone ring need not be installed. Furthermore, this approach could eliminate the problem hydrogenation of the lactone benzyl position encountered with deprotection of Cbz- groups of LGX precursor **77**. Additionally, the carboxyl group side reactions encountered during attachment of biomimetic sequences to the NH_2 would be eliminated. This would be the case whether the biomimetics were attached before the fluorophore was fully constructed as was the current strategy, or after.

Simplification of the Grignard reagents required to install the top ring system to xanthone would also be noted, as no protected carboxyl precursor is required. Selective functionalisation of the upper ring in any position to produce a single regioisomer would also be enabled. This was a considerable advantage over the traditional production method for upper ring functionalisation, shown in Figure 66. The SGs could also be constructed from the parent xanthenes which our synthetic investigations had started from. A conveniently smooth progression into their investigation was consequently possible at this stage.

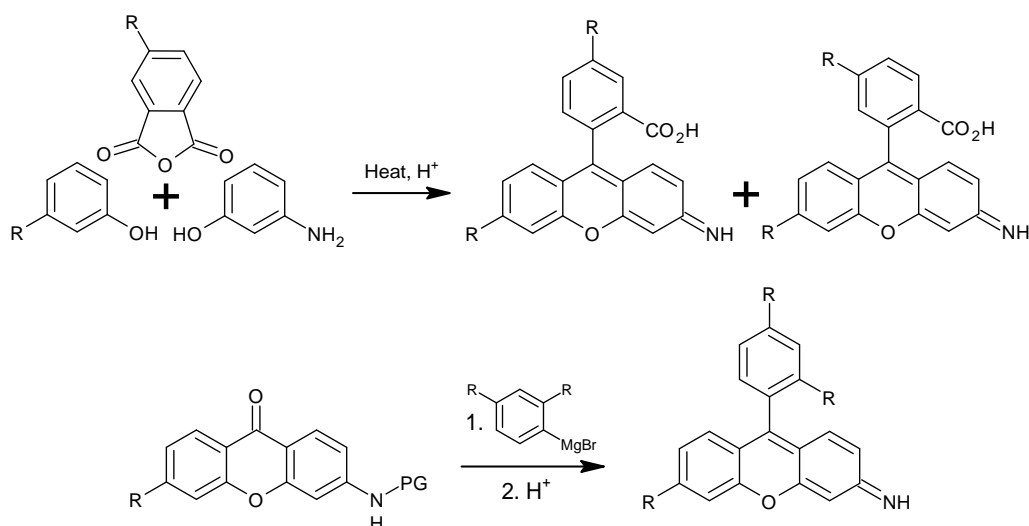


Figure 66. Condensation of a substituted phthalic anhydride to produce an upper ring substituted rhodamine analogue yields a mixture of difficult to separate isomers. A Grignard reaction installing the substituted upper ring results in only a single isomer.

With the adjusted strategy, additional elaboration to the xanthone core was undertaken to produce the modified structure from which the fluorophores would be constructed. Maintenance of the un-symmetric nature of the core was always important, as well as the need for conversion of the nitro group into a compatible functional group to avoid the problems previously noted.

Diazotization of the amine group of **108** followed by quenching in hot water yielded the hydroxy derivative 3-hydroxy-6-nitro-xanthen-9-one **117** in near quantitative yield without the need for further purification. Alkylation of the hydroxyl group of **117** followed this, facilitated by iodomethane. The product 3-methoxy-6-nitro-xanthen-9-one **118** was produced efficiently and in excellent yield, again without requiring further purification.

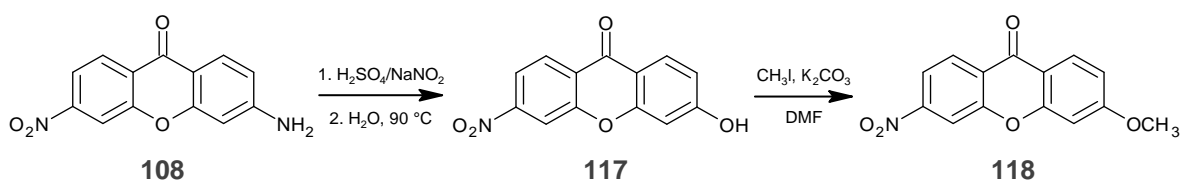


Figure 67. Conversion of 3-amino-6-nitro-xanthen-9-one **108** to 3-methoxy-6-nitro-xanthen-9-one **118** via diazotisation, hydrolysis and subsequent alkylation.

Following alkylation of the hydroxyl group to produce **118**, attention was turned to providing the handle for attachment of a biomimetic or recognition sequence. Reduction of the nitro group of **118** with tin(II)chloride afforded the required amino derivative, 3-amino-6-methoxy-xanthen-9-one **119** in quantitative yield, yet again without purification.

With the xanthenone **119** which the fluorophores would be constructed from in hand, protection of the NH_2 group was the undertaken. This was achieved using the acid labile trityl group, attached effectively using trityl chloride in 60 minutes, purification by precipitation in a large volume of hexane yielded pure product **120**.

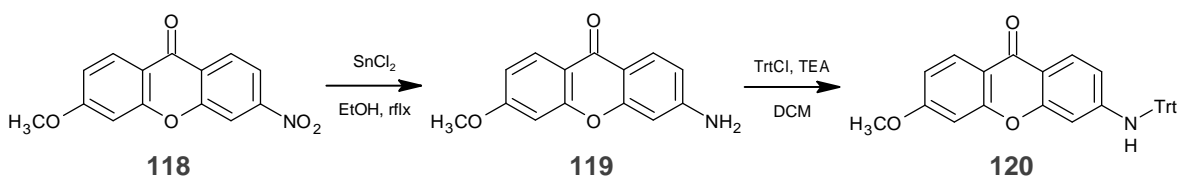


Figure 68. Conversion of 3-methoxy-6-nitro-xanthen-9-one **118** to 3-amino-6-methoxy-xanthen-9-one **119** via reduction and subsequent trityl protection to yield **120**.

With the protected xanthenone **120** ready, the Grignard addition of **121** followed reproducing the orphan fluorophore Singapore Green (SG1, **116**), the first step into the investigation of this novel class. This part of the synthesis was performed in accordance with the published procedure to ensure its applicability.¹⁶⁵

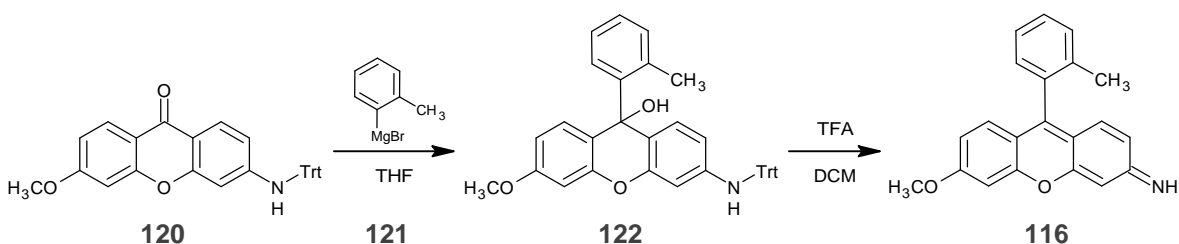


Figure 69. Conversion of xanthenone **120** to SG1 **116** via addition of Grignard reagent **121**, followed by acidic deprotection and dehydration of intermediate **122**.

Commercially obtained Grignard reagent **121** was introduced into a THF solution of protected xanthenone **120** at room temperature, then refluxed for 16 hours, TLC examination followed. A further portion of the Grignard was then added as starting material **120** was still strongly apparent in the TLC, indicating its low reactivity. Further investigation of the

TLC revealed a strongly fluorescent high polarity component which appeared after several seconds. As none of the reaction products were expected to be so fluorescent at this stage, it was reasoned that the silica of the TLC plate had catalysed deprotection and dehydration to form the fluorescent SG1 **116**. Reflux for a further 16 hours followed the second Grignard addition. Further TLC analysis revealed that the starting material had been more thoroughly consumed at this point, although total consumption had not occurred.

Following quenching and workup, purification was attempted on tertiary alcohol **122**. Gradient column chromatography using a 0 - 10 % MeOH/DCM mobile phase led to significant streaking, converse to that detailed in the literature.¹⁶⁵ It was determined that deprotection and dehydration were occurring *in situ* leading to variable rates of elution for the same components, confounding purification. It is notable that the literature cites no spectroscopic evidence whatsoever for isolation of the tertiary alcohol intermediate, likely for the same reason mentioned here.¹⁶⁵ Although the trityl group is normally expected to survive silica chromatography, in this case a significant increase in conjugation throughout the molecule is gained upon dehydration. There is also an increase in steric crowding associated with conversion of the trityl protected amine to an imine following dehydration (Figure 70). It is conceivable that this increased the acid lability of the trityl group sufficiently to allow deprotection on silica, going some way toward explaining this observation.

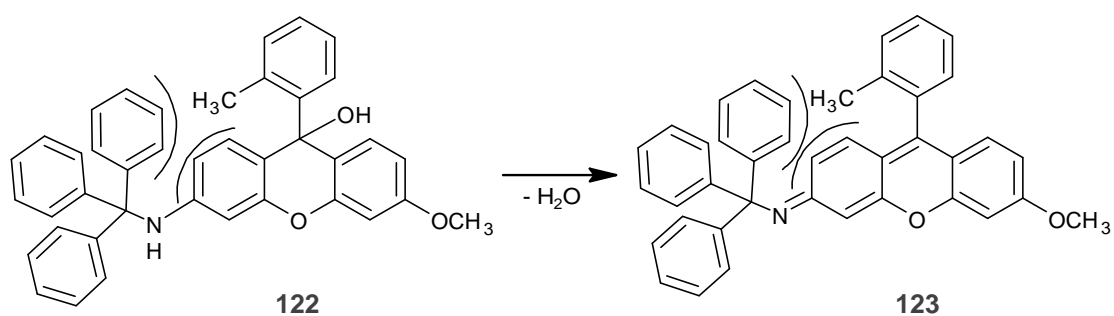


Figure 70. Dehydration of **122** with concurrent imine formation results in decreased bond length and increased steric clash between the trityl group and the xanthone rings in **123**.

After concluding that deprotection and dehydration were occurring on the column and at variable points, it was decided that the best course of action would be to fully deprotect the crude and purify the final product in one step. This was achieved in the traditional way using trifluoroacetic acid in DCM, after which the same purification conditions were successful. This confirmed the method to produce the highly fluorescent Singapore Green, SG1 116.

2.3.2 Synthesis of a Novel Singapore Green Library

With a working method to produce new fluorophores, generation of a selection of novel analogues was the next course of action. Several substituted aromatic bromides were obtained from which to generate the associated Grignard reagents. Following their generation, the protected xanthone would be exposed to form a small library of novel SGs.

The aromatic bromide 2-bromobenzotrifluoride **124** was obtained, its Grignard reagent **125** generated, and a simple test reaction on cyclohexanone **96** was run to ensure applicability. This was met with success in generation of tertiary alcohol **126**, the identity of which was confirmed spectroscopically. The same conditions were applied to generate further Grignard reagents for production of other SGs.

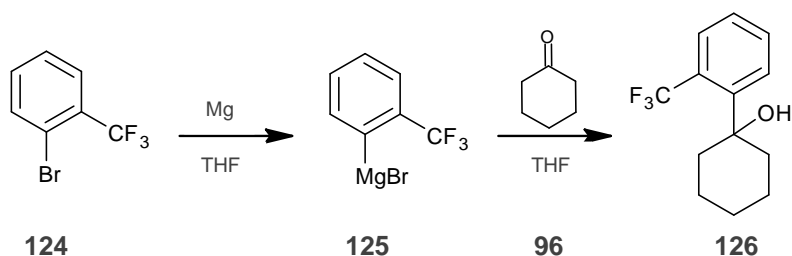


Figure 71. Test reaction to validate method of Grignard reagent generation.

The second Singapore Green (SG2 **127**, Figure 73) was generated in a similar manner to the first, using Grignard reagent **125** under the same conditions. Two additions of the reagent 16 hours apart resulted in incomplete consumption of the starting material even under reflux, further confirming the lack of electrophilicity of the parent xanthone.

Quenching, workup and trityl deprotection yielded the crude fluorophore which was then purified in the same manner as SG1 **116**. The product isolated was the novel fluorophore SG2 **127**, the first accompaniment to the orphan SG1 **116** in this class.

To improve yields and simplify handling of the precursor, a solid supported strategy was adopted. Polymer bound 2-chlorotrityl chloride resin was chosen as the solid support as a result of its simplicity of use and applicability to protection of the NH₂ group of xanthone **119**. A 2-chlorotrityl chloride resin of 1.6 mmol/g loading, 100 – 200 mesh, 1 % DVB crosslinked was used for support.

Loading of the resin was achieved using a stoichiometric quantity of xanthone **120** with respect to resin binding sites. This was performed in the presence of 10 equivalents of pyridine base and in accordance with published procedure.¹⁶⁰ The binding mixture was agitated for 24 hours in freshly silyl protected solid phase glassware, after which the binding solution was removed, resin washed with DMF x 5, MeOH x 10 and DCM x 10 and dried under vacuum. Following this the resin was methanol capped using a 17:2:1 DCM:MeOH:DIEA mix, agitated for 60 minutes and washed with DCM x 3, DMF x 3, MeOH x 3, DCM x 3, vacuum desiccated at 50 °C for 24 hours and stored under dry nitrogen until required. Quantification of loading was determined *via* quantitative NMR (qNMR) and performed for each batch of polymer bound xanthone for use in reaction stoichiometry.

Novel fluorophores SG2 – SG9 **127 – 134** were produced using the 2-chlorotrityl supported xanthone under reflux while agitating. Each of these were subjected to three separate Grignard additions of 12 equivalents, the consumed reagent having been removed each time a new portion was added. Cleavage from the resin was achieved using a 5 % TFA/DCM solution in which the resin was stirred for 20 minutes. The resin was then washed three additional times with the cleavage solution and the washings combined. Purification was again *via* column chromatography using a 0 – 10 % MeOH/DCM gradient mobile phase.

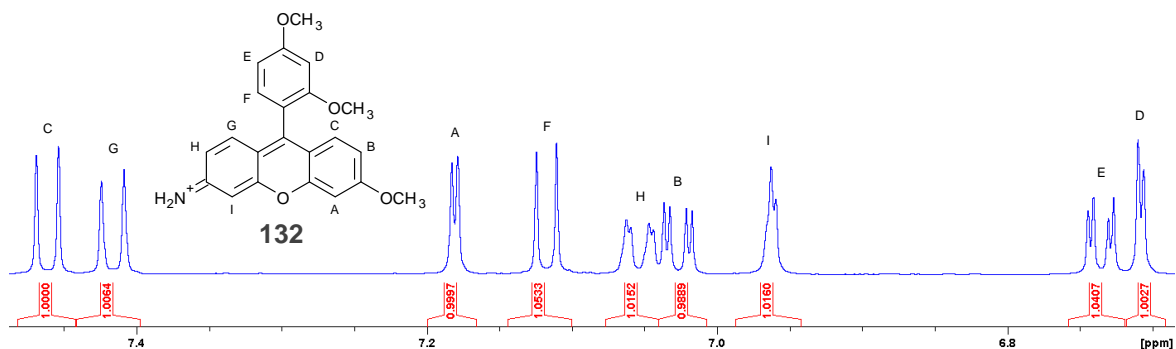


Figure 72. Expansion of aromatic region of ¹H-NMR spectrum of fluorophore SG7 **147** with associated aromatic proton assignments.

With a small library of novel fluorophores SG1 - 9 in hand, their spectral properties were investigated. Fluorescence quantum yield, extinction coefficient and $\lambda_{\text{ex}}/\lambda_{\text{em}}$ were determined for each of the Singapore Green fluorophores SG1, 2 – 9, **116**, **127** - **134** Figure 73.

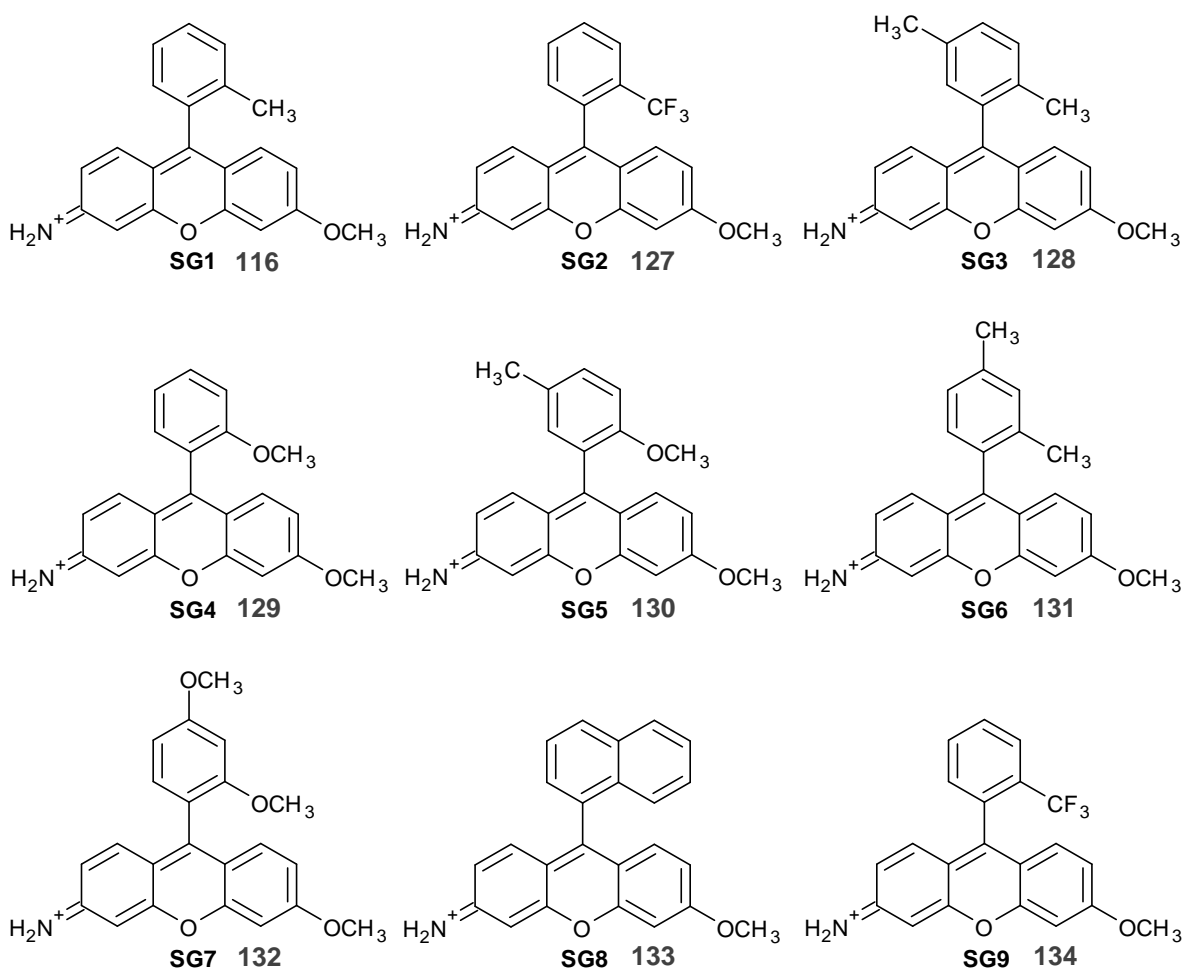


Figure 73. Singapore Greens 1 – 9 (SG1, 2 – 9, 116, 127 – 134). N.B. SG1 – 8.TFA, SG9.HCl.

2.3.3 Spectral Analysis of Singapore Greens

Quantum yield provided the quotient of photons absorbed to those re-emitted as fluorescence. Relative fluorescence quantum yield was measured using fluorescein as the standard.¹⁶⁶ The equation used for quantum yield determination was as follows:

$$\Phi_x = \Phi_{st} (m_x/m_{st})(\eta_x^2/\eta_{st}^2)$$

Where: Φ_x = quantum yield of SG,

Φ_{st} = quantum yield of fluorescein.

m_x = gradient of \int fluorescence intensity vs absorbance of SG,

m_{st} = gradient of \int fluorescence intensity vs absorbance of fluorescein.

Chapter 2 – Results and Discussion

η_x = refractive index of ethanol (1.361),

η_{st} = refractive index of 0.1 M NaOH (1.334).

Molar extinction coefficient was determined using the standard formula:

$$A = \epsilon cl$$

Where: **A** = Absorbance.

ϵ = Molar extinction coefficient ($M^{-1}cm^{-1}$).

c = concentration (M).

l = path length (cm).

Fluorophore	QY	ϵ ($M^{-1}cm^{-1}$)	λ_{ex} (nm)	λ_{em} (nm)
SG1.TFA 116	0.64	46044	492	519
SG2.HCl 127	0.56	25695	499	526
SG3.TFA 128	0.63	26450	491	519
SG4.TFA 129	0.48	44527	492	526
SG5.TFA 130	0.015	35411	501	527
SG6.TFA 131	0.39	22822	497	532
SG7.TFA 132	0.0098	38279	505	525
SG8.TFA 133	0.56	36186	496	526
SG9.TFA 134	0.65	17178	498	525

Table 8. Spectral characteristics of the Singapore Green fluorophores SG1 – 9.

Interestingly, the two di-methyl analogues, SG3 **128** and SG6 **131** exhibit markedly different quantum yields of 0.63 and 0.39 respectively, despite differing only by disposition of the methyl groups on the upper ring. This may be as a consequence of the methyl groups of SG6 **131** being arranged meta to one another. The result of this is that both of these groups inductively donate electron density to the same two positions, one of which

links the upper ring to the lower xantheno system. As PeT is analogous to an ionisation process, and both electron releasing methyl groups donate electron density to this junction, its ionisation energy is plausibly lowered. With this effect in mind, it is conceivable that ionisation occurs here more easily and so the rate of PeT to the xantheno system is increased more substantially than expected, quenching fluorescence more significantly. This same effect is not seen in SG3 **128** due to the para disposition of methyl groups to one another, in this case both oppose each other's electron donation to any specific position on the ring, nullifying the enhancement to PeT when compared to SG6 **131**.

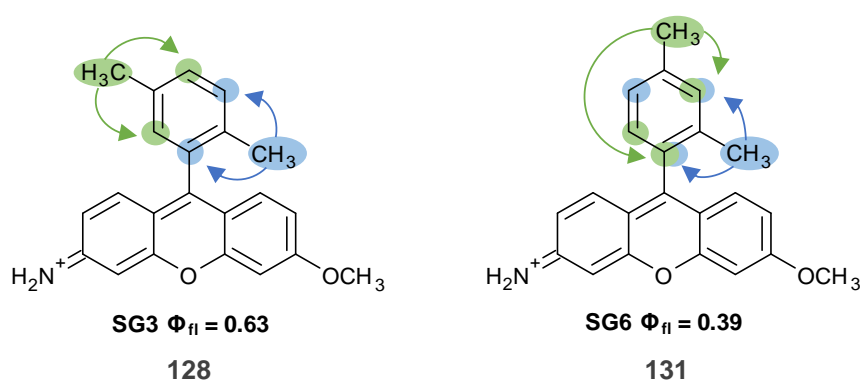


Figure 74. Disposition of methyl groups on SG3 **128** oppose each other's electron donating effect, in SG6 **131** they work in conjunction to enhance electron density in positions indicated. The result is a disproportionate increase in rate of PeT in SG6 **131** over SG3 **128** with corresponding drop in quantum yield, despite having the same relative electron density in the upper ring system.

Remarkably, there is a huge difference in quantum yield between the mono-methoxy substituted SG4 **129**, and the methyl-methoxy substituted SG5 **130**, with quantum yields of 0.48 and 0.015 respectively. The difference between their upper rings being only a mildly electron donating methyl group, which would be predicted to make little difference. This result implies there is a threshold electron density which exists for the upper ring. Above this threshold, PeT is the dominant depopulator of the excited state, at which point fluorescence quantum yield drops off massively. Naturally SG7 **132** being di-methoxy substituted and consequently more electron rich, places it above the aforementioned PeT threshold, so PeT dominates and its quantum yield is negligible at 0.0098.

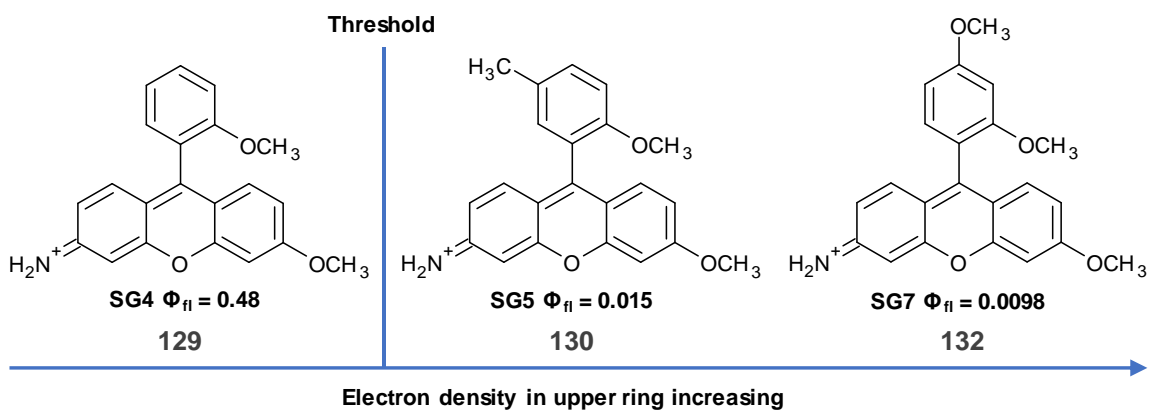


Figure 75. Comparison of SG4 **129**, SG5 **130** and SG7 **132** fluorescence quantum yields. A large drop is observed between SG4 and SG5 despite only a modest increase in upper ring electron density, this is indicative of a threshold above which PeT becomes the dominant process.

The three most fluorescent of the Singapore Greens, SG1 **116**, SG8 **133**, and SG9 **134** also follow suit in the observation that the relative electron densities of their upper rings show the expected inverse correlation with quantum yield. The least electron dense CF_3 variant SG9 **134** being most fluorescent and the slightly more electron rich naphthyl substituted SG8 **133** the least of the three, with SG1 **116** in between (Figure 76).

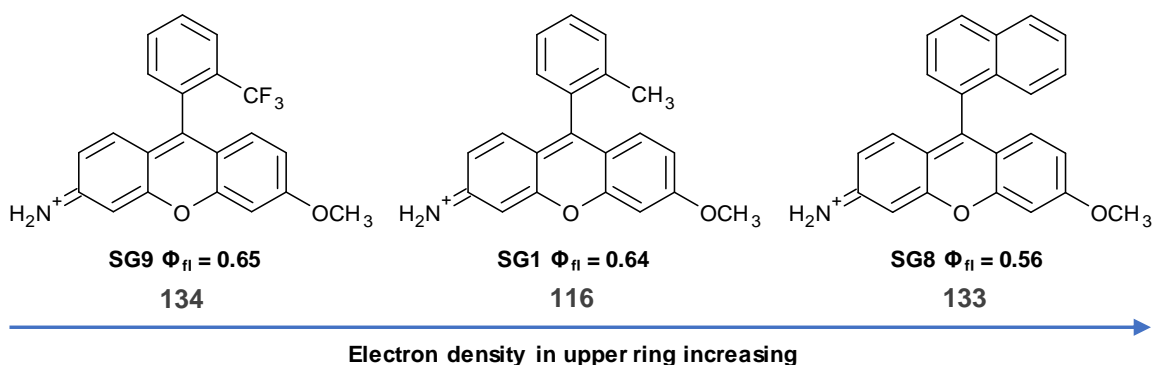


Figure 76. Fluorescence quantum yield decreases as upper ring electron density increases.

Considering these observations, it may be concluded that the same PeT quenching mechanism applies to Singapore Greens as it does to Tokyo Greens. This relationship is not in direct proportionality to electron density, but contains a threshold after which PeT dominates and fluorescence drops off rapidly. Additionally, mesomeric effects appear dominant over those observed from inductive effects in terms of upper ring electron

density and PeT rate. This dominance of mesomeric over inductive effect is similar to that observed in electrophilic aromatic substitution *via* resonance stabilisation of positive charge brought about through PeT ionisation.

Furthermore, as with the Tokyo Greens we have also demonstrated that removal and replacement of the upper carboxyl group with a variety substituents has very little effect on the $\lambda_{\text{ex}}/\lambda_{\text{em}}$. Only very slight variations are noted on these properties associated with experimental and equipment-based imperfections. The similarity in $\lambda_{\text{ex}}/\lambda_{\text{em}}$ to fluorescein and rhodamine 110 **7** is useful, as the same incident radiation source in the form of the 488 nm argon ion laser is compatible with all of them.

The measured values for the molar extinction coefficient (ϵ) appear to show a modest correlation to molecular cross-sectional area. The most electron deficient and therefore conceivably contracted CF_3 analogue SG9 **134** produces the lowest value, with the more functionalised and conceivably larger analogues eliciting higher values. However, SG1 **116** exhibits the highest extinction coefficient, which is difficult to equate to it possessing a larger molecular cross-sectional area than the naphthyl derivative SG8 **133**, which has a lower coefficient. Therefore, the only conclusion that can be drawn is that other steric, electronic, solvatochromic or agglomeration effects account for the variations seen, and these cannot be sufficiently addressed herein.

2.3.4 Fluorescence Quenching of Singapore Greens via Acylation

Having successfully produced a small library of novel Singapore Green fluorophores, acylation of some examples was undertaken in order to determine their comparative quantum yield and extinction coefficients. The variation in these properties would be the basis for fluorescence contrast change in any future probe built upon these fluorophores.

Acetic anhydride was applied in the presence of pyridine as solvent to initially yield an unexpected spirocyclic bis-acylated analogue of SG1 **116**, named SG1BisAc **135**. This bis-acyl product decomposed rapidly in the presence of light to form the target compound

SG1Ac **136**. The molecule was re-synthesised and its photolysis monitored periodically *via* NMR until complete decomposition had occurred. The photochemical nature of decomposition was proven conclusively by holding **135** under light free conditions within the magnet of a 600 MHz NMR spectrometer for 70 hours at 293 K. The period of 70 hours was chosen as in normal daylight at 293 K SG1BisAc **135** had fully decomposed to SG1Ac **136** with concurrent elimination of acetic acid, observed at around 2.02 ppm. After 70 hours of darkness in the NMR magnet at a fixed temperature of 293 K no change was recorded in the spectrum, proving that the decomposition was indeed light induced.

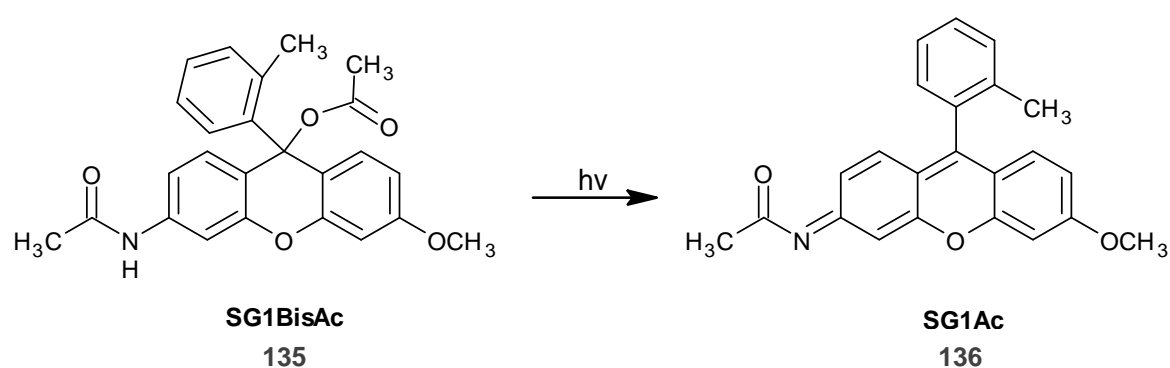


Figure 77. Acylation of SG1 **116** resulted in the spirocyclic bis-acetyl analogue SG1BisAc **135** which rapidly decomposed in light to furnish the target product SG1Ac **136**.

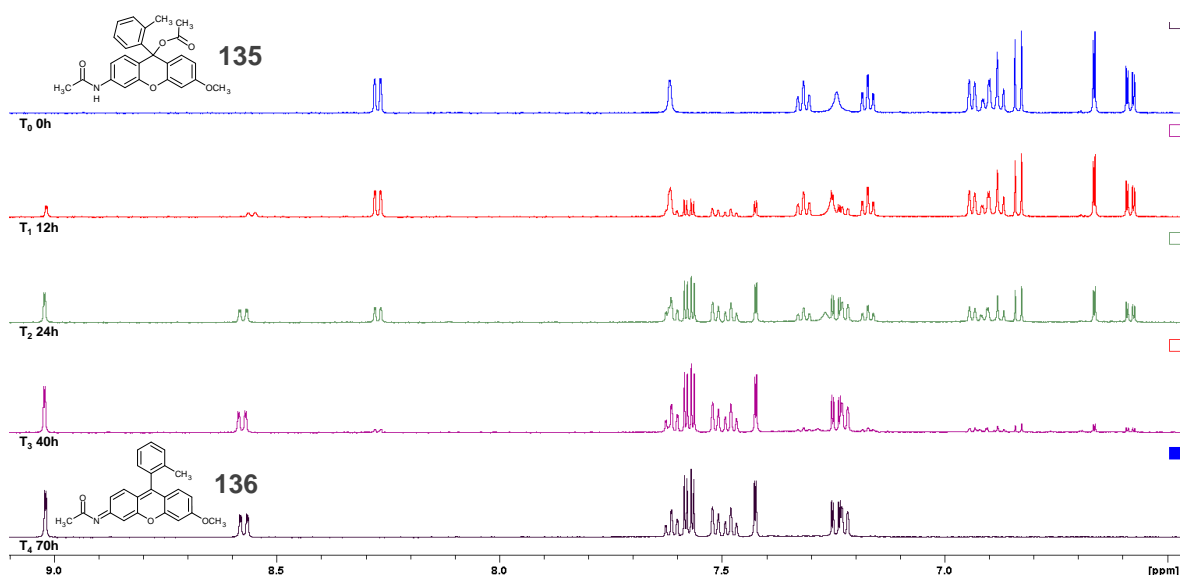


Figure 78. Changes in aromatic region of ^1H -NMR spectrum upon decomposition of SG1BisAc **135** to SG1Ac **136** in light over a 70 hour period. Specific timings marked under each spectrum.

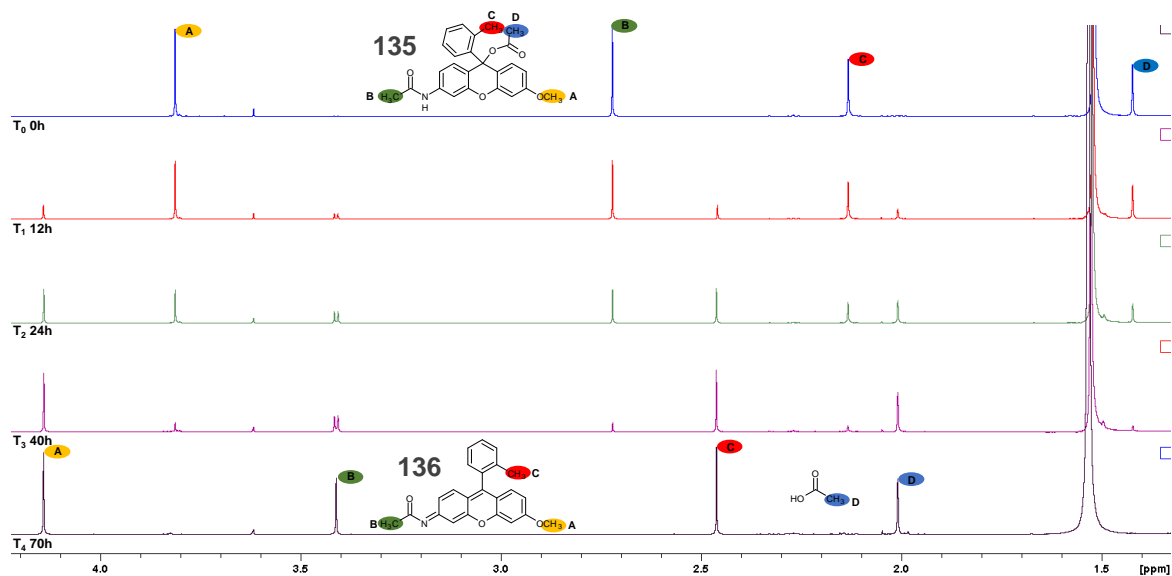


Figure 79. Changes in aliphatic region of $^1\text{H-NMR}$ spectrum upon decomposition of SG1BisAc **135** to SG1Ac **136** with CH_3 groups colour coded for clarity. Timings marked under each spectrum.

Acylation of SG5 **130** and SG7 **132** was undertaken in the same manner as that of SG1 **116**, both under the same conditions to efficiently yield the spirocyclic bis-acyl products as seen with SG1 **116**. However, unlike SG1BisAc **135**, exposure to light did not induce photolysis in either of them, this was evidenced by the fact that after more than a week of exposure to daylight no change was seen visually or *via* NMR. This was in direct contrast to that seen with SG1BisAc **135**, with all other variables held the same.

In order to further study the photostability of the two bis-acylates SG5BisAc **137** and SG8BisAc **139**, the samples were subjected to both soft (365 nm) and hard (254 nm) UV irradiation. Both samples were initially exposed to 365 nm irradiation with $^1\text{H-NMR}$ s run at 5 minute intervals up to 60 minutes, throughout this time no change was seen visually or *via* NMR. Following this, both were exposed to 254 nm UV irradiation, again with measurements at 5 minute intervals up to 320 minutes. No photolysis was observed under these conditions either, with no change seen visually or *via* NMR spectroscopy. In light of the contradictory photo stability observed for the bis-acylates SG5BisAc **137** and SG8BisAc **139** when compared to SG1BisAc **135** the implication is that there exists a steric barrier to photolysis. Despite the differing electron densities in the upper rings of the

other bis-acylates, the most significant difference is the steric properties of the upper rings. As SG1BisAc **135** decomposed readily in normal daylight while the two others were highly resistant even to prolonged irradiation with hard UV, the only conclusion that can be made is that there is a steric barrier. This steric barrier appears to prevent both SG5BisAc **137** and SG8BisAc **139** from adopting the correct orientation for photolysis to occur, rendering them kinetically/orientationally stabilised with respect to photolysis.

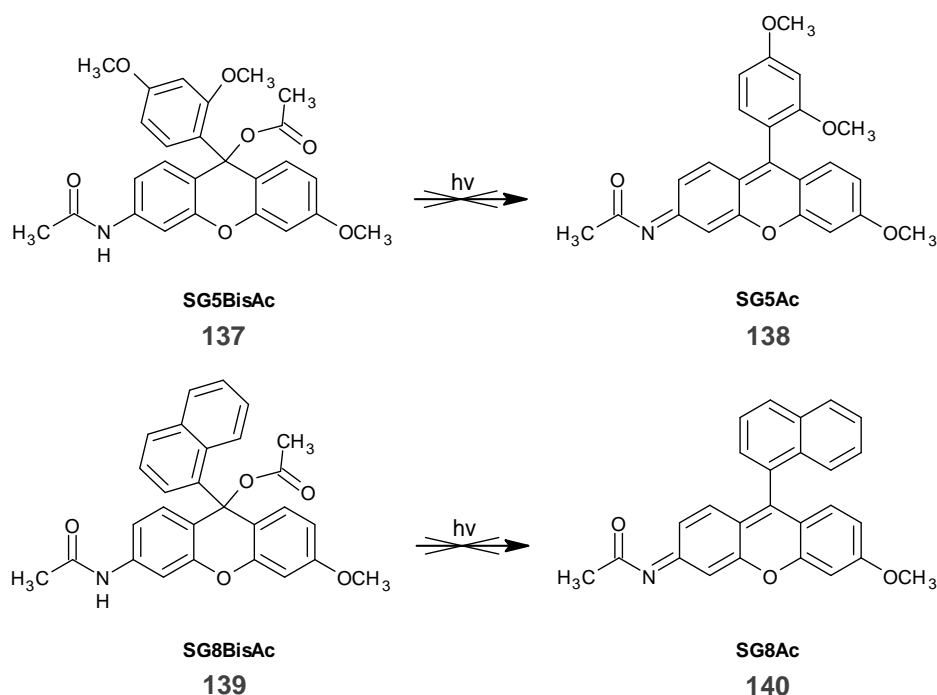


Figure 80. Both bis-acylates SG5BisAc **137** and SG8BisAc **139** are highly resistant to photolysis under normal lighting and UV irradiation of 365 or 254 nm.

Having successfully acylated the SG1 **116** to form SG1Ac **136**, their relative quantum yields and extinction coefficients could be measured for comparison with the non-acylated equivalent. This would provide a proof of concept measurement as to the effectiveness of fluorescence quenching when the fluorophore was bound to a biomimetic or other recognition sequence, as it would be in a probe. The value obtained for brightness ($\Phi \times \epsilon$) and the difference measured would provide the basis for fluorescence contrast change in any fluorescent probe utilising this fluorophore.

2.3.5 Spectral analysis of Singapore Green Acyls

Fluorophore	QY (Φ)	ϵ ($M^{-1}cm^{-1}$)	Brightness ($\Phi \times \epsilon$)
SG1 116	0.64	46044	29810.35
SG1Ac 136	0.12	225	27.19874

Table 9. Comparative fluorescence, extinction coefficient and brightness values of SG1 **116** and SG1Ac **136**.

The brightness differential between SG1 **116** and SG1Ac **136** was found to be of excellent magnitude, with values of 29810 and 27 respectively. This represents a brightness change of 99.909 % or approximately an 1100-fold increase in brightness between the acylated and free fluorophore. This contrast change would be sufficient for utilisation in future fluorogenic probes and proves the concept and utility this class of fluorophore. Furthermore, there is scope for improvement upon this value based on the variation in fluorescence quantum yield observed upon modulation of upper ring electron density.

2.4 Conclusions

Optimisation and scale up of the synthesis of the *S. aureus* probe LGX was successful, with a more than fourfold improvement to the isolated yield. This enables its production to be further scaled up with an aim to eventually form part of an ultra-fast detection system for use in healthcare environments. This could form an effective first line of defence for the control of troublesome bacterial strains *via* accurately targeted antibiotic therapy. A previously unencountered synthetic complication in the form of over hydrogenation was identified and efficiently circumvented *via* a modification to the synthetic route. This is of particular value as hydrogenation of any benzyl ester could be reversed by DDQ. This would have utility in the production of other probes containing protected arginine, should the steric conditions be appropriate. This complication highlighted the troublesome nature and side reactivity of the upper lactone system in rhodamine prompting a reassessment of probe construction order. Investigation of non-symmetric fluorophores which could be constructed following peptide attachment further highlighted the need for simplification of the synthetic route.

Building on the lessons learned from the LGX project, an orphan class of fluorophore coined Singapore Green was investigated. A small library of nine novel fluorophores based on this motif were synthesised and fully characterised. It was also confirmed that the upper lactone ring system is not essential for fluorescence, while upper ring electron density modulates fluorescence quantum yield through varying PeT-based quenching. It was further evidenced that the correlation between electron density and quantum yield is not linear, rather a threshold exists beyond which PeT predominates and quantum yield drops significantly.

The characterisation of this novel group of fluorophores has demonstrated they possess good quantum yields and extinction coefficients as well as demonstrating their compatibility with existing two-channel fluorescence instruments utilising the argon ion laser. Their excellent fluorescent properties, coupled with the ease of synthesis and

functionalisation (compared with the rhodamine class) provides considerable scope and potential for their utilisation for rapid protease detection systems. This is potentially of considerable value in the detection of proteases which are characteristic of a disease state or indicate the presence of problem pathogens, in light of the grave and continuing problem of antibiotic resistance.

2.5 Future Work

Having synthesised and scaled up the LGX probe successfully, as well as proven the favourable fluorescence properties of the Singapore Green fluorophores, the next logical step would be to combine the two. However, before selection of the best Singapore Green candidate to move forward with, further investigation in terms of extension of lower xanthene ring systems should be undertaken (Figure 81). The same synthetic methodology to synthesise the xanthone precursors up may be used to achieve this. This modification is likely to reveal useful information as to how their $\lambda_{ex}/\lambda_{em}$ may be modulated, as other work on analogous structures has demonstrated this elicits a bathochromic shift in $\lambda_{ex}/\lambda_{em}$.¹¹⁶

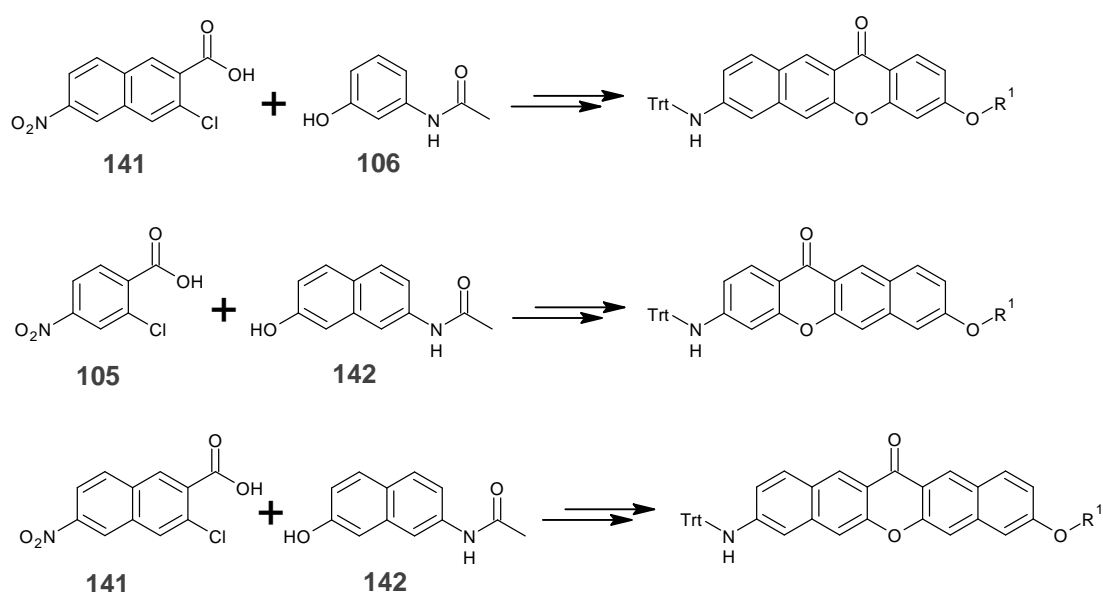


Figure 81. Extension of lower xanthene ring systems on Singapore Green precursors. $R^1 = CH_3$, C_2H_5 , C_3H_7 etc.

Chapter 2 – Results and Discussion

Variation of substituents on the upper and lower ring systems is also likely to give rise to changes in quantum yield of fluorescence as observed in this work, warranting further investigation (Figure 82).

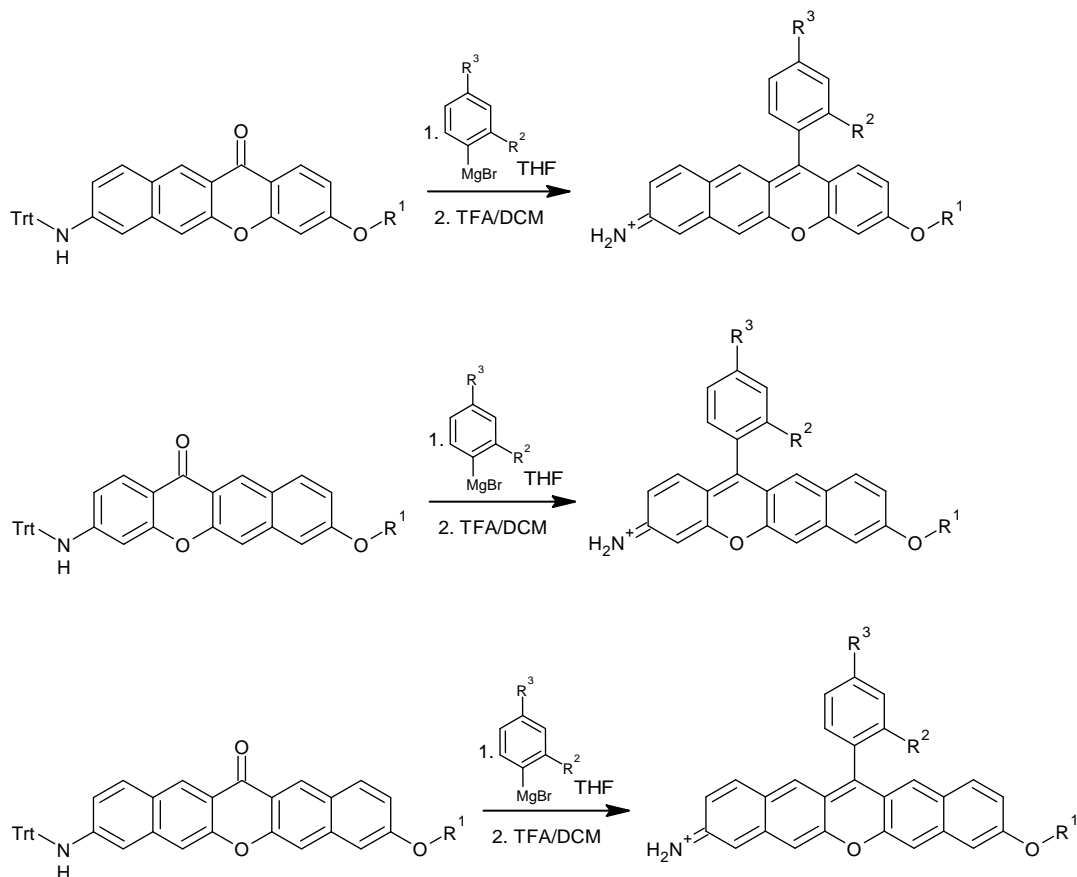


Figure 82. Synthesis of Singapore Greens with extended lower xanthene ring systems as well as variation of ring substituents R^1 , R^2 and R^3 to determine their effects on spectral characteristics. R^1 = CH_3 , C_2H_5 , C_3H_7 ; R^2 = CH_3 , OCH_3 , CF_3 ; R^3 = H , CH_3 , OCH_3 , CF_3 etc.

Following this, determination of the new analogues' full spectral properties including fluorescence quantum yield would conclusively determine the best candidate to move forward with. This candidate would then form the central core for a next generation *Staphylococcus aureus* probe (Figure 83).

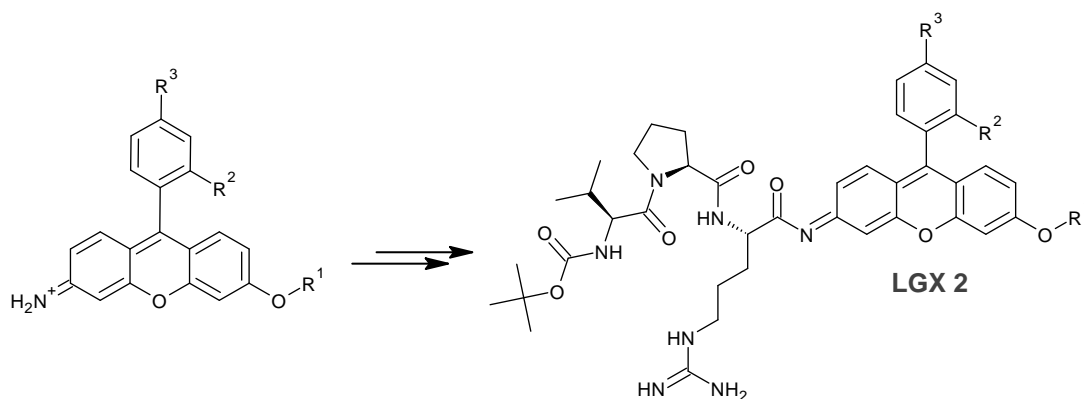


Figure 83. The most favourable Singapore Green analogue would be used as the core for a next generation *S. aureus* probe using the proven synthetic route to LGX.

As the synthesis of LGX has been optimised, and the Singapore Green fluorophores simplified relative to rhodamine, construction of the new probe should proceed relatively smoothly. Once this has been achieved, biological testing should be undertaken in order to allow direct comparison to the LGX probe in terms of sensitivity and selectivity. If these test prove favourable, the new probe could be eventually patented and put into production as a rapid detection system for *S. aureus* in healthcare environments.

Chapter 3 – Experimental

3.1 General Experimental Methods

3.1.1 Physical Methods

All ^1H -NMR spectra were recorded at either 400 MHz on a Brüker AV400 FT-NMR spectrometer equipped with a BB- $^1\text{H}/\text{D}$ Z-GRD probe head (broadband multinuclear with autotune) or a 600 MHz Bruker AV600 equipped with a PATXI $^1\text{H}/\text{D}$ - $^{13}\text{C}/^{15}\text{N}$ Z-GRD probe. ^{13}C -NMR spectra were recorded at 100 MHz using the Brüker AV400 or at 125 MHz using the Brüker AV600. ^{19}F spectra were obtained at 376 MHz on the Brüker AV400. All NMR spectra were recorded using NMR tubes of specification 5 mm o/d, No Z107374, Brüker BioSpin AG, Switzerland. NMR spectral measurements were carried out in solution using deuterated chloroform, deuterated dichloromethane, deuterated dimethyl sulfoxide, or deuterated methanol as the solvent. All NMR signals quoted are in ppm as downfield δ chemical shifts from either the internal tetramethylsilane (TMS) standard at $\delta = 0.00$ or from the residual CHCl_3 resonance at $\delta = 7.26$ ppm, residual DCM resonance at $\delta = 5.32$, residual DMSO resonance at $\delta = 2.50$ ppm, or the residual MeOD resonance at $\delta = 3.31$ ppm. All coupling constants are quoted in Hz. Sample analysis was carried out using standard procedure for sweep width optimisation and parameter sets for proton dimension in correlation spectra. The final spectra were obtained following standard Fourier transform NMR processing for the averaged transients. The data was processed manually using TopSpin 3.5 pl7 (c) 2017 Brüker BioSpin.

TLC analysis was performed using Fluka glass backed silica gel plates 60 F₂₅₄, 250 μm or Merck aluminium backed aluminium oxide 60 F₂₅₄ and visualised at either 254 or 365 nm UV by a UVP UVGL – 58 multiband UV lamp, or using KMnO_4 , Iodine, Vanillin or Ninhydrin stains. Flash column chromatography was performed at ambient temperature using high purity Merck 63 - 200 μm silica gel at moderate pressure, or with a Biotage Isolera Spektra Four system using Biotage ZIP 40 – 60 μm flash cartridges.

Gas Chromatography – Mass Spectrometry was performed using a Shimadzu GCMS-QP2010 SE and undertaken using a 1 ppm – 1 ppb solution of each compound. The

samples were introduced into the GC-MS and analysed under standard procedure. Chromatograph peaks were then checked for the mass, and then the mass spectral fragmentation pattern was cross referenced *in silico* against the inbuilt fragmentation pattern database where applicable.

Low resolution mass spectra (LR MS): EI (electron impact); ES (electro spray); CI (chemical ionisation) and High resolution mass spectra (HR MS) were obtained *via* MEDAC Ltd. in accordance with BS EN ISO 9001:2008 provision for microanalysis service.

Infra-red analysis was performed using either a small quantity of the neat oil or a solid powdered sample coated onto the analysis plate of a ThermoScientific Nicolet 869-142500 iD5 Diamond ATR FT-IR spectrophotometer, or coated onto either a KBr or NaCl disc and analysed using a ThermoScientific Nicolet iS5 FT-IR spectrophotometer.

UV-Vis spectrophotometry was performed using an Agilent Cary 7000 UMS spectrophotometer using ultra-pure optically matched, stoppered rectangular Spectrosil quartz fluorimeter cells, type 23-Q-10 with a 10 mm path length. A scan rate of 600 nm/min was employed.

Fluorescence measurement was performed using an Agilent Cary Eclipse fluorescence spectrophotometer using the same ultra-pure optically matched, stoppered rectangular Spectrosil quartz fluorimeter cells, type 23-Q-10 with a 10 mm path length.

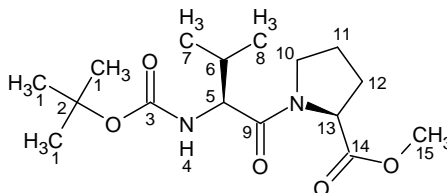
3.1.2 Reagents, Solvents and Reaction Conditions

All chemicals were purchased from commercial vendor Sigma-Aldrich chemicals unless otherwise stated, and purchased at the highest possible grade (at least > 95 %) and used as received. All anhydrous solvents were also purchased at the highest possible grade from commercial vendor Sigma-Aldrich chemicals and obtained in SureSeal™ packaging and stored under nitrogen at 4 °C. Other solvents were of SLR grade from the same vendor. Anhydrous reactions were performed using oven then flame dried glassware

Chapter 3 - Experimental

under vacuum, and carried out under an anhydrous nitrogen atmosphere. Water refers to deionised water, LiCl solutions are saturated and brine is a saturated aqueous solution of sodium chloride. Where no reaction temperature is given, reactions were carried out at an ambient temperature of 20 °C. Evaporation of solvents was performed on a Büchi RE111 Rotovapor in conjunction with a Büchi 461 water bath.

3.2 Experimental Methods

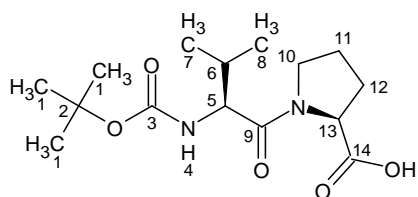
Boc-NH-Val-Pro-OMe, **64**

To a solution of Boc-L-Valine-OH **62** (1.00 g, 4.60 mmol) in anhydrous DCM (20 ml) was added COMU (2.36 g, 5.52 mmol) and triethylamine (2.79 g, 3.84 ml, 27.6 mmol). The resulting solution was then stirred for 30 minutes under a dry nitrogen atmosphere. L-proline methyl ester **63** (0.76 g, 4.6 mmol) was added to the resulting solution and stirred for a further 24 hours. The crude mixture was washed with 1 M aqueous HCl solution (3 x 10 ml), saturated NaHCO₃ solution (3 x 10 ml), water (3 x 10 ml) and brine (2 x 10 ml). The organics were then dried over Na₂SO₄ and concentrated under vacuum. Purification was achieved *via* silica flash chromatography using an ethyl acetate:petroleum ether (40 - 60) 1:1 mix to yield a white amorphous solid.¹⁶⁷ (0.950 g, 63 %, 1:1 ethyl acetate:petroleum ether (40 – 60) R_f = 0.3).

¹H-NMR (400 MHz; CDCl₃) δ = 0.87 (3H, d, J=6.80 Hz, CH₃-7), 0.96 (3H, d, J=6.80 Hz, CH₃-8), 1.36 (9H, s, CH₃-1), 1.94 (4H, m, CH₂-11,12), 2.15 (1H, m, CH-6), 3.59 (1H, m, CH-10), 3.65 (3H, s, CH₃-15), 3.71 (1H, m, CH-10'), 4.21 (1H, dd, J=6.24, 9.43 Hz, CH-13), 4.46 (1H, dd, J=4.64, 9.23 Hz, CH-5), 5.17 (1H, d, J=9.23 Hz, NH-4).

¹³C-NMR (100 MHz; CDCl₃) δ = 17.56, 19.38, 25.10, 28.48, 29.17, 31.43, 47.32, 52.33, 57.02, 58.97, 79.70, 156.07, 171.53, 172.55.

Boc-NH-Val-Pro-OH, 76



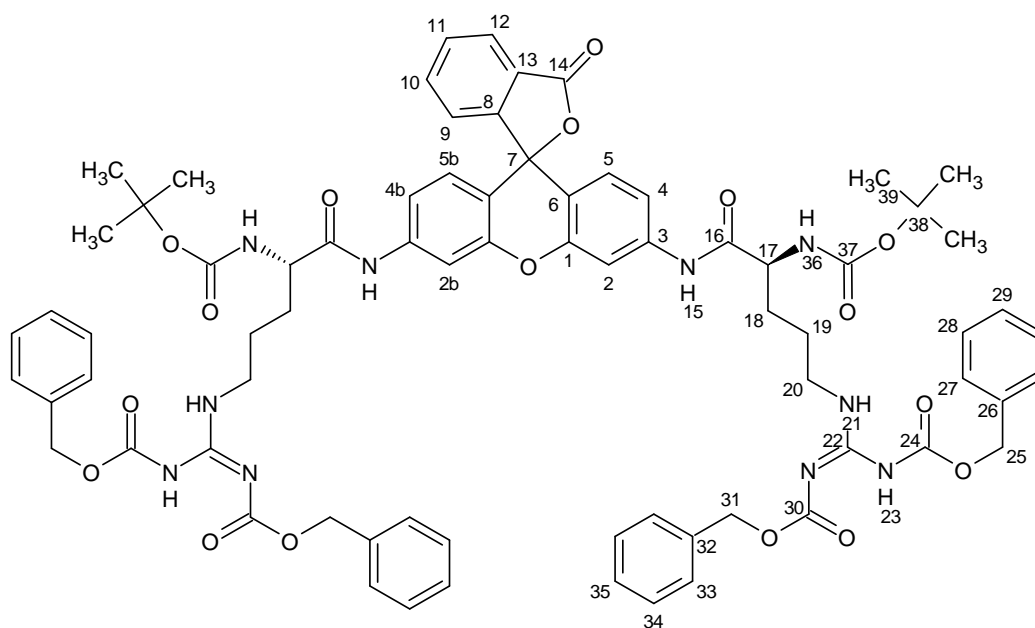
To a solution of Boc-Val-Pro-OMe **64** (0.85 g, 2.60 mmol) in THF was added a 1M aqueous solution of LiOH (100 ml), the resulting solution was stirred at room temperature for 2 hours. Following this the solution was concentrated under vacuum, washed with 1M HCl solution (3 x 40 ml) and extracted with ethyl acetate (3 x 30 ml), dried over Na₂SO₄ and the solvent removed under vacuum. Purification was achieved *via* recrystallisation from DCM:petroleum ether (40 - 60) to yield a fluffy white solid. (0.590 g, 63 %).

¹H-NMR (400 MHz; CDCl₃) δ = 0.93 (3H, d, J=6.80 Hz, CH-7), 0.99 (3H, d, J=6.80 Hz, CH-8), 1.42 (9H, s, CH₃-1), 2.11 (5H, m, CH-6, CH₂-11,12), 3.65 (1H, m, CH-10), 3.80 (1H, m, CH-10'), 4.27 (1H, dd, J=6.83, 9.27 Hz, CH-13), 4.58 (1H, m, CH-5), 5.29 (1H, d, J=9.35 Hz, NH-4).

¹³C-NMR (100 MHz; CDCl₃) δ = 17.52, 19.22, 24.87, 28.08, 28.31, 31.26, 47.61, 56.94, 59.32, 79.74, 155.86, 172.92, 173.81.

LR MS (EI) m/z = 315.2, requires 315.2 [M + H]⁺.

HR MS (ES) m/z = 313.2523, requires 313.1760 [M - H]⁺.

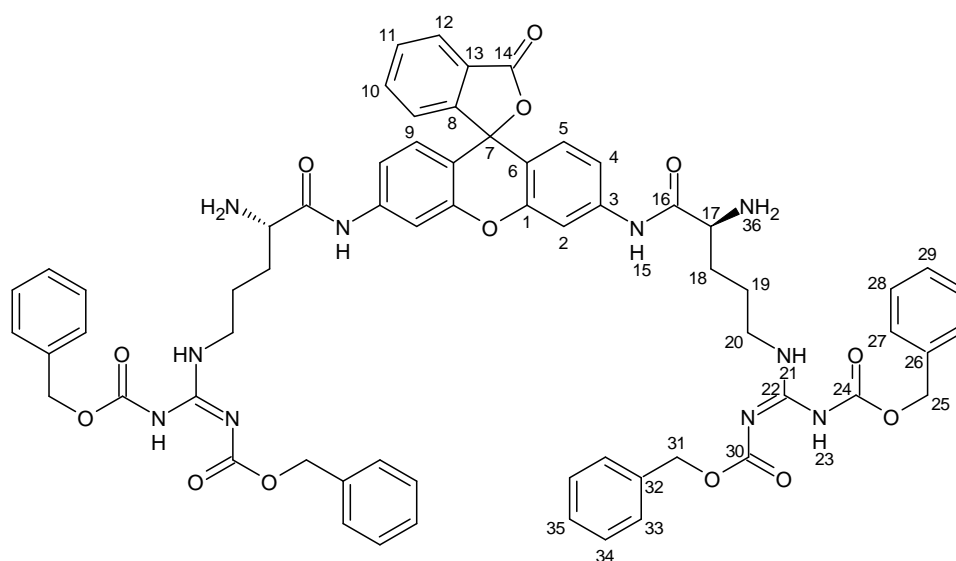
Rhodamine-(Arg(Cbz)₂-NHBoc)₂, 69

To a solution of HO-Arg(Cbz)₂-NH-Boc **68** (0.81 g, 1.50 mmol) in anhydrous DMF (10 ml) under a dry nitrogen atmosphere was added HATU (0.62 g, 1.64 mmol) and DIEA (0.31 g, 0.42 ml, 2.40 mmol). The resulting solution was stirred for 30 minutes before addition of rhodamine 110 (0.250 g, 0.682 mmol). The solution was stirred at room temperature for 20 hours. Purification was achieved *via* isocratic silica flash chromatography using ethyl acetate:chloroform in a 3:7 ratio as a glassy white amorphous solid. (0.231 g, 25 %, 3:7 ethyl acetate:CHCl₃, R_f = 0.3).

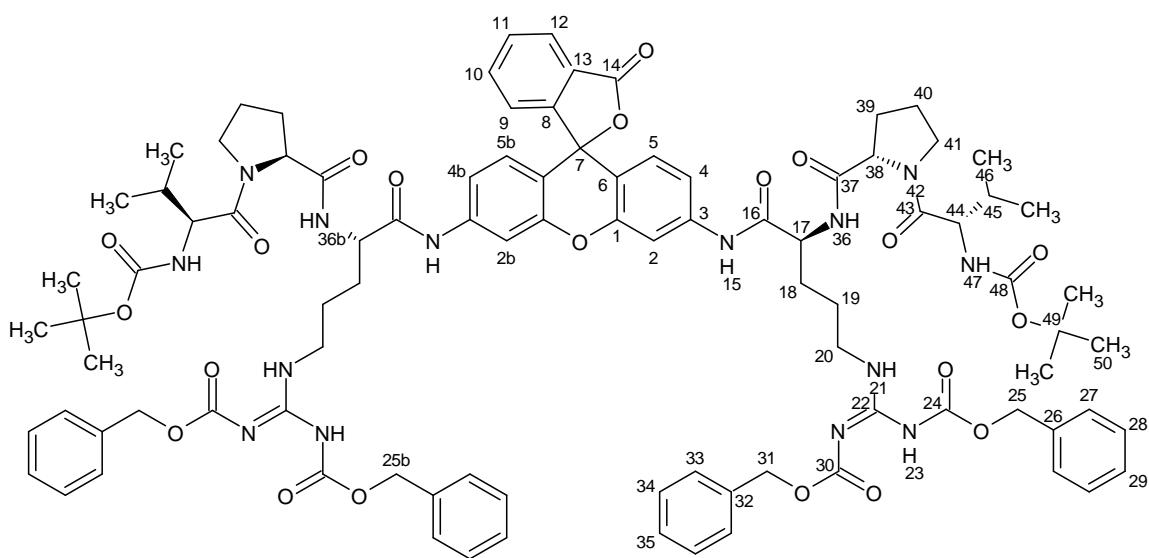
¹H-NMR (400 MHz; CDCl₃) δ = 1.43 (18H, s, CH₃-39), 1.81 (8H, m, CH₂-18, 19), 3.97 (4H, m, CH₂-20), 4.41 (2H, m, CH-17), 5.13 (8H, m, CH₂-25, 31), 5.82 (2H, br s, NH-36), 6.54 (2H, dd, J=2.12, 8.59 Hz, CH-5, 5b), 6.72 (1H, d, J=8.59 Hz, CH-4), 6.77 (1H, d, J=8.59 Hz, CH-4b), 7.04 (1H, dd, J=1.40, 7.00 Hz, CH-9), 7.28 (20H, m, CH-27, 28, 29, 33, 34, 35), 7.46 (2H, s, CH-2, 2b), 7.62 (2H, m, CH-10, 11), 8.01 (1H, dd, J=1.86, 6.42 Hz, CH-12), 8.78 (2H, br s, NH-15), 9.32 (2H, br s, NH-21), 9.44 (2H, br s, NH-23).

¹³C-NMR (100 MHz; CDCl₃) δ = 24.93, 28.28, 28.49, 44.12, 54.61, 67.42, 69.25, 80.44, 82.48, 108.18, 108.24, 114.42, 115.76, 124.04, 125.17, 126.38, 128.16, 128.25, 128.31, 128.51, 128.65, 128.98, 129.09, 129.86, 134.59, 134.60, 135.17, 136.36, 139.66, 151.55, 153.41, 155.87, 161.00, 163.60, 169.60, 171.06.

HR MS (ES) m/z = 1379.5876, requires 1379.5619 [M + H]⁺.

Rhodamine-(Arg(Cbz)₂-NH₂)₂, 75

To a solution of Rhodamine-(Arg(Cbz)₂-NH₂)₂ **69** (0.02 g, 0.0140 mmol) in anhydrous DCM (3 ml) under a dry nitrogen atmosphere was added TFA (3 ml) and stirred for 4 hours at room temperature. The mixture was then washed with 1 M aqueous NaOH (3 x 2 ml) and the organic layer separated. The aqueous layer was then washed with DCM (3 x 2 ml) and the organics combined, these were then washed with brine (2 x 2 ml), dried over anhydrous Na₂SO₄ and under vacuum to yield a colourless glassy solid which was used immediately for the next reaction step without further purification. (0.015 g, 93 %).

Rhodamine-(Arg(Cbz)₂-Pro-Val-NHBoc)₂, **77**

To a solution of Boc-Val-Pro-OH **76** (0.028g, 0.0880 mmol) in anhydrous DMF (7 ml) under a dry nitrogen atmosphere was added HATU (0.037 g, 0.0960 mmol), the resulting mixture was stirred for 10 minutes at room temperature, after which DIEA (0.0 g, 0.512 ml, 0.296 mmol) was added. The solution was stirred for a further 30 minutes, at which point Rhodamine-(Arg(Cbz)₂-NH₂)₂ **75** (0.016 g, 0.0520 mmol) was added. The reaction was followed by TLC analysis and was found to have ceased after 18 hours. The crude reaction mixture was diluted with ethyl acetate (15 ml), washed with saturated NaHCO₃ (3 x 3 ml), saturated LiCl (3 x 3 ml), brine (1 x 2 ml) and dried over anhydrous Na₂SO₄. Solvent was removed under vacuum to yield an off white foamy solid. Purification was achieved *via* preparative silica TLC using 100 % ethyl acetate to yield a clear glassy solid. (0.044 g, 47 %, 100 % ethyl acetate, R_f = 0.7).

¹H-NMR (400 MHz; CDCl₃) δ = 0.86 (12H, m, CH-46), 1.43 (18H, s, CH₃-50), 1.89 (18H, m, CH-18, 19, 39, 40, 45), 3.54 (2H, m, CH-41), 3.69 (2H, m, CH-41'), 4.03 (4H, m, CH₂-20), 4.22 (2H, m, CH-44), 4.30 (4H, m, CH-38), 4.50 (2H, m, CH-17), 5.02 (2H, d, J=9.13 Hz, CH-25), 5.16 (2H, d, J=9.13 Hz, CH-25'), 5.25 (4H, s, CH-31), 6.66 (1H, d, J=7.55 Hz, CH-5), 6.67 (1H, d, J=7.55 Hz, CH-5b), 6.99 (1H, m, CH-4), 7.07 (1H, m, CH-4b), 7.09 (1H, m, CH-9), 7.25 (6H, m, CH-34, 35), 7.37 (10H, m, CH-27, 28, 29), 7.53 (1H, s, NH-36), 7.54 (1H, s, NH-36b), 7.61 (3H, m, CH-2, 10, 11), 7.75 (1H, s, CH-2b), 8.03 (1H, d, J=7.36 Hz, CH-12), 8.83 (2H, m, NH-21), 9.41 (2H, m, NH-23).

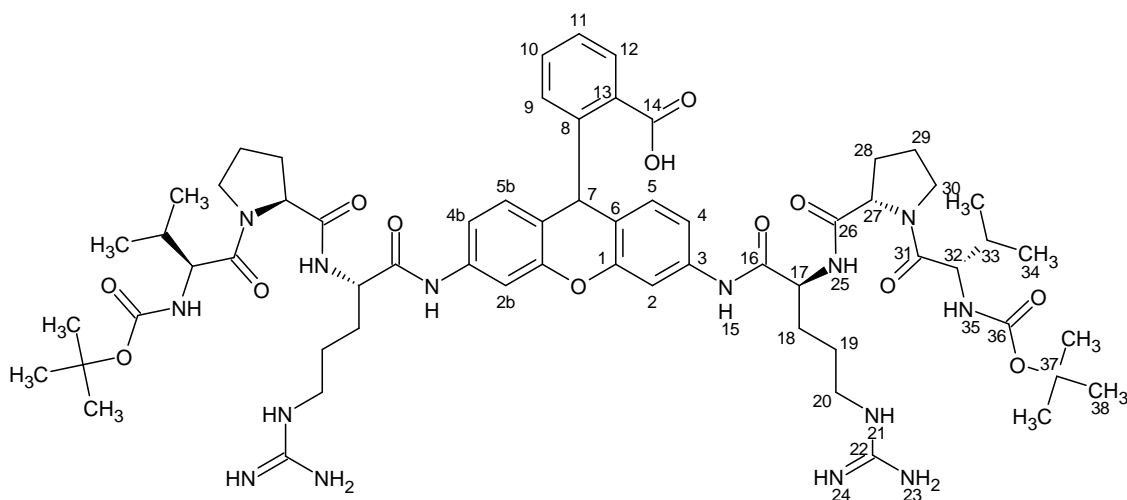
¹³C-NMR (100 MHz; CDCl₃) δ = 14.26, 17.60, 17.65, 19.52, 25.12, 25.32, 28.50, 29.84, 31.37, 44.14, 47.76, 54.16, 57.29, 57.38, 60.45, 60.57, 67.36, 69.26, 79.82, 82.66,

Chapter 3 - Experimental

108.30, 114.33, 123.99, 125.18, 126.42, 128.25, 128.30, 128.39, 128.50, 128.62, 128.64, 128.97, 129.05, 129.83, 134.62, 135.15, 136.34, 140.08, 151.66, 156.00, 161.26, 163.60, 170.13, 172.12.

LR MS (EI) $m/z = 1772.0$, requires $1771.8 [M + H]^+$.

HR MS (ES) $m/z = 1771.8899$ requires $1771.8005 [M + H]^+$.

Rhodamine-(H₂)-(Arg-Pro-Val-NHBoc)₂, **78**

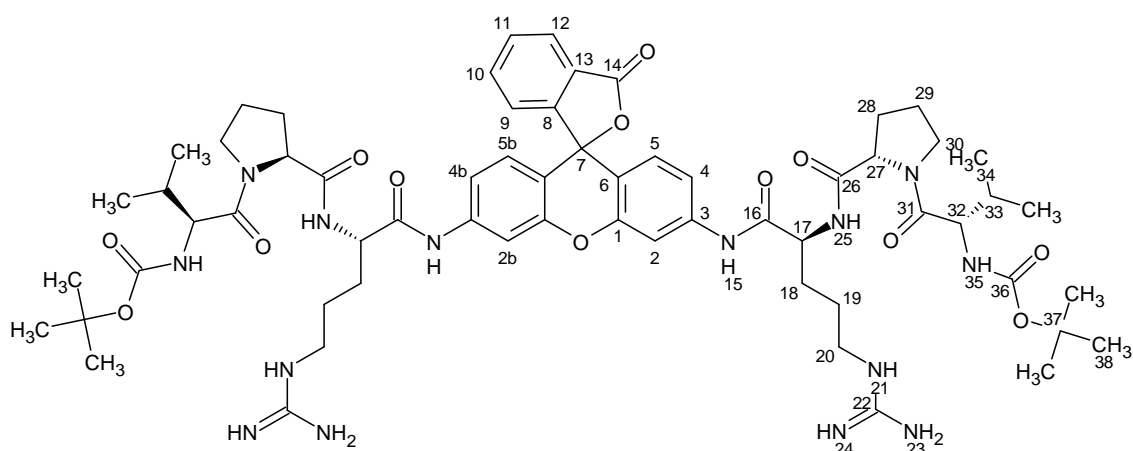
Into a solution of Rho-(Arg(Cbz)₂-Pro-Val-NHBoc)₂ **77** (0.032 g, 0.0182 mmol) in anhydrous DMF (0.5 ml) and anhydrous methanol (0.5 ml) was added 10 % Pd/C (0.001 g). The resulting mixture was then stirred under a dry hydrogen atmosphere for 48 h. The crude reaction mixture was then concentrated under vacuum, reconstituted in anhydrous methanol and filtered through Celite. The filtrate was dried under high vacuum to yield the product as an amorphous white solid. (0.024 g, 80 %).

¹H-NMR (600 MHz; CD₃OD) δ = 0.99 (12H, m, CH₃-34), 1.45 (18H, s, CH₃-38), 1.87 (2H, m, CH-29'), 2.00 (6H, m, CH-28, CH-29, CH-33), 2.12 (2H, m, CH-28'), 2.28 (4H, m, CH₂-18), 3.24 (4H, m, CH₂-20), 3.70 (2H, m, CH-30), 3.93 (2H, m, CH-30'), 4.20 (2H, m, CH-32), 4.74 (4H, m, CH-17, 27), 6.05 (1H, s, CH-7), 6.70 (1H, d, J=7.80, CH-5), 6.90 (1H, d, J=7.80, CH-5b), 7.00 (1H, d, J=7.80, CH-4), 7.02 (1H, d, J=8.50, CH-9), 7.05 (1H, d, J=7.80, CH-4b), 7.23 (1H, dd, J=6.91, 8.50, CH-10), 7.25 (1H, dd, J=6.91, 8.50, CH-11), 7.42 (1H, s, CH-2), 7.44 (1H, s, CH-2b), 7.46 (1H, d, J=8.50, CH-12), 8.17 (2H, s, NH-15), 8.48 (2H, d, J=7.00, NH-25), 10.11 (2H, d, J=7.70 Hz, NH-24).

¹³C-NMR (125 MHz; CD₃OD) δ = 17.2, 18.4, 22.3, 24.7, 24.9, 27.3, 28.9, 29.2, 29.4, 30.2, 35.6, 40.7, 44.1, 48.3, 48.6, 53.7, 58.0, 60.4, 73.3, 76.5, 79.2, 82.7, 107.4, 114.1, 115.6, 123.7, 124.3, 126.2, 127.0, 134.4, 139.5, 149.5, 154.6, 155.4, 162.2, 169.6, 170.0, 171.1, 172.2

LR MS (EI) m/z = 1236.3 (z = 1), requires 1236.7 [M + 2H]⁺.

HR MS (ES) m/z = 619.6222 (z = 2), requires 619.3362 [M + 2H]⁺.

LGX; Rhodamine-(Arg-Pro-Val-NHBoc)₂, 61

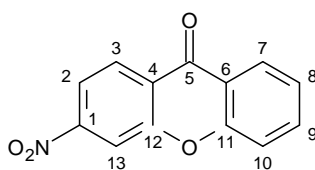
Into a solution of rhodamine-(H₂)-(Arg-Pro-Val-NHBoc)₂ **78** (0.032 g, 0.0182 mmol) in anhydrous methanol (0.5 ml) and anhydrous DMF (0.5 ml) under a dry nitrogen atmosphere was added 2,3-dichloro-5,6-dicyano-1,4-benzoquinone (0.033 g, 0.146 mmol). The resulting mixture was stirred at room temperature for 30 minutes while monitoring *via* TLC analysis. Purification was achieved *via* MDAP and dried under high vacuum to yield the product as an amorphous white solid. (0.022 g, 83 %).

¹H-NMR (600 MHz; CD₃OD) δ = 0.99 (12H, m, CH₃-34), 1.45 (18H, s, CH₃-38), 1.87 (2H, m, CH-29), 2.00 (6H, m, CH-28, 29', 33), 2.12 (2H, m, CH-28'), 2.28 (4H, m, CH₂-18), 3.24 (4H, m, CH₂-20), 3.70 (2H, m, CH-30), 3.93 (2H, m, CH-30'), 4.20 (2H, m, CH-32), 4.74 (4H, m, CH-17, 27), 6.65 (1H, J=7.80, NH-35), 6.75 (1H, d, J=7.80, CH-5), 6.75 (1H, d, J=7.80, CH-5b), 7.19 (1H, d, J=7.80, NH-35b), 7.21 (1H, d, J=8.50, CH-9), 7.22 (1H, d, J=7.80, CH-4), 7.41 (2H, s, NH-21), 7.73 (1H, dd, J=6.90, 8.50, CH-10), 7.79 (1H, dd, J=6.90, 8.50, CH-11), 7.82 (1H, s, CH-2), 7.89 (1H, s, CH-2b), 8.05 (1H, d, J=8.50, CH-12), 8.17 (2H, s, NH-15), 8.48 (2H, d, J=7.00, NH-25), 10.11 (1H, s, NH-24) 10.11 (1H, s, NH-24b).

¹³C NMR (125 MHz; CD₃OD) δ = 17.2, 18.4, 22.3, 24.7, 24.9, 27.3, 28.9, 29.2, 29.4, 30.2, 35.6, 40.7, 44.1, 48.3, 48.6, 53.7, 58.0, 60.4, 73.3, 79.2, 82.7, 107.4, 114.1, 115.6, 123.7, 124.6, 126.2, 128.0, 130.0, 135.4, 140.7, 151.5, 156.7, 157.4, 163.8, 169.8, 171.0, 172.2, 173.2. (Three additional peaks for C-2b, C-4b and C-5b).

HR MS (EI) m/z = 618.3322 (z = 2), requires 618.3283 [M + 2H]⁺.

3-Nitroxanthone-9-one, 82a



Two routes:

Into concentrated sulphuric acid at 0 °C was slowly added concentrated nitric acid with stirring to form a 1:1 mixture, this was stirred at 0 °C for 30 minutes, after which xanthone (1.50 g, 7.65 mmol) was slowly added. The resulting mixture was stirred at 0 °C for a further 40 minutes after which it was poured over ice (500 ml) and stirred until a precipitate formed. This was isolated and re-suspended in 20 % Na₂CO₃ with stirring until evolution of CO₂ had ceased. The solid was then washed with water (3 x 100 ml) and air dried. Purification was achieved *via* silica flash column chromatography using an Ethyl acetate:petroleum ether (40 - 60) gradient of 1:9 to 4:6, yielding a white crystalline solid. (0.331 g, 1.377 mmol, 18 %, 3:7 ethyl acetate:petroleum ether (40 – 60) R_f = 0.5).

To a stirred solution of phenol (18.3 g, 194 mmol) in DMF (200 ml) was added K₂CO₃ (26.81 g, 194 mmol). To the resulting solution was added 2-chloro-4-nitro-benzoic acid (19.6 g, 97.0 mmol) and copper powder (1.23 g, 19.4 mmol). The mixture was then refluxed at 130 °C for 40 hours, cooled to room temperature, poured over concentrated icy HCl (600 ml) and stirred until a brown precipitate formed. The pH was adjusted to 1 and the solid isolated, washed with excess cold water and air dried. The dry isolated solid was added portionwise to concentrated H₂SO₄ (150 ml) and heated to 80 °C with stirring for 1.5 hours and cooled to room temperature. The crude mixture was slowly poured over ice (500 ml) and stirred until a brown/beige precipitate formed, this was isolated and stirred in solution of 20 % Na₂CO₃ until evolution of CO₂ ceased and washed with excess water. Purification was achieved *via* isocratic silica flash column chromatography using ethyl acetate:petroleum ether (40 - 60) in a 3:7 ratio yielding a white crystalline solid. (7.95 g, 34 %, 3:7 ethyl acetate:petroleum ether (40 – 60) R_f = 0.5).

¹H-NMR (400 MHz; d⁶ - DMSO) δ = 7.54 (1H, ddd, J=0.91, 7.15, 7.98 Hz, CH-8), 7.70 (1H, dd, J=0.91, 8.56 Hz, CH-10), 7.94 (1H, ddd, J=1.72, 7.15, 8.56 Hz, CH-9), 8.20 (1H, dd, J=2.04, 8.73 Hz, CH-2), 8.20 (1H, dd, J=1.72, 7.98 Hz, CH-7), 8.40 (1H, d, J=8.73 Hz, CH-3), 8.45 (1H, d, J=2.04 Hz, CH-13).

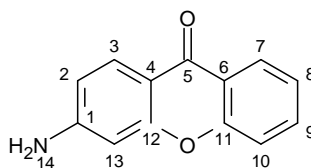
Chapter 3 - Experimental

^{13}C -NMR (100 MHz; d^6 - DMSO) δ = 114.14, 118.22, 118.23, 121.14, 124.94, 125.06, 126.05, 128.10, 136.26, 151.04, 155.11, 155.87, 175.24.

IR (ATR): ν = 3092, 1667, 1614, 1575, 1522.

LR MS (EI) m/z = found 241.0, requires 241.0 $[\text{M}]^+$.

3-Aminoxanthen-9-one, 82

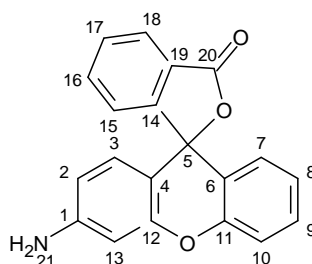


To a stirred suspension of 3-nitroxanthen-9-one **82a** (0.90 g, 3.70 mmol) in industrial methylated spirit (50 ml) was added tin(II) chloride (3.34 g, 14.80 mmol). The resulting mixture was heated to reflux for 2 hours, after which TLC analysis confirmed consumption of the starting material. The crude mixture was cooled to room temperature, the solvent removed under vacuum, saturated aqueous NaHCO₃ (30 ml) added and mixture stirred for 30 minutes. The mixture was then filtered and washed with excess water and dried in air. The dry residue was ground to a fine powder and subjected to ultrasonication in chloroform several times, the organic extracts were combined, washed with water (3 x 25 ml), brine (2 x 25 ml) and dried over Na₂SO₄ to yield the pure product as a yellow/beige solid. (0.802 g, 79 %).¹⁶⁸

¹H-NMR (400 MHz; d⁶ - DMSO) δ = 6.41 (2H, s, NH₂-14), 6.47 (1H, d, J=2.04 Hz, CH-13), 6.61 (1H, dd, J=2.04, 8.71 Hz, CH-2), 7.33 (1H, ddd, J=0.81, 7.17, 7.87 Hz, CH-8), 7.46 (1H, d, J=8.31, 0.81 Hz, CH-10), 7.68 (1H, ddd, J=1.63, 7.17, 8.31 Hz, CH-19), 7.79 (1H, d, J=8.71 Hz, CH-3), 8.04 (1H, dd, J=1.63, 7.87 Hz, CH-7).

¹³C-NMR (100 MHz; d⁶ - DMSO) δ = 107.01, 120.27, 122.00, 127.06, 131.02, 133.20, 135.18, 137.02, 143.61, 164.87, 165.28, 167.55, 183.39.

LR MS (EI) m/z = found 212.1, requires 212.1 [M + H]⁺.

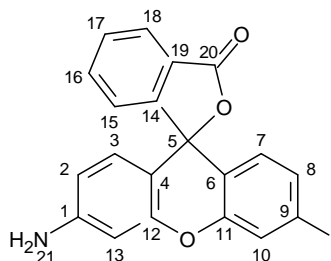
3'-Aminospiro[isobenzofuran-3,9'-xanthene]-1-one, 85

To a solution of phenol (2.00 g, 21.3 mmol) in anhydrous methansulfonic acid (30 ml) under a dry nitrogen atmosphere, were added 3-aminophenol (2.32 g, 21.3 mmol) and phthalic anhydride (3.15 g, 21.3 mmol) with vigorous stirring. The mixture was heated to 140 °C for 48 hours, cooled to room temperature and poured over ice (400 ml). The crude mixture was stirred for 30 minutes until a suspension was formed, and its pH was adjusted to 8 using a 10 % aqueous NaOH solution. The aqueous phase was filtered, and the residue subjected to ultrasonication in DCM (3 x 30 ml) followed by chloroform (3 x 30 ml). The organic extracts were combined and washed with 10 % aqueous NaOH solution (3 x 50 ml), brine (2 x 25 ml), dried over Na₂SO₄, the solvent was then removed under vacuum. Purification was achieved *via* successive dry loaded isocratic flash column chromatography, using a mobile phase of 1.5:98.5 methanol:DCM followed by 1:99 to yield a deep red fluffy solid. (0.103 g, 13 %, 1:99 methanol:DCM R_f = 0.3).

¹H-NMR (400 MHz; CD₂Cl₂) δ = 4.00 (2H, s, NH₂-21), 6.38 (1H, dd, J=2.28, 8.55 Hz, CH-2), 6.55 (1H, d, J=2.28 Hz, CH-13), 6.56 (1H, d, J=8.55 Hz, CH-3), 6.77 (1H, dd, J=1.47, 7.91 Hz, CH-10), 7.02 (1H, ddd, J=0.97, 7.17, 7.91 Hz, CH-9), 7.17 (1H, d, J=7.47 Hz, CH-15), 7.27 (1H, dd, J=0.97, 8.42 Hz, CH-7), 7.40 (1H, ddd, J=1.47, 7.17, 8.42 Hz, CH-8), 7.63 (1H, ddd, J=1.02, 7.41, 7.47 Hz, CH-16), 7.69 (1H, ddd, J=1.25, 7.41, 7.51 Hz, CH-17), 7.99 (1H, d, J=7.51 Hz, CH-18).

¹³C-NMR (100 MHz; CD₂Cl₂) δ = 101.04, 111.51, 116.99, 119.38, 123.41, 123.89, 124.78, 127.05, 127.96, 129.07, 129.65, 130.43, 134.96, 139.55, 143.43, 149.27, 151.43, 152.45, 153.17, 155.55.

HR MS (ES) m/z = 316.0976, requires 316.0968 [M + H]⁺.

3'-Amino-6'-iodo-spiro[isobenzofuran-3,9'-xanthene]-1-one, 89

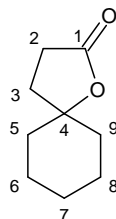
To a solution of 3-aminophenol (4.00 g, 36.7 mmol) in anhydrous methanesulfonic acid (35 ml) under a dry nitrogen atmosphere, were added 3-iodophenol (8.06 g, 36.65 mmol) and phthalic anhydride (5.42 g, 36.7 mmol) with vigorous stirring. The resulting suspension was heated to 140 °C for 40 hours and cooled to room temperature. The crude mixture was then poured over ice (300 ml) and stirred until a brown suspension formed, the pH was then adjusted to 7 using 10 % aqueous NaOH solution. The crude mixture was extracted with DCM (3 x 50 ml), the organics combined and washed with 10 % aqueous NaOH solution (3 x 50 ml), brine (2 x 25 ml), dried over Na₂SO₄ and concentrated to yield a crude brown solid. Purification was achieved *via* dry loaded flash column chromatography using a gradient of 3:7 ethyl acetate:petroleum ether (40 - 60) to 1:1, followed by standard isocratic flash column chromatography using 3:97 methanol:DCM to yield the product as a fluffy pink solid.¹⁶⁹ (1.136 g, 7 %, 3:97 methanol:DCM R_f = 0.3).

¹H-NMR (400 MHz; d⁶ - DMSO) δ = 5.67 (2H, s, NH₂-21), 6.36 (1H, dd, J=2.04, 8.55 Hz, CH-2), 6.39 (1H, d, J=8.55 Hz, CH-3), 6.45 (1H, d, J=2.04 Hz, CH-13), 6.50 (1H, d, J=8.31 Hz, CH-7), 7.28 (1H, dd, J=0.90, 7.62 Hz, CH-15), 7.42 (1H, dd, J=1.72, 8.31 Hz, CH-8), 7.72 (1H, ddd, J=0.90, 7.45, 7.56 Hz, CH-17), 7.76 (1H, d, J=1.72 Hz, CH-10), 7.79 (1H, ddd, J=0.87, 7.45, 7.62 Hz, CH-16), 7.99 (1H, dd, J= 0.87, 7.56 Hz, CH-18).

¹³C-NMR (100 MHz; d⁶ - DMSO) δ = 82.64, 96.06, 99.05, 104.68, 111.50, 119.07, 123.91, 124.58, 125.33, 125.97, 128.37, 129.44, 130.08, 132.42, 135.54, 151.24, 151.40, 151.49, 152.12, 168.49.

HR MS (ES) m/z = 441.9946, requires 441.9935 [M + H]⁺.

1-Oxaspiro[4.5]decan-2-one, 97



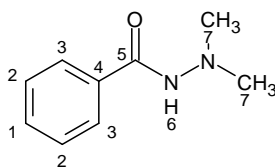
Into a stirred solution of SmI_2 (0.13 M, 20 ml, 2.64 mmol) in dry THF under a dry nitrogen atmosphere was added a solution of cyclohexanone (0.10 g, 0.11 ml, 1.06 mmol), ethyl acrylate (0.11 g, 0.11 ml, 1.06 mmol) and *s*-BuOH (0.08 g, 0.10 ml, 1.06 mmol) in dry THF drop-wise. The resulting solution was stirred at room temperature for 20 h. The reaction mixture was dried *in vacuo*, taken up into DCM and washed with 1M HCl x 2, dried over Na_2SO_4 and purified *via* flash column chromatography in 1:3 ethyl acetate:petroleum ether (40 - 60) to yield a colourless oil. (0.108 g, 66 %, 1:3 ethyl acetate:petroleum ether (40 - 60) $R_f = 0.5$).

^1H NMR (400 MHz; CDCl_3) $\delta = 1.32 - 1.61$ (m, 6H, CH_2 -6, 7, 8) 1.64 - 1.73 (m, 2H, CH_2 -9) 1.73 - 1.82 (m, 2H, CH_2 -5) 1.99 (t, $J=8.34$ Hz, 2H, CH_2 -3) 2.57 (t, $J=8.34$ Hz, 2H, CH_2 -2)

^{13}C NMR (100 MHz; CDCl_3) $\delta = 22.53, 24.87, 28.54, 32.79, 36.85, 86.34, 176.74$.

IT (ATR): $\nu = 2933, 2860, 1762$.

HR MS (ES) $m/z = 155.0994$, requires 155.1063 $[\text{M} + \text{H}]^+$.

***N,N*-dimethylbenzohydrazide, 100**

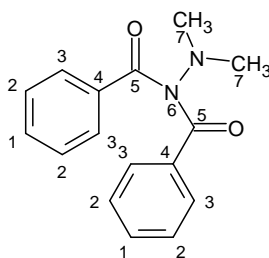
To a vigorously stirred biphasic mixture of diethyl ether (40 ml), 10 % aqueous NaOH solution (20 ml) and dimethylhydrazine (2.57 g, 3.25 ml, 42.7 mmol) at 0 °C, benzoyl chloride (6.00 g, 4.95 ml, 42.7 mmol) was slowly added over 20 minutes, the solution was maintained at 0 °C for 1 hour. The resulting solution was followed *via* TLC analysis for a further 5 hours, after which the starting material had been consumed. The crude mixture was separated, and the aqueous layer washed with diethyl ether (3 x 30 ml), the organics were combined and washed with 10 % aqueous NaOH solution. The organics were dried over Na₂SO₄, and the solvent removed under vacuum. Purification was achieved *via* trituration in petroleum ether (40 - 60) followed by recrystallisation from petroleum ether (40 - 60):ethyl acetate, to yield lustrous rod shaped crystals.¹⁷⁰ (4.830 g, 70 %).

¹H-NMR (400 MHz; CDCl₃) δ = 2.66 (6H, s, CH₃-7), 7.09 (1H, br s, NH-6), 7.37 (2H, m, CH-3), 7.45 (1H, m, CH-1), 7.71 (2H, m, CH-2).

¹³C-NMR (100 MHz; CDCl₃) δ = 47.49, 126.99, 128.43, 131.45, 133.65, 165.65.

LR MS (EI) *m/z* = 187.1, requires 187.1 [M + Na]⁺.

HR MS (ES) *m/z* = 164.0955, requires 164.0950 [M]⁺.

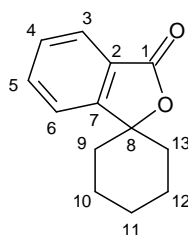
***N*-benzoyl-*N,N*-dimethylbenzohydrazide, 101**

To a vigorously stirred biphasic mixture of diethyl ether (40 ml), 10 % aqueous NaOH solution (20 ml) and dimethylhydrazine (2.57 g, 3.25 ml, 42.7 mmol), benzoyl chloride (6.00 g, 4.95 ml, 42.7 mmol) was slowly added over 20 minutes, the solution was maintained at 0 °C for 1 hour. The resulting solution was followed *via* TLC analysis for a further 5 hours, after which the starting material had been consumed. The crude mixture was separated, and the aqueous layer washed with diethyl ether (3 x 30 ml), the organics were combined and washed with 10 % aqueous NaOH solution. The organics were dried over Na₂SO₄, and the solvent removed under vacuum. Purification was achieved *via* trituration in petroleum ether (40 - 60) followed by recrystallisation from petroleum ether (40 - 60):ethyl acetate, to yield large diamond shaped crystals.¹⁷¹ (1.374 g, 12 %).

¹H-NMR (400 MHz; CDCl₃) δ = 2.94 (6H, s, CH₃-7), 7.39 (4H, m, CH-2), 7.49 (2H, m, CH-1), 7.70 (4H, m, CH-3).

¹³C-NMR (100 MHz; CDCl₃) δ = 44.04, 128.25, 128.54, 132.05, 135.15, 173.56.

LR MS (EI) m/z = 269.2, requires 269.1 [M + H]⁺.

3*H*-spiro[2-benzofuran-1-1'-cyclohexan]-3-one, 103

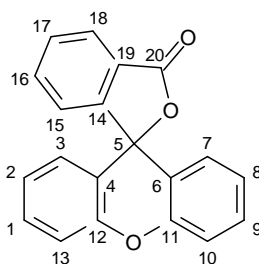
To a solution of *s*-BuLi (1.40 M, 0.25 ml, 3.05 mmol) at -78 °C in anhydrous THF (10 ml) under a dry nitrogen atmosphere was added *N,N*'-dimethylbenzohydrazide **100** (0.20 g, 1.22 mmol) and TMEDA (0.14 g, 0.18 ml, 2.44 mmol). Cyclohexanone (0.24 g, 0.25 ml, 2.44 mmol, 0.8 eq) was then added dropwise; the resulting solution was stirred at -78 °C for a further 4 hours before further stirring at room temperature for 16 hours. The reaction was then quenched with cold water, the water layer separated, washed with DCM (3 x 5 ml), the organics combined and washed with brine (2 x 3 ml), dried over anhydrous Na₂SO₄ and concentrated under vacuum. Purification was achieved *via* silica flash column chromatography using 1:4 ethyl acetate:petroleum ether (40 - 60) to yield a fragrant colourless oil. (0.061 g, 0.302 mmol, 25 %, 1:4 ethyl acetate:petroleum ether (40 - 60) R_f = 0.4).

¹H NMR (400 MHz; CDCl₃) δ = 1.67 - 1.78 (4H, m, CH₂-9, 13) 1.78 - 1.92 (6H, m, CH₂-10, 11, 12) 7.38 (1H, d, J=7.65 Hz, CH-6) 7.48 (1H, m, CH-4) 7.63 (1H, m, CH-5) 7.84 (1H, d, J=7.65 Hz, CH-3).

¹³C NMR (100 MHz; CDCl₃) δ = 22.22, 24.62, 36.24, 86.87, 120.89, 125.38, 125.66, 128.83, 133.83, 154.81, 170.01.

IR (ATR): ν = 3052, 2934, 2861, 1746, 1614, 1600.

HR MS (ES) *m/z* = 202.0987, requires 202.0993 [M]⁺.

Spiro[isobenzofuran-3,9'-xanthene]-1-one, **104**

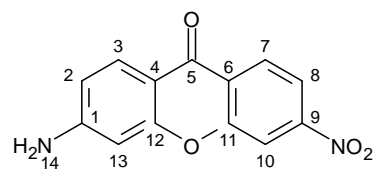
To a solution of *N,N*-dimethylbenzohydrazide **100** (0.200 g, 1.22 mmol) in anhydrous THF (5 ml) at -78 °C under a dry nitrogen atmosphere containing TMEDA (0.14 g, 1.22 mmol), was slowly added a 1.40 M solution of *s*-BuLi in THF (2.18 ml, 3.05 mmol). The solution was stirred at -78 °C for 1 hour, after which a solution of xanthone in THF (5 ml, 0.24 g, 1.22 mmol) was added dropwise. The reaction mixture was maintained at -78 °C for 1 further hour, after which was warmed to room temperature and stirred for 4 hours. The crude mixture was quenched with water (10 ml) and the organic layer washed with DCM (3 x 10 ml), the organics combined, washed with water (3 x 10 ml) dried over Na₂SO₄ and the solvent removed under vacuum. The crude was reconstituted in THF (20 ml) and acidified with 6 M aqueous HCl solution (10 ml) and let stand for 12 hours, after which the pure product had crystallised out of solution as needle like crystals. These were isolated, washed with diethyl ether (3 x 5 ml) and dried under vacuum. (0.059 g, 16 %).

¹H-NMR (400 MHz; CD₂Cl₂) δ = 6.85 (2H, dd, J=1.58, 8.00 Hz, CH-13), 7.06 (2H, ddd, J=1.21, 7.11, 8.00 Hz, CH-1, 9), 7.16 (1H, m, CH-15), 7.33 (2H, dd, J=1.21, 8.33 Hz, CH-3, 7), 7.44 (2H, ddd, J=1.58, 7.11, 8.33 Hz, CH-2, 8), 7.65 (2H, ddd, J=1.27, 7.39, 7.39 Hz, CH-17), 7.69 (1H, ddd, J=1.47, 7.39, 7.39 Hz, CH-16), 8.02 (1H, m, CH-18).

¹³C NMR (100 MHz; CD₂Cl₂) δ = 82.66, 117.69, 119.57, 124.26, 124.37, 125.57, 126.69, 128.46, 130.44, 131.26, 135.76, 151.70, 153.95, 169.71.

IR (ATR): ν = 3055, 3043, 1765, 1605, 1573.

HR MS (ES) m/z = found 301.0870, requires 301.0865 [M + H]⁺.

3-Amino-6-nitro-xanthen-9-one, 108

To a stirred suspension of 3-acetamidophenol (18.10 g, 120 mmol) in anhydrous DMF (200 ml) under a dry nitrogen atmosphere, was added anhydrous K_2CO_3 (16.60 g, 120 mmol), 2-chloro-4-nitrobenzoic acid and copper powder (0.40 g, 6.00 mmol). The resulting mixture was heated to 130 °C for 16 hours, then cooled to room temperature. The crude mixture was quenched by pouring over 500 ml of iced 5 M HCl solution and adjusted to pH 1 *via* further HCl addition. The mixture was stirred until a pale brown solid had precipitated, the solid was then isolated, washed with cold water and dried in air. The solid was then slowly dissolved in concentrated H_2SO_4 (100 ml) and heated to 80 °C for 1 hour with stirring. After cooling to room temperature, the mixture was poured over ice (300 ml) and stirred until a brown solid formed, the solid was isolated and stirred with 20 % w/v Na_2CO_3 until evolution of CO_2 ceased. The crude product was washed with water and dried under vacuum. Purification was achieved *via* successive reverse recrystallisation and decantation using ethyl acetate:petroleum ether (40 - 60) 1:1 to pure ethyl acetate. The pure product was isolated as a bright yellow powder. (9.220 g, 30 %, 1:1 ethyl acetate:petroleum ether (40 – 60) $R_f = 0.2$).

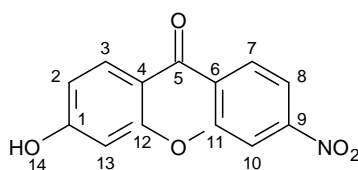
1H -NMR (400 MHz; d^6 - DMSO) $\delta = 6.56$ (1H, d, $J=2.04$ Hz, CH-13), 6.70 (2H, s, NH_2 -14), 6.71 (1H, dd, $J=2.04, 8.79$ Hz, CH-2), 7.87 (1H, d, $J=8.79$ Hz, CH-3), 8.14 (1H, dd, $J=2.14, 8.65$ Hz, CH-8), 8.31 (1H, d, $J=8.65$ Hz, CH-7), 8.34 (1H, d, $J=2.14$ Hz, CH-10).

^{13}C -NMR (100 MHz; d^6 - DMSO) $\delta = 97.33, 110.67, 113.15, 113.49, 117.76, 125.69, 127.60, 127.71, 150.23, 154.81, 156.46, 158.32, 172.38$.

IR (ATR): $\nu = 3479, 3345, 3223, 3105, 1646, 1630, 1608, 1573, 1543$.

LR MS (EI) $m/z =$ found 257.1, requires 257.1 $[M + H]^+$.

3-Hydroxy-6-nitro-xanthen-9-one, 117



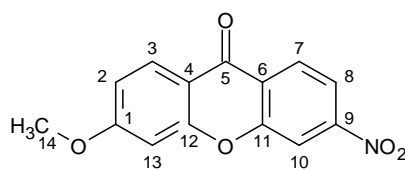
To a stirred solution of 3-amino-6-nitro-xanthen-9-one **108** (1.48 g, 5.78 mmol) in a mixture of concentrated H₂SO₄ (30 ml) and water (15 ml) at 0 °C, a solution of NaNO₂ (1.20 g, 17.3 mmol) in water (10 ml) was added dropwise. The mixture was stirred for 1 hour at 0 °C, then poured into boiling water (1000 ml) and held at 90 °C for a 1 hour. The reaction was cooled to room temperature, the solid isolated, washed with excess cold water and dried under vacuum to yield the pure product as a light brown powder. (1.283 g, 86 %).

¹H-NMR (400 MHz; d⁶ - DMSO) δ = 6.88 (1H, d, J=2.20 Hz, CH-13), 6.94 (1H, dd, J=2.20, 8.75 Hz, CH-2), 8.03 (1H, d, J=8.75 Hz, CH-3), 8.15 (1H, dd, J=2.16, 8.67 Hz, CH-8), 8.33 (1H, d, J=8.67 Hz, CH-7), 8.36 (1H, d, J=2.16 Hz, CH-10), 11.12 (1H, s, OH-14).

¹³C-NMR (100 MHz; d⁶ - DMSO) δ = 102.16, 113.77, 113.92, 114.85, 118.05, 125.13, 127.85, 128.11, 150.57, 154.98, 157.85, 164.65, 173.63.

IR (ATR): ν = 3074 br, 1649, 1607, 1565, 1528.

LR MS (EI) m/z = found 256.0, requires 256.0 [M - H]⁺.

3-Methoxy-6-nitro-xanthen-9-one, 118

To a suspension of 3-hydroxy-6-nitro-xanthen-9-one **117** (1.28 g, 4.98 mmol) in anhydrous DMF (30 ml) under a dry nitrogen atmosphere, was added anhydrous K_2CO_3 (1.38 g, 9.98 mmol). The suspension was stirred for 20 minutes, after which iodomethane (0.850 g, 5.99 mmol) was added dropwise. The resulting mixture was stirred at room temperature for 18 hours, after which TLC analysis showed complete disappearance of starting material. The crude reaction mixture was diluted with chloroform (30 ml), filtered, the residue washed several times with chloroform and the organic extracts combined. The organic extracts were washed with saturated aqueous LiCl solution (3 x 50 ml), and the LiCl layers back extracted with chloroform. The organics were combined, washed with saturated aqueous $NaHCO_3$ (3 x 50 ml), water (2 x 50 ml) and brine (2 x 50 ml). The washing process was repeated until the organic layer was clean *via* TLC, after which it was dried over Na_2SO_4 followed by vacuum, to yield a beige powder. (1.086 g, 80 %).

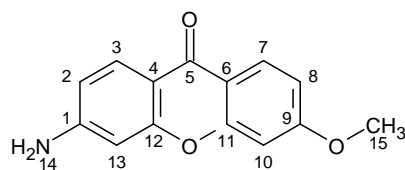
1H -NMR (400 MHz; d^6 - DMSO) δ = 3.98 (3H, s, CH_3 -14), 6.95 (1H, d, J =2.36 Hz, CH-13), 7.02 (1H, dd, J =2.36, 8.91 Hz, CH-2), 8.18 (1H, dd, J =2.12, 8.67 Hz, CH-8), 8.27 (1H, d, J =8.91 Hz, CH-3), 8.36 (1H, dd, J =0.32, 2.12 Hz, CH-10), 8.50 (1H, dd, J =0.32, 8.67 Hz, CH-7).

^{13}C -NMR (100 MHz; d^6 - DMSO) δ = 56.27, 100.69, 113.79, 114.36, 114.95, 118.28, 125.17, 127.73, 127.96, 150.75, 155.09, 157.92, 165.51, 173.91.

IR (ATR): ν = 3104, 1668, 1615, 1575, 1524.

LR MS (EI) m/z = found 271.0, requires 271.1 $[M]^+$.

3-Amino-6-methoxy-xanthen-9-one, 119



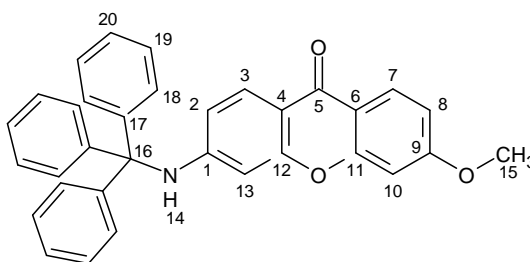
To a stirred suspension of 3-methoxy-6-nitro-xanthen-9-one **118** (1.09 g, 4.00 mmol) in absolute ethanol (30 ml), was added tin(II) chloride (2.43 g, 12.8 mmol). The resulting mixture was heated to reflux for 20 hours, after which TLC analysis showed complete consumption of the starting material. The crude mixture was cooled to room temperature, the ethanol was removed under vacuum, quenched with saturated aqueous NaHCO₃ (50 ml) and stirred for 30 minutes. The crude solid was isolated and washed with water (3 x 30 ml), then air dried for 12 hours. The resulting solid was ground into a fine powder, suspended in acetone, subjected to ultrasonication, filtered and the acetone filtrate retained. The residue was repeatedly subjected to this process until the acetone filtrate became colourless. The organic extracts were combined and dried under vacuum to yield a shiny fluorescent yellow solid requiring no further purification. (0.941 g, 98 %).

¹H-NMR (400 MHz; d⁶ - DMSO) δ = 3.90 (3H, s, CH₃15), 6.34 (2H, s, NH₂-14), 6.51 (1H, d, J=2.05 Hz, CH-13), 6.64 (1H, dd, J=2.05, 8.65 Hz, CH-2), 6.95 (1H, dd, J=2.40, 8.80 Hz, CH-8), 7.03 (1H, d, J=2.40 Hz, CH-10), 7.82 (1H, d, J=8.65 Hz, CH-3), 8.00 (1H, d, J=8.80 Hz, CH-7).

¹³C-NMR (100 MHz; d⁶ - DMSO) δ = 55.95, 97.53, 100.44, 110.66, 112.16, 112.55, 115.20, 127.16, 127.35, 155.34, 157.17, 158.02, 163.90, 173.26.

IR (ATR): ν = 3373, 3336, 3216, 1649, 1596.

LR MS (EI) m/z = 229.1, requires 229.1 [M]⁺.

3-Methoxy-6-(tritylamino)xanthen-9-one, 120

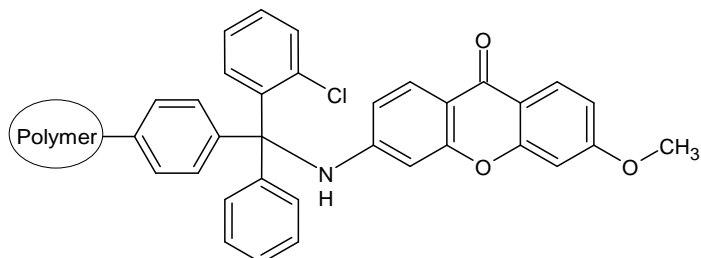
To a solution of 3-amino-6-methoxy-xanthen-9-one **119** (0.94 g, 3.90 mmol) in anhydrous DCM (60 ml), was added triethylamine (1.58 g, 2.18 ml, 15.6 mmol) followed by trityl chloride (2.17 g, 7.80 mmol). The reaction was stirred at room temperature while monitoring *via* TLC analysis, complete consumption of the starting material was noted after 1 hour. The crude reaction mixture was then diluted with water (50 ml), the aqueous portion separated and successively washed with DCM (3 x 50 ml). The organics were then combined, washed with water (3 x 50 ml), brine (2 x 50 ml), dried over anhydrous Na₂SO₄ and the solvent removed under vacuum. Purification was achieved *via* dissolution in DCM and subsequent precipitation in excess vigorously stirred n-hexane. The product was isolated, washed several times with 10:1 to 20:1 n-hexane:ethyl acetate and dried under vacuum to yield a very light yellow powder. (1.523 g, 81 %).

¹H-NMR (400 MHz; CDCl₃) δ = 3.85 (3H, s, CH₃-15), 5.66 (2H, s, NH-14), 6.07 (1H, d, J=2.26 Hz, CH-13), 6.54 (1H, dd, J=2.26, 8.77 Hz, CH-2), 6.69 (1H, d, J=2.44 Hz, CH-10), 6.84 (1H, dd, J=2.44, 8.87 Hz, CH-8), 7.94 (1H, d, J=8.77 Hz, CH-3), 8.14 (1H, d, J=8.87 Hz, CH-7).

¹³C-NMR (100 MHz; CDCl₃) δ = 55.82, 71.92, 100.22, 101.45, 112.53, 113.16, 114.03, 116.09, 127.09, 127.47, 128.03, 128.41, 129.21, 144.45, 151.93, 157.62, 157.92, 164.30, 175.40.

IR (ATR): ν = 3316, 1601, 1520.

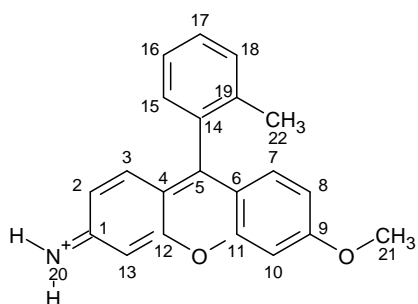
HR MS (ES) m/z = found 484.1925, requires 484.1913 [M + H]⁺.

2-Chlorotriptyl resin bound methoxyaminoxanthone, 3-Methoxy-6-(tritylamino)xanthen-9-one 119p

The 2-chlorotriptyl chloride resin (2.60 g, 4.16 mmol trityl sites) was swelled in anhydrous DCM (50 ml) under a nitrogen atmosphere for 30 minutes, the solvent was removed and the resin rinsed with anhydrous DCM (2 x 10 ml). The resin was then dried under a stream of nitrogen, after which a pyridine (3.29 g, 41.6 mmol, 3.36 ml) and a solution of 3-methoxy-6-(tritylamino)xanthen-9-one (1.00 g, 4.16 mmol) in anhydrous DCM/DMF (50 ml/10 ml) was added. The resulting suspension was agitated for 36 hours, after which the solution was removed under positive nitrogen pressure. The crude resin was washed with anhydrous DMF (5 x 30 ml), anhydrous methanol (10 x 20 ml) and anhydrous DCM (10 x 20 ml), then dried under a nitrogen stream.

A solution of DCM:Methanol:DIEA (34 ml:4 ml:2 ml) was then added to the resin under a dry nitrogen atmosphere and the resulting suspension was agitated for 1 hour at room temperature. The capping solution was then removed under positive nitrogen pressure and washed with DCM (3 x 20 ml), DMF (3 x 20 ml), methanol (3 x 20 ml) and DCM (3 x 20 ml), dried under a nitrogen stream and vacuum desiccated at 50 °C for 48 h, then stored under nitrogen.

SG1.TFA; 6-Methoxy-9-(o-tolyl)xanthen-3-iminium trifluoroacetate, 116



Under a dry nitrogen atmosphere, a stirred 2 M solution of o-tolylmagnesium bromide (2.58 ml, 1.03 mmol) was diluted to 0.5 M with anhydrous THF (7.73 ml). Into this was added a 0.1 M solution of 3-methoxy-6-(tritylamino)xanthen-9-one **120** (0.50 g, 1.03 mmol) dropwise at room temperature. The solution was then heated to 60 °C and stirred for 16 h, after which an additional portion of o-tolylmagnesium bromide (1.03 ml, 2.06 mmol) was slowly added and maintained at 60 °C for a further 16 h while following with TLC analysis. The reaction was then quenched with water (20 ml), then acidified to pH 7 *via* slow addition of cold aqueous 1 M HCl. The solution was extracted with diethyl ether (3 x 15 ml) and ethyl acetate (1 x 15 ml). The organics were combined, washed with water (2 x 15 ml) and brine (1 x 15 ml), dried over anhydrous Na₂SO₄ and concentrated under vacuum.

The crude product was reconstituted in DCM (14 ml), to which water (4 ml) and trifluoroacetic acid (2 ml) were added with stirring at room temperature. The mixture was stirred for 30 minutes after which water (10 ml) was added, and the organic layer separated. The organics were washed with saturated NaHCO₃ (2 x 10 ml), water (1 x 10 ml) and brine (1 x 10 ml), then dried over anhydrous Na₂SO₄ and concentrated under vacuum. Purification was achieved *via* flash column chromatography using a gradient elution of 0 – 10 % methanol:DCM, to yield the product as a foamy red solid. (0.025 g, 7.7 %, 1:99 methanol:DCM R_f = 0.1).

Manual Grignard preparation

Into a flask containing magnesium turnings (0.13 g, 5.15 mmol) under a dry nitrogen atmosphere was added anhydrous diethyl ether (7.7 ml). Into this was added a solution 1-bromo-2-methyl benzene (0.88 g, 5.15 mmol, 0.89 ml) in anhydrous THF (2.6 ml) dropwise, with stirring and heating to mild reflux. Upon Grignard initiation, heating was

removed and the remaining bromide continued to be added dropwise with stirring to maintain a mild reflux until all bromide was added. The mixture was stirred for a further 1h at which point a solution of 3-methoxy-6-(tritylamino)xanthen-9-one **120** (0.50 g, 1.03 mmol) in anhydrous THF (10 ml) was added dropwise over 30 minutes, followed by heating to 60 °C. The mixture was maintained at 60 °C for 16 hours and followed by TLC analysis, after which a second portion of Grignard reagent was added, prepared in the same manner as before using magnesium (0.13 g, 5.15 mmol) and bromo-2-methyl benzene (1.04 g, 2.06 mmol, 1.03 ml) in anhydrous THF (4 ml). Following addition, the mixture was stirred for a further 18 h at 60 °C and followed by TLC analysis. After 36 h the reaction was quenched with water (10 ml), stirred for 30 min and slowly acidified to pH 7 with cold aqueous 1M HCl. Subsequently the solution was extracted with diethyl ether (3 x 10 ml) and ethyl acetate (1 x 10 ml), the organics combined and washed with water (2 x 10 ml) and brine (1 x 10ml), then dried over anhydrous Na₂SO₄ and concentrated under vacuum.

The crude product was reconstituted in DCM (14 ml), to which water (4 ml) and trifluoroacetic acid (2 ml) were added with stirring at room temperature. The mixture was stirred for 30 minutes after which water (10 ml) was added, and the organic layer separated. The organics were washed with saturated NaHCO₃ (2 x 10 ml), water (1 x 10 ml) and brine (1 x 10 ml), then dried over anhydrous Na₂SO₄ and concentrated under vacuum. Purification was achieved *via* flash column chromatography using a gradient elution of 0 – 10 % methanol:DCM, to yield the product as a foamy red solid. (0.035 g, 10.9 %, 1:99 methanol:DCM R_f = 0.1).

¹H-NMR (600 MHz; MeOD) δ = 2.05 (3H, s, CH₃-22), 4.08 (3H, s, CH₃-21), 7.00 (1H, d, J=1.92 Hz, CH-13), 7.07 (1H, dd, J=1.92, 9.36 Hz, CH-2), 7.17 (1H, dd, J=2.34, 9.12 Hz, CH-8), 7.28 (1H, d, J=7.50 Hz CH-15), 7.31 (1H, d, J=9.36 Hz, CH-5), 7.34 (1H, d, J=9.12 Hz, CH-7), 7.45 (1H, d, J=2.34 Hz, CH-10), 7.49 (1H, dd, J=7.50, 7.50 Hz, CH-16), 7.54 (1H, d, J=7.68 Hz, CH-18), 7.60 (1H, dd, J=7.50, 7.50 Hz, CH-17), 8.72 (2H, br d, J=56.89 Hz, NH₂-20).

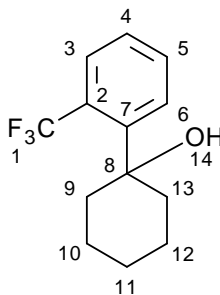
¹³C-NMR (150 MHz; MeOD) δ = 19.66, 57.57, 98.56, 98.63, 101.55, 116.65, 118.29, 121.31, 121.38, 127.37, 130.07, 131.63, 131.98, 132.27, 132.71, 134.34, 137.21, 158.49, 161.51, 161.73, 164.19, 164.30, 169.67.

¹⁹F-NMR (376 MHz; MeOD) δ = -76.77.

IR (ATR): ν = 2917 br, 1645, 1596, 1549.

HR MS (ES) m/z = found 316.1341, calculated 316.1338 [M]⁺.

1-[2-(Trifluoromethyl)phenyl]cyclohexan-1-ol, 126



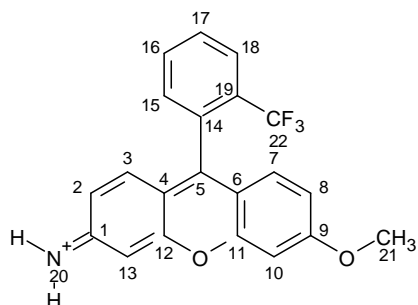
Into a flask containing magnesium turnings (0.14 g, 5.56 mmol) under a dry nitrogen atmosphere was added anhydrous THF (8 ml). Into this was added 2-bromobenzotrifluoride (1.00 g, 0.61 ml, 4.44 mmol) dropwise with stirring, while simultaneously heating to mild reflux. Upon Grignard initiation, the bromide continued to be added to maintain a mild reflux until addition completed, after which the resulting mixture was stirred for an additional 20 minutes. A cyclohexanone (0.22 g, 2.22 mmol, 0.23 ml) solution in anhydrous THF (1 ml) was then added dropwise and stirred for 18h at room temperature and monitored *via* TLC analysis. The reaction was acidified to pH 6 with 5 % aqueous HCl. The solution was then extracted with diethyl ether (2 x 5 ml) and ethyl acetate (1 x 5 ml) and the organics combined. The organics were then washed with water (1 x 5 ml) and brine (1 x 5ml) dried over Na₂SO₄ and concentrated under vacuum. Purification was achieved *via* flash column chromatography using gradient elution 0:1 - 3:7 EtOAc:petroleum ether (40 - 60) to yield a fragrant colourless oil (0.215 g, 40 %, 1:3 ethyl acetate:petroleum ether (40 - 60) R_f = 0.3).

¹H NMR (400 MHz, CD₂Cl₂) δ = 1.31 (1H, br s, OH-14), 1.65 (2H, m, CH₂-11), 1.83 (8H, m, CH₂-9, 10, 12, 13), 7.35 (1H, m, CH-4), 7.52 (1H, m, CH-5), 7.61 (1H, dd, J=0.73, 8.02 Hz, CH-6), 7.77 (1H, dd, J=0.88, 7.96 Hz, CH-3).

¹³C NMR (100 MHz, CD₂Cl₂) δ = 22.31, 25.77, 39.46, 39.48, 74.84, 124.30, 127.02, 127.07, 128.28, 128.40, 129.73, 131.96, 131.97.

IT (ATR): ν = 3612, 2931, 2858, 1604, 1577.

HR MS (ES) m/z = 244.1084, requires 244.1075 [M]⁺.

SG2.HCl; 6-Methoxy-9-[2-(trifluoromethyl)phenyl]xanthen-3-iminium hydrochloride, 127

Into a flask containing magnesium turnings (0.16 g, 6.51 mmol) under a dry nitrogen atmosphere was added anhydrous THF (6 ml). Into this, a solution of 2-bromobenzotrifluoride (1.47 g, 6.51 mmol, 0.89 ml) in anhydrous THF (4 ml) was added dropwise, with stirring and heating to mild reflux. Upon Grignard initiation, heating was removed and the remaining bromide continued to be added dropwise with stirring to maintain a mild reflux until all was added. The mixture was then stirred for a further 1 h at which point a solution of 3-methoxy-6-(tritylamino)xanthen-9-one **120** (0.45 g, 0.930 mmol) in anhydrous THF was added dropwise over 30 minutes, followed by heating to 60 °C. The mixture was maintained at 60 °C for 18 h and followed by TLC analysis. After the initial 18h a second portion of Grignard reagent was added, prepared in the same manner as before using magnesium (0.11 g, 4.65 mmol) and 2-bromobenzotrifluoride (1.05 g, 4.65 mmol, 0.63 ml) in anhydrous THF (4 ml). Following addition, the mixture was stirred for a further 18h at 60 °C and followed by TLC analysis. After 36 h the reaction was quenched with water (10 ml), stirred for 30 min and slowly acidified to pH 7 with cold aqueous 1 M HCl. Subsequently the solution was extracted with diethyl ether (3 x 10 ml) and ethyl acetate (1 x 10 ml), the organics combined and washed with water (2 x 10 ml) and brine (1 x 10ml), then dried over anhydrous Na₂SO₄ and concentrated under vacuum.

The crude product was reconstituted in THF (30 ml), to which 6 M aqueous HCl (30 ml) was added. The solution was stirred and followed by TLC analysis and after 1h the deprotection was deemed complete. Saturated NaHCO₃ solution (30 ml) was then added to the resulting mixture with stirring until CO₂ evolution ceased. The mixture was basified to pH 7 with 10 % aqueous NaOH. The mixture was then extracted with DCM (5 x 20 ml), the organics washed with water (3 x 10 ml) and brine (1 x 20 ml), then dried over anhydrous Na₂SO₄ and concentrated under vacuum. Purification was achieved *via* flash

column chromatography using a gradient elution 0 – 10 % Methanol:DCM to yield a fluffy red solid. (0.050 g, 13.2 %, 1:99 methanol:DCM R_f = 0.1).

$^1\text{H-NMR}$ (600 MHz; MeOD) δ = 4.08 (3H, s, CH_3 -21), 7.00 (1H, d, $J=2.04$ Hz, CH-13), 7.07 (1H, dd, $J=2.04, 9.36$ Hz, CH-2), 7.16 (1H, dd, $J=2.40, 9.12$ Hz, CH-8), 7.23 (2H, d, $J=9.36$ Hz, CH-3), 7.24 (1H, d, $J=9.12$ Hz, CH-7), 7.47 (1H, d, $J=2.40$ Hz, CH-10), 7.55 (1H, m, CH15), 7.93 (2H, m, CH-16,17), 8.07 (1H, m, CH-18).

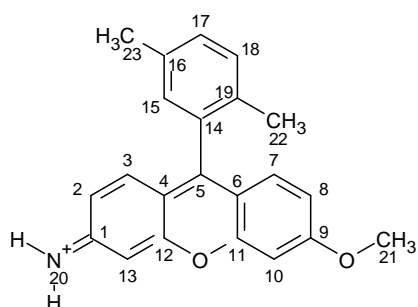
$^{13}\text{C-NMR}$ (150 MHz; MeOD) δ = 57.62, 98.57, 101.42, 117.00, 118.25, 118.80, 121.49, 128.15, 129.99, 130.19, 131.24, 132.02, 132.20, 132.34, 133.92, 134.49, 158.13, 158.19, 161.29, 164.45, 169.72.

$^{19}\text{F-NMR}$ (376 MHz; MeOD) δ = -60.12 (CF_3)

IR (ATR): ν = 3400 br, 1649, 1451.

HR MS (ES) m/z = found 370.1053, calculated 370.1055 $[\text{M}]^+$.

SG3.TFA; 9-(2,5-Dimethylphenyl)-6-methoxy-xanthen-3-iminium trifluoroacetate, 128



Into a flask containing magnesium turnings (0.23 g, 9.49 mmol) under a dry nitrogen atmosphere was added anhydrous THF (4 ml). Into this a solution of 2-bromo-1,4-dimethyl benzene (1.69 g, 9.11 mmol, 1.26 ml) in anhydrous THF (4 ml) was added dropwise, with stirring and heating to mild reflux. Upon Grignard initiation, heating was removed and the remaining bromide continued to be added dropwise over 30 minutes with stirring to maintain a mild reflux until all bromide was added, the reaction was then stirred for a further 1 h at room temperature. The 2-chlorotryl chloride resin bound 3-methoxy-6-(tritylamino)xanthen-9-one **119p** (0.27 mg/mg loading by qNMR, 0.69 g resin, 0.18 g loading, 0.759 mmol) was swelled in anhydrous THF (10 ml) for 30 minutes prior to use, the solvent was then removed, after which the Grignard reagent was added and heated to 60 °C. The reaction was agitated and maintained at 60 °C for 24 h while following *via* TLC analysis. After the initial 16 h the reaction solvent was removed and a second portion of Grignard reagent was added (12 equivalents), prepared in the same manner as before. Again, this was agitated at 60 °C for a further 16 h, after which the reaction mixture was removed and a third portion of Grignard (12 equivalents) was added as before and agitated at 60 °C for 16 h. Following this, the reaction mixture was cooled to room temperature, removed, and the resin washed with DMF (5 x 10 ml), methanol (10 x 10 ml), DCM (10 x 10 ml) and diethyl ether (5 x 10 ml), then dried under a stream of nitrogen and vacuum desiccated.

The resin was then stirred in a 5 % trifluoroacetic acid solution in DCM (1 ml/20 ml) for 20 minutes, the solution was removed, retained and the resin further washed with 5 % trifluoroacetic acid in DCM (3 x 20 ml). The extracts were combined and concentrated under vacuum. Purification was achieved *via* flash column chromatography using a gradient elution of 0 – 10 % methanol:DCM, to yield a red foam. (0.061 g, 18.1 %, 1:99 methanol:DCM $R_f = 0.1$).

$^1\text{H-NMR}$ (600 MHz; CD_2Cl_2) δ = 1.96 (3H, s, CH_3 -22), 2.39 (3H, s, CH_3 -23), 4.01 (3H, s, CH_3 -21), 6.98 (1H, br s, CH-15), 7.00 (1H, dd, $J=2.46, 9.06$ Hz, CH-8), 7.14 (1H, br s, CH-13), 7.15 (1H, dd, $J=1.80, 9.06$ Hz, CH-2), 7.21 (1H, d, $J=2.46$ Hz, CH-10), 7.23 (1H, d, $J=9.06$ Hz, CH-3), 7.27 (1H, d, $J=9.06$ Hz, CH-7), 7.33 (2H, m, CH-17,18), 8.93 (2H, br d, $J=240.23$ Hz, NH_2 -20).

$^{13}\text{C-NMR}$ (150 MHz; CD_2Cl_2) δ = 19.31, 21.02, 57.26, 57.56, 98.70, 100.53, 100.73, 115.85, 117.56, 117.65, 121.05, 129.59, 131.16, 131.39, 131.58, 131.65, 133.17, 133.58, 136.51, 157.45, 160.23, 161.22, 162.56, 168.39.

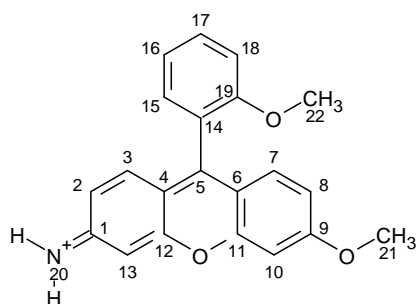
$^{19}\text{F-NMR}$ (376 MHz; CD_2Cl_2) δ = -75.93.

IR (ATR): ν = 3313 br, 3069 br, 1644, 1597, 1544.

HR MS (ES) m/z = found 330.1507, calculated 330.1494 $[\text{M}]^+$.

All subsequent Grignard reactions were performed using the same solid supported procedure, their stoichiometries for preparation of the Grignard reagent are quoted. The crude product was also cleaved from the resins using the same method.

SG4.TFA; 6-Methoxy-9-(2-methoxyphenyl)xanthen-3-iminium trifluoroacetate, 129



2-Bromoanisole (2.33 g, 12.4 mmol, 1.55 ml), magnesium turnings (0.32 g, 13.0 mmol) x 3 portions.

2-chlorotritylchloride resin bound 3-methoxy-6-(tritylamino)xanthen-9-one **119p** (0.27 mg/mg loading by qNMR, 0.94 g resin, 0.25 g loading, 1.04 mmol).

Purification achieved *via* flash column chromatography using gradient elution 2 – 10 % methanol:DCM to yield a foamy red solid. (0.67 g, 14.5 %, 1:99 methanol:DCM $R_f = 0.1$).

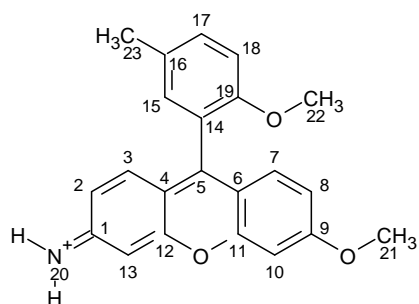
$^1\text{H-NMR}$ (600 MHz; CD_2Cl_2) $\delta = 3.70$ (3H, s, CH-22), 4.01 (3H, s, CH-21), 6.99 (1H, dd, $J=2.46, 9.12$ Hz, CH-8), 7.17 (1H, d, $J=2.46$ Hz, CH-10), 7.17 (1H, br d, $J=8.40$ Hz, CH-18), 7.20 (2H, m, CH-15, 16), 7.30 (1H, d, $J=1.83$ Hz, CH-13), 7.30 (1H, d, $J=9.39$ Hz, CH-3), 7.35 (1H, dd, $J=1.83, 9.39$ Hz, CH-2), 7.36 (1H, d, $J=9.12$ Hz, CH-7), 7.63 (1H, m, CH-17), 9.33 (2H, br d, $J=156.75$ Hz, NH_2 -20).

$^{13}\text{C-NMR}$ (150 MHz; CD_2Cl_2) $\delta = 56.05, 57.05, 98.55, 100.34, 112.01, 115.83, 116.61, 118.13, 120.70, 121.20, 121.41, 131.03, 131.46, 132.60, 133.43, 156.93, 157.04, 157.09, 159.95, 163.17, 167.42$.

$^{19}\text{F-NMR}$ (376 MHz; CD_2Cl_2) $\delta = -75.52$.

IR (ATR): $\nu = 3012$ br, 1644, 1598, 1546.

HR MS (ES) $m/z =$ found 332.1291, calculated 332.1287 $[\text{M}]^+$.

SG5.TFA; 6-Methoxy-9-(2-methoxy-5-methyl-phenyl)xanthen-3-iminium trifluoroacetate, 130

2-Bromo-4-methylanisole (2.65 g, 13.2 mmol, 1.91 ml), magnesium turnings (0.33 g, 13.7 mmol) x 3 portions.

2-chlorotriptylchloride resin bound 3-methoxy-6-(tritylamino)xanthen-9-one **119p** (0.27 mg/mg loading by qNMR, 1.00 g resin, 0.26 g loading, 1.10 mmol).

Purification achieved *via* flash column chromatography using gradient elution 2 – 10 % methanol:DCM to yield a foamy red solid. (0.158 g, 32.3 %, 1:99 methanol:DCM R_f = 0.1).

$^1\text{H-NMR}$ (600 MHz; CD_2Cl_2) δ = 2.37 (3H, s, CH_3 -23), 3.66 (3H, s, CH_3 -22), 4.02 (3H, s, CH_3 -21), 6.99 (2H, m, CH-13, 15), 7.02 (1H, dd, J =2.45, 9.04 Hz, CH-8), 7.06 (2H, m, CH-3, 17), 7.20 (1H, d, J =2.45 Hz, CH-10), 7.37 (1H, d, J =9.42 Hz, CH-18), 7.41 (1H, d, J =9.04 Hz, CH-7), 7.42 (1H, dd, J =2.15, 9.18 Hz, CH-2), 8.58 (2H, br d, J =94.34 Hz, NH_2 -20).

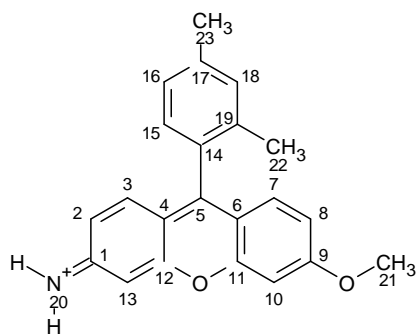
$^{13}\text{C-NMR}$ (150 MHz; CD_2Cl_2) δ = 20.47, 56.06, 57.10, 98.12, 100.31, 111.97, 115.95, 116.94, 117.85, 120.27, 120.67, 130.91, 131.25, 131.78, 133.06, 133.91, 154.95, 157.12, 158.35, 160.28, 162.81, 167.80.

$^{19}\text{F-NMR}$ (376 MHz; CD_2Cl_2) δ = -75.97.

IR (ATR): ν = 3080 br, 1678, 1644, 1599, 1544.

HR MS (ES) m/z = found 346.1455, calculated 346.1443[M] $^+$.

SG6.TFA; 9-(2,4-Dimethylphenyl)-6-methoxy-xanthen-3-iminium trifluoroacetate, 131



1-bromo-2,4-dimethylbenzene (1.84 g, 9.94 mmol, 1.34 ml), magnesium turnings (0.25 g, 10.4 mmol) x 3 portions.

2-chlorotriylchloride resin bound 3-methoxy-6-(tritylamino)xanthen-9-one **119p** (0.30 mg/mg loading by qNMR, 0.67 g resin, 0.20 g xanthone, 0.829 mmol).

Purification achieved *via* flash column chromatography using gradient elution 2 – 10 % methanol:DCM to yield a foamy red solid. (0.135 g, 36.7 %, 1:99 methanol:DCM R_f = 0.1).

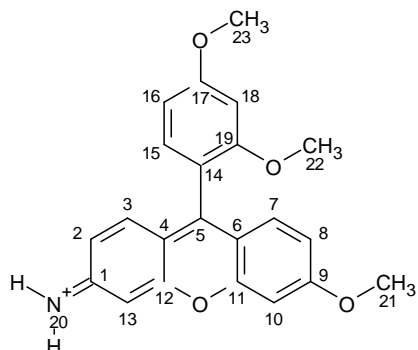
$^1\text{H-NMR}$ (600 MHz; CD_2Cl_2) δ = 1.98 (3H, s, CH_3 -22), 2.47 (3H, s, CH_3 -23), 4.07 (3H, s, CH_3 -21), 6.99 (1H, br s, CH-13), 7.07 (1H, d, $J=7.68$ Hz, CH-15), 7.11 (1H, dd, $J=2.46$, 9.27 Hz, CH-8), 7.25 (1H, br d, $J=7.68$ Hz, CH-16), 7.29 (1H, d, $J=9.48$ Hz, CH-3), 7.29 (1H, br s, CH-18), 7.37 (1H, d, $J=2.46$ Hz, CH-10), 7.40 (1H, d, $J=9.27$ Hz, CH-7), 7.69 (1H, d, $J=9.48$ Hz, CH-2), 11.45 (2H, br s, NH_2 -20).

$^{13}\text{C-NMR}$ (150 MHz; CD_2Cl_2) δ = 24.53, 26.21, 62.67, 106.42, 122.02, 123.64, 124.22, 125.19, 132.84, 134.44, 135.03, 137.34, 137.52, 137.63, 142.06, 145.13, 147.17, 161.28, 163.73, 164.43, 168.88, 175.38.

$^{19}\text{F-NMR}$ (376 MHz; CD_2Cl_2) δ = -75.88.

IR (ATR): ν = 3066 br, 1688, 1595, 1548.

HR MS (ES) m/z = found 364.1097, calculated= 364.1104 $[\text{M} - \text{H} + \text{Cl}]^+$.

SG7.TFA; 9-(2,4-Dimethoxyphenyl)-6-methoxy-xanthen-3-iminium trifluoroacetate, 132

1-bromo-2,4-dimethoxy benzene (2.16 g, 9.95 mmol, 1.43 ml), magnesium turnings (0.25 g, 10.4 mmol) x 3 portions.

2-chlorotritylchloride resin bound 3-methoxy-6-(tritylamino)xanthen-9-one **119p** (0.21 mg/mg loading by qNMR, 0.96 g resin, 0.20 g xanthone loading, 0.829 mmol).

Purification achieved *via* flash column chromatography using gradient elution 2 – 10 % methanol:DCM to yield a foamy red solid. (0.68 g, 17.3 %, 1:99 methanol:DCM $R_f = 0.1$).

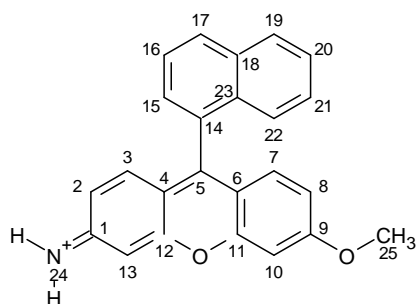
¹H-NMR (600 MHz; CD₂Cl₂) δ = 3.68 (3H, s, CH₃-22), 3.93 (3H, s, CH₃-23), 4.01 (1H, s, CH₃-21), 6.71 (1H, d, J=2.22 Hz, CH-18), 6.74 (1H, dd, J=2.22, 8.34 Hz, CH-16), 6.96 (1H, d, J=1.83 Hz, CH-13), 7.03 (1H, dd, J=2.46, 9.18 Hz, CH-8), 7.05 (1H, dd, J=1.83, 9.36 Hz, CH-2), 7.12 (1H, d, J=8.34 Hz, CH-15), 7.18 (1H, d, J=2.46 Hz, CH-10), 7.42 (1H, d, J=9.36 Hz, CH-3), 7.46 (1H, d, J=9.18 Hz, CH-7), 8.41 (2H, br d, J=61.33, NH₂-20).

¹³C-NMR (150 MHz; CD₂Cl₂) δ = 55.61, 55.71, 56.67, 97.63, 97.70, 99.01, 99.87, 105.42, 112.51, 115.80, 117.61, 119.99, 131.52, 131.77, 133.60, 156.76, 158.05, 159.89, 162.16, 162.27, 163.45, 167.36.

IR (ATR): ν = 2919 br, 2850, 1693, 1665, 1598, 1543.

HR MS (ES) m/z = found 362.1387, calculated 362.1392 [M]⁺.

SG8.TFA; 6-Methoxy-9-(1-naphthyl)xanthen-3-iminium trifluoroacetate, 133



1-bromonaphthalene (1.80 g, 8.70 mmol, 1.22 ml), magnesium turnings (0.22 g, 9.06 mmol) x 3 portions.

2-chlorotritylchloride resin bound 3-methoxy-6-(tritylamino)xanthen-9-one **119p** (0.21 mg/mg loading by qNMR, 0.84 g resin, 0.18 g xanthone, 0.725 mmol).

Purification achieved *via* flash column chromatography using gradient elution 2 – 10 % methanol:DCM to yield a foamy red solid. (0.45 g, 13.3 %, 1:99 methanol:DCM R_f = 0.1).

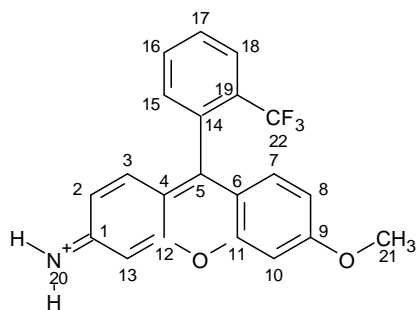
$^1\text{H-NMR}$ (600 MHz; CD_2Cl_2) δ = 4.02 (3H, s, CH_3 -25), 6.92 (1H, dd, J =2.46, 9.18 Hz, CH-8), 6.98 (1H, dd, J =2.07, 9.42 Hz, CH-2), 7.10 (1H, d, J =2.07 Hz, CH-13), 7.17 (1H, d, J =9.42 Hz, CH-3), 7.18 (1H, d, J =9.18 Hz, CH-7), 7.26 (2H, m, CH-10, 19), 7.40 (1H, ddd, J =1.34, 6.93, 8.36 Hz, CH-20), 7.47 (1H, dd, J =1.05, 7.01 Hz, CH-15), 7.58 (1H, ddd, J =1.14, 6.93, 8.34 Hz, CH-21), 7.71 (1H, dd, J =8.31, 7.01 Hz, CH-16), 8.04 (1H, d, J =8.34 Hz, CH-22), 8.16 (1H, d, J =8.31 Hz, CH-17), 8.77 (1H, d, J =215.03 Hz, NH_2 -24).

$^{13}\text{C-NMR}$ (150 MHz; CD_2Cl_2) δ = 57.18, 98.46, 100.57, 116.34, 117.16, 118.53, 121.16, 125.36, 125.51, 127.39, 128.02, 128.19, 129.12, 129.45, 131.19, 131.69, 131.77, 133.61, 133.86, 157.10, 158.81, 160.16, 163.10, 168.08.

IR (ATR): ν = 3064 br, 1674, 1643, 1595, 1545.

HR MS (ES) m/z = found 352.1353, requires 352.1338 $[\text{M}]^+$.

SG9.TFA; 6-Methoxy-9-[2-(trifluoromethyl)phenyl]xanthen-3-iminium trifluoroacetate, 134



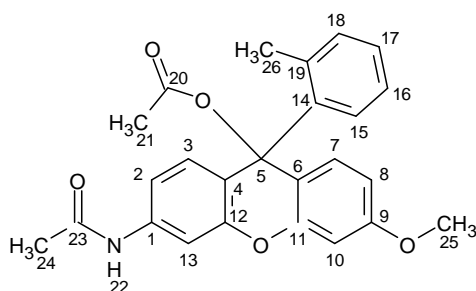
Under a dry nitrogen atmosphere, Amberlyst A21 basic resin (0.50 g) was washed with a 5:1 DCM/methanol mixture (2 x 10 ml), followed by DCM (5 x 10 ml), methanol (5 x 10 ml) and an addition DCM wash (5 x 10 ml). The resin was then dried under a stream of nitrogen followed by high vacuum. SG2.HCl **127** (0.01 g, 0.0296 mmol) was then reconstituted into DCM/methanol solution of 5:1 (20 ml), to which the clean dry Amberlyst A21 resin was then added and stirred for 20 h. The resin was filtered off and washed several times with the reaction solution. The washings were combined, the solvent removed under high vacuum and stored under nitrogen. The dry compound was reconstituted in a 10 % trifluoroacetic acid solution in DCM and stirred under nitrogen for 24 h, the solvent was then removed under high vacuum for several days, to yield a deep red solid. (0.012 g, 0.0248 mmol, 84 %, 1:99 methanol:DCM $R_f = 0.1$).

$^1\text{H-NMR}$ (600 MHz; MeOD) $\delta = 4.08$ (3H, s, CH_3 -21), 6.99 (1H, d, $J=2.04$ Hz, CH-13), 7.05 (1H, dd, $J=2.04, 9.42$ Hz, CH-2), 7.16 (1H, dd, $J=2.40, 9.42$ Hz, CH-8), 7.23 (1H, d, $J=9.42$ Hz, CH-3), 7.24 (1H, d, $J=9.42$ Hz, CH-7), 7.47 (1H, d, $J=2.40$ Hz, CH-10), 7.54 (1H, m, CH-15), 7.92 (2H, m, CH-16, 17), 8.07 (1H, m, CH-18).

$^{13}\text{C-NMR}$ (150 MHz; MeOD) $\delta = 57.60, 98.55, 101.42, 117.02, 118.26, 118.81, 121.48, 128.15, 130.01, 130.22, 131.27, 132.03, 132.19, 132.35, 133.91, 134.51, 158.14, 158.21, 161.31, 164.46, 169.72$.

$^{19}\text{F-NMR}$ (376 MHz; CD_2Cl_2) $\delta = -59.17, -76.23$.

HR MS (ES) $m/z =$ found 370.1060, requires 370.1055 $[\text{M}]^+$.

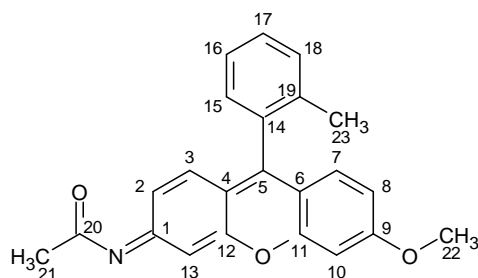
SG1BisAc; [3-Acetamido-6-methoxy-9-(*o*-tolyl)xanthen-9-yl] acetate, 135

Into a stirred solution of SG1.TFA **116** (0.01 g, 0.0230 mmol) in anhydrous pyridine under a dry nitrogen atmosphere, acetic anhydride (0.01 g, 0.115 mmol, 0.01 ml) was added dropwise. The resulting solution was stirred at room temperature for 16 h while monitoring *via* TLC analysis, and then evaporated to dryness under high vacuum at 40 °C. The crude mixture was reconstituted in DCM (10 ml), washed with 0.5 M aqueous HCl solution (3 x 5 ml), saturated NaHCO₃ (2 x 5 ml), brine (1 x 10 ml), dried over anhydrous Na₂SO₄ and finally evaporated to dryness under high vacuum. Purification was achieved *via* flash column chromatography using a gradient elution of 0 - 5 % methanol:DCM to yield an orange solid. (0.007 g, 73 %, 1:9 methanol:DCM R_f = 0.4).

¹H-NMR (600 MHz; CD₂Cl₂) δ = 1.43 (3H, s, CH₃-21), 2.14 (3H, s, CH₃-26), 2.73 (3H, s, CH₃-24), 3.82 (3H, s, CH₃-25), 6.59 (1H, dd, J=2.52, 8.70 Hz, CH-8), 6.67 (1H, d, J=2.52 Hz, CH-10), 6.85 (1H, d, J=8.70 Hz, CH-7), 6.89 (1H, d, J=8.46 Hz, CH-3), 6.92 (1H, dd, J=1.95, 8.46 Hz, CH-2), 6.95 (1H, dd, J=7.41, 0.78 Hz, CH-18), 7.18 (1H, ddd, J=7.41, 7.41, 1.38 Hz, CH-17), 7.26 (1H, br s, NH-23), 7.33 (1H, ddd, J=7.92, 7.41, 0.78 Hz, CH-16), 7.63 (1H, d, J=1.95 Hz, CH-13), 8.28 (1H, dd, J=1.38, 7.92 Hz, CH-15).

¹³C-NMR HSQC (150 MHz; CD₂Cl₂) δ = 131.76, 130.03, 129.60, 127.32, 125.10, 114.58, 114.58, 111.08, 99.50, 55.40, 49.18, 24.52, 20.08.

HR MS (ES) m/z = found 358.1442, requires 358.1443 [M – OAc]⁺.

SG1Ac; *N*-[6-methoxy-9-(*o*-tolyl)xanthen-3-ylidene]acetamide, **136**

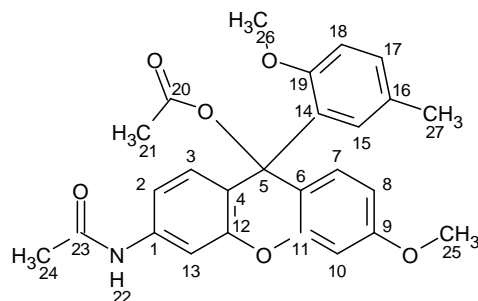
[3-Acetamido-6-methoxy-9-(*o*-tolyl)xanthen-9-yl] acetate **135** was exposed to sunlight over 70 h at 20 °C to induce photolysis to form the elimination product SG1Ac **136** as an orange brown solid. (0.006 g, 100 %).

$^1\text{H-NMR}$ (600 MHz; CD_2Cl_2) δ = 2.46 (3H, s, CH_3 -23), 3.41 (3H, s, CH_3 -21), 4.15 (3H, s, CH_3 -22), 7.23 (1H, dd, $J=1.26, 7.56$ Hz, CH-15), 7.25 (1H, dd, $J=2.34, 9.24$ Hz, CH-8), 7.44 (1H, d, $J=2.34$ Hz, CH-10), 7.49 (1H, ddd, $J=0.78, 7.56, 7.65$ Hz, CH-16), 7.52 (1H, dd, $J=7.65, 0.78$ Hz, CH-18), 7.58 (1H, d, $J=9.24$ Hz, CH-7), 7.59 (1H, d, $J=9.42$ Hz, CH-3), 7.62 (1H, ddd, $J=1.26, 7.65, 7.65$ Hz, CH-17), 8.56 (1H, d, $J=9.42$ Hz, CH-2), 9.02 (1H, d, $J=1.10$ Hz, CH-13).

$^{13}\text{C-NMR}$ HSQC (150 MHz; CD_2Cl_2) δ = 131.89, 131.23, 131.10, 128.80, 126.30, 120.35, 99.89, 57.66, 25.13, 19.67.

HR MS (ES) m/z = found 358.1446, requires 358.1443 $[\text{M}]^+$.

SG5BisAc; [3-Acetamido-6-methoxy-9-(2-methoxy-5-methyl-phenyl)xanthen-9-yl] acetate, 137



Into a stirred solution of SG5.TFA **130** (0.042 g, 0.0910 mmol) in anhydrous pyridine under a dry nitrogen atmosphere, acetic anhydride (0.047 g, 0.457 mmol, 0.044 ml) was added dropwise. The resulting solution was stirred at room temperature for 16 h while monitoring *via* TLC analysis, after which an additional portion of acetic anhydride (0.141 g, 1.37 mmol, 0.132 ml) was added dropwise. After an additional 4 h the reaction mixture was evaporated to dryness under high vacuum at 40 °C. The crude mixture was reconstituted in DCM (10 ml), washed with 0.5 M aqueous HCl solution (3 x 5 ml), saturated NaHCO₃ (2 x 5 ml), brine (1 x 10 ml), dried over anhydrous Na₂SO₄ and finally evaporated to dryness under high vacuum. Purification was achieved *via* flash column chromatography using a gradient elution of 0 - 5 % methanol:DCM to yield an deep orange solid. (0.010 g, 25 %, 1:9 methanol:DCM R_f = 0.4).

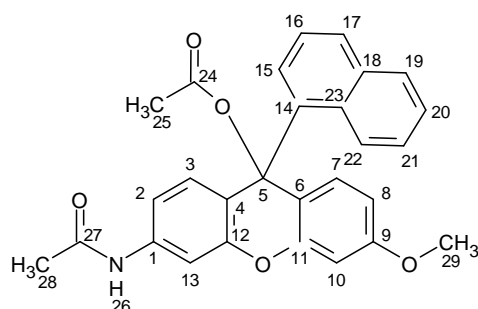
¹H-NMR (600 MHz; CD₂Cl₂) δ = 2.13 (3H, s, CH₃-21), 2.39 (3H, s, CH₃-27), 2.79 (3H, s, CH₃-24), 3.11 (3H, s, CH₃-23), 3.80 (3H, s, CH₃-25), 6.55 (1H, dd, J=2.55, 8.58 Hz, CH₃-8), 6.57 (1H, d, J=8.22 Hz, CH-18), 6.65 (1H, d, J=2.55 Hz, CH-10), 6.91 (1H, dd, J=1.89, 8.46 Hz, CH-2), 6.95 (1H, d, J=8.58 Hz, CH-7), 6.99 (1H, d, J=8.46 Hz, CH-3), 7.02 (1H, dd, J=2.28, 8.22 Hz, CH-17), 7.30 (1H, s, NH-22), 7.54 (1H, d, J=1.89 Hz, CH-13), 7.93 (1H, d, J=2.28 Hz, CH-15).

¹³C-NMR (150 MHz; CD₂Cl₂) δ = 21.08, 24.83, 49.98, 55.75, 56.30, 73.10, 99.98, 106.36, 110.38, 113.53, 114.34, 115.71, 119.44, 126.17, 128.89, 129.01, 129.33, 129.87, 137.42, 138.68, 152.91, 153.45, 154.29, 160.27, 168.56.

IR (ATR): ν = 3300, 2934, 2834, 1668, 1612, 1586, 1536.

HR MS (ES) m/z = found 388.1553, requires 388.1549 [M – OAc]⁺.

SG8BisAc; [3-Acetamido-6-methoxy-9-(naphthyl)xanthen-9-yl] acetate, 139



Into a stirred solution of SG8.TFA **133** (0.079 g, 0.170 mmol) in anhydrous pyridine under a dry nitrogen atmosphere, acetic anhydride (0.868 g, 8.50 mmol, 0.803 ml) was added dropwise. The resulting solution was stirred at room temperature for 14 h while monitoring *via* TLC analysis, after which it was evaporated to dryness under high vacuum at 40 °C. The crude mixture was reconstituted in DCM (10 ml), washed with 0.5 M aqueous HCl solution (3 x 5 ml), saturated NaHCO₃ (2 x 5 ml), brine (1 x 10 ml), dried over anhydrous Na₂SO₄ and finally evaporated to dryness under high vacuum. Purification was achieved *via* flash column chromatography using a gradient elution of 0 - 5 % methanol:DCM to yield a deep orange solid. (0.014 g, 18 %, 1:9 methanol:DCM R_f = 0.4).

¹H-NMR (600 MHz; CD₂Cl₂) δ = 2.12 (3H, s, CH₃-25), 2.80 (3H, s, CH₃-4), 3.80 (3H, s, CH₃-29), 6.50 (1H, dd, J=2.55, 8.70 Hz, CH-8), 6.77 (1H, d, J=2.55 Hz, CH-10), 6.79 (1H, dd, J=2.04, 8.46 Hz, CH-2), 6.82 (1H, d, J=8.70 Hz, CH-7), 6.84 (1H, d, J=8.46 Hz, CH-3), 7.00 (1H, ddd, J=1.55, 6.84, 8.69 Hz, CH-20), 7.20 (1H, m, CH-19), 7.23 (1H, ddd, J=1.11, 8.04, 6.84 Hz, CH-21), 7.32 (1H, s, NH-26), 7.62 (1H, dd, J=7.41, 8.10 Hz, CH-16), 7.77 (2H, m, CH-22, 13), 7.84 (1H, d, J=8.10 Hz, CH-17), 8.52 (1H, dd, J=0.69, 7.41 Hz, CH-15).

¹³C-NMR (150 MHz; CD₂Cl₂) δ = 24.83, 49.51, 55.82, 74.65, 100.33, 106.69, 111.41, 115.06, 115.64, 119.16, 125.00, 125.02, 125.05, 125.18, 125.63, 129.13, 129.25, 129.82, 130.24, 130.27, 135.04, 139.42, 141.44, 152.48, 153.06, 160.89, 168.66, 168.68.

IR (ATR): ν = 3306, 3051, 2932, 1725, 1671, 1611, 1584, 1537.

HR MS (ES) m/z = found 394.1444, requires 394.1443 [M + H – OAc]⁺.

Chapter 4 – References

Chapter 4 - References

- ¹ Hibbetts K, Hines B, Williams D. An overview of proteinase inhibitors. *Journal of veterinary internal medicine*. 1999 Jul;13(4):302-8.
- ² Diamond SL. Methods for mapping protease specificity. *Current opinion in chemical biology*. 2007 Feb 1;11(1):46-51.
- ³ Puente XS, Sánchez LM, Overall CM, López-Otín C. Human and mouse proteases: a comparative genomic approach. *Nature Reviews Genetics*. 2003 Jul;4(7):544-548.
- ⁴ Vogler EA, Siedlecki CA. Contact activation of blood-plasma coagulation. *Biomaterials*. 2009 Apr 1;30(10):1857-69.
- ⁵ Mansour K, Taher AT, Musallam KM, Alam S. Aspirin resistance. *Advances in hematology*. 2009 Feb 15;2009(1):1-10.
- ⁶ Vergnolle N. Protease-activated receptors as drug targets in inflammation and pain. *Pharmacology & therapeutics*. 2009 Sep 1;123(3):292-309.
- ⁷ Strongin AY. Proteolytic and non-proteolytic roles of membrane type-1 matrix metalloproteinase in malignancy. *Biochimica et Biophysica Acta (BBA)-Molecular Cell Research*. 2010 Jan 1;1803(1):133-41.
- ⁸ Wilkinson RD, Williams R, Scott CJ, Burden RE. Cathepsin S: therapeutic, diagnostic, and prognostic potential. *Biological chemistry*. 2015 Aug 1;396(8):867-82.
- ⁹ Yuan J, Yankner BA. Apoptosis in the nervous system. *Nature*. 2000 Oct 12;407(6805):802.
- ¹⁰ Doucet A, Overall CM. Protease proteomics: revealing protease in vivo functions using systems biology approaches. *Molecular aspects of medicine*. 2008 Oct 1;29(5):339-58.
- ¹¹ Havale SH, Pal M. Medicinal chemistry approaches to the inhibition of dipeptidyl peptidase-4 for the treatment of type 2 diabetes. *Bioorganic & medicinal chemistry*. 2009 Mar 1;17(5):1783-802.
- ¹² Haim H, Salas I, Sodroski J. Proteolytic processing of the human immunodeficiency virus envelope glycoprotein precursor decreases conformational flexibility. *Journal of virology*. 2013 Feb;87(3):1884-9.
- ¹³ Oda K. JB Review New families of carboxyl peptidases: serine-carboxyl. *J. Biochem*. 2012;151(1):13-25.
- ¹⁴ Brik A, Wong CH. HIV-1 protease: mechanism and drug discovery. *Organic & biomolecular chemistry*. 2003;1(1):5-14.
- ¹⁵ Rzychon M, Chmiel D, Stec-Niemczyk J. Modes of inhibition of cysteine proteases. *Acta Biochim. Pol.* 2004 Jan 1;51(4):861-73.
- ¹⁶ Menard R, Carriere J, Laflamme P, Plouffe C, Khouri HE, Vernet T, Tessier DC, Thomas DY, Storer AC. Contribution of the glutamine 19 side chain to transition-state stabilization in the oxyanion hole of papain. *Biochemistry*. 1991 Sep;30(37):8924-8.
- ¹⁷ Otto HH, Schirmeister T. Cysteine proteases and their inhibitors. *Chemical reviews*. 1997 Feb 5;97(1):133-72.

- ¹⁸ Arafet K, Ferrer S, Moliner V. Computational study of the catalytic mechanism of the cruzain cysteine protease. *ACS Catalysis*. 2017 Jan 11;7(2):1207-15.
- ¹⁹ Rauwerdink A, Kazlauskas RJ. How the same core catalytic machinery catalyzes 17 different reactions: The serine-histidine-aspartate catalytic triad of α/β -hydrolase fold enzymes. *ACS catalysis*. 2015 Sep 22;5(10):6153-76.
- ²⁰ Wang X, Wu S, Xu D, Xie D, Guo H. Inhibitor and substrate binding by angiotensin-converting enzyme: quantum mechanical/molecular mechanical molecular dynamics studies. *Journal of chemical information and modeling*. 2011 Apr 26;51(5):1074-82.
- ²¹ Zhang C, Wu S, Xu D. Catalytic mechanism of angiotensin-converting enzyme and effects of the chloride ion. *The Journal of Physical Chemistry B*. 2013 May 23;117(22):6635-45.
- ²² Mu X, Zhang C, Xu D. QM/MM investigation of the catalytic mechanism of angiotensin-converting enzyme. *Journal of molecular modeling*. 2016 Jun 1;22(6):132.
- ²³ Piddock LJ. The crisis of no new antibiotics—what is the way forward? *The Lancet infectious diseases*. 2012 Mar 1;12(3):249-53.
- ²⁴ White AR, BSAC Working Party on The Urgent Need: Regenerating Antibacterial Drug Discovery and Development, Blaser M, Carrs O, Cassell G, Fishman N, Guidos R, Levy S, Powers J, Norrby R, Tillotson G. Effective antibacterials: at what cost? The economics of antibacterial resistance and its control. *Journal of antimicrobial chemotherapy*. 2011 Jun 23;66(9):1948-53.
- ²⁵ White AR. The pharmaceutical company approach to antibiotic policies. In *Antibiotic Policies 2005* (pp. 673-699). Springer, Boston, MA.
- ²⁶ Payne DJ, Gwynn MN, Holmes DJ, Pompliano DL. Drugs for bad bugs: Confronting the challenges of antibacterial discovery. *Nature reviews Drug discovery*. 2007 Jan;6(1):29.
- ²⁷ Payne DJ, Miller LF, Findlay D, Anderson J, Marks L. Time for a change: addressing R&D and commercialization challenges for antibacterials. *Philosophical Transactions of the Royal Society B: Biological Sciences*. 2015 Jun 5;370(1670):20140086.
- ²⁸ ECDC E. The Bacterial Challenge—Time to react a call to narrow the gap between multidrug-resistant bacteria in the EU and development of new antibacterial agents. Solna: ECDC & EMEA Joint press release. 2009.
- ²⁹ Resistance to Antibiotics: The spread of superbugs. What can be done about the rising risk of antibiotic resistance? (2011). *The Economist*, 399(8727).
- ³⁰ Kaplan W, Laing R. Priority medicines for Europe and the world. Geneva: WHO; 2004 Nov. [cited 12 April 2019]. Available from: <http://stroma.se/wp-content/uploads/2016/04/Priority-Medicines-for-Europe-and-the-World.pdf>
- ³¹ World Health Organization. The global burden of disease: 2004 update. [cited 12 April 2019]. Available from: https://apps.who.int/iris/bitstream/handle/10665/43942/9789241563710_eng.pdf
- ³² Magill SS, Edwards JR, Bamberg W, Beldavs ZG, Dumyati G, Kainer MA, Lynfield R, Maloney M, McAllister-Hollod L, Nadle J, Ray SM. Multistate point-prevalence survey of

health care–associated infections. *New England Journal of Medicine*. 2014 Mar 27;370(13):1198-208.

³³ Kollef MH, Shorr A, Tabak YP, Gupta V, Liu LZ, Johannes RS. Epidemiology and outcomes of health-care–associated pneumonia: results from a large US database of culture-positive pneumonia. *Chest*. 2005 Dec 1;128(6):3854-62.

³⁴ Kollef MH, Sherman G, Ward S, Fraser VJ. Inadequate antimicrobial treatment of infections: a risk factor for hospital mortality among critically ill patients. *Chest*. 1999 Feb 1;115(2):462-74.

³⁵ Kumar A, Roberts D, Wood KE, Light B, Parrillo JE, Sharma S, Suppes R, Feinstein D, Zanotti S, Taiberg L, Gurka D. Duration of hypotension before initiation of effective antimicrobial therapy is the critical determinant of survival in human septic shock. *Critical care medicine*. 2006 Jun 1;34(6):1589-96.

³⁶ McKinnell JA, Corman S, Patel D, Leung GH, Gordon LM, Lodise TP. Effective antimicrobial stewardship strategies for cost-effective utilization of telavancin for the treatment of patients with hospital-acquired bacterial pneumonia caused by *Staphylococcus aureus*. *Clinical therapeutics*. 2018 Mar 1;40(3):406-14.

³⁷ Caliendo AM, Gilbert DN, Ginocchio CC, Hanson KE, May L, Quinn TC, Tenover FC, Alland D, Blaschke AJ, Bonomo RA, Carroll KC. Better tests, better care: improved diagnostics for infectious diseases. *Clinical Infectious Diseases*. 2013 Dec 1;57(suppl_3):S139-70.

³⁸ World Health Organisation. World Health Day 2011, Urgent action necessary to safeguard drug treatments. [Internet]. Who.int. 2019 [cited 16 April 2019] Available from: https://www.who.int/mediacentre/news/releases/2011/whd_20110406/en/

³⁹ Sethi S, Breton J, Wynne B. Efficacy and safety of pharmacokinetically enhanced amoxicillin-clavulanate at 2,000/125 milligrams twice daily for 5 days versus amoxicillin-clavulanate at 875/125 milligrams twice daily for 7 days in the treatment of acute exacerbations of chronic bronchitis. *Antimicrobial agents and chemotherapy*. 2005 Jan 1;49(1):153-60.

⁴⁰ Ong IL, Yang KL. Recent developments in protease activity assays and sensors. *Analyst*. 2017;142(11):1867-81.

⁴¹ López-Otín C, Overall CM. Protease degradomics: a new challenge for proteomics. *Nature reviews Molecular cell biology*. 2002 Jul;3(7):509-19.

⁴² Edgington LE, Verdoes M, Bogyo M. Functional imaging of proteases: recent advances in the design and application of substrate-based and activity-based probes. *Current opinion in chemical biology*. 2011 Dec 1;15(6):798-805.

⁴³ Fonovic M, Bogyo M. Activity based probes for proteases: applications to biomarker discovery, molecular imaging and drug screening. *Current pharmaceutical design*. 2007 Jan 1;13(3):253-61.

⁴⁴ Deu E, Verdoes M, Bogyo M. New approaches for dissecting protease functions to improve probe development and drug discovery. *Nature Structural and Molecular Biology*. 2012 Jan;19(1):9-16.

- ⁴⁵ Turk V, Stoka V, Vasiljeva O, Renko M, Sun T, Turk B, Turk D. Cysteine cathepsins: from structure, function and regulation to new frontiers. *Biochimica et Biophysica Acta (BBA)-Proteins and Proteomics*. 2012 Jan 1;1824(1):68-88.
- ⁴⁶ Halfon S, Patel S, Vega F, Zurawski S, Zurawski G. Autocatalytic activation of human legumain at aspartic acid residues. *FEBS letters*. 1998 Oct 30;438(1-2):114-8.
- ⁴⁷ Dix MM, Simon GM, Cravatt BF. Global mapping of the topography and magnitude of proteolytic events in apoptosis. *Cell*. 2008 Aug 22;134(4):679-91.
- ⁴⁸ Crawford ED, Wells JA. Caspase substrates and cellular remodeling. *Annual review of biochemistry*. 2011 Jul 7;80:1055-87.
- ⁴⁹ Sanman LE, Bogoy M. Activity-based profiling of proteases. *Annual review of biochemistry*. 2014 Jun 2;83:249-73.
- ⁵⁰ Garland M, Yim JJ, Bogoy M. A bright future for precision medicine: advances in fluorescent chemical probe design and their clinical application. *Cell chemical biology*. 2016 Jan 21;23(1):122-36.
- ⁵¹ Otsuji T, Okuda-Ashitaka E, Kojima S, Akiyama H, Ito S, Ohmiya Y. Monitoring for dynamic biological processing by intramolecular bioluminescence resonance energy transfer system using secreted luciferase. *Analytical biochemistry*. 2004 Jun 15;329(2):230-7.
- ⁵² Kim GB, Kim KH, Park YH, Ko S, Kim YP. Colorimetric assay of matrix metalloproteinase activity based on metal-induced self-assembly of carboxy gold nanoparticles. *Biosensors and Bioelectronics*. 2013 Mar 15;41:833-9.
- ⁵³ Mizukami S, Takikawa R, Sugihara F, Hori Y, Tochio H, Wälchli M, Shirakawa M, Kikuchi K. Paramagnetic relaxation-based ¹⁹F MRI probe to detect protease activity. *Journal of the American Chemical Society*. 2008 Jan 23;130(3):794-5.
- ⁵⁴ Tyas L, Brophy VA, Pope A, Rivett AJ, Tavaré JM. Rapid caspase-3 activation during apoptosis revealed using fluorescence-resonance energy transfer. *EMBO reports*. 2000 Sep 1;1(3):266-70.
- ⁵⁵ Poreba M, Drag M. Current strategies for probing substrate specificity of proteases. *Current medicinal chemistry*. 2010 Jan 1;17(33):3968-95.
- ⁵⁶ Powers JC, Asgjan JL, Ekici ÖD, James KE. Irreversible inhibitors of serine, cysteine, and threonine proteases. *Chemical reviews*. 2002 Dec 11;102(12):4639-750.
- ⁵⁷ Chau DM, Crump CJ, Villa JC, Scheinberg DA, Li YM. Familial Alzheimer disease presenilin-1 mutations alter the active site conformation of γ -secretase. *The Journal of Biological Chemistry*. 2012 May 18;287(21):17288-96.
- ⁵⁸ Puri AW, Broz P, Shen A, Monack DM, Bogoy M. Caspase-1 activity is required to bypass macrophage apoptosis upon *Salmonella* infection. *Nature chemical biology*. 2012 Sep;8(9):745-47.
- ⁵⁹ Lakowicz J. *Principles of fluorescence spectroscopy*. 3rd ed. New York: Springer; 2006.

- ⁶⁰ Lavis LD, Raines RT. Bright building blocks for chemical biology. *ACS chemical biology*. 2014 Mar 20;9(4):855-66.
- ⁶¹ Sun WC, Gee KR, Haugland RP. Synthesis of novel fluorinated coumarins: Excellent UV-light excitable fluorescent dyes. *Bioorganic & medicinal chemistry letters*. 1998 Nov 17;8(22):3107-10.
- ⁶² De Wael EV, Pardoën JA, Van Koeveringe JA, Lugtenburg J. Pyrromethene-BF₂ complexes (4, 4'-difluoro-4-bora-3a, 4a-diaza-s-indacenes). *Synthesis and luminescence properties. Recueil des Travaux Chimiques des Pays-Bas*. 1977;96(12):306-9.
- ⁶³ Haugland RP. *The handbook: a guide to fluorescent probes and labeling technologies. Molecular probes*; 2005.
- ⁶⁴ Bueno C, Villegas ML, Bertolotti SG, Previtali CM, Neumann MG, Encinas AV. The excited-state interaction of resazurin and resorufin with amines in aqueous solutions. *photophysics and photochemical reactions. Photochemistry and photobiology*. 2002 Oct;76(4):385-90.
- ⁶⁵ Mujumdar RB, Ernst LA, Mujumdar SR, Lewis CJ, Waggoner AS. Cyanine dye labeling reagents: sulfoindocyanine succinimidyl esters. *Bioconjugate chemistry*. 1993 Mar 1;4(2):105-11.
- ⁶⁶ Waggoner A. Fluorescent labels for proteomics and genomics. *Current opinion in chemical biology*. 2006 Feb 1;10(1):62-6.
- ⁶⁷ Waggoner A. Covalent labeling of proteins and nucleic acids with fluorophores. *Methods in enzymology*. 1995;246:362-73.
- ⁶⁸ Grimm JB, Sung AJ, Legant WR, Hulamm P, Matlosz SM, Betzig E, Lavis LD. Carbofluoresceins and carborhodamines as scaffolds for high-contrast fluorogenic probes. *ACS chemical biology*. 2013 Apr 24;8(6):1303-10.
- ⁶⁹ Bywaters L, Mulcahy-Ryan L, Fielder M, Sinclair A, Le Gresley A. Synthetic scale-up of a novel fluorescent probe and its biological evaluation for surface detection of *Staphylococcus aureus*. *Molecular and cellular probes*. 2017 Dec 1;36:1-9.
- ⁷⁰ Sinclair A, Mulcahy LE, Geldeard L, Malik S, Fielder MD, Le Gresley A. Development of an *in situ* culture-free screening test for the rapid detection of *Staphylococcus aureus* within healthcare environments. *Organic & biomolecular chemistry*. 2013;11(20):3307-13.
- ⁷¹ Riveiro ME, De Kimpe N, Moglioni A, Vazquez R, Monczor F, Shayo C, Davio C. Coumarins: old compounds with novel promising therapeutic perspectives. *Current medicinal chemistry*. 2010 May 1;17(13):1325-38.
- ⁷² Sun WC, Gee KR, Haugland RP. Synthesis of novel fluorinated coumarins: Excellent UV-light excitable fluorescent dyes. *Bioorganic & medicinal chemistry letters*. 1998 Nov 17;8(22):3107-10.
- ⁷³ Uttamapinant C, White KA, Baruah H, Thompson S, Fernández-Suárez M, Puthenveetil S, Ting AY. A fluorophore ligase for site-specific protein labeling inside living cells. *Proceedings of the National Academy of Sciences*. 2010 Jun 15;107(24):10914-9.

- ⁷⁴ Lavis LD, Chao TY, Raines RT. Latent blue and red fluorophores based on the trimethyl lock. *ChemBioChem*. 2006 Aug 4;7(8):1151-4.
- ⁷⁵ Nizamov S, Willig KI, Sednev MV, Belov VN, Hell SW. Phosphorylated 3-heteroarylcoumarins and their use in fluorescence microscopy and nanoscopy. *Chemistry—A European Journal*. 2012 Dec 14;18(51):16339-48.
- ⁷⁶ Von Pechmann H, Duisberg C. Ueber die verbindungen der phenole mit acetessigäther. *Berichte der deutschen chemischen Gesellschaft*. 1883 Jul;16(2):2119-28.
- ⁷⁷ Maly DJ, Leonetti F, Backes BJ, Dauber DS, Harris JL, Craik CS, Ellman JA. Expedient solid-phase synthesis of fluorogenic protease substrates using the 7-amino-4-carbamoylmethylcoumarin (ACC) fluorophore. *The Journal of organic chemistry*. 2002 Feb 8;67(3):910-5.
- ⁷⁸ Jin X, Uttamapinant C, Ting AY. Synthesis of 7-Aminocoumarin by Buchwald–Hartwig cross coupling for specific protein labeling in living cells. *ChemBioChem*. 2011 Jan 3;12(1):65-70.
- ⁷⁹ Jones G. The Knoevenagel condensation. *Organic reactions*. 2004 Apr 15;15:204-599.
- ⁸⁰ Loudet A, Burgess K. BODIPY dyes and their derivatives: Syntheses and spectroscopic properties. *Chemical Reviews*. 2007;11(107):4891-932.
- ⁸¹ Ulrich G, Zissel R, Harriman A. The chemistry of fluorescent bodipy dyes: versatility unsurpassed. *Angewandte Chemie International Edition*. 2008 Feb 1;47(7):1184-201.
- ⁸² De Wael EV, Pardoen JA, Van Koevinge JA, Lugtenburg J. Pyrromethene-BF₂ complexes (4, 4'-difluoro-4-bora-3a, 4a-diaza-s-indacenes). Synthesis and luminescence properties. *Recueil des Travaux Chimiques des Pays-Bas*. 1977;96(12):306-9.
- ⁸³ Schmitt A, Hinkeldey B, Wild M, Jung G. Synthesis of the core compound of the BODIPY dye class: 4, 4'-difluoro-4-bora-(3a, 4a)-diaza-s-indacene. *Journal of fluorescence*. 2009 Jul 1;19(4):755-8.
- ⁸⁴ Hinkeldey B, Schmitt A, Jung G. Comparative photostability studies of BODIPY and fluorescein dyes by using fluorescence correlation spectroscopy. *ChemPhysChem*. 2008 Oct 6;9(14):2019-27.
- ⁸⁵ Loudet A, Bandichhor R, Burgess K, Palma A, McDonnell SO, Hall MJ, O'Shea DF. B, O-Chelated azadipyrromethenes as near-IR probes. *Organic letters*. 2008 Sep 25;10(21):4771-4.
- ⁸⁶ Kamiya M, Johnsson K. Localizable and highly sensitive calcium indicator based on a BODIPY fluorophore. *Analytical chemistry*. 2010 Jun 30;82(15):6472-9.
- ⁸⁷ Carreira EM, Zhao W. Conformationally restricted aza-BODIPY: A highly fluorescent, stable, near-infrared-absorbing dye. *Angewandte Chemie. International Edition*. 2005;44(11):1677-9.
- ⁸⁸ Kojima R, Takakura H, Ozawa T, Tada Y, Nagano T, Urano Y. Rational design and development of near-infrared-emitting firefly luciferins available in vivo. *Angewandte Chemie International Edition*. 2013 Jan 21;52(4):1175-9.

- ⁸⁹ Flores-Rizo JO, Esnal I, Osorio-Martínez CA, Gómez-Durán CF, Bañuelos J, López Arbeloa I, Pannell KH, Metta-Magaña AJ, Peña-Cabrera E. 8-Alkoxy-and 8-aryloxy-BODIPYs: straightforward fluorescent tagging of alcohols and phenols. *The Journal of organic chemistry*. 2013 Jun 11;78(12):5867-77.
- ⁹⁰ Carlson JC, Meimetis LG, Hilderbrand SA, Weissleder R. BODIPY–tetrazine derivatives as superbright bioorthogonal turn-on probes. *Angewandte Chemie International Edition*. 2013 Jul 1;52(27):6917-20.
- ⁹¹ Jose J, Burgess K. Benzophenoxazine-based fluorescent dyes for labeling biomolecules. *Tetrahedron*. 2006 Nov 27;62(48):11021-37.
- ⁹² Beecken H, Gottschalk EM, v Gizycki U, Krämer H, Maassen D, Matthies HG, Musso H, Rathjen C, Zdhorszky UI. Orcein and litmus. *Biotechnic & histochemistry*. 2003 Dec 1;78(6):289-302.
- ⁹³ Hofmann J, Sernetz M. Immobilized enzyme kinetics analyzed by flow-through microfluorimetry: resorufin- β -D-galactopyranoside as a new fluorogenic substrate for β -galactosidase. *Analytica Chimica Acta*. 1984 Jan 1;163:67-72.
- ⁹⁴ Theriot JA, Mitchison TJ. Actin microfilament dynamics in locomoting cells. *Nature*. 1991 Jul;352(6331):126-31.
- ⁹⁵ Zhou M, Diwu Z, Panchuk-Voloshina N, Haugland RP. A stable nonfluorescent derivative of resorufin for the fluorometric determination of trace hydrogen peroxide: applications in detecting the activity of phagocyte NADPH oxidase and other oxidases. *Analytical biochemistry*. 1997 Nov 15;253(2):162-8.
- ⁹⁶ Greenspan P, Mayer EP, Fowler SD. Nile red: a selective fluorescent stain for intracellular lipid droplets. *The Journal of cell biology*. 1985 Mar 1;100(3):965-73.
- ⁹⁷ Sharonov A, Hochstrasser RM. Wide-field subdiffraction imaging by accumulated binding of diffusing probes. *Proceedings of the National Academy of Sciences*. 2006 Dec 12;103(50):18911-6.
- ⁹⁸ Corey PF, Trimmer RW, Biddlecom WG. A new chromogenic β -galactosidase substrate: 7- β -D-galactopyranosyloxy-9, 9-dimethyl-9H-acridin-2-one. *Angewandte Chemie International Edition in English*. 1991 Dec;30(12):1646-8.
- ⁹⁹ Warther D, Bolze F, Léonard J, Gug S, Specht A, Puliti D, Sun XH, Kessler P, Lutz Y, Vonesch JL, Winsor B. Live-cell one-and two-photon uncaging of a far-red emitting acridinone fluorophore. *Journal of the American Chemical Society*. 2010 Feb 8;132(8):2585-90.
- ¹⁰⁰ Klein C, Batz HG, Herrmann R, inventors; Roche Diagnostics GmbH, assignee. Resorufin derivatives. United States patent US 6.800.765. 1990.
- ¹⁰¹ Mujumdar RB, Ernst LA, Mujumdar SR, Lewis CJ, Waggoner AS. Cyanine dye labeling reagents: sulfoindocyanine succinimidyl esters. *Bioconjugate chemistry*. 1993 Mar 1;4(2):105-11.
- ¹⁰² Waggoner AS. Dye indicators of membrane potential. *Annual review of biophysics and bioengineering*. 1979 Jun;8(1):47-68.

- ¹⁰³ Rye HS, Yue S, Wemmer DE, Quesada MA, Haugland RP, Mathies RA, Glazer AN. Stable fluorescent complexes of double-stranded DNA with bis-intercalating asymmetric cyanine dyes: properties and applications. *Nucleic acids research*. 1992 Jun 11;20(11):2803-12.
- ¹⁰⁴ Yuan L, Lin W, Yang Y, Chen H. A unique class of near-infrared functional fluorescent dyes with carboxylic-acid-modulated fluorescence ON/OFF switching: rational design, synthesis, optical properties, theoretical calculations, and applications for fluorescence imaging in living animals. *Journal of the American Chemical Society*. 2012 Jan 6;134(2):1200-11.
- ¹⁰⁵ Richard JA, Massonneau M, Renard PY, Romieu A. 7-Hydroxycoumarin–hemicyanine hybrids: a new class of far-red emitting fluorogenic dyes. *Organic letters*. 2008 Sep 3;10(19):4175-8.
- ¹⁰⁶ Xiong X, Song F, Chen G, Sun W, Wang J, Gao P, Zhang Y, Qiao B, Li W, Sun S, Fan J. Construction of long-wavelength fluorescein analogues and their application as fluorescent probes. *Chemistry—A European Journal*. 2013 May 17;19(21):6538-45.
- ¹⁰⁷ Panigrahi M, Dash S, Patel S, Mishra BK. Syntheses of cyanines: a review. *Tetrahedron*. 2012;3(68):781-805.
- ¹⁰⁸ Kothavale S, Jadhav AG, Sekar N. Deep red emitting triphenylamine based coumarin-rhodamine hybrids with large Stokes shift and viscosity sensing: synthesis, photophysical properties and DFT studies of their spirocyclic and open forms. *Dyes and Pigments*. 2017 Feb 1;137:329-41.
- ¹⁰⁹ Adie EJ, Kalinka S, Smith L, Francis MJ, Marengi A, Cooper ME, Briggs M, Michael NP, Milligan G, Game S. A pH-sensitive fluor, CypHer™ 5, used to monitor agonist-induced G protein-coupled receptor internalization in live cells. *Biotechniques*. 2002 Nov 1;33(5):1152-7.
- ¹¹⁰ Maurel D, Banala S, Laroche T, Johnsson K. Photoactivatable and photoconvertible fluorescent probes for protein labeling. *ACS chemical biology*. 2010 Mar 24;5(5):507-16.
- ¹¹¹ Baeyer A. Ueber eine neue Klasse von Farbstoffen. *Berichte der deutschen chemischen Gesellschaft*. 1871 Jun;4(2):555-8.
- ¹¹² Lavis LD, Rutkoski TJ, Raines RT. Tuning the pK_a of fluorescein to optimize binding assays. *Analytical chemistry*. 2007 Sep 1;79(17):6775-82.
- ¹¹³ Sun WC, Gee KR, Klaubert DH, Haugland RP. Synthesis of fluorinated fluoresceins. *The Journal of Organic Chemistry*. 1997 Sep 19;62(19):6469-75.
- ¹¹⁴ Tian L, Yang Y, Wysocki LM, Arnold AC, Hu A, Ravichandran B, Sternson SM, Looger LL, Lavis LD. Selective esterase–ester pair for targeting small molecules with cellular specificity. *Proceedings of the National Academy of Sciences*. 2012 Mar 27;109(13):4756-61.
- ¹¹⁵ Fleming GR, Knight AW, Morris JM, Morrison RJ, Robinson GW. Picosecond fluorescence studies of xanthene dyes. *Journal of the American Chemical Society*. 1977 Jun;99(13):4306-11.

- ¹¹⁶ Azuma E, Nakamura N, Kuramochi K, Sasamori T, Tokitoh N, Sagami I, Tsubaki K. Exhaustive syntheses of naphthofluoresceins and their functions. *The Journal of organic chemistry*. 2012 Mar 28;77(7):3492-500.
- ¹¹⁷ Pluth MD, Chan MR, McQuade LE, Lippard SJ. Seminaphthofluorescein-based fluorescent probes for imaging nitric oxide in live cells. *Inorganic chemistry*. 2011 Sep 7;50(19):9385-92.
- ¹¹⁸ Yang Y, Lowry M, Xu X, Escobedo JO, Sibrian-Vazquez M, Wong L, Schowalter CM, Jensen TJ, Fronczek FR, Warner IM, Strongin RM. Seminaphthofluorones are a family of water-soluble, low molecular weight, NIR-emitting fluorophores. *Proceedings of the National Academy of Sciences*. 2008 Jul 1;105(26):8829-34.
- ¹¹⁹ Hammershøj P, Thyraug E, Harris P, Ek PK, Andresen TL, Clausen MH. Convenient one-step synthesis of 5-carboxy-seminaphthofluoresceins. *Tetrahedron Letters*. 2017 Apr 19;58(16):1611-5.
- ¹²⁰ Yue X, Li W, Chen W, Zhang L, Li G, Sheng J. A dual-response naphthofluorescein-based fluorescent probe for multiple-channel imaging of cysteine/homocysteine in living cells. *Tetrahedron Letters*. 2018 Jun 6;59(23):2232-7.
- ¹²¹ Egawa T, Koide Y, Hanaoka K, Komatsu T, Terai T, Nagano T. Development of a fluorescein analogue, TokyoMagenta, as a novel scaffold for fluorescence probes in red region. *Chemical Communications*. 2011;47(14):4162-4.
- ¹²² Lavis, L. D., Chao, T.-Y., and Raines, R. T. (2011) Synthesis and utility of fluorogenic acetoxymethyl ethers. *Chem. Sci.* 2, 521–530.
- ¹²³ Yang Y, Zhao Q, Feng W, Li F. Luminescent chemodosimeters for bioimaging. *Chemical Reviews*. 2012 Jun 18;113(1):192-270.
- ¹²⁴ Wysocki LM, Grimm JB, Tkachuk AN, Brown TA, Betzig E, Lavis LD. Facile and general synthesis of photoactivatable xanthene dyes. *Angewandte Chemie International Edition*. 2011 Nov 18;50(47):11206-9.
- ¹²⁵ Egawa T, Hirabayashi K, Koide Y, Kobayashi C, Takahashi N, Mineno T, Terai T, Ueno T, Komatsu T, Ikegaya Y, Matsuki N. Red fluorescent probe for monitoring the dynamics of cytoplasmic calcium ions. *Angew. Chem. Int. Ed.* 2013;52:3874-7.
- ¹²⁶ Ceresole M. Verfahren zur darstellung von farbstoffen aus der gruppe des meta-amidophenolphtaleïns. DR patent. 1887 Nov(44002).
- ¹²⁷ Khanna PL, Ullman EF. 4', 5'-Dimethoxy-6-carboxyfluorescein: a novel dipole-dipole coupled fluorescence energy transfer acceptor useful for fluorescence immunoassays. *Analytical biochemistry*. 1980 Oct 1;108(1):156-61.
- ¹²⁸ Lavis LD, Chao TY, Raines RT. Fluorogenic label for biomolecular imaging. *ACS chemical biology*. 2006 May 19;1(4):252-60.
- ¹²⁹ Panchuk-Voloshina N, Haugland RP, Bishop-Stewart J, Bhargat MK, Millard PJ, Mao F, Leung WY, Haugland RP. Alexa dyes, a series of new fluorescent dyes that yield exceptionally bright, photostable conjugates. *Journal of Histochemistry & Cytochemistry*. 1999 Sep;47(9):1179-88.

- ¹³⁰ Levine MN, Raines RT. Sensitive fluorogenic substrate for alkaline phosphatase. *Analytical biochemistry*. 2011 Nov 15;418(2):247-52.
- ¹³¹ Levine MN, Hoang TT, Raines RT. Fluorogenic probe for constitutive cellular endocytosis. *Chemistry & biology*. 2013 Apr 18;20(4):614-8.
- ¹³² Arden-Jacob J, Frantzeskos J, Kemnitzer NU, Zilles A, Drexhage KH. New fluorescent markers for the red region. *Spectrochimica Acta Part A: Molecular and Biomolecular Spectroscopy*. 2001 Sep 14;57(11):2271-83.
- ¹³³ Koide Y, Urano Y, Hanaoka K, Terai T, Nagano T. Evolution of group 14 rhodamines as platforms for near-infrared fluorescence probes utilizing photoinduced electron transfer. *ACS chemical biology*. 2011 Mar 17;6(6):600-8.
- ¹³⁴ Koide Y, Urano Y, Hanaoka K, Piao W, Kusakabe M, Saito N, Terai T, Okabe T, Nagano T. Development of NIR fluorescent dyes based on Si-rhodamine for in vivo imaging. *Journal of the American Chemical Society*. 2012 Mar 7;134(11):5029-31.
- ¹³⁵ Ioffe IS, Otten VF. Investigations in field of rhodamine dyestuffs and compounds related to them. 1. Parent substance of rhodamines, its preparation and properties. *Zhurnal Obshchei Khimii*. 1961 Jan 1;31(5):1511-16.
- ¹³⁶ Grimm JB, Lavis LD. Synthesis of rhodamines from fluoresceins using Pd-catalyzed C–N cross-coupling. *Organic letters*. 2011 Nov 17;13(24):6354-7.
- ¹³⁷ Wu L, Burgess K. Synthesis and spectroscopic properties of rosamines with cyclic amine substituents. *The Journal of organic chemistry*. 2008 Oct 18;73(22):8711-18.
- ¹³⁸ Lukinavičius G, Umezawa K, Olivier N, Honigmann A, Yang G, Plass T, Mueller V, Reymond L, Corrêa Jr IR, Luo ZG, Schultz C. A near-infrared fluorophore for live-cell super-resolution microscopy of cellular proteins. *Nature chemistry*. 2013 Feb 1;5(2):132-9.
- ¹³⁹ Mitronova GY, Belov VN, Bossi ML, Wurm CA, Meyer L, Medda R, Moneron G, Bretschneider S, Eggeling C, Jakobs S, Hell SW. New fluorinated rhodamines for optical microscopy and nanoscopy. *Chemistry—A European Journal*. 2010 Apr 19;16(15):4477-88.
- ¹⁴⁰ Fölling J, Belov V, Kunetsky R, Medda R, Schönle A, Egnér A, Eggeling C, Bossi M, Hell SE. Photochromic rhodamines provide nanoscopy with optical sectioning. *Angewandte Chemie International Edition*. 2007 Aug 20;46(33):6266-70.
- ¹⁴¹ Yang Y, Zhao Q, Feng W, Li F. Luminescent chemodosimeters for bioimaging. *Chemical Reviews*. 2012 Jun 18;113(1):192-270.
- ¹⁴² Chan J, Dodani SC, Chang CJ. Reaction-based small-molecule fluorescent probes for chemoselective bioimaging. *Nature chemistry*. 2012 Dec;4(12):973.
- ¹⁴³ El-Faham A, Albericio F. COMU: A third generation of uronium-type coupling reagents. *Journal of peptide science: an official publication of the European Peptide Society*. 2010 Jan;16(1):6-9.
- ¹⁴⁴ Bunnett JF, Davis GT. The nucleophilic reactivity of aniline, hydrazine and phenoxide ion toward 2, 4-dinitrochlorobenzene. *Journal of the American Chemical Society*. 1958 Aug;80(16):4337-9.

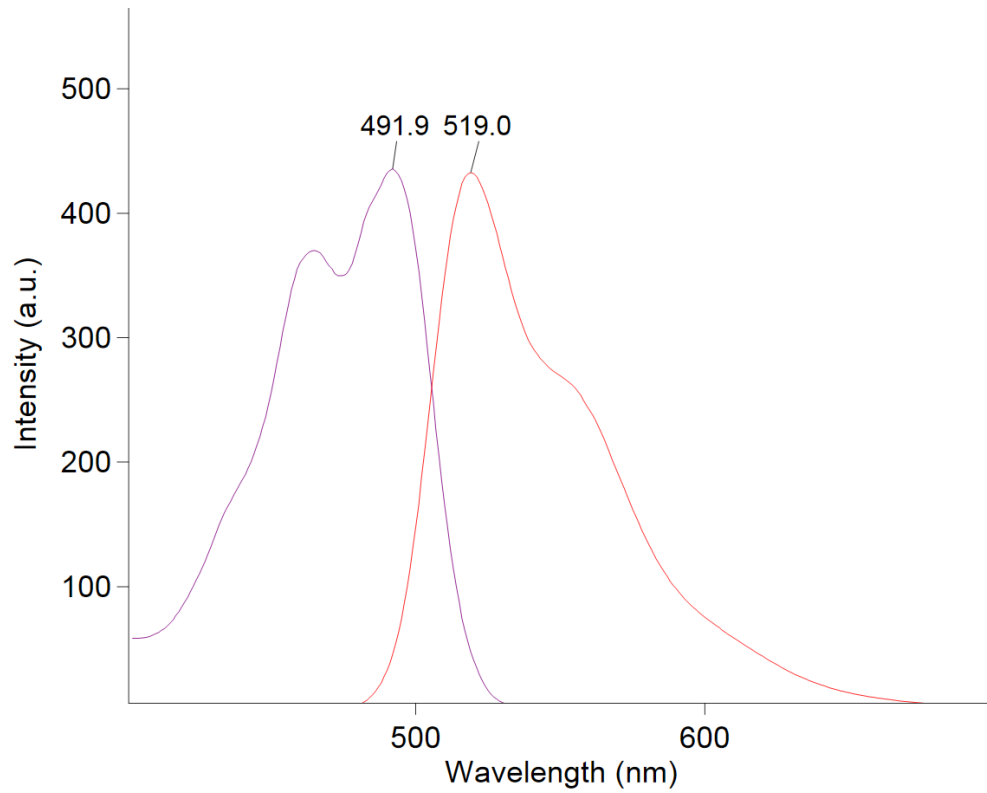
- ¹⁴⁵ Rink H, Sieber P, Raschdorf F. Conversion of urethane protected arginine to ornithine in peptide solid phase synthesis. *Tetrahedron letters*. 1984 Jan 1;25(6):621-4.
- ¹⁴⁶ Paul R, Anderson GW, Callahan FM. Some side reactions of nitro-L-arginine. *The Journal of Organic Chemistry*. 1961 Sep;26(9):3347-50.
- ¹⁴⁷ Al-Warhi TI, Al-Hazimi HM, El-Faham A. Recent development in peptide coupling reagents. *Journal of Saudi Chemical Society*. 2012 Apr 1;16(2):97-116.
- ¹⁴⁸ Austin PR, Bousquet EW, Lazier WA. Phthalide. I. The hydrogenation of phthalic anhydride. *Journal of the American Chemical Society*. 1937 May;59(5):864-6.
- ¹⁴⁹ Wardman P. Fluorescent and luminescent probes for measurement of oxidative and nitrosative species in cells and tissues: progress, pitfalls, and prospects. *Free radical biology and medicine*. 2007 Oct 1;43(7):995-1022.
- ¹⁵⁰ Leytus SP, Melhado LL, Mangel WF. Rhodamine-based compounds as fluorogenic substrates for serine proteinases. *Biochemical Journal*. 1983 Feb 1;209(2):299-307.
- ¹⁵¹ Gorska K, Manicardi A, Barluenga S, Winssinger N. DNA-templated release of functional molecules with an azide-reduction-triggered immolative linker. *Chemical Communications*. 2011;47(15):4364-6.
- ¹⁵² Fukuzawa SI, Nakanishi A, Fujinami T, Sakai S. Reductive coupling of ketones or aldehydes with electron-deficient alkenes promoted by samarium di-iodide. *Journal of the Chemical Society, Chemical Communications*. 1986(8):624-5.
- ¹⁵³ Fukuzawa SI, Nakanishi A, Fujinami T, Sakai S. Samarium (II) di-iodide induced reductive coupling of α , β -unsaturated esters with carbonyl compounds leading to a facile synthesis of γ -lactone. *Journal of the Chemical Society, Perkin Transactions 1*. 1988(7):1669-75.
- ¹⁵⁴ Sono M, Doi N, Yoshino E, Onishi S, Fujii D, Tori M. Samarium (II) iodide-induced intermolecular coupling of α , β -unsaturated esters with ketones: reactions of methyl propiolate and ethyl buta-2, 3-dienoate with cyclohexanone and its application to synthesis of a terpene carboxylic acid. *Tetrahedron Letters*. 2013 Apr 10;54(15):1947-50.
- ¹⁵⁵ Liu LY, Zhang Y, Huang KM, Chang WX, Li J. 1, 3-Dichloro-tetra-n-butyl-distannoxane: a new application for catalyzing the direct substitution of 9H-xanthen-9-ol at room temperature. *Applied Organometallic Chemistry*. 2012 Jan;26(1):9-15.
- ¹⁵⁶ Szostak M, Spain M, Procter DJ. Preparation of samarium (II) iodide: quantitative evaluation of the effect of water, oxygen, and peroxide content, preparative methods, and the activation of samarium metal. *The Journal of organic chemistry*. 2012 Mar 20;77(7):3049-59.
- ¹⁵⁷ Imamoto T, Ono M. The reaction of samarium (III) iodide with samarium metal in tetrahydrofuran, a new method for the preparation of samarium (II) iodide. *Chemistry Letters*. 1987 Mar 5;16(3):501-2.
- ¹⁵⁸ Martínez A, Hernández-Marin E, Galano A. Xanthenes as antioxidants: a theoretical study on the thermodynamics and kinetics of the single electron transfer mechanism. *Food & function*. 2012;3(4):442-50.

- ¹⁵⁹ Pratt SA, Goble MP, Mulvaney MJ, Wuts PG. Dialkylhydrazides for directed orthometalations. *Tetrahedron Letters*. 2000 May 6;41(19):3559-62.
- ¹⁶⁰ Ahn YH, Lee JS, Chang YT. Combinatorial rosamine library and application to in vivo glutathione probe. *Journal of the American Chemical Society*. 2007 Apr 18;129(15):4510-1.
- ¹⁶¹ Bartoli G, Palmieri G, Bosco M, Dalpozzo R. The reaction of vinyl Grignard reagents with 2-substituted nitroarenes: a new approach to the synthesis of 7-substituted indoles. *Tetrahedron Letters*. 1989 Jan 1;30(16):2129-32.
- ¹⁶² Hirano T, Kikuchi K, Urano Y, Higuchi T, Nagano T. Highly zinc-selective fluorescent sensor molecules suitable for biological applications. *Journal of the American Chemical Society*. 2000 Dec 13;122(49):12399-400.
- ¹⁶³ Lindqvist L, Lundeen GW. Radiationless transitions in xanthene dyes. *The Journal of Chemical Physics*. 1966 Feb 15;44(4):1711-2.
- ¹⁶⁴ Urano Y, Kamiya M, Kanda K, Ueno T, Hirose K, Nagano T. Evolution of fluorescein as a platform for finely tunable fluorescence probes. *Journal of the American Chemical Society*. 2005 Apr 6;127(13):4888-94.
- ¹⁶⁵ Li J, Yao SQ. "Singapore Green": a new fluorescent dye for microarray and bioimaging applications. *Organic letters*. 2008 Dec 19;11(2):405-8.
- ¹⁶⁶ Povrozin, Yevgen, and Ewald Terpetschnig. "Measurement of fluorescence quantum yields on ISS instrumentation using vinci." (2011).
- ¹⁶⁷ Agbowuro AA, Mazraani R, McCaughey LC, Huston WM, Gamble AB, Tyndall JD. Stereochemical basis for the anti-chlamydial activity of the phosphonate protease inhibitor JO146. *Tetrahedron*. 2018 Mar 22;74(12):1184-90.
- ¹⁶⁸ Goldberg AA, Walker HA. 277. Synthesis of diaminoxanthenes. *Journal of the Chemical Society (Resumed)*. 1953:1348-57.
- ¹⁶⁹ Pianowski Z, Gorska K, Oswald L, Merten CA, Winssinger N. Imaging of mRNA in live cells using nucleic acid-templated reduction of azidorhodamine probes. *Journal of the American Chemical Society*. 2009 Apr 20;131(18):6492-7.
- ¹⁷⁰ Susinskis I, Mekss P, Hmelnickis J. Method development for the determination of 1, 1-dimethylhydrazine by the high-performance liquid chromatography–mass spectrometry technique. *European Journal of Mass Spectrometry*. 2018 Aug;24(4):352-9.
- ¹⁷¹ Glover SA, Rosser AA, Spence RM. Studies of the structure, amidicity, and reactivity of *N*-chlorohydroxamic esters and *N*-chloro- β , β -dialkylhydrazides: anomeric amides with low resonance energies. *Australian Journal of Chemistry*. 2014 Sep 23;67(9):1344-52.

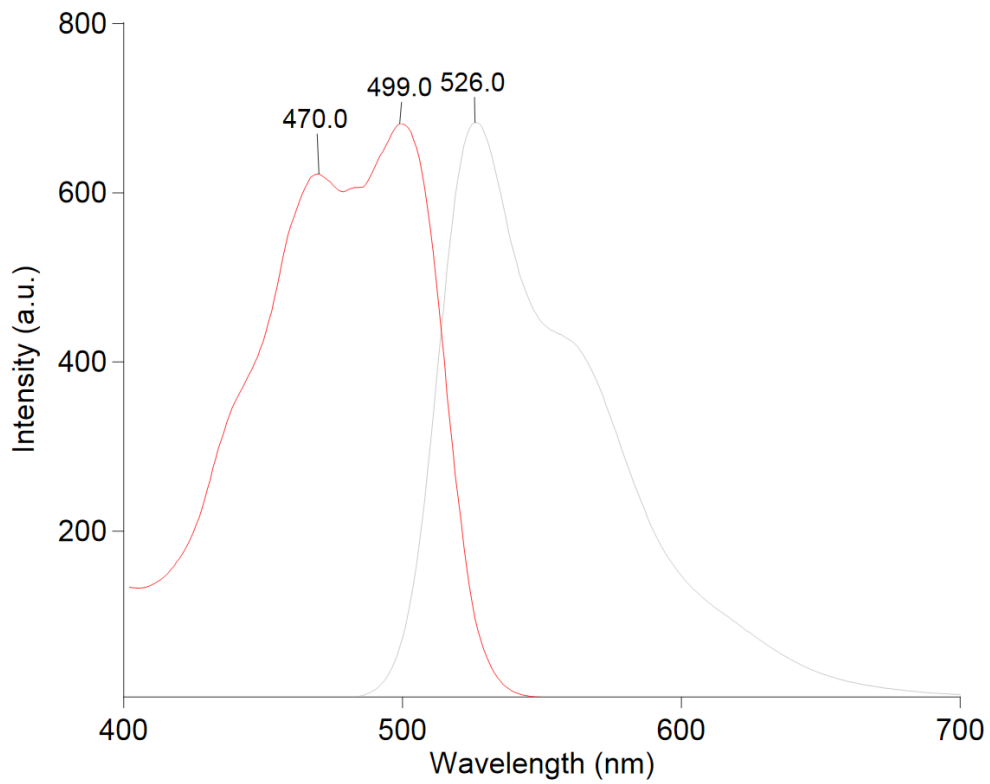
Chapter 5 – Appendix

5.1 Excitation vs Emission Maxima for Singapore Greens

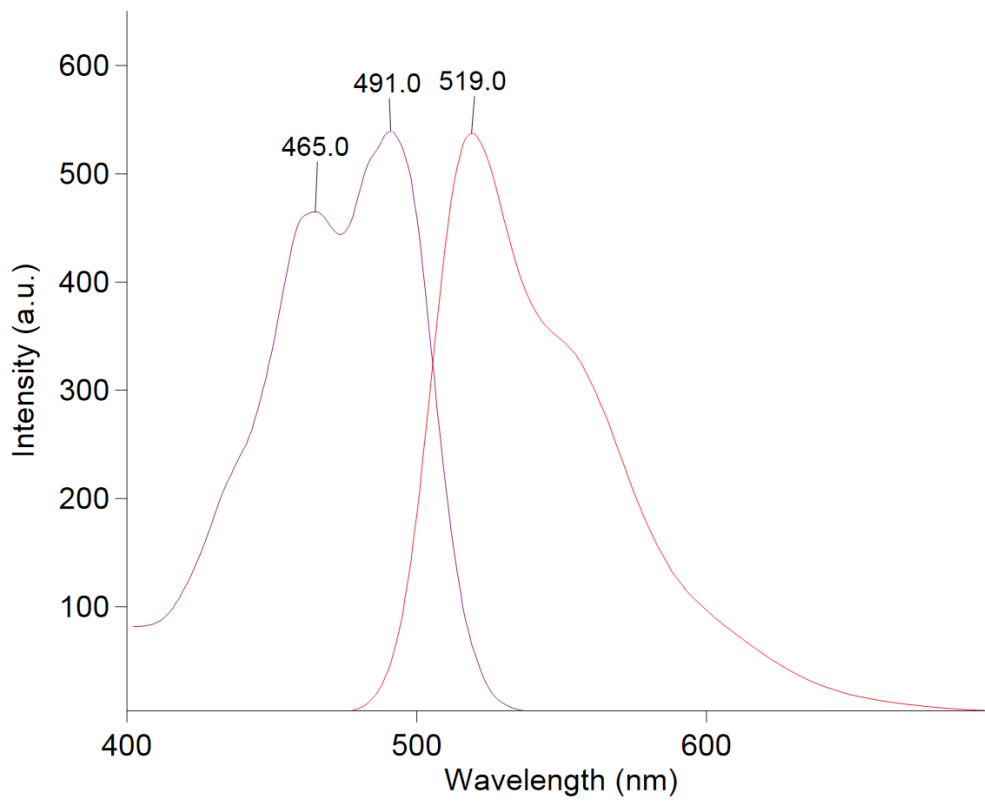
SG1.TFA



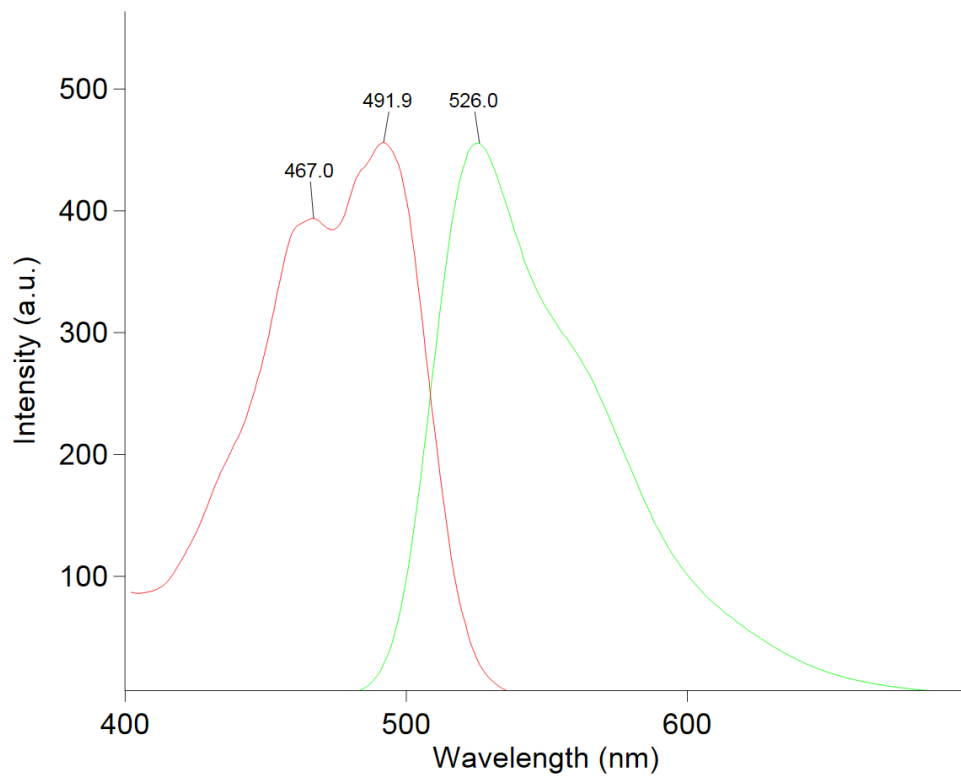
SG2.HCI



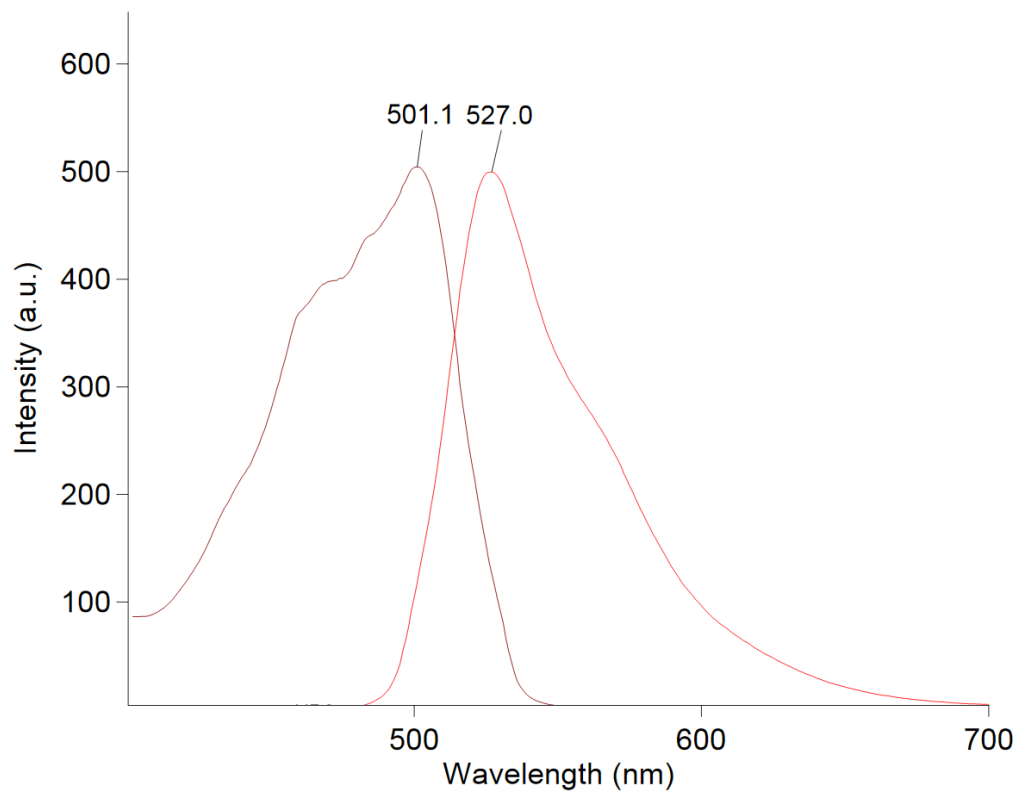
SG3.TFA



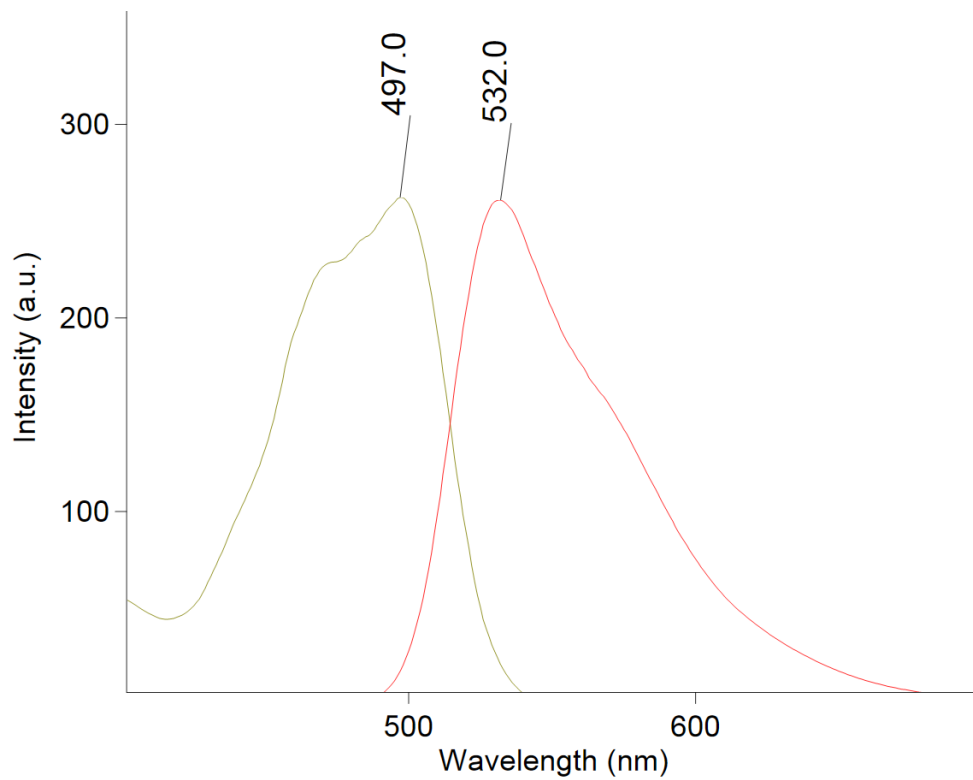
SG4.TFA



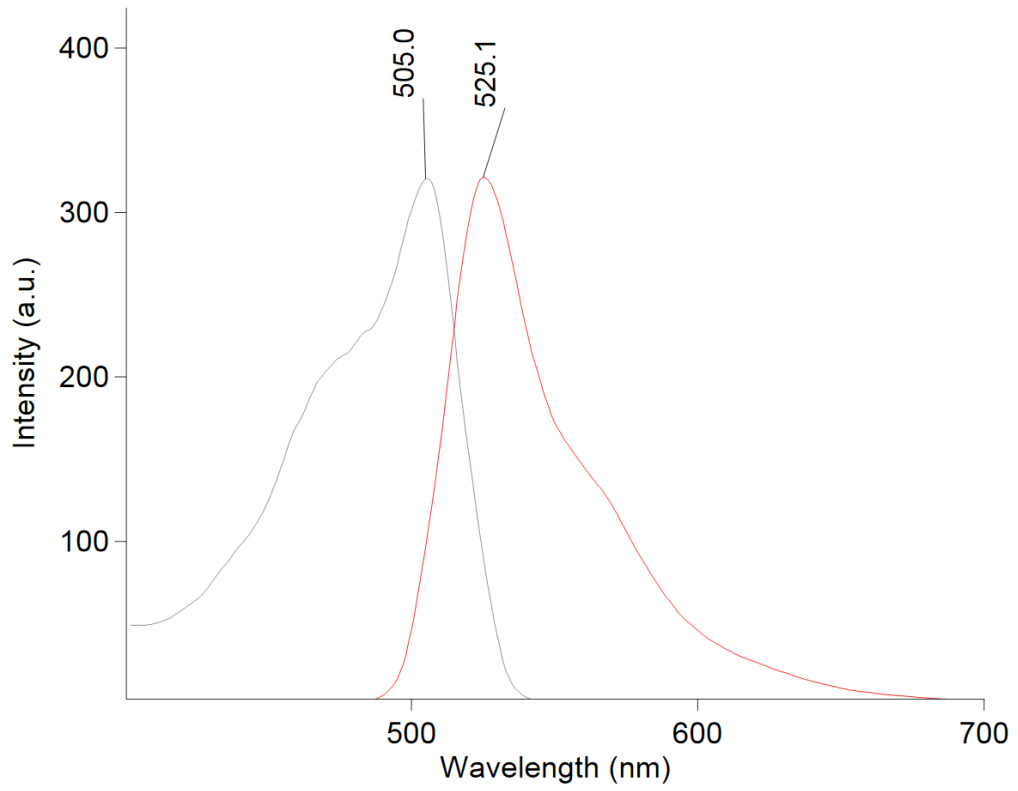
SG5.TFA



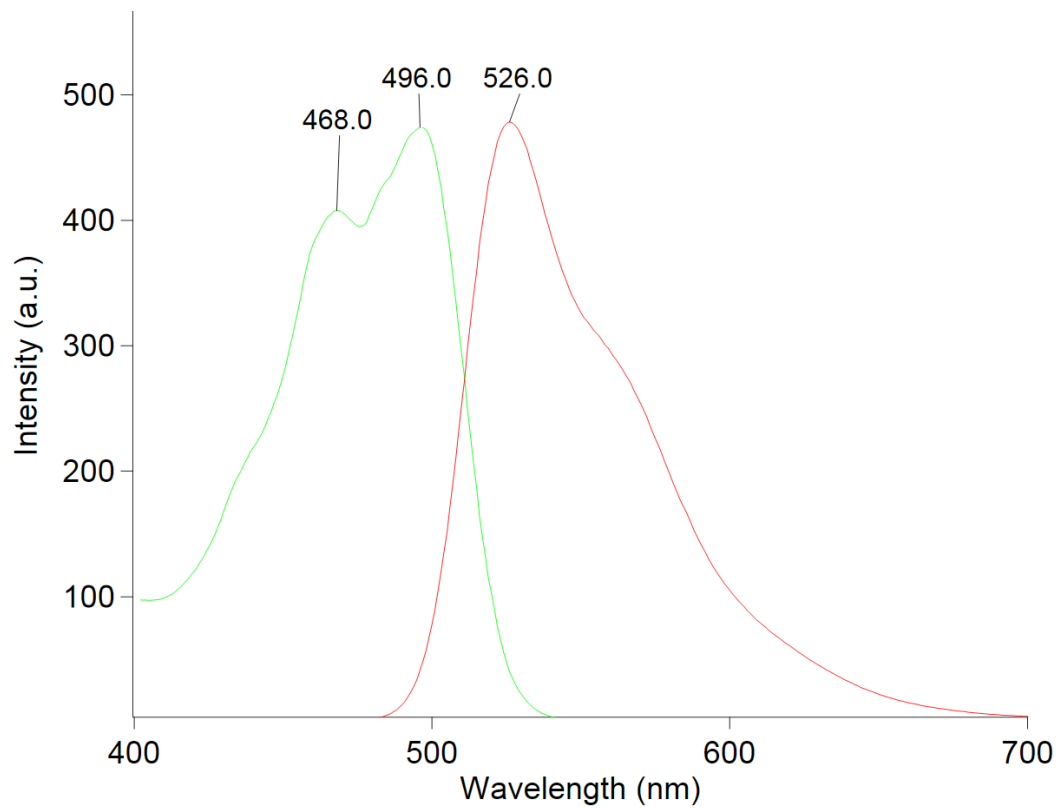
SG6.TFA



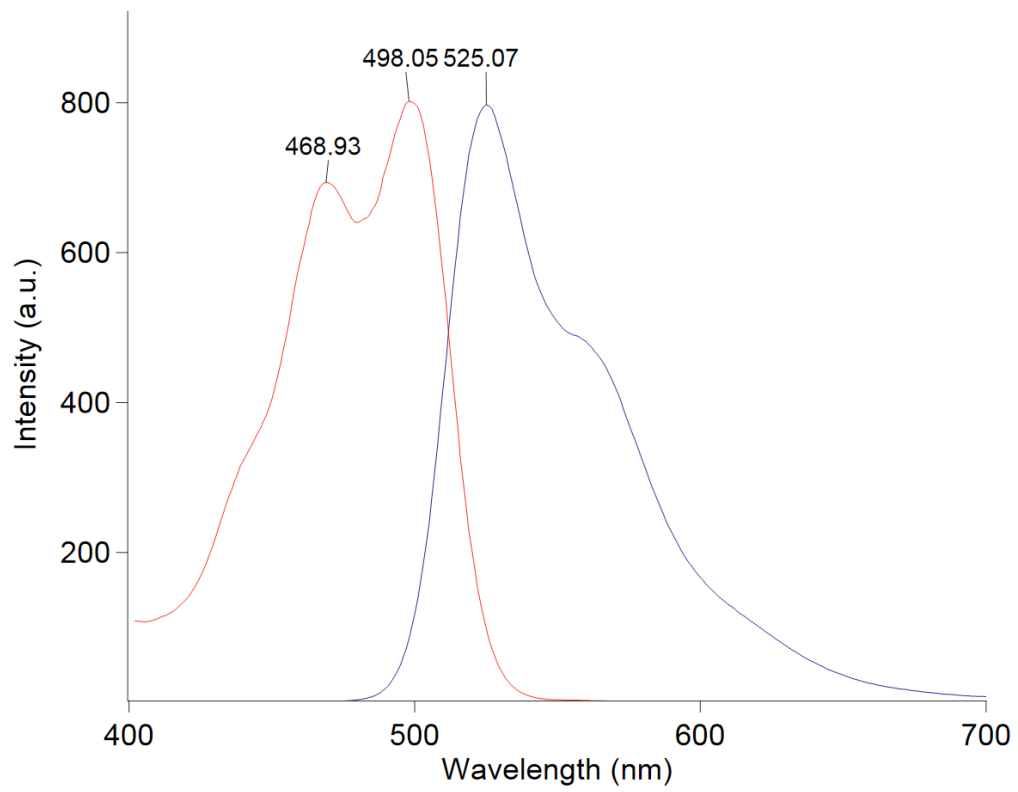
SG7.TFA



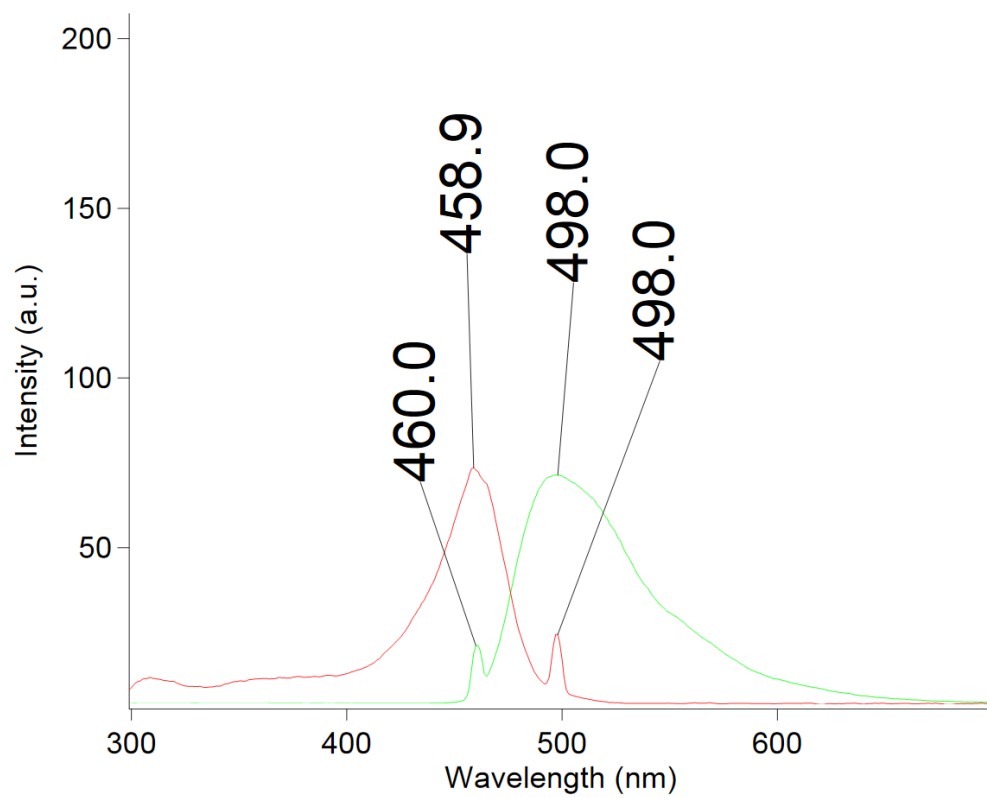
SG8.TFA



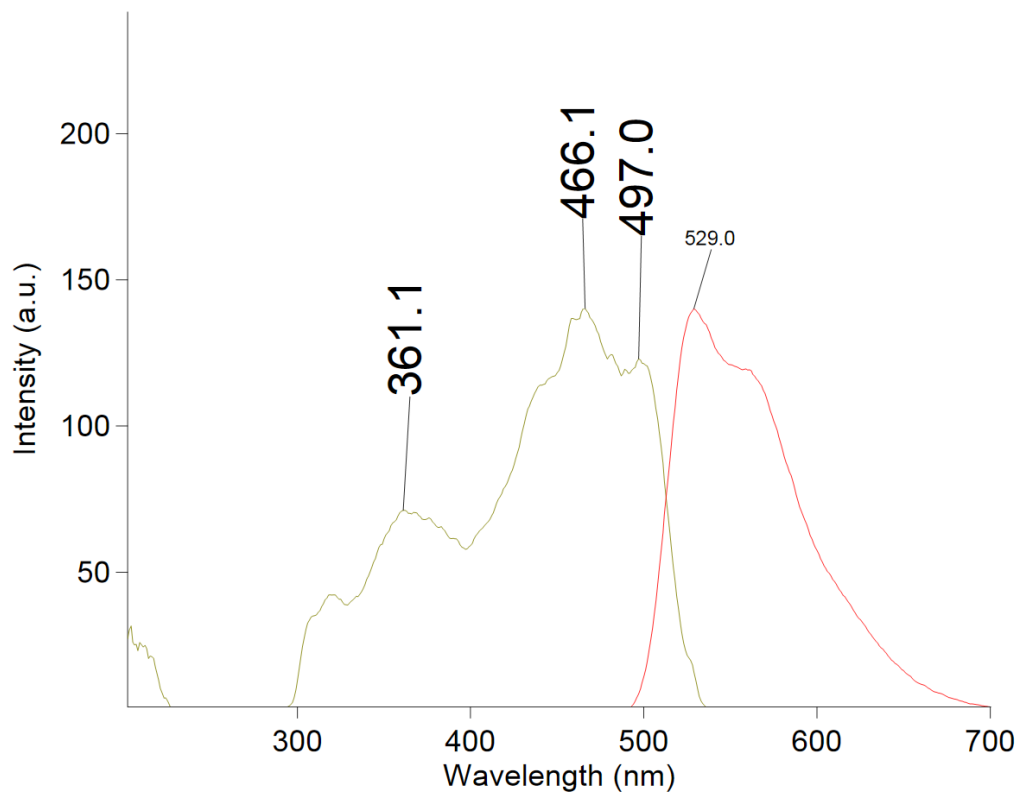
SG9.TFA



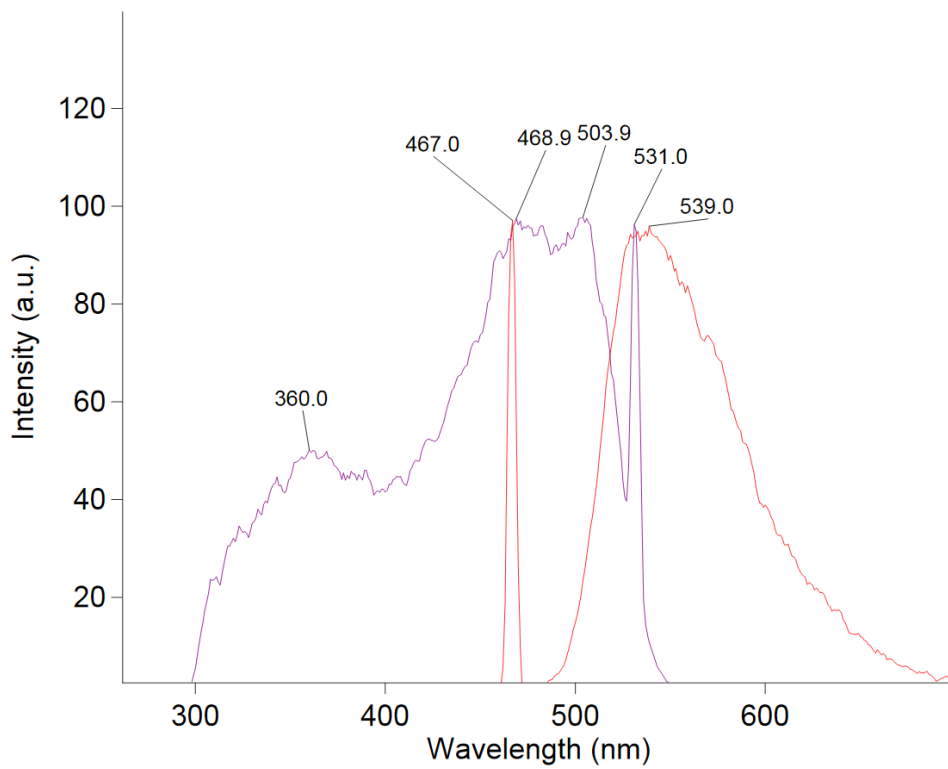
SG1BisAc



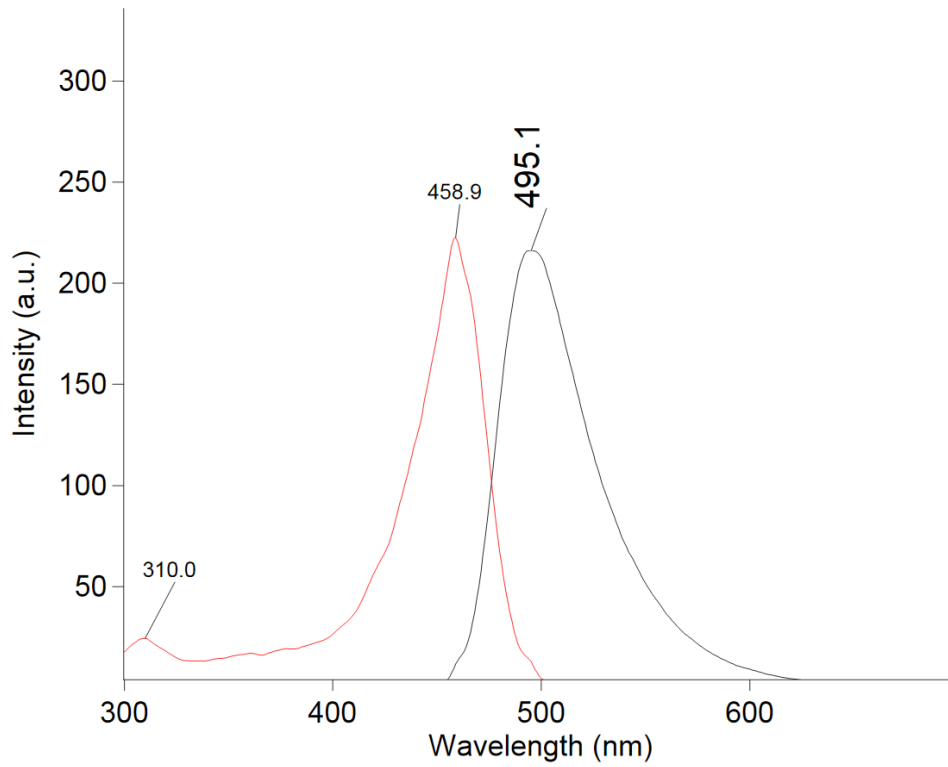
SG5BisAc



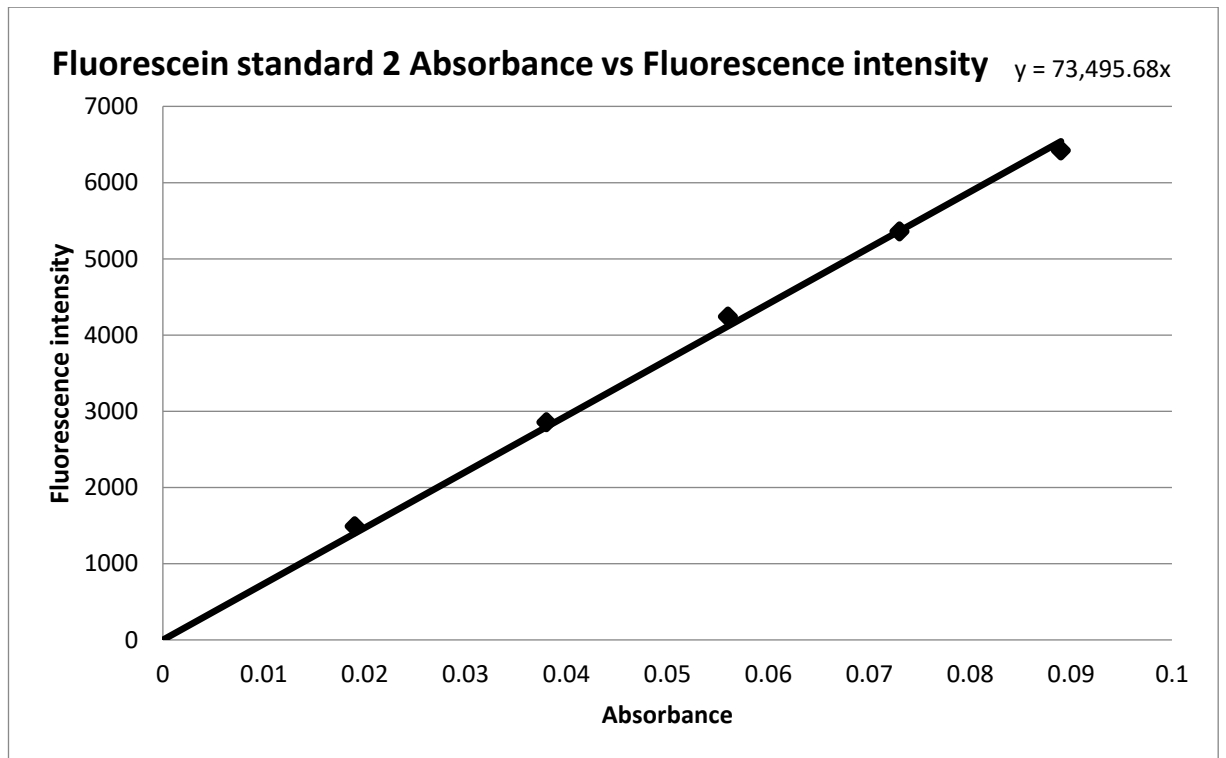
SG8BisAc

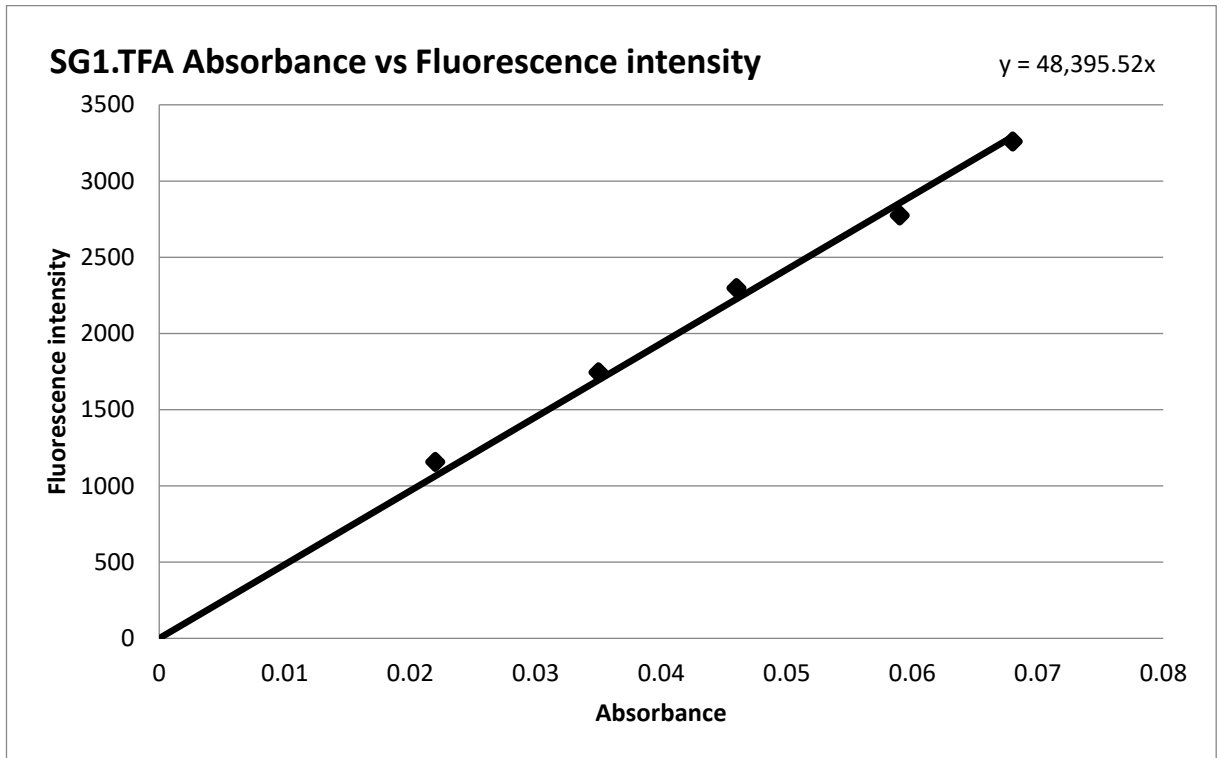


SG1MonoAc

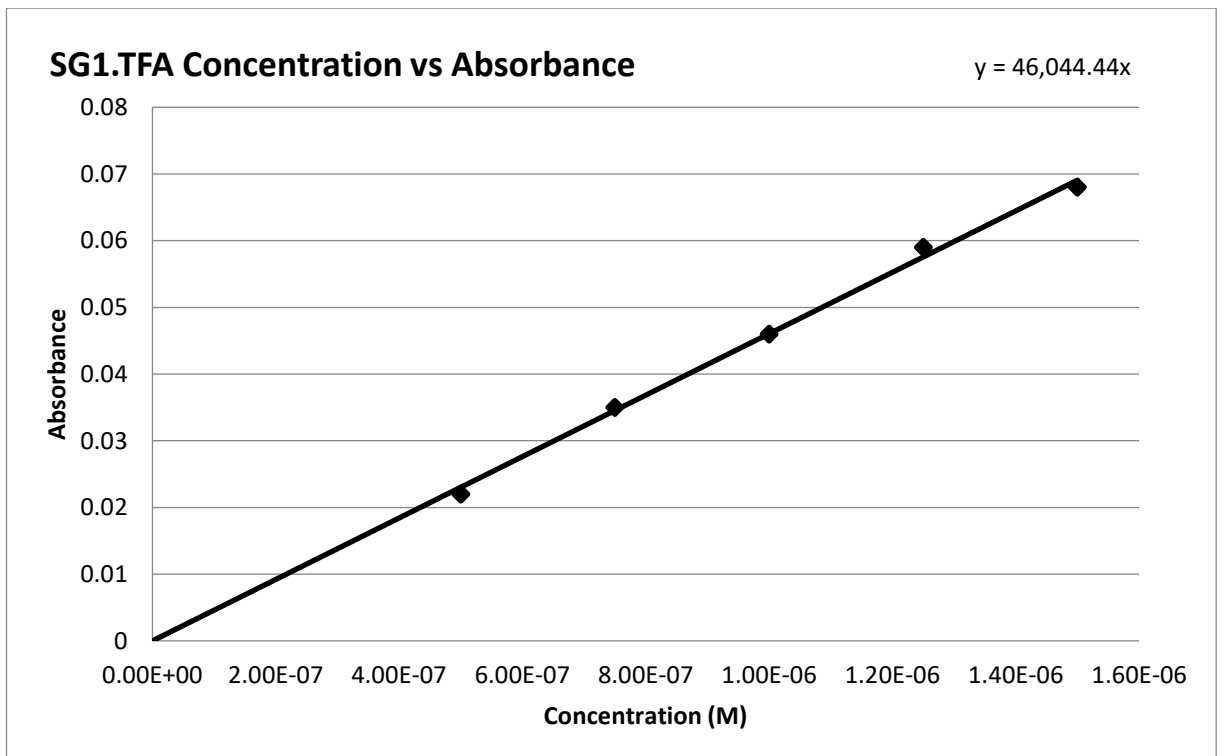


5.2 Plots for Fluorescence Quantum Yield Determinations of Singapore Greens

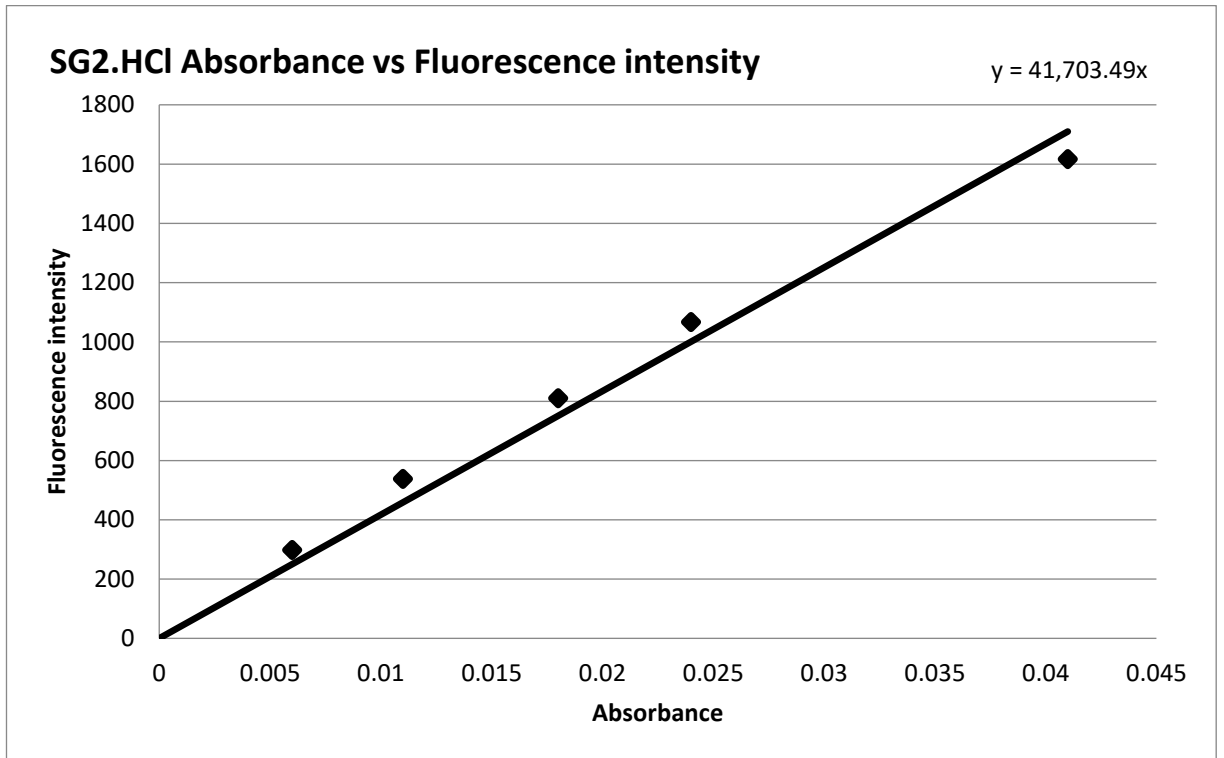




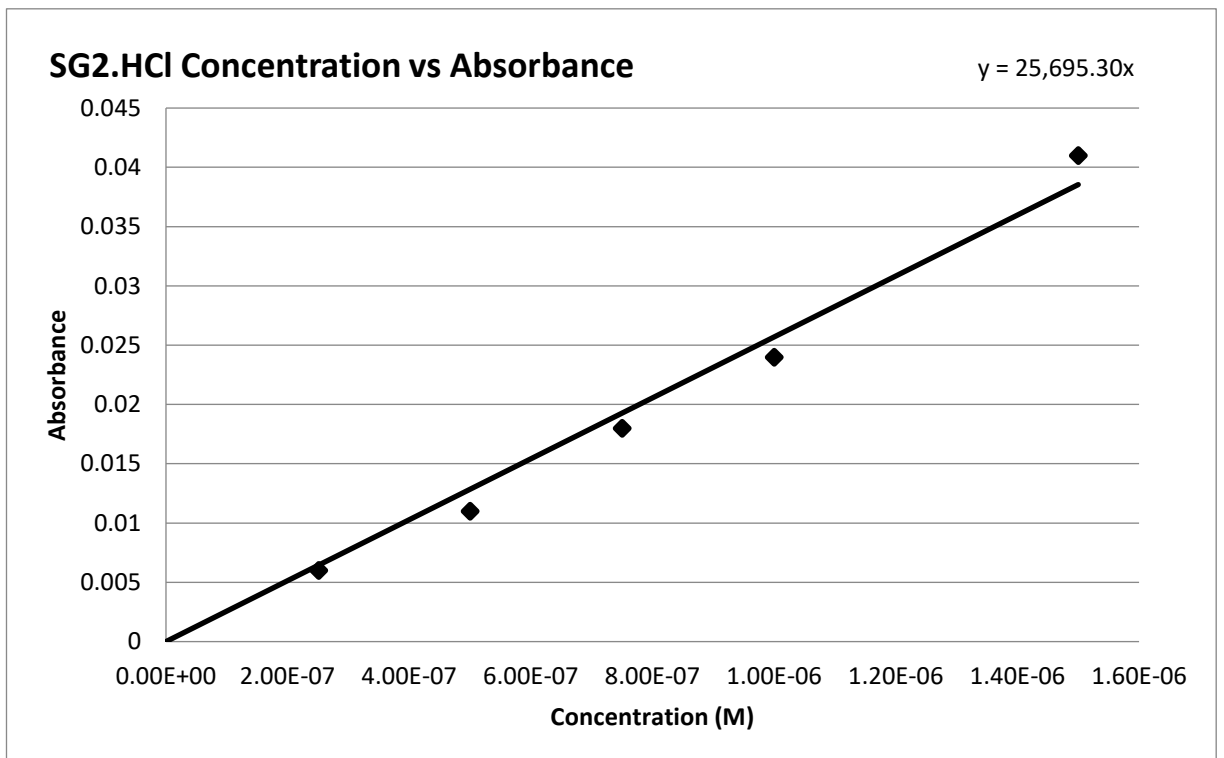
SG1 QY = 0.647431877



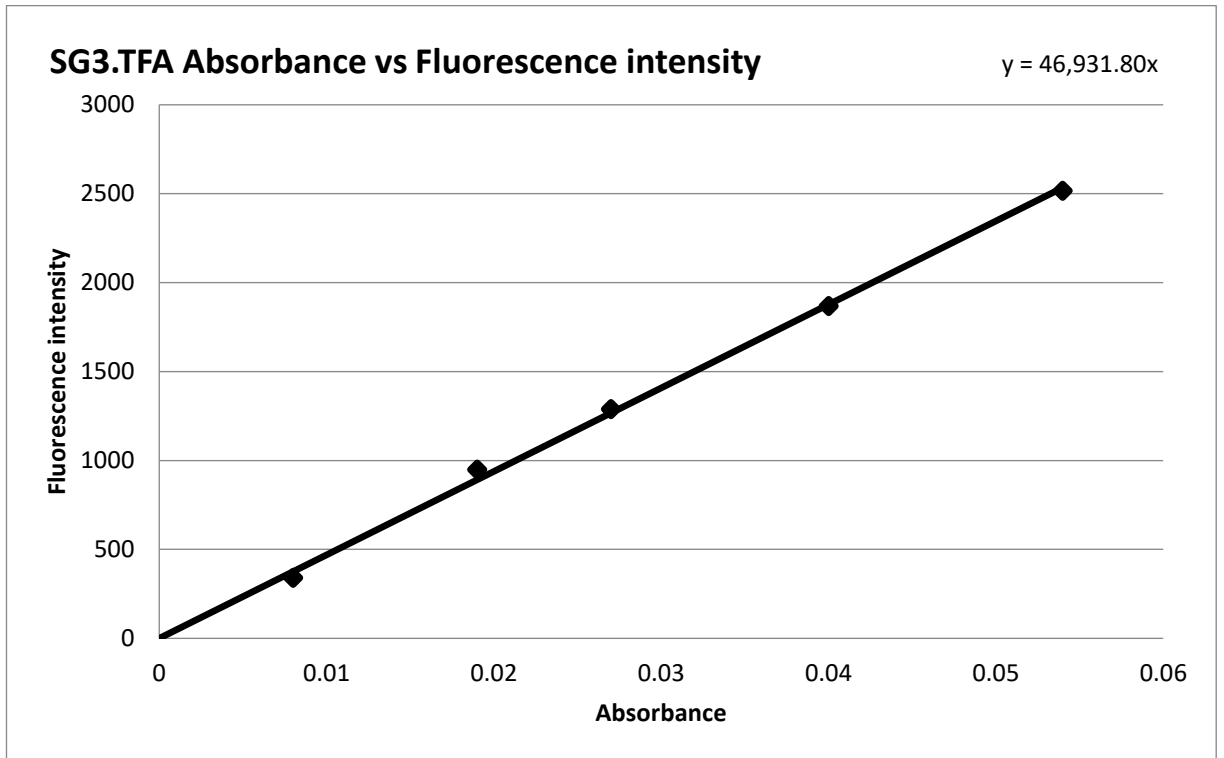
SG1 $\epsilon = 46044 \text{ M}^{-1}\text{cm}^{-1}$



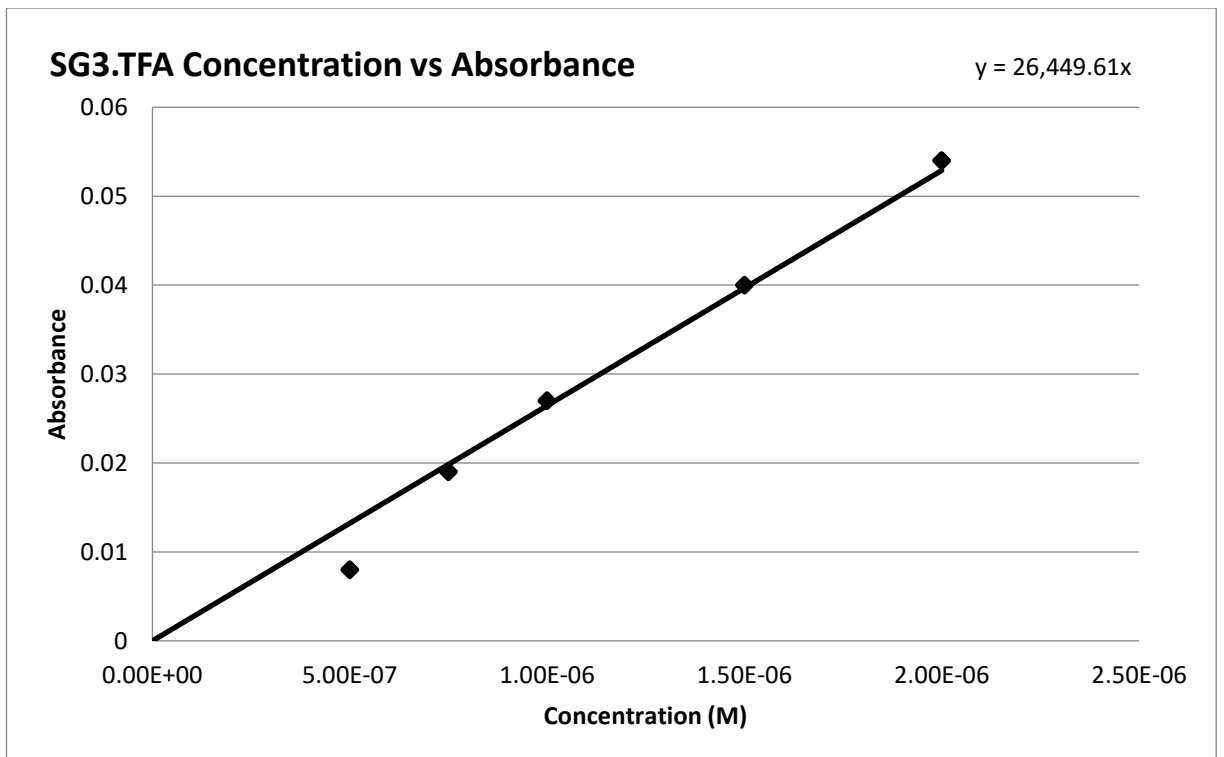
SG2 QY = 0.561098083



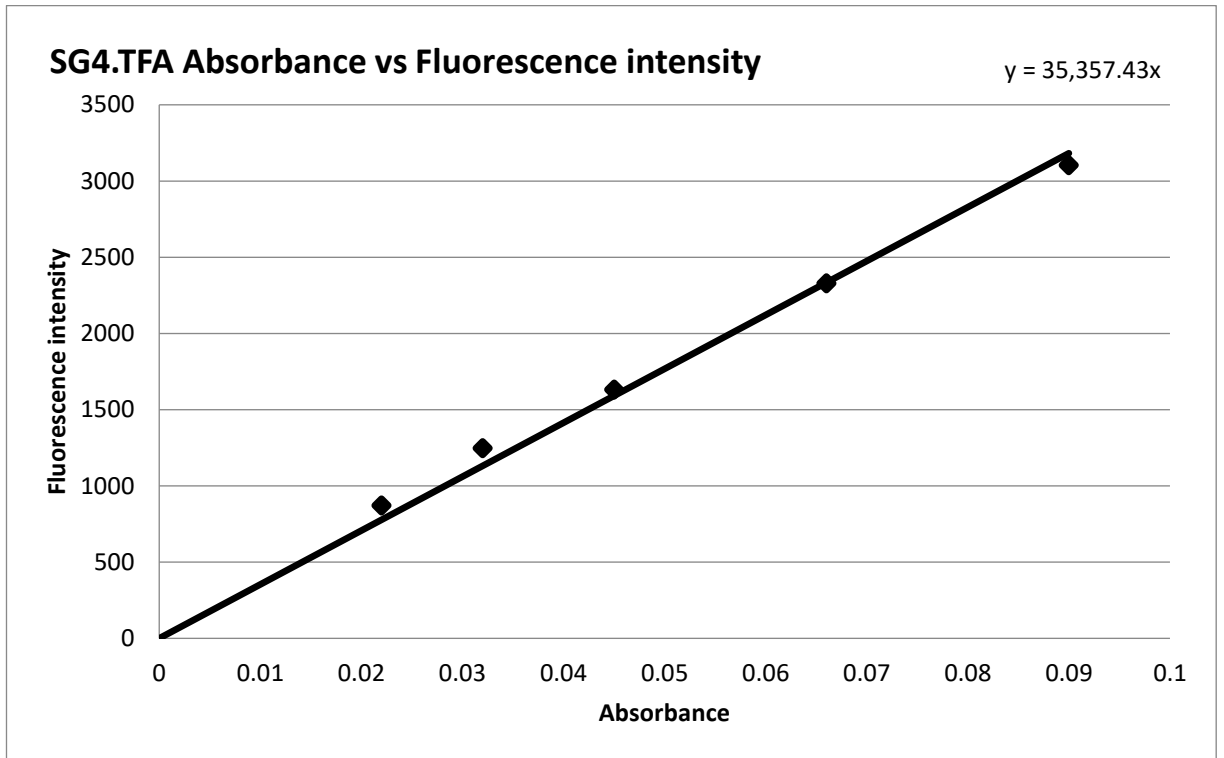
SG2 $\epsilon = 25695 \text{ M}^{-1}\text{cm}^{-1}$



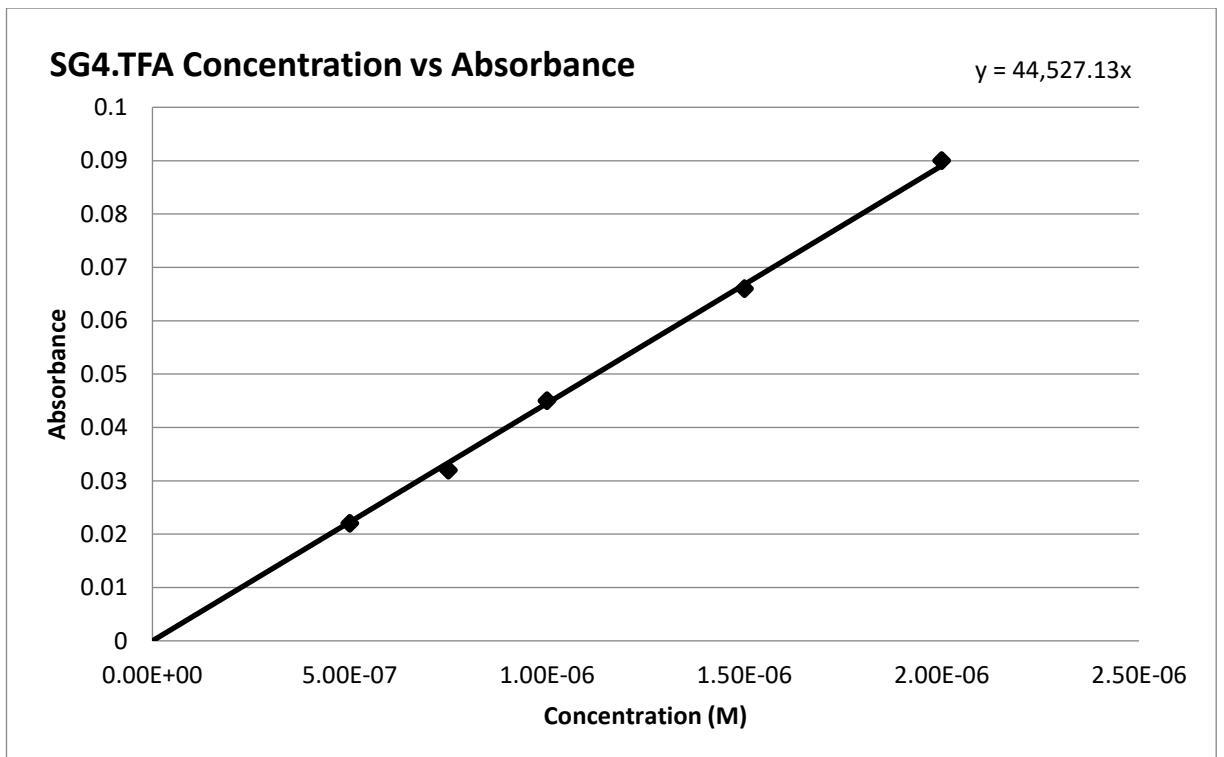
SG3 QY = 0.63144219



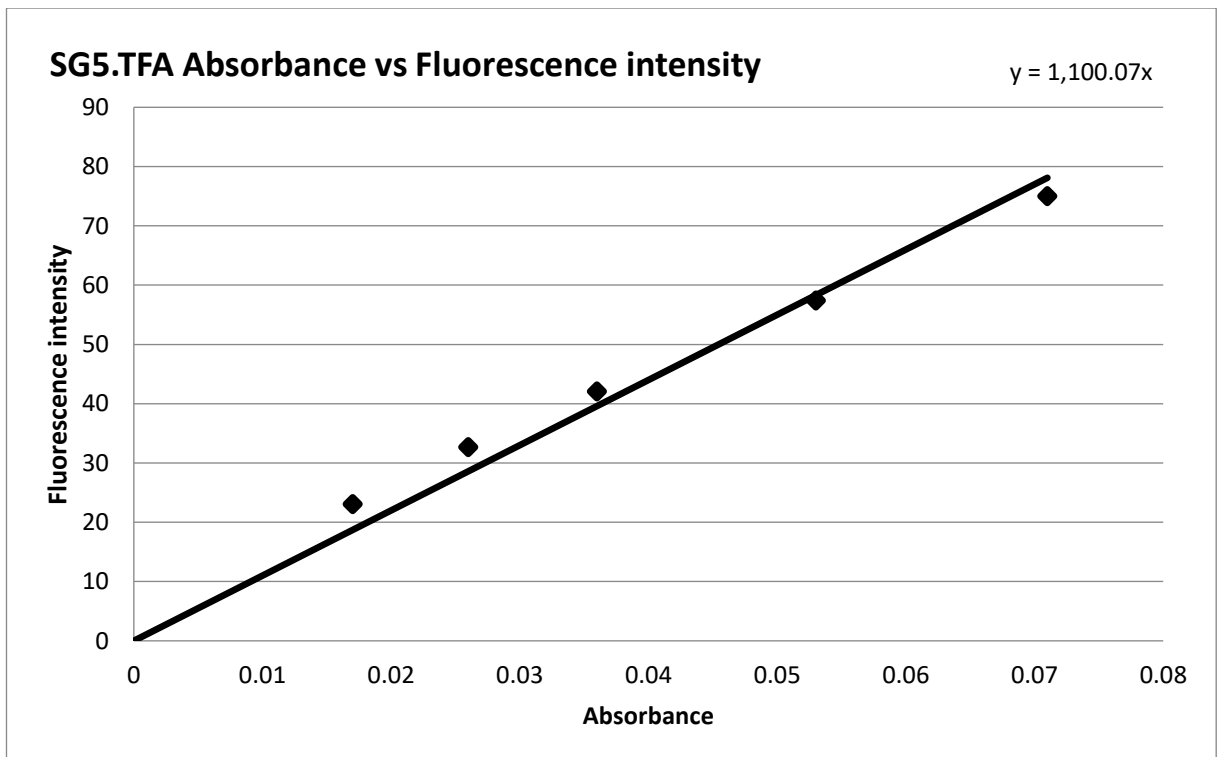
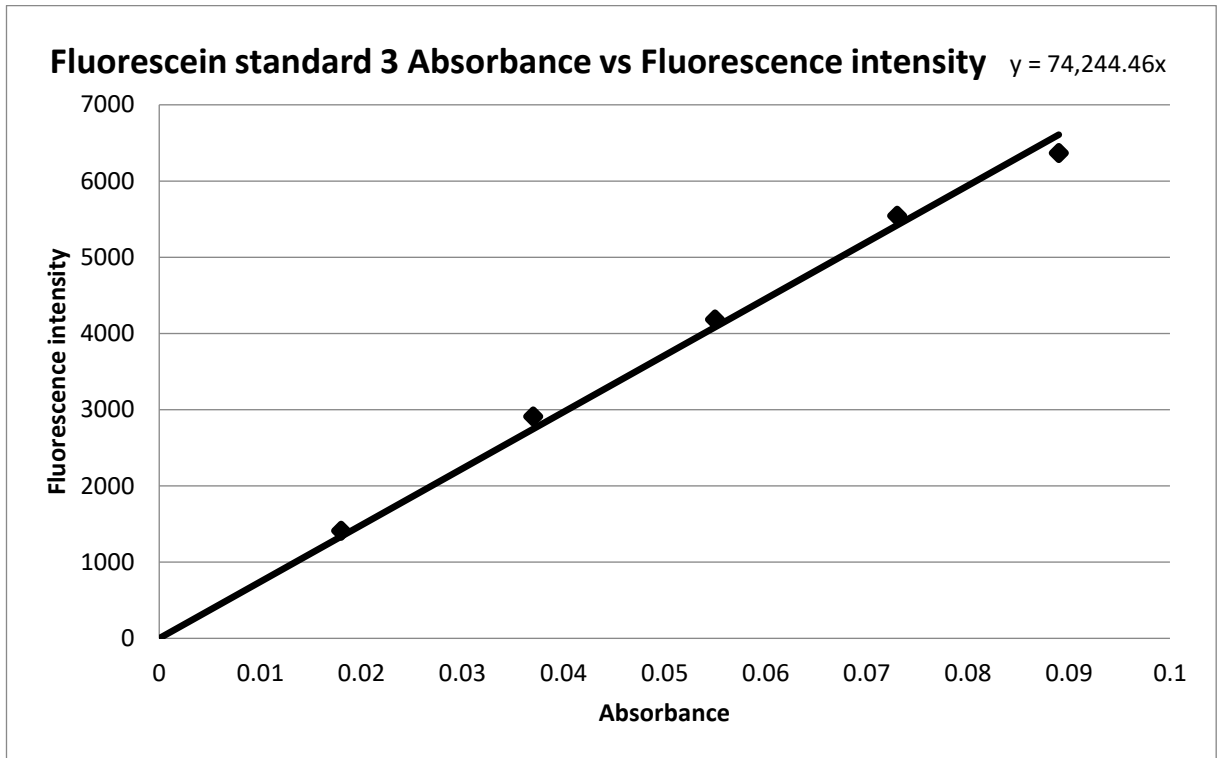
SG3 $\epsilon = 26450 \text{ M}^{-1}\text{cm}^{-1}$



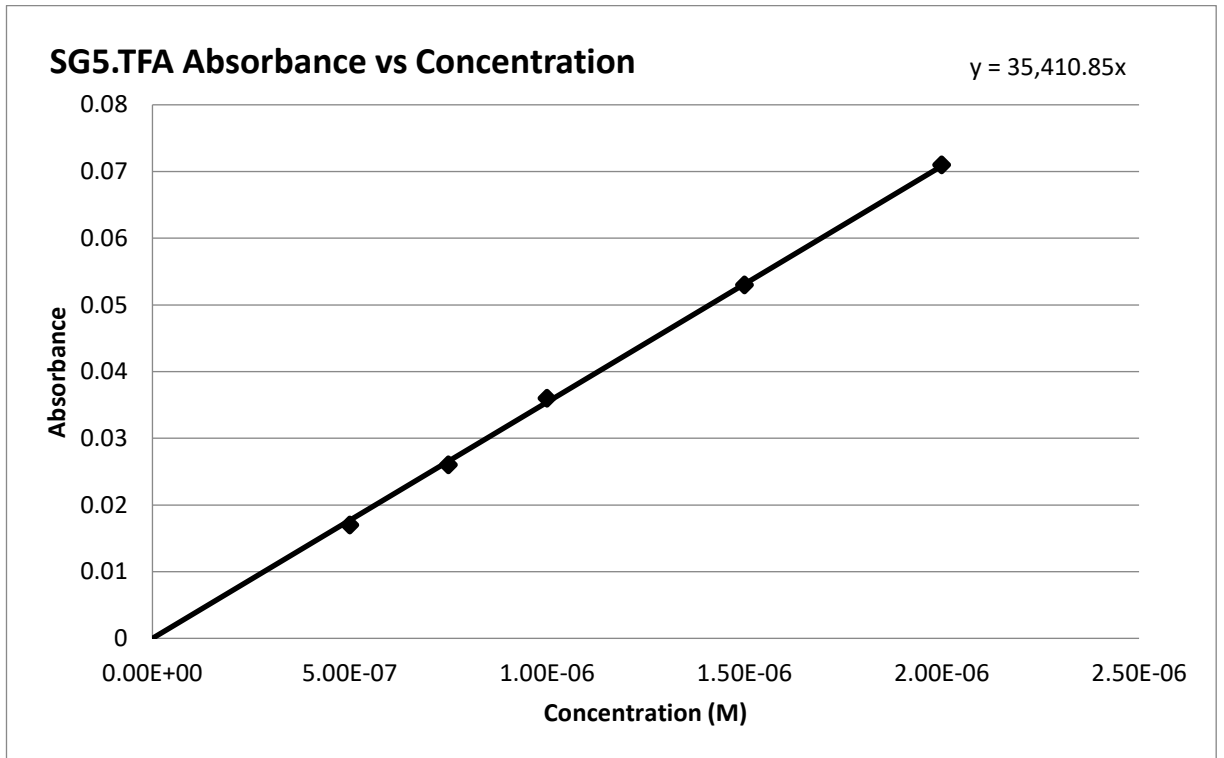
QY = 0.475715251



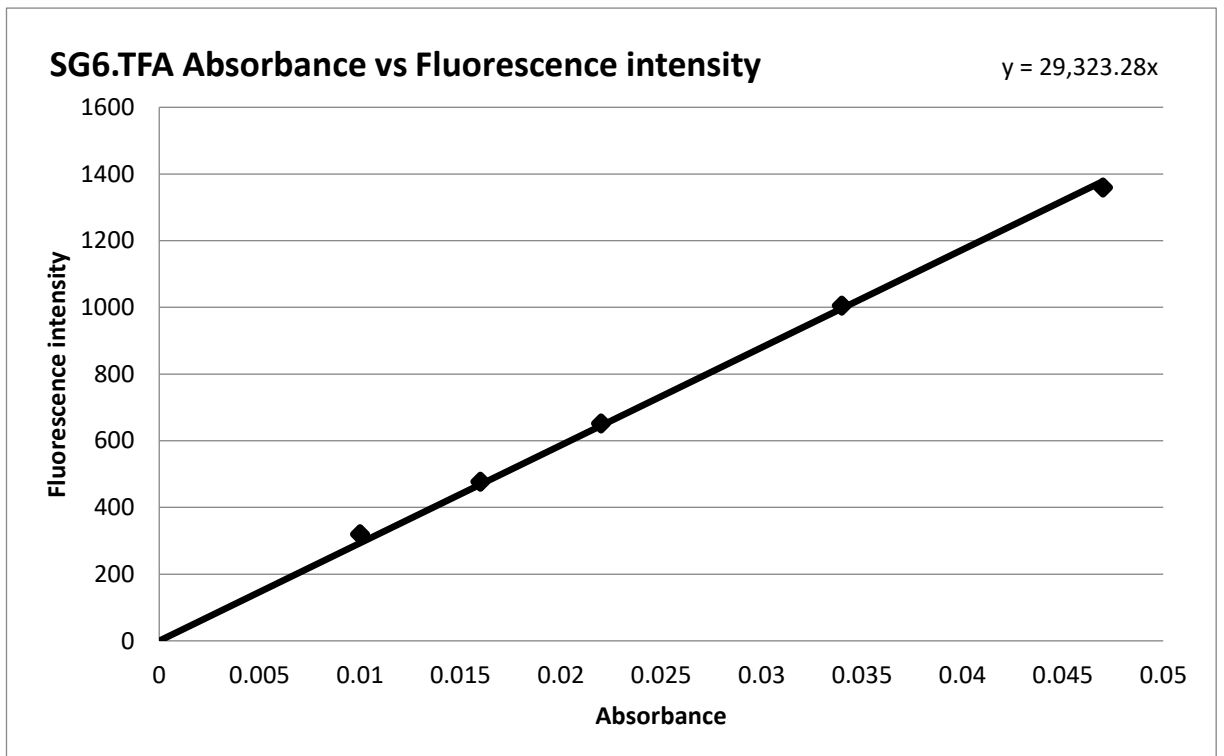
SG4 $\epsilon = 44527 \text{ M}^{-1}\text{cm}^{-1}$



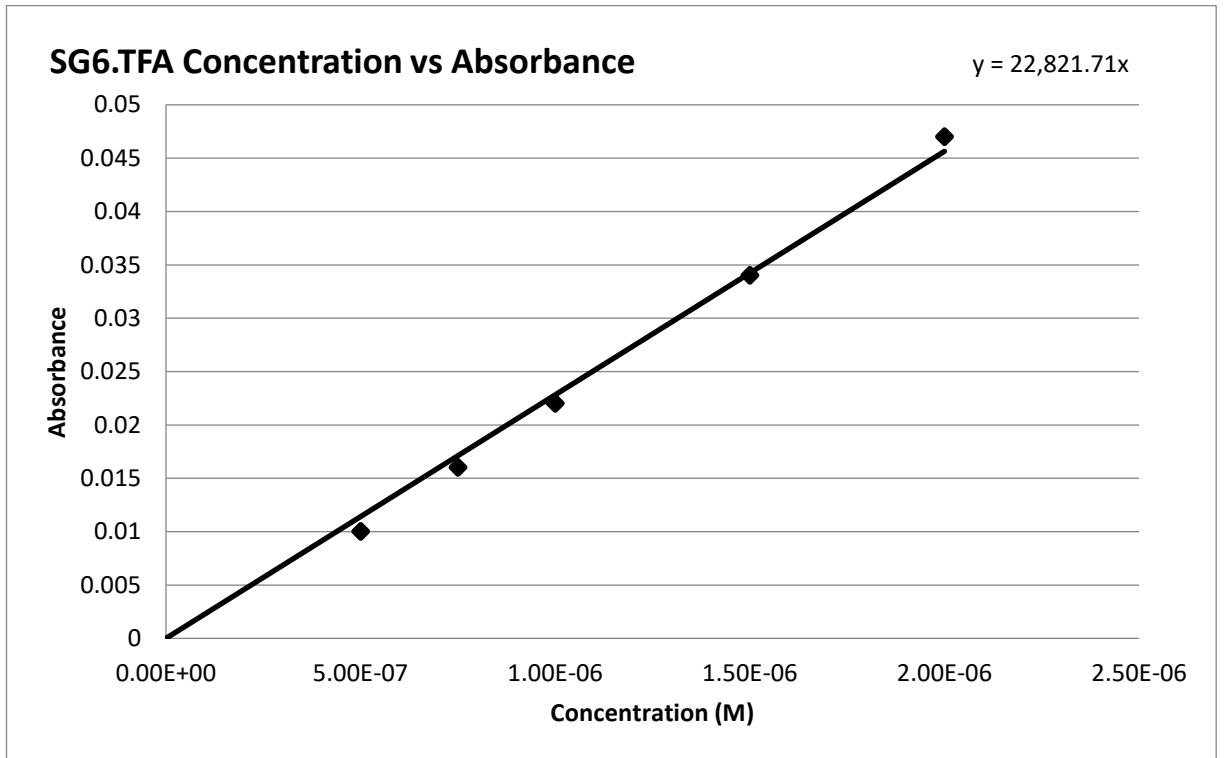
QY = 0.014651641



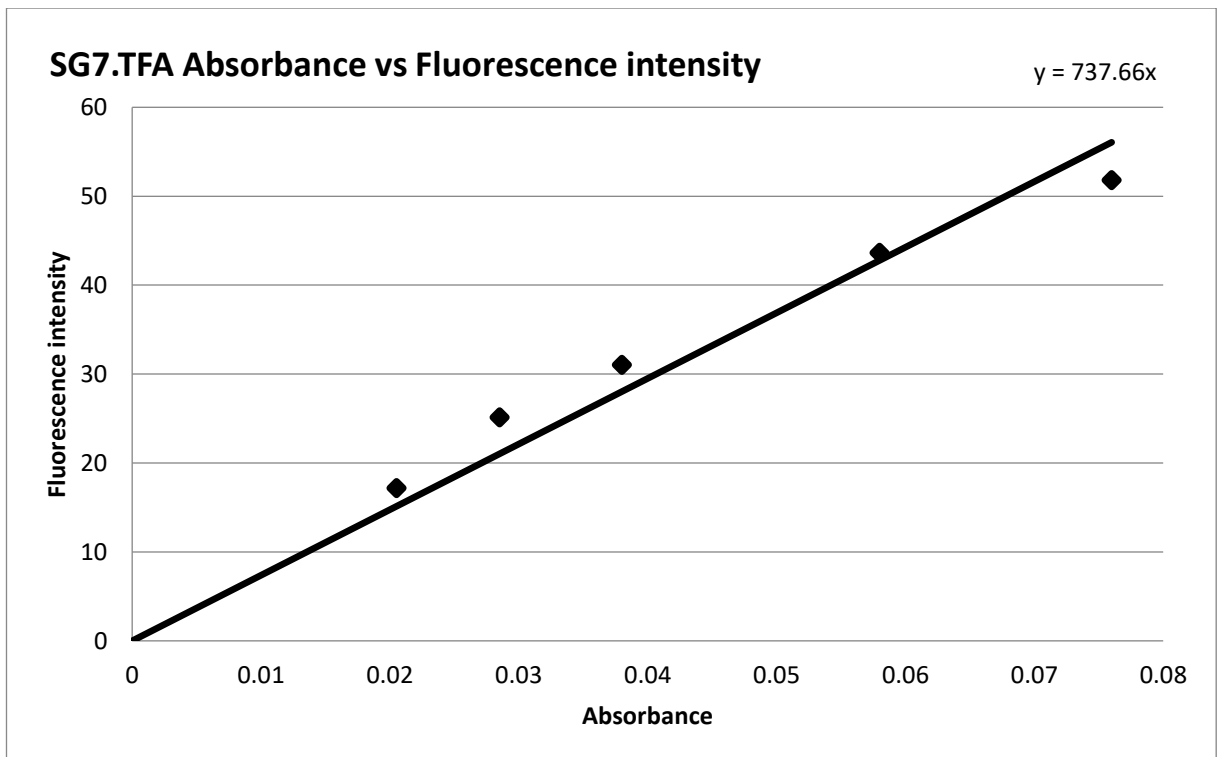
SG5 $\epsilon = 35411 \text{ M}^{-1}\text{cm}^{-1}$



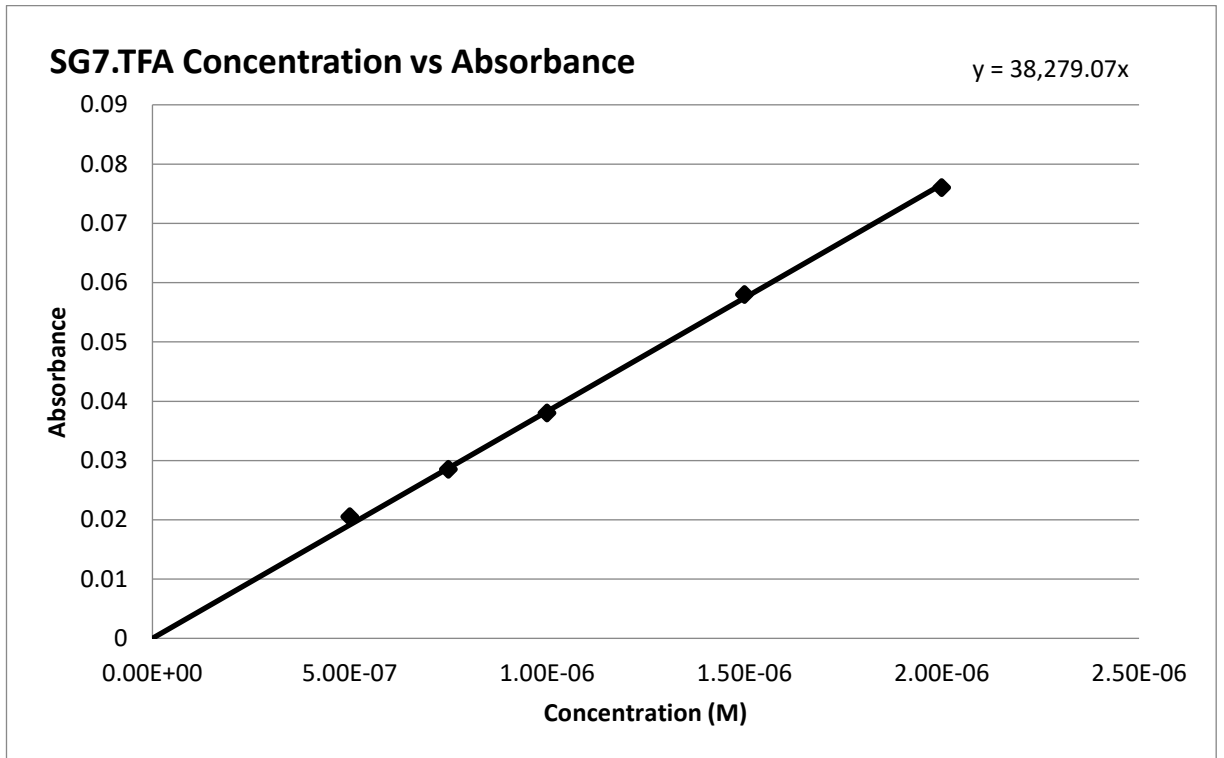
QY = 0.390550111



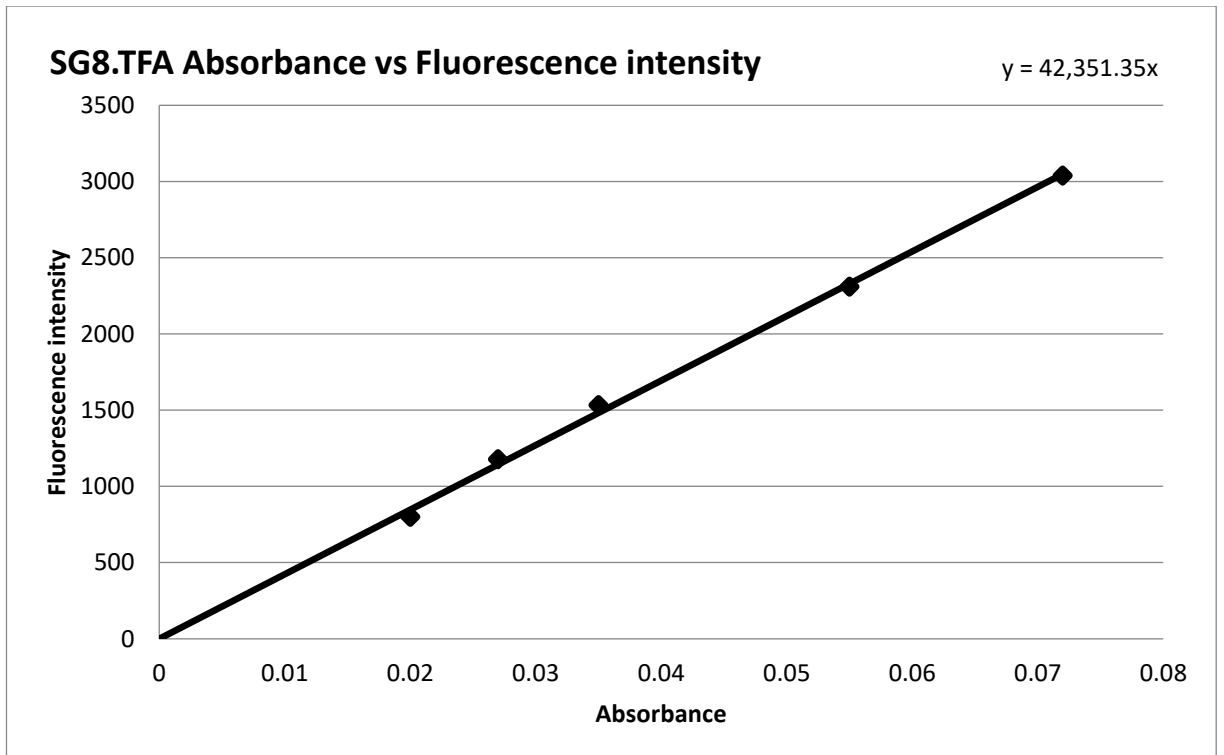
SG6 $\epsilon = 22822 \text{ M}^{-1}\text{cm}^{-1}$



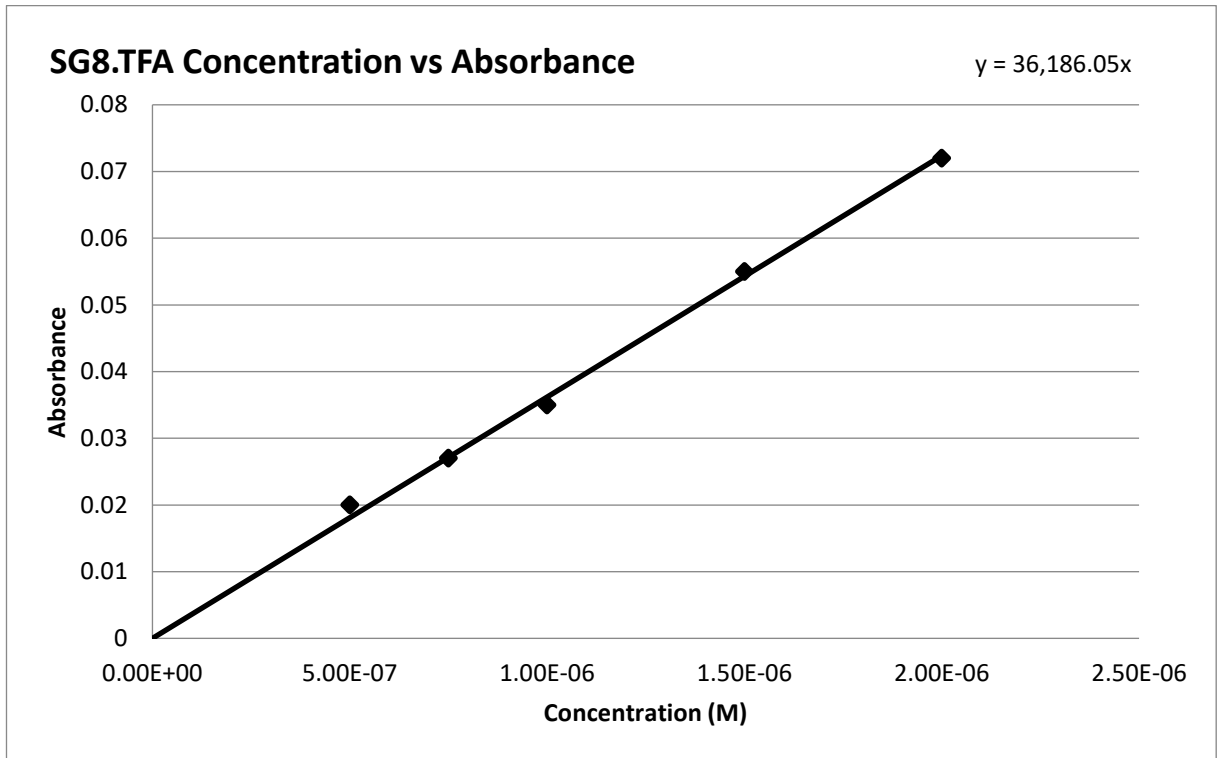
QY = 0.009824684



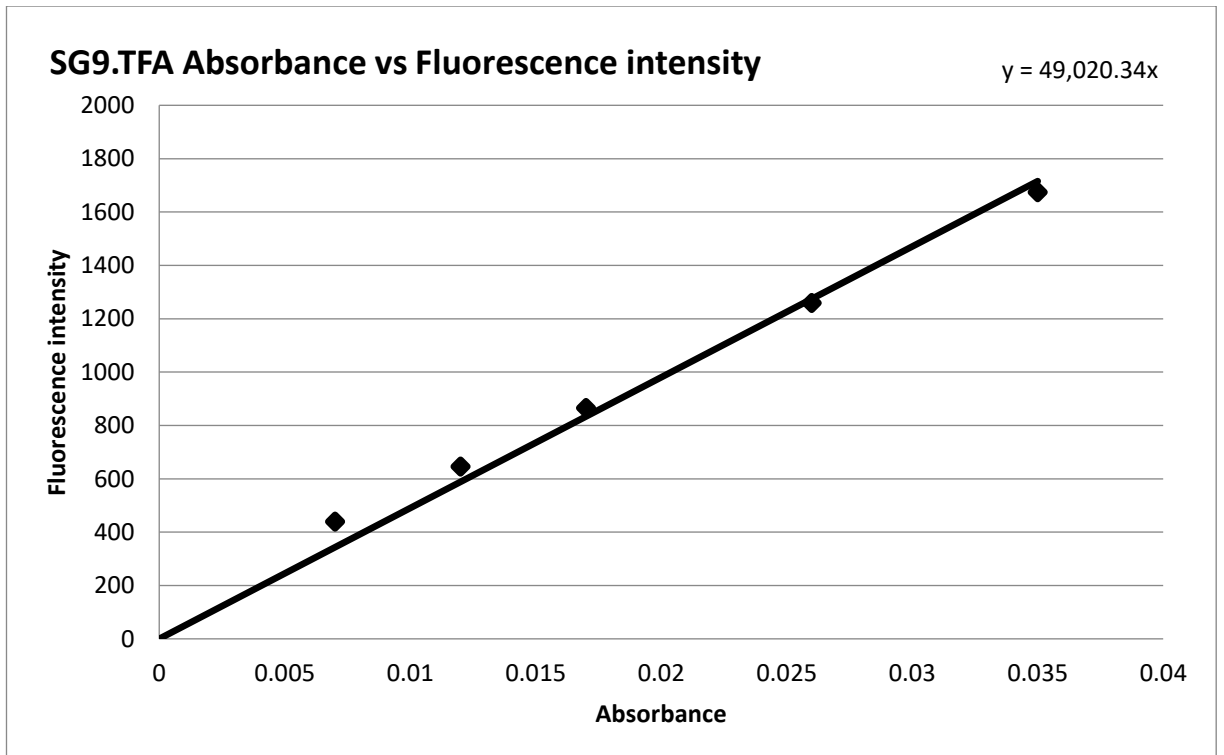
SG7 $\epsilon = 38279 \text{ M}^{-1}\text{cm}^{-1}$



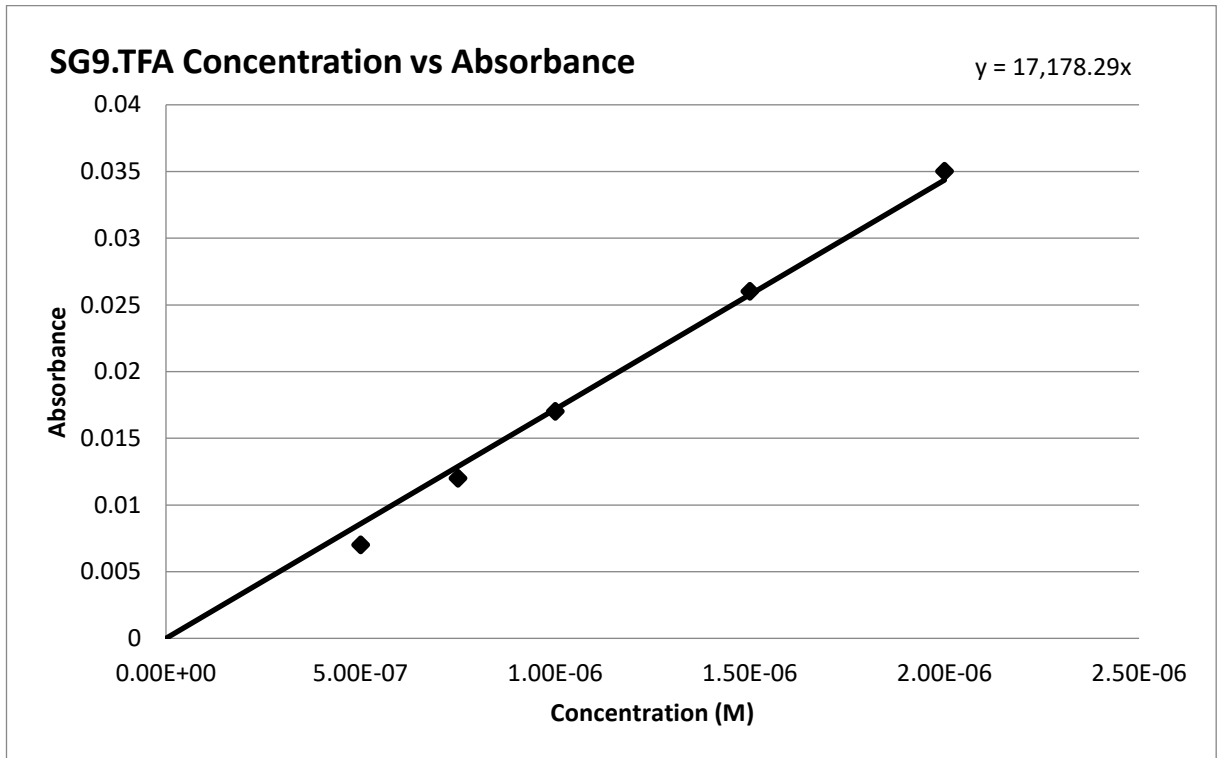
QY = 0.564067922



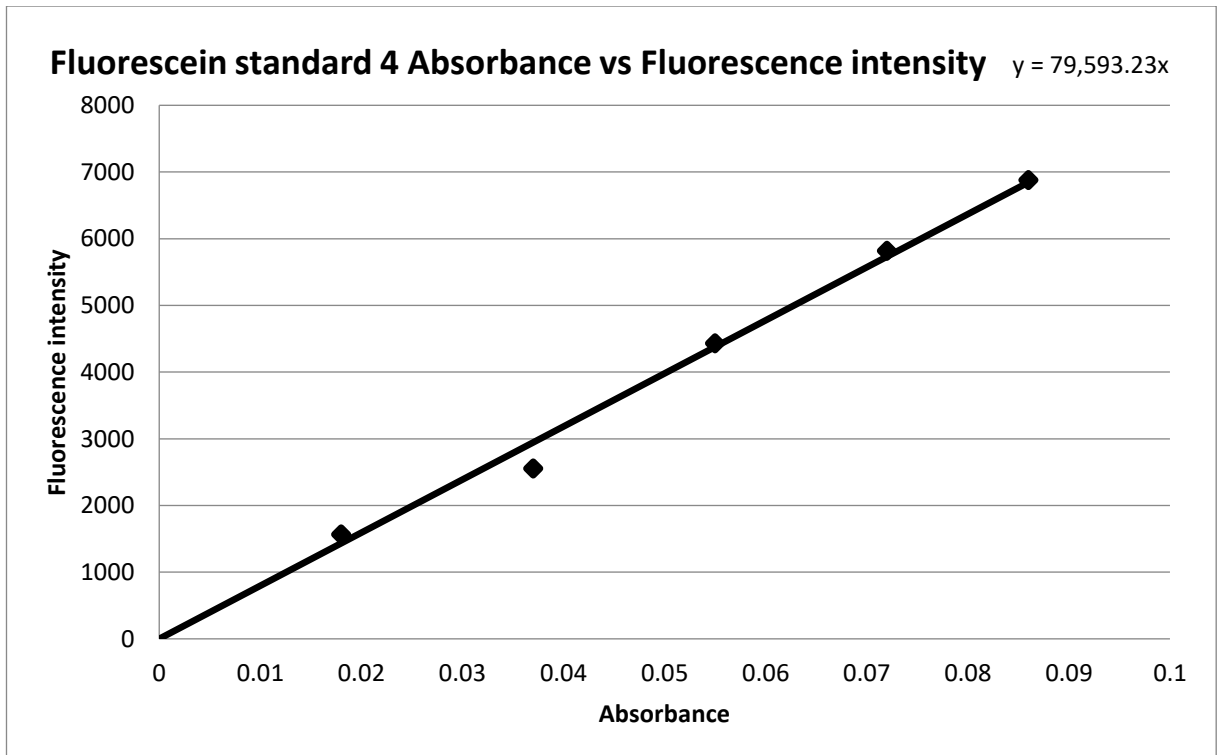
SG8 $\epsilon = 36186 \text{ M}^{-1}\text{cm}^{-1}$

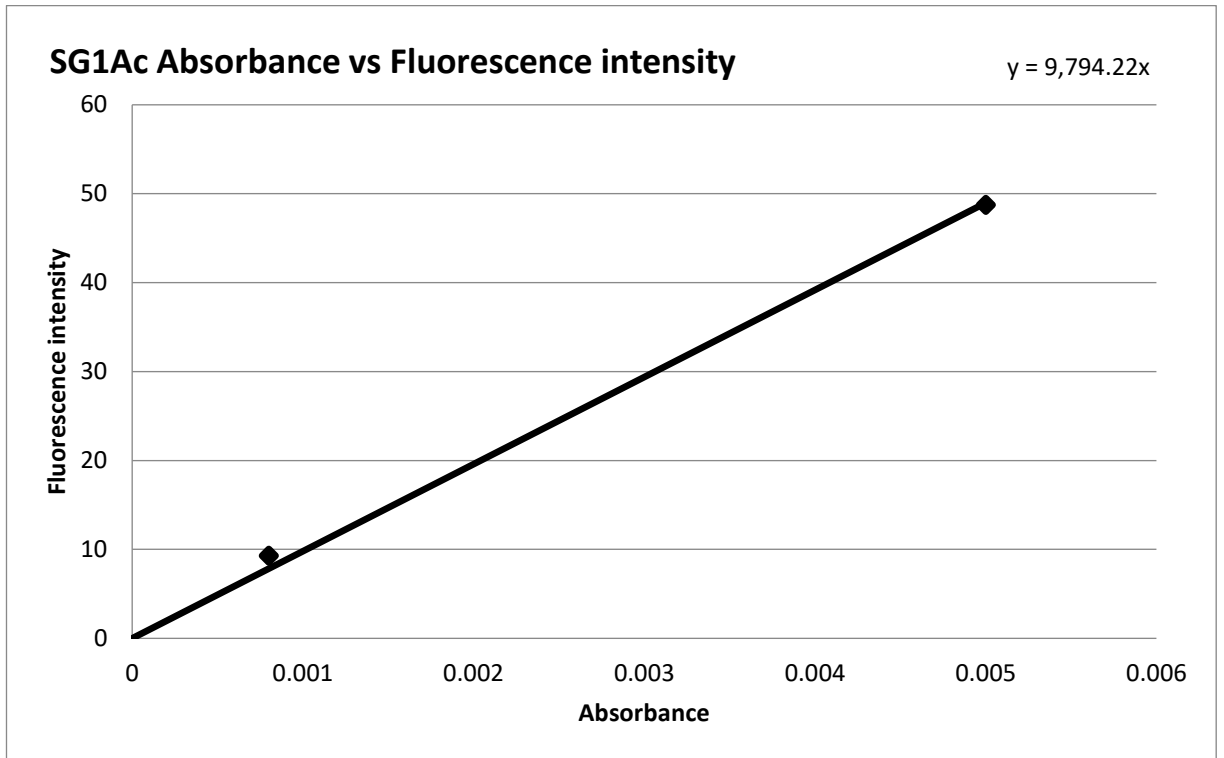


QY = 0.652890671

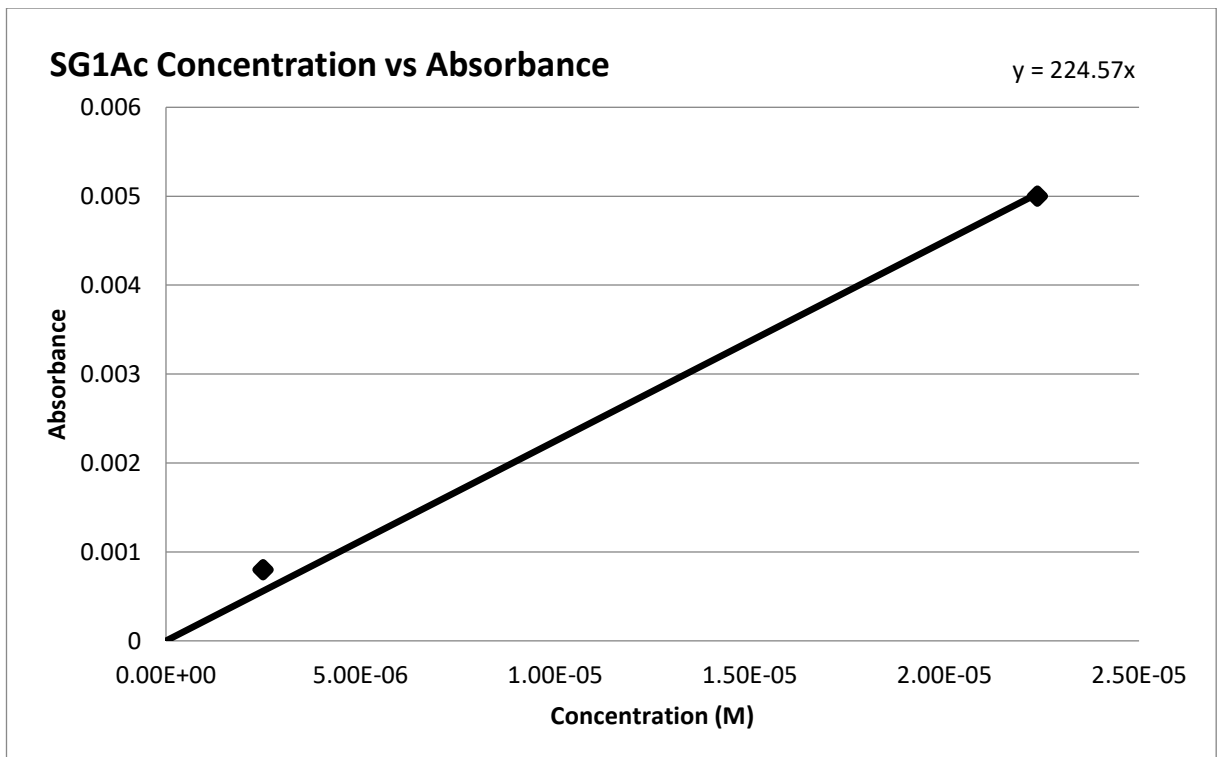


SG9 $\epsilon = 17178 \text{ M}^{-1}\text{cm}^{-1}$





SG1Ac QY = 0.120883283



SG1Ac $\epsilon = 225 \text{ M}^{-1}\text{cm}^{-1}$